UCRL-5675

PLOWSHARE SERIES

Proceedings of the Second Plowshare Symposium
MAY 13-15, 1959 San Francisco, California

PART I

Phenomenology of Underground Nuclear Explosions

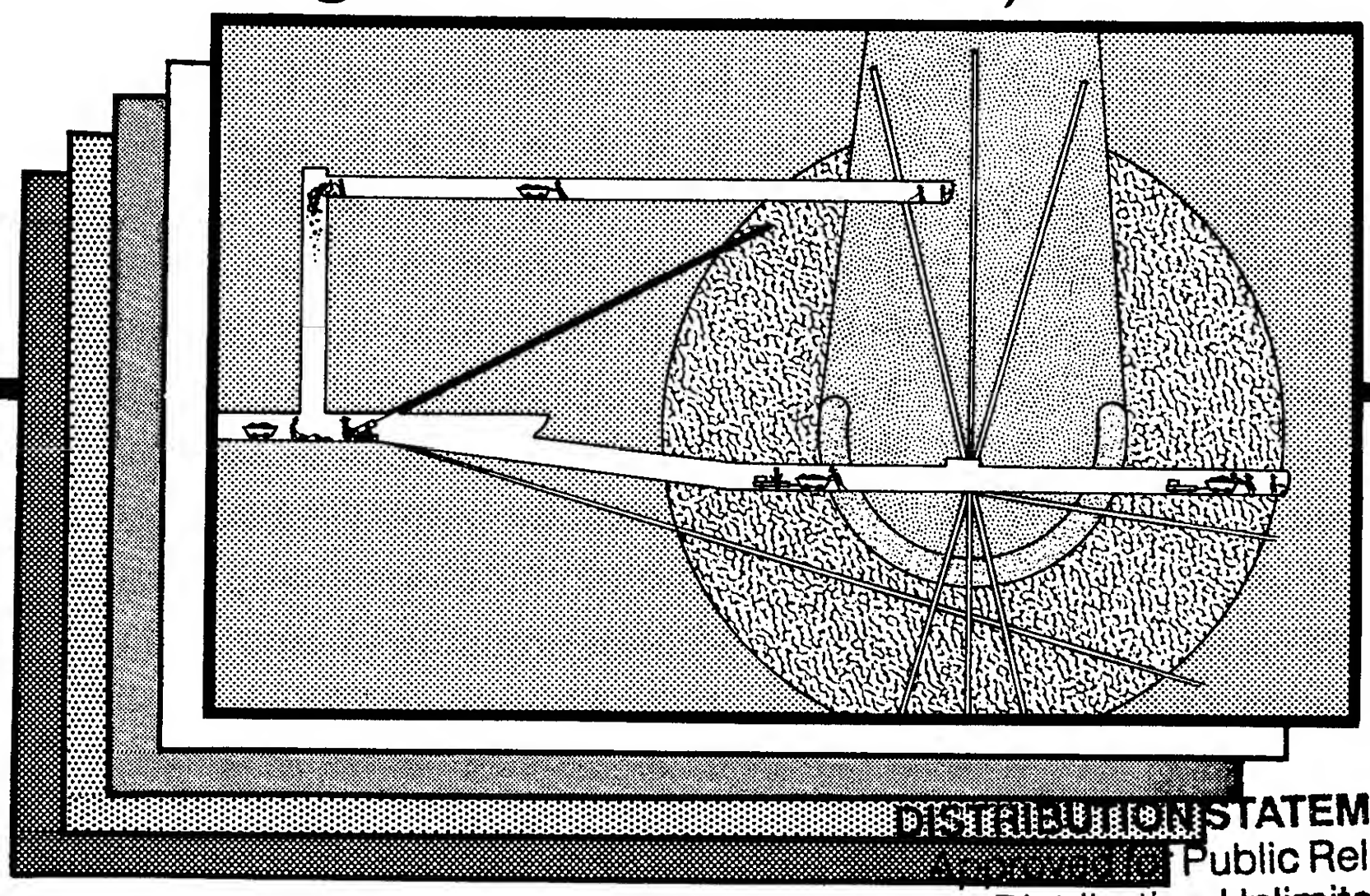

LAWRENCE RADIATION LABORATORY — LIVERMORE

and

AEC — SAN FRANCISCO OPERATIONS OFFICE

UCRL-5675
Nuclear Explosions
Peaceful Applications
TID-4500, UC-35 (15th Ed.)

UNIVERSITY OF CALIFORNIA
Lawrence Radiation Laboratory
Livermore, California

and

San Francisco Operations Office
U. S. Atomic Energy Commission

Contract No. W-7405-eng-48

Plowshare Series: Report No. 2

Proceedings of the Second Plowshare Symposium

Part I

May 15, 1959

Phenomenology of Underground Nuclear Explosions

Printed for the U. S. Atomic Energy Commission

PREFACE

The Second Plowshare Symposium was held in San Francisco, California, on May 13-15, 1959. The main topics covered were: Underground Explosion Phenomenology, Excavation with Nuclear Explosives, Power and Isotope Recovery Studies, Industrial Applications, and Scientific Experiments. In order to publish the proceedings in volumes of a reasonable size, each of the major sessions is being published separately.

As is indicated by the topic headings, the meeting followed a planned sequence from the past, through the present, and ended with some future plans and ideas. The order of presentation was (1) the data on past underground explosions, (2) the current theories on phenomena produced in underground explosions, (3) the extrapolation of these facts and theories to excavation and power-recovery projects planned for the near future, and (4) some thoughts on industrial and scientific applications envisioned somewhat farther in the future. This first volume contains the talks of the first day, May 13, concerning the underground nuclear explosions that took place in Nevada in 1957 and 1958.

In addition to the speakers, many people contributed to the successful carrying out of the symposium. Marshall Peterson handled the meeting arrangements; Rodney Southwick was responsible for the news coverage and public information releases; David Rabb, Nanette Jaffe, and Harlan Zodtner helped in editing the papers and session recordings for publication; the staff of the Technical Information Division was responsible for the preparation, publication and distribution of the symposium reports.

W. J. Frank

TABLE OF CONTENTS

TABLE OF CONTENTS (Contd.)

A. Opening Talks

1. INTRODUCTORY REMARKS

Harold Brown

Lawrence Radiation Laboratory, Livermore

The first Plowshare Symposium was held somewhat over two years ago. It would seem appropriate at this time to take a look at where we now stand, at what we've done since that first Symposium. That is one reason for this second Symposium.

Perhaps an even more important reason is to help those people who are interested in Plowshare, or have heard something of Plowshare, learn what's going on in the subject, by hearing the people who are working in it say what they are doing, instead of by reading scattered and sometimes overpopularized articles. In particular, we hope that you will realize that this program does not consist of a group of physicists in a back room drawing conclusions about geology, chemical processing, or economics, but that qualified people have been brought in as participants in the program and as consultants for each specific application which is being considered.

I don't think it's my job, particularly at the beginning of a meeting of this kind, to evaluate the progress of the last two years; but I do think that two points should be made. First, there have now been a number of underground nuclear explosions. These have not been Plowshare experiments in the sense that they were entirely motivated by the Plowshare program; they had other motivations as well. However, they have cast a considerable amount of light on the characteristic effects of underground explosions and on the specific Plowshare applications which use, or might use, those effects.

Second, in evaluating the Plowshare program, one important criterion (it's not the only one) is whether we are learning more. That is, a criterion of the success of the program is whether we are learning more and whether what we have learned is favorable or unfavorable to the specific applications that we have in mind. Although I think the accomplishment of specific projects is in the long run the most important criterion of progress, it is by no means the only test of progress, and I think we should keep that in mind as we listen to the subsequent papers.

2. WELCOMING ADDRESS

Ellison C. Shute

San Francisco Operations Office, USAEC

On behalf of the University of California Lawrence Radiation Laboratory, and the Atomic Energy Commission, I extend a wholehearted welcome to all of you attending the Second Plowshare Symposium. It is our hope that these discussions will stimulate the exchange of ideas on the peaceful applications of nuclear explosives and will further contribute to our knowledge in this field. The intriguing possibility of using nuclear explosives for peacetime purposes was considered as early as fourteen years ago at the inception of the atomic energy program. In more recent years, scientists and engineers in our laboratories and in industrial and private institutions have continued to consider ways and means in which this new explosive could be put to work. The Lawrence Radiation Laboratory at Livermore provided the initiative, starting a formal program of investigation which has become known as the Plowshare program. A first major step in this direction, as Dr. Brown indicated, was the First Plowshare Symposium held in February 1957. Although it was conducted as a classified meeting, most of the papers presented there were subsequently declassified and published. Additional emphasis was given to the program by the underground weapons tests conducted at the Nevada Test Site in 1957 and 1958. Those tests have proved to be a valuable source of reference data in considering possible uses of nuclear detonations for entirely peaceful purposes such as mining, excavation, and earth-moving jobs previously entirely impractical or impossible before the advent of this new dimension in explosives. Other possibilities worth investigating are the production of power and isotopes, and the replenishment of ground water. Nuclear explosives have been known to the public only as nuclear weapons and as such have gained a somewhat fearsome reputation. History indicates, however, that this preoccupation of wartime application is not entirely justified. Many other explosives have been invented for wartime use and were considered horrible; in the long run, however, peacetime uses have proved to be far more numerous than the military uses.

Two formal projects are currently under way in the Plowshare program. They are: Project Gnome which is a proposed detonation of a 10-kiloton

device in the salt beds near Carlsbad, New Mexico, for the purpose of investigating the feasibility of recovering power and isotopes, and Project Chariot which is a proposed experiment to use two 200-kiloton and three 20-kiloton devices to demonstrate the feasibility of excavation for such purposes as harbors and canals. In addition, there have been discussions with the petroleum industry regarding its interest in supporting an AEC-U.S. Bureau of Mines project to investigate the practicability of using nuclear devices to crush oil shales thereby permitting the recovery of oil by in-situ retorting. Let me re-emphasize that the Gnome and Chariot Projects are under study. Thorough consideration is being given to every phase of these projects and the Commission requires that every precaution be taken to assure the public health and safety. Extensive studies and surveys are being and will be conducted to determine all possible effects of blast, radiation, and heat on any environment being considered. The Commission will give us approval to proceed only after such studies have established that the nuclear explosives can be used with complete safety. We all look forward to hearing the ideas and papers being presented and the discussions that I am sure will follow. I hope you will find the sessions both informative and interesting.

3. THE PLOWSHARE PROGRAM

Edward Teller

Lawrence Radiation Laboratory, Livermore

It is a very great pleasure to see all of you here. It's rather a bigger gathering than we had two years ago, and I think that what we know about the subject is also a little bit larger. I will try to give you, in a very few minutes, some sort of a perspective on what we are after.

Conventional explosives have been used in peacetime as much, perhaps more, than they have been used in wartime. They have been used in the main for two purposes. They have been used for transportation in the sense that obstacles have been removed in building roads, waterways and other similar things. And they have been used in mining. You will see that, according to our present ideas, these are also the two main uses of nuclear explosives, although you will hear about other classes of possible applications.

The reason that nuclear explosives have been so slow in entering our ideas for peaceful purposes is twofold. One reason is that nuclear explosives have sort of biggish effects with the result that one tends to think twice or perhaps even more than twice before one actually tries to undertake something. The other reason is that nuclear explosives produce radioactivity. This radioactivity in the immediate neighborhood of the nuclear explosive can, indeed, be quite dangerous; one has to take, and we are going to take, as Mr. Shute has just told you, the most conscientious precautions that this radioactivity will do no harm. Of course, one should also realize that radioactivity in exceedingly small doses (a subject that often enters the public discussion) is really far from dangerous; one cannot even determine sometimes whether a danger exists.

I should say right away that many of the applications are underground explosions where the radioactivity is completely contained and where, provided one pays serious attention to the question of possible ground water contamination, the danger will be quite negligible. Furthermore, I should tell you that the radioactivity we are likely to release underground is very much smaller than the radioactivity that one buries when one tries to dispose of reactor products. The difficulties due to possible contamination merit serious and conscientious consideration. But they are by no means insurmountable.

It has been an exceedingly wise act of the Atomic Energy Commission to have declassified the whole subject of Plowshare with one exception, with the exception of the black box which contains the main actor in the drama. This item we cannot at the present time declassify. I would like to say that all of us who are involved in this business are very anxious to conduct it with the greatest possible openness and to give you information about the nuclear explosive itself insofar as this should prove compatible with the information which we have to guard for military reasons. Actually, almost everything that needs to be said for an effective application can be said in an unclassified manner and will be said here.

I have told you that two great difficulties connected with Plowshare are the fact that nuclear explosives are big and that they produce radioactivity. I would like to assure you that we are working very hard on these two topics. It stands to reason that the full effect of nuclear explosives can be exploited only if the biggest kind of nuclear explosions are included in our program and in the long run we hope to include them. At the same time it will add a very great deal to the flexibility and the scope of the program if smaller nuclear explosions can be carried out and particularly if they can be carried out cheaply. This is one of the aims of continued research into nuclear explosives and I only wish I could tell you more about this exceedingly interesting topic. Perhaps someday I shall be able, or somebody shall be able, to do so.

Second, I should like to tell you that the difficulty of radioactive contamination is also something which we can attack. Even at the present time we know how to make big nuclear explosions fairly clean. We are hard at work to make big and small nuclear explosions as clean as possible and, hopefully, we may make them completely clean. It will require invention, it will require work, but if we could get rid of radioactive contamination, the applicability of this new tool would be very, very greatly increased, and this is one of the most important aims toward which our experiments are, and must be, directed.

Now, as to the program itself, we need help. We have knowledge – good knowledge, reliable knowledge – about nuclear explosives: how to make them, how to handle them, how to apply them. We acquired some knowledge of the behavior of nuclear explosives in the air quite some time ago, and underground more recently. This knowledge comes in very handy, but we have to have more knowledge, particularly about underground nuclear explosions.

However, there are very, very big areas where we are in dire need of advice and cooperation; in fact, this program cannot prosper without a great number of people, earth scientists, chemists of every description, scientific people of every kind. If these people will participate, and I know many of you are in these various fields, then the program will prosper; otherwise it will not.

Let me sketch briefly the state of our prospects and ideas. First of all, we have the earth-moving projects – building harbors, building canals. To move earth, and to move earth cheaply, is something that we know we can do today. We do not know the best way to do it, we do not know in every detail how the radioactivity can be handled, and we can only hope that the radioactivity might be avoided altogether, as I have told you. But, the question does not end here. Today we can dig a harbor for the price, or for less than the price, that it costs to equip that harbor. But, when you want to dig a harbor, the question immediately arises "where?" Where is it worthwhile to dig a harbor? Will that harbor last or will it silt up? Again, for a canal, the same kind of economic questions arise. These are tasks which we can perform, which we hope to perform wisely with the help of a wide and thorough discussion both with respect to safety and with respect to the question of whether the projects are worthwhile.

Then, there are many projects which do not depend on the moving of earth but which depend on the breaking up of rock. These include possible regulation of underground flow of water, storage of water, and all manner of mining including oil production. These two words, water and oil, are magic. Oil is our most important fuel and the lifeblood of modern industry. It may be a strange reversal when nuclear energy will be used to make the main source of conventional energy cheaper and more plentiful. We seem to be putting some cart before some horse.

Water is even more important; but whether these things can be done in a practical sense is an exceedingly difficult question. In fact, I think that any thing or project of this description is likely to turn out to be not feasible, at least for the time being. We have found that we can crush rock; but, we also have found out that this rock may solidify again. We have found out that we can break up rock, but only one kind of rock – volcanic ash; we do not know whether we can break up granite, limestone, or oil shale, and in what precise

manner. Yet, for these applications of water storage, underground regulation of water flow, mining, oil production, these questions of breaking up rock are of basic significance.

And here arises the point that Harold Brown has so correctly mentioned – we must for the next few years consider ourselves successful if we have gathered information about these important things. We may have a chance, a small chance, a 10% chance, or a smaller chance even, greatly to enrich the oil reserves of the world by making available oil sands or oil shales. The odds may be long, but the stakes are high and our investment need not be very great.

There is a big area of, in my opinion, even more adventurous thought. We can produce heat and we can mine the heat. If we can make the capital investment of piping and other things serve for many shots in the same place, we can hope to do this in a really economical way and to have really cheap and abundant thermonuclear power. We can make isotopes of all descriptions underground; some of these isotopes will be very valuable, provided we can extract them in a cheap and effective manner.

Now I would like to mention to you two fields which, I believe, have been considered much too little. They have been considered, but the consideration has not been sufficient. One is the use of nuclear explosions for purely scientific purposes. A nuclear explosion underground is a source of geophysical disturbance, a smallish earthquake which can be used to find out more about the crust and interior of our earth. A nuclear explosion is a source of radiation and neutrons; we can use nuclear explosives to find out more about neutrons and nuclear physics in general. One can use a nuclear explosive as it was used unintentionally in the first big nuclear explosion in the Pacific: to capture many successive neutrons in the same nucleus and thereby get to a new species which then can be studied. One can use nuclear explosives for various strange purposes to find out the properties of the upper atmosphere and the earth's magnetic field, as it has been done by the well-publicized Argus experiment. I am sure that this does not begin to exhaust the list. We haven't thought enough about the subject and we shall hear about it during this symposium. I also should like to tell you that, in order to discuss this matter more fully, with complete knowledge of what exactly goes into and comes out of the black box, a classified conference is being planned during the summer at Los Alamos.

I hope it will be very successful and produce new scientific ideas and new scientific approaches.

There is another and very practical field which also has been neglected — at least neglected in comparison with its enormous potential. One of our good friends, John Grebe, will talk to you about this field: the use of a nuclear explosion underground to produce the heat and pressure to induce chemical reactions.

I should like to start this topic in a somewhat lighter vein by mentioning to you a relatively small and interesting object which actually commands more interest than is justified. I have diamonds in mind. Now, I don't think that diamonds are important, except in some industrial processes, and if we ever succeed in making diamonds, all we are going to accomplish is to ruin the diamond market. The importance of diamonds cannot compare with the importance of oil and water. But, just for the fun of it, let me talk for a moment about diamonds.

We happen to know diamonds can be produced if we have three things — high pressure, low temperature, and time; then diamonds will grow out of pure carbon. Now, high pressure from nuclear explosives we have, but low temperatures we do not. Perhaps if we are very clever about it we might be able to arrange conditions so as to give in certain regions high pressure without excessive temperature. This much I think could be done. What we do not have in nuclear explosions is time. We cannot maintain the high pressure for a long period. This should not necessarily be discouraging. Maybe time can be replaced by exceedingly high pressure, and perhaps we have a chance to produce this exceedingly high pressure. Even so, I don't have a hope for the Hope diamond. What we are much more likely to produce, lest the diamond industry react to my remarks, is very fine and very imperfect diamond powder.

All this I am using only as an example. Maybe we can initiate geochemical and geophysical transformations which usually go on deep inside the earth and reproduce types of materials never seen near the surface of the earth.

We can produce a number of chemical reactions in the strange reactors which we will have underground. Provided we can make the products either volatile or fluid, and some of them will be, it will not be very difficult to get them to the surface, and our chemical industry might be seriously interested. Now this kind of thing cannot be done without the cooperation of chemists,

chemical engineers, and economists. In a laboratory whose aims are really a little bit different, we cannot do much more than give you the means, draw the opportunities to your attention, and then hope for the best.

This group here, if you'll pardon me for saying so, seems to be similar to a bunch of starved and blind people stumbling around in an extremely rich garden. The food, I'm sure, is there to pick; the only question you have to decide is in which direction you want to extend your hand; then you have to rely on the best methods of touch, smell, and intelligence lest you bite into a bitter fruit. I am sure that the opportunity is here. I'm sure that somewhere among you there is the idea, the initiative, the perseverance and the genius which will bring this Plowshare program to fruitation.

B. The Data from Underground Nuclear Explosions

1. SOME BASIC DATA ON UNDERGROUND NUCLEAR EXPLOSIONS

Gerald W. Johnson

Lawrence Radiation Laboratory, Livermore

General Description of an Underground Explosion

In discussing the phenomenology of underground explosions, it is useful to consider several different time scales, with their associated phenomena. The Rainier event, in which 1.7 kilotons of energy (1.7×10^{12} calories, 6.7×10^{9} Btu, or 2.0×10^{6} kw-hr) were released in a room 6 feet square, 7 feet high, and 800 feet below the surface of the earth, will be used as an example.

a. Nuclear Phase (Microseconds). The energy of the nuclear explosive is generated in a few tenths of a microsecond, vaporizing the assembly materials and forming a rapidly growing fireball. The material in the Rainier room reached a temperature of ten million degrees Fahrenheit and a pressure of seven million atmospheres.

b. Hydrodynamic Phase (Milliseconds). A shock wave proceeds outward vaporizing, melting, and crushing the surrounding medium. A cavity is formed by the outward motion of the rock near the center of the explosion. In Rainier, the shock vaporized a 3-foot thickness of rock (about 100 tons), melted 7 more feet (about 600 tons), and crushed rock out to 130 feet. The cavity in Rainier reached its final radius of 55 feet in about a hundred milliseconds.

c. Quasi-static Phase (Seconds to Minutes). The cavity cools and collapses when the internal pressure can no longer support it. In Rainier, the pressure dropped to forty atmospheres in about a minute. A fissure must then have opened, allowing the gases to escape and releasing the internal pressure; the roof caved in and a chimney of rubble was formed. About two hundred thousand tons of broken rock were produced.

d. Long-term Phase (Days to Years). A slow transport of heat through the rock takes place, and the radioactive products decay. In Rainier, the

water present in the rock (20% by weight) vaporized and distributed the heat over a large volume; the highest temperature now present is at the boiling point of water.

Containment and Cratering Data

Nine past explosions will be of particular interest in this symposium. Several were near the surface and were thus not contained; they gave useful data for cratering studies. Several were completely contained, producing no craters and releasing no radioactivity to the atmosphere. Table I summarizes the yield, cratering, and released radioactivity data. The cratering information will be dealt with in more detail in subsequent papers. The containment data may be summarized by saying that for depths of burial greater than $D = 450\ W^{1/3}$ (where W is the yield in kilotons) the radioactivity will be completely confined.

Geological Data

The six explosions which were contained or nearly contained took place in a geological formation known as Oak Springs tuff. This formation, which is some 1900 feet in thickness in the tunnel area, has been divided into eight lithologic units, TOS_1 through TOS_8. The rocks composing these units are fine to coarse, grained-bedded to massive tuffs, welded tuff tuffaceous sandstones, tuff breccias, and agglomerates. The rocks of the Oak Springs formation are siliceous and contain from 65 to 75% SiO_2. Vesicles average 6% of the volume of the nonwelded tuffs, but only 3.5% of the volume of welded tuffs.

The tuffs can be divided into three groups: welded tuff, units TOS_6 and TOS_8; friable tuff, unit TOS_7; and bedded tuff, units TOS_1 through TOS_5.

Welded tuff forms the cap rock of the mesa (unit TOS_8). The color of welded tuff ranges from reddish purple to gray. Phenocrysts of quartz, feldspar, and biotite are common. The rock is hard and dense.

The rocks of the friable tuff, unit TOS_7, are weak. Samples can easily be broken by hand, and drill core recovery is poor. Most beds are light gray or brown and consist of granules of lapilli and fragments of quartz and feldspar. Biotite is relatively conspicuous; fragments of quartzite and welded tuff are locally abundant. It was in this zone that the Rainier event took place.

Table I. Cratering and Containment Data.

Event	Date	Yield (W) (kt)	Medium	Vertical burial depth (D) (feet)	Scaled depth, $D/W^{1/3}$	Measured radioactivity deposited on surface (%)	Crater volume (yd^3)	Crater volume/kt (yd^3)
Jangle-S	11/19/51	1.2 ±0.1	Alluvium	-3.5[a]	-3.3[a]	>65	1,650	1,400
Jangle-U	11/29/51	1.2 ±0.1	Alluvium	17	16	>80	37,000	31,000
Teapot-Ess	3/23/55	1.2 ±0.1	Alluvium	67	63	90	96,000	80,000
Neptune	10/14/58	0.090±0.020	Bedded tuff	99	220	< 2	33,000	370,000[b]
Blanca	10/30/58	19.0 ±1.5	Bedded tuff	835	310	< 0.5	0[c]	0
Logan	10/16/58	5.0 ±0.4	Bedded tuff	830	485	0	0	0
Rainier	9/19/57	1.7 ±0.1	Bedded tuff	790	670	0	0	0
Tamalpais	10/ 8/58	0.07 ±0.01	Bedded tuff	330	780	0[d]	0	0
Evans	10/29/58	0.055±0.030	Bedded tuff	840	2200	0[e]	0	0

[a] 3.5 feet above surface.

[b] This explosion took place in bedded tuff under a sloping surface (with a slope of 1:3) so the crater is probably larger than would be expected on a level surface.

[c] A small crater was formed by the chimney formation reaching from the cavity to the surface, but its details were obscured by slides on the side of the mesa.

[d] No breakthrough to surface but radioactive gases in large quantities leaked into the tunnel.

[e] No breakthrough to surface but stemming failed, releasing radioactivity into the tunnel.

Bedded tuff comprises units TOS_1 through TOS_5. They are not welded but are composed of zeolitized ash shards and pumice, fragments of welded tuff and quartzite, and phenocrysts of quartz, feldspar, and biotite, all cemented together by zeolite minerals. The unit is well bedded with individual distinctive beds ranging from a few inches to a few tens of feet in thickness. Most of the beds are nearly white or reddish purple. Pumice fragments are abundant in most beds, and in parts of unit TOS_5 they comprise a large part of the rock. The Blanca event occurred in unit TOS_4 of this group.

The "basement" rock of the formation is carbonate, with limestone as the dominating type. Figure 1.1 shows the bedding structure for the Rainier and Blanca shots.

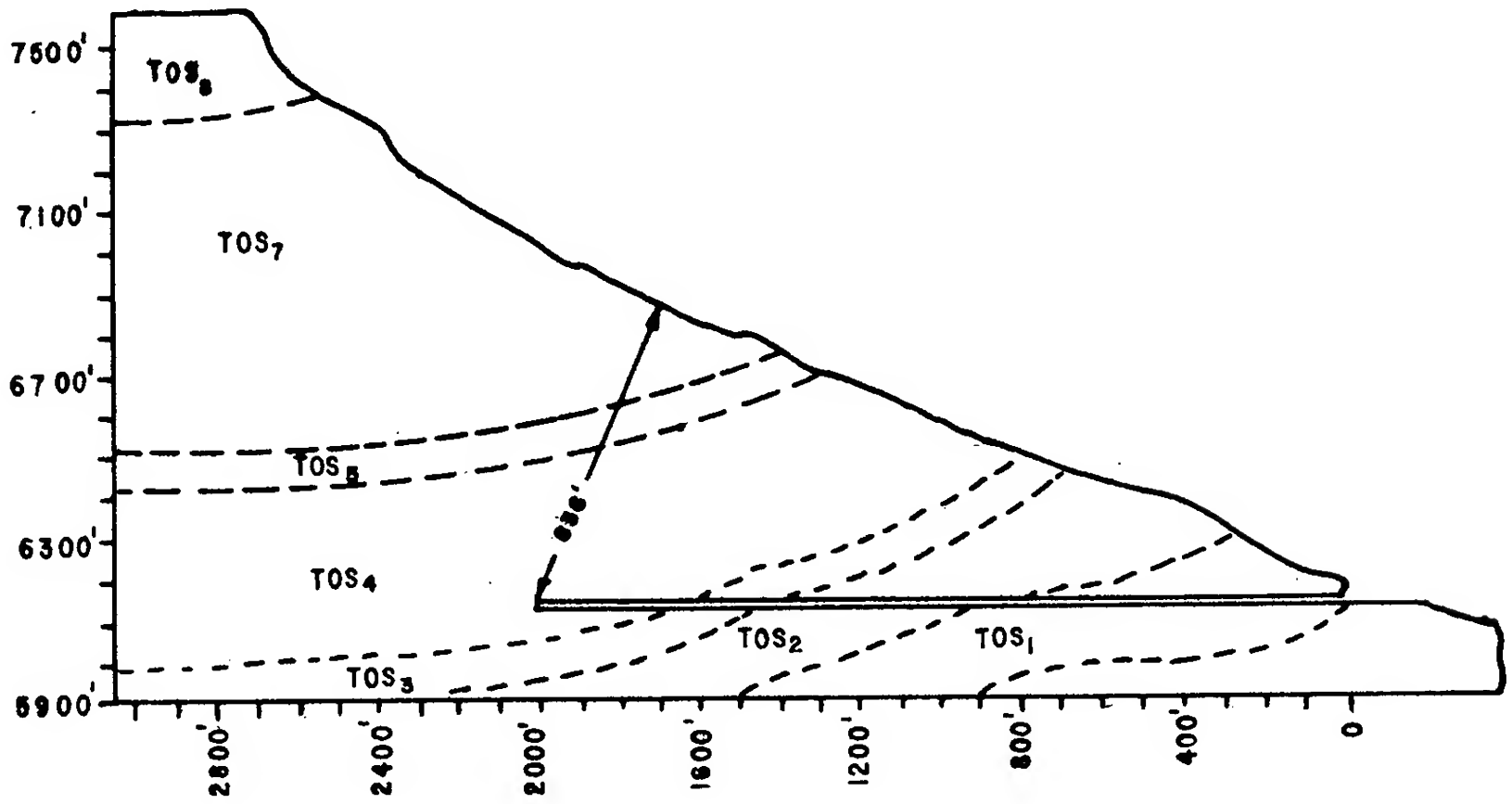

BLANCA

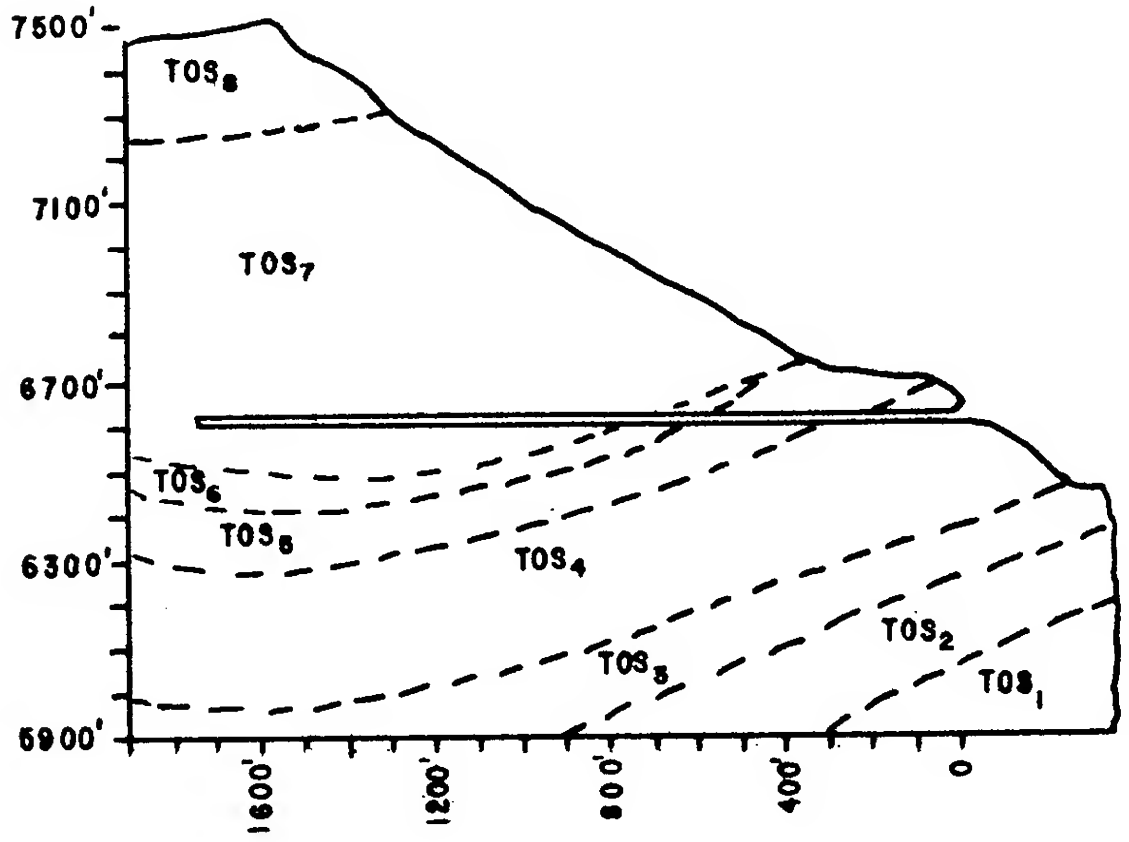

MUL-10217

RAINIER

Fig. 1.1. Bedding structures for the Rainier and Blanca events.

2. THE EARLY CAVITY HISTORY OF RAINIER AND COMMENTS ON ENERGY STORAGE

George C. Kennedy

Institute of Geophysics, University of California, Los Angeles

There are three major chemical environments in which underground shots can be made. The knowledge of explosions in these environments is important if they are to be used for the underground storage of heat. The behavior of these three systems, which are (1) silicate (lava, granite, slate), (2) limestone ($CaCO_3$), and (3) salt (NaCl), is grossly contrasting. Since Dr. Higgins and I have worked out in some detail the phenomenology of a shot in silicate[1] (the tuff in the Rainier event), I would like to review that first. A surprisingly detailed history of temperatures and pressures in the underground cavity produced by the Rainier Event can be worked out by physical examination of the samples obtained by drilling and tunneling in the shot vicinity, and by radiochemical analysis of these samples.

Several milliseconds after detonation of the device, a cavity was formed, lined with approximately 10 cm of fused rock at high temperatures. The total quantity of fused rock has been estimated from the concentrations of radioactive products contained in various samples to be approximately 700 metric tons. The gradient of the temperature between the shell of fused rock and the surrounding unfused rock was very steep. Rhyolite glass is exceedingly viscous up to temperatures as high as 1400°C and flows very slowly at lower temperatures. However, numerous thin, small fragments showing contact between unfused rock and molten rock were recovered in drill cores. These fragments show a maximum of 1/4 inch of glass adhering to unfused rock. Through that 1/4 inch the temperature difference must have been on the order of 300-400°C. Unaltered tuff fuses at about 1100°C, which may serve as an approximate boundary temperature between the glass lining and the unfused rhyolite. However, 1/4 inch in toward the shot chamber from the fused margin, the rhyolite was sufficiently hot to be fluid and fall as minute droplets, which suggests that temperatures on the inside of this 1/4 inch rim of glass may have been on the order of 1500°C.

---

[1] G. C. Kennedy and G. H. Higgins, Temperatures and Pressures Associated with the Cavity Produced by the Rainier Event, UCRL-5281, July 1958.

Numerous small droplets, beads, and shot-like particles of glass were found mixed with the collapsed rubble recovered from the bottom of the cavity (see Fig. 2. 1). These beads apparently are droplets of glass that dripped from the roof and walls of the chamber early in the sequence of events following the explosion. An interesting phenomenon appears upon close examination of these droplets of glass. Although they were obviously once quite fluid, there is no evidence of indentation as would be expected if they fell from the roof of the chamber and reached the floor while still fluid. Presumably during the several seconds of fall from the roof of the chamber to the floor of the chamber, these droplets changed in temperature very rapidly and on impact with the bottom were cool enough so that the glass was quite stiff if not solid. Exceedingly rapid and early cooling apparently occurred within the shot chamber.

An estimate of the vapor pressure of water in the chamber at the time these glass droplets froze may be obtained. The glass beads vesiculate (that is, become filled with small cavities) excessively and fuse at around 920°C. They vesiculate due to evolution of water from the glass and from the very minute bubbles within the glass. A few of these beads were weighed, heated to outgas them, and reweighed. A sample of vesiculated material recovered from the site and a sample of the vesiculated material produced by heating the bead are shown in Fig. 2. 2. About 40 atmospheres of H_2O vapor pressure at 1200-1500°C in the chamber is required to account for all the water in the glass and the bubbles, assuming of course that the glass beads were in equilibrium with the vapor inside the chamber.

It is clear, however, that though these droplets were quenched during fall at a pressure of approximately 40 atmospheres, the pressure of water vapor in the shot chamber was dropping rapidly. A puddle of glass (several inches thick, as sampled by core drilling) had earlier accumulated on the floor of the chamber by slumping of the 10 cm glass lining of the chamber. This puddle was saturated with water; but before it could freeze, the water pressure in the shot chamber had dropped sufficiently to make the puddle vesiculate extensively as it outgassed (see Fig. 2. 2). Thus the evidence strongly points to the fact that though the vapor pressure was 40 atmospheres inside the chamber immediately after the shot while the glass droplets were still falling from the roof of the chamber, a minute or two later the pressure

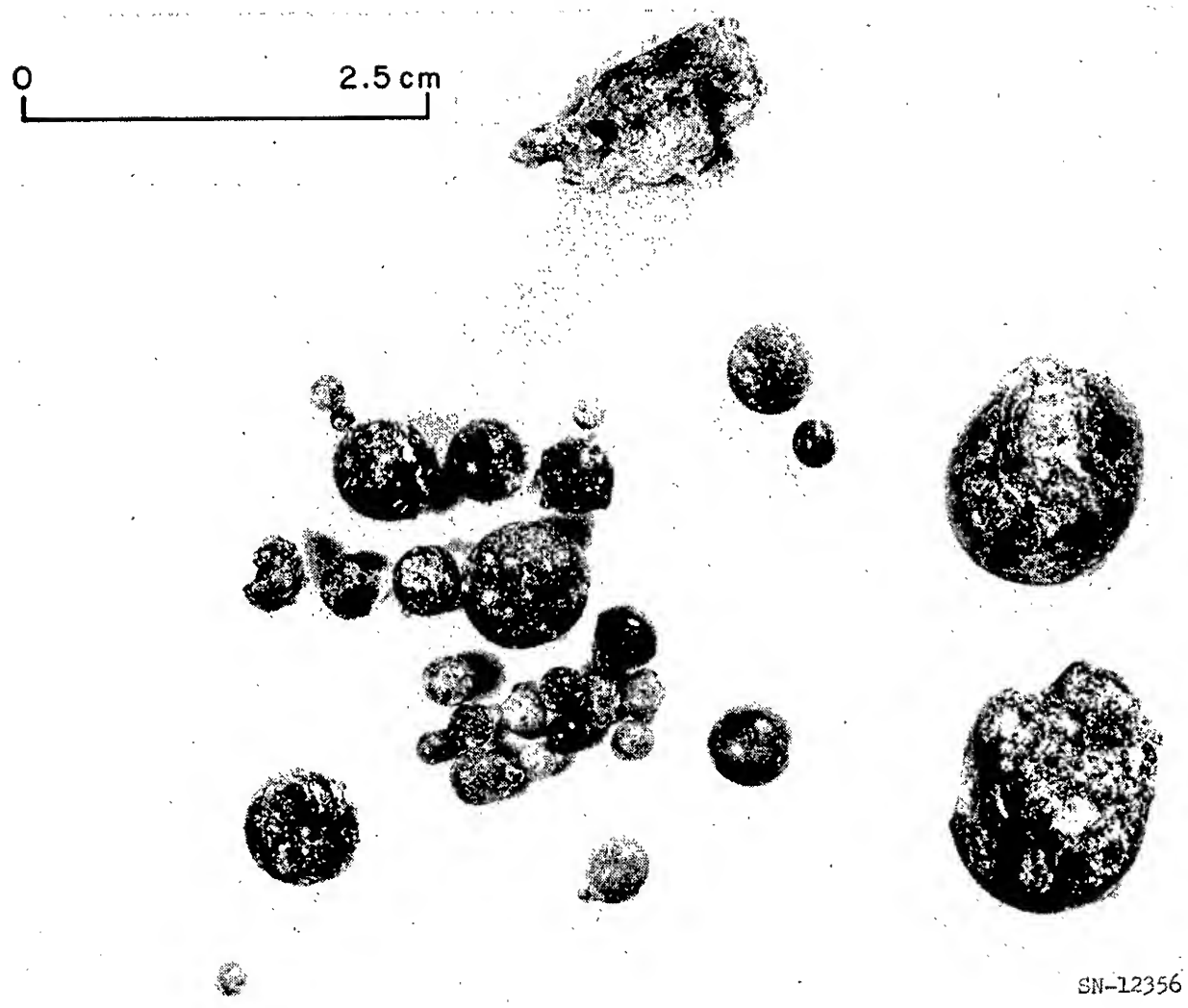

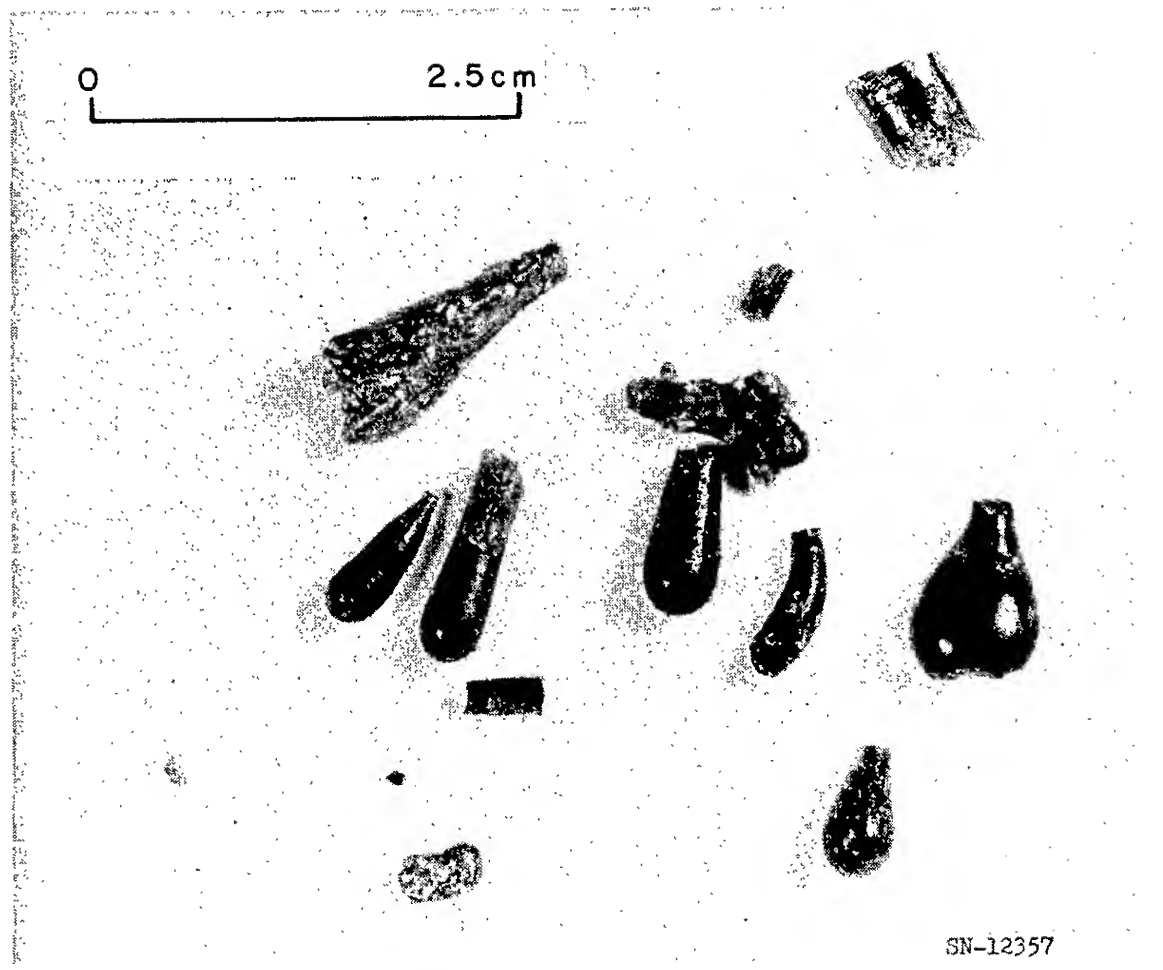

Fig. 2.1. Photographs of the small droplets and round beads of fused material recovered from the interior of the Rainier cavity.

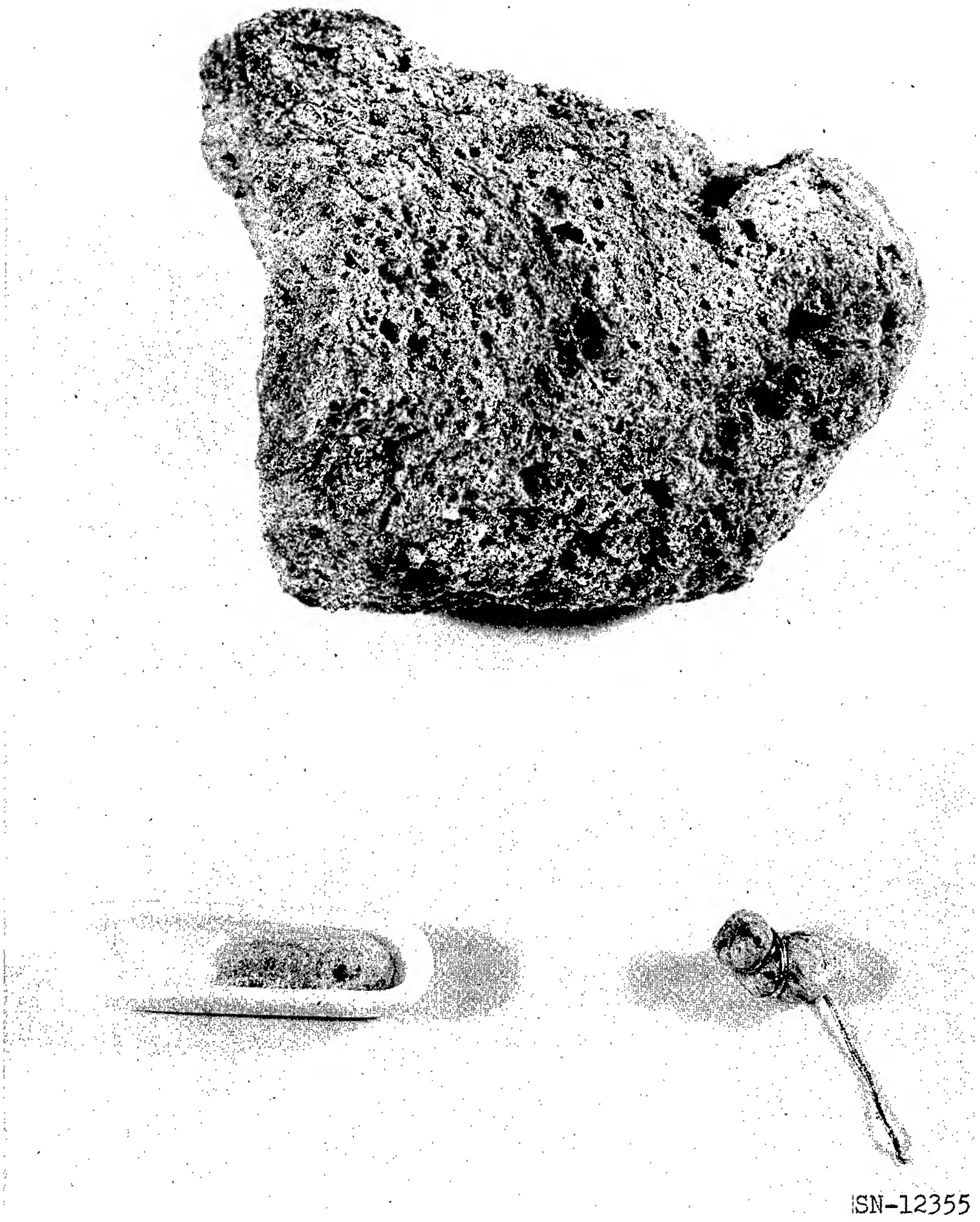

Fig. 2.2. Material like that shown in Fig. 2.1 after it has been heated to approximately 1000°C is pictured in the boat and on the end of the wire. The large piece of vesiculated material was recovered from the bottom of the cavity in a solid core about 1 ft long and has not been heated.

had dropped to only a few atmospheres. A heating experiment on the vesiculated glass from the bottom of the chamber indicated that it had been nearly completely outgassed. This particular material does not vesiculate on heating as do the glass droplets.

Two more observations concerning the small droplets of glass which solidified as beads early in the history of the shot throw some light on the sequence of events inside the shot chamber. Most of the droplets of quenched glass show minute bumps and pimples all over their surfaces. These pimples are apparently the result of other exceedingly small droplets of glass collecting and adhering to the larger droplets during cooling. They suggest that the cavity contained numerous very minute dust particles which probably condensed from the vapor phase and, because of their small size, cooled very quickly and adhered to various glass beads and other free surfaces. Two glass beads, 1/2 and 3/4 of an inch in diameter, do show slight flattening on the bottom as though they had not entirely chilled during the time of fall from the roof to the bottom. All those smaller than 1/2 inch show no sign of flattening or no sign of being molten on reaching the bottom of the chamber.

Thus we can reconstruct the pressure-temperature history of the chamber, starting with an initial water-vapor pressure based on the assumption that approximately 700 metric tons of tuff containing something on the order of 15% water were melted, vaporizing approximately 10^8 grams of water. This water vapor filled the cavity, whose volume was approximately 2×10^{10} cm^3. Thus the specific volume of water in the chamber was approximately 200 cm^3/g, corresponding to a pressure of almost exactly 40 atmospheres at a temperature of 1500°C. The agreement between this computed pressure, based on the estimated amount of rock fused and its initial water concentration, with the pressure based on measurements of the amount of water in the quenched glass droplets is remarkable. Because the thin puddle of glass that formed early on the bottom of the chamber soon vesiculated, we can deduce that the pressure dropped rapidly after the shot. Coincident with the pressure drop was a very sharp and marked cooling as evidenced by the glass beads quenched during fall. It seems quite likely that the extremely rapid cooling was due to the expansion of the gas in the chamber.

Radiometric analyses of the unfused rock immediately adjacent to the molten shell strongly suggest that the water vapor and radioactive gases in

the chamber did not escape by a general outward diffusion. Levels of radioactivity in the unfused rock adjacent to the shell were not detectable above background. Since an appreciable quantity of gaseous radioactive products resulted from the explosion, it is clear that the highly compacted tuff adjacent to the walls of the chamber was essentially impermeable to gases.

Evidence of the vesiculated melt at the bottom of the chamber, the quenched beads of glass, the marked loss of such short-lived volatile radioactive products as krypton and xenon from the chamber, and the marked asymmetry of the post-shot thermal-energy distribution strongly suggests the chamber vented through one or at the most a few major fractures. Apparently none of these fractures communicated with the surface as no activity was observed on the surface of the ground after the shot. One of these escape channels was probably intersected by a core drill hole 75 to 80 feet beyond the shot site and diametrically opposite to the access tunnel. The nonvolatile decay products of the short-lived radioactive gases were highly concentrated in the fused rock along this channel.

Since the decay of the gaseous products into nonvolatile elements is known to be exponential with time, the percentage loss of volatile precursers is a direct indication of the time of escape. Times of escape have been computed for a number of elements and a number of analyses. The range of times of escape computed by this method is remarkably narrow and suggests that the chamber vented between 30 seconds and two minutes after the shot. The time of venting derived from examination of the glasses in the chamber and the time derived from radiochemical sampling are in close agreement.

Coincident with the accumulation of the puddle of glass on the floor of the chamber and with the venting during the first minute or two after the shot, other phenomena were taking place in the cavity. The dense, highly compressed tuff of the walls, with a water content of approximately 15%, was steadily increasing in temperature owing to conduction of heat outward from the adjacent thin, molten shell. A series of implosions of the shell into the cavity was probably due in large part to expansions of water in the dense tuff. Nowhere in drill holes or tunnel opening has the original glass-lined wall been seen. This wall material was all imploded into the cavity. These implosions continued over a considerable time. They began before all the melt had accumulated on the bottom of the cavity and continued until sometime after the cavity had vented and the general collapse of the roof had begun.

It is interesting to compare the initial gas pressure in the cavity with the weight of the column of rock overlying the cavity. If an overburden of 850 feet of tuff with a density of approximately 2.0 g/cc is assumed, the rock pressure on the cavity is 50 to 55 atmospheres, which is counterbalanced by the initial gas pressure in the cavity of approximately 40 atmospheres. Thus it seems likely that very shortly after the gas escaped from the cavity and the pressure dropped to a few atmospheres, the roof would collapse. Most of this roof collapse did take place after the cavity had cooled and the gas had escaped. The total absence of fragments of rock in the puddle of molten lava at the base of the cavity shows that all the lava had vesiculated and cooled before collapse of the cavity took place.

NaCl as a chemical environment for the storage of heat will be studied in the Gnome experiment. Surprisingly enough the $NaCl \cdot H_2O$ system is almost unexplored, but recently we have made a large number of measurements on its chemistry. I will describe these measurements later in this symposium (see p. 4 of UCRL-5678, Part IV of the Symposium proceedings), and will only summarize a few of the details now.

A most unexpected result was the discovery that the concentration of salt in steam is almost independent of temperature up to 600°C. Further, at high pressures, the concentration of salt in steam decreases as the temperature rises toward 600°C; there is a highly optimum temperature in the system at which there is a low salt content in the steam, amounting to around 200-300 parts per million.

The least explored system today is that of $CaCO_3 \cdot H_2O$, and I think particularly serious consideration should be given to its detailed examination. A casual glance suggests that it is one of the most interesting of all systems in which to store energy because of its self-sealing nature and because of the high fluidity of the molten phase. Solubility of $CaCO_3$ in gases is small, and limestone environments are geologically abundant.

Suppose we examine the details of an explosion in limestone. Immediately after the shot, $CaCO_3$ is melted at a temperature of approximately 1220°C and a pressure of 40 atmospheres of CO_2. However, in the $CaCO_3 \cdot CaO$ system, there is a minimum in the melting point curve.

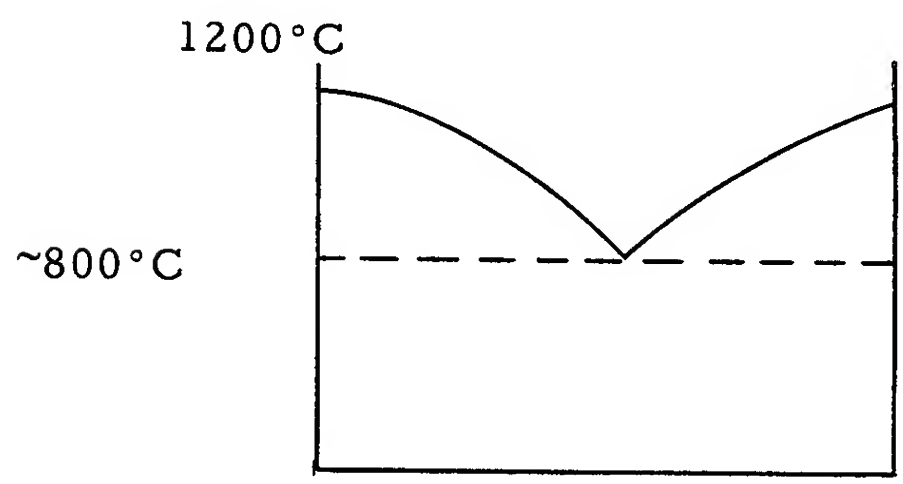

Consequently as soon as a little CO_2 is formed, CaO will form in equilibrium with $CaCO_3$. As some of the CO_2 gas streams off, the melting temperature will drop sharply to around 900°C; there is the possibility of having a large fluid body of a low temperature melt in the system $CaCO_3 \cdot CaO$ with relatively low CO_2 vapor pressure, because of the shape of the vapor pressure vs temperature curve in a reaction of this kind.

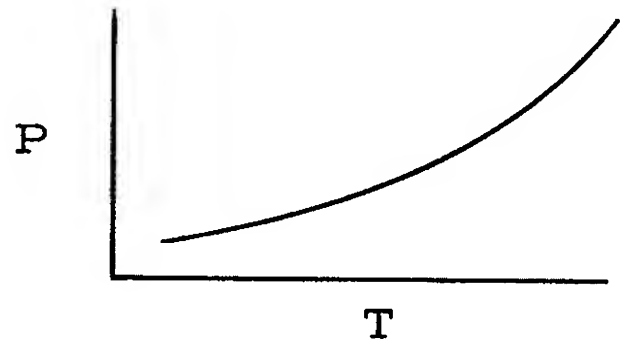

Furthermore, the addition of water at 1000 atmospheres will probably lower the temperature approximately another 200°C. Therefore, there is a good probability of obtaining highly fluid melts at temperatures of 700-800°C.

Limestone beds thus may make effective reservoirs for the storage of heat. In addition, they have certain properties that NaCl beds do not have. For instance, they are self-sealing in case of a crack. If we have a ball of melt

underground in the system $CaCO_3 \cdot H_2O$, and a crack opens up in the surrounding rock and melt starts leaking away, the lowering of the water pressure due to escape of gas will raise the melting point of the carbonate. The melt in the crack will becomes solid and seal off any further escape of the melt. The system thus tends to be self-sealing like a bullet proof gas tank.

To summarize this talk, I wish to emphasize that the phenomenology of underground nuclear explosions in the three most likely chemical environments is greatly contrasting. Particularly serious attention, I think, should be given to the detailed examination of $CaCO_3 \cdot H_2O$ systems, as this is the system which is the most interesting and which is least explored today in terms of physical behavior.

3. CLOSE-IN SHOCK TIME-OF-ARRIVAL MEASUREMENTS AND HYDRODYNAMIC YIELD[1]

F. B. Porzel

Senior Scientific Advisor

Armour Research Foundation of the Illinois Institute of Technology

Part A

This paper briefly describes the principal ideas in the theory, experimental techniques and results for the programs entitled, "Close-In Shock Time-of-Arrival Measurements," which were performed by Armour Research Foundation (ARF) on Operations Rainier (1957) and Hardtack II (1958) under contract to the University of California Lawrence Radiation Laboratory. The end purpose of the ARF programs was to determine the hydrodynamic yield; they exploited methods previously used by ARF for similar purposes for the Navy in Operations Wigwam (1955) and Hardtack I (1958), and are based in turn on similar measurements by Group J-10 of the Los Alamos Scientific Laboratory on Operation Jangle (1951) at the Nevada Test Site. Another immediate and more basic purpose of these measurements is to provide better understanding of the phenomenology of underground explosions.

This paper covers four topics: experimental techniques, theory, Rainier results, and Hardtack II results.

---

[1] This paper is in two parts. Part A is primarily concerned with close-in shock time-of-arrival measurements for the determination of hydrodynamic yield, on operations Rainier and Hardtack II. This part is essentially the verbal presentation made by the author at the Plowshare Symposium in May, 1959 at San Francisco. The test report for Operation Rainier covers this section in detail: WT-1495, Project 25.1, "Close-In Time-of-Arrival Measurements for Yield of Underground Rainier Shot," University of California, Lawrence Radiation Laboratory.

Part B is primarily concerned with the theoretical concepts used in Part A, and in particular, discusses some implications of the theory for these measurements which apply to control and use of explosions, aside from the specific test operations described in Part A. [Editor's Note: Part B proved too long to publish as part of the Plowshare Symposium. Sections I, II, III, VII, and VIII, which are directly referred to in Part A, have been included. The other sections can be obtained in Armour Research Foundation Technical Memorandum 421, "New Concepts for Control and Use of Nuclear Explosions," F. B. Porzel.]

I. Experimental Techniques

Two principal experimental techniques have been used: time-of-arrival switches and Doppler. By far the greatest reliance so far has been placed on the switches and the experimental arrangement for Rainier is shown schematically in Fig. 3.1. The switches are placed at essentially equal logarithmic spacings from the nuclear device out to the expected limit of crushing, beyond which distance the shock velocity becomes sonic and hence ambiguous for diagnosis of hydrodynamic effects. The blast switch itself is essentially an open terminal of a coaxial cable whose inner conductor is closed by crushing of an outer conductor upon it when the main shock pulse arrives. The switch is designed not to close from weak precursor sound signals. The signals from a single string of switches are electronically coded for pulse length and pulse width in a "mixing box," then transmitted on a single cable to a shelter outside the tunnel, where they are displayed on an oscilloscope at a 20,000 cps raster sweep and recorded on a GR No. 651-AH streak camera. Time is measured with almost arbitrary accuracy because the abrupt pulse rise on the raster can be read to one microsecond whereas the hydrodynamic events occur on a millisecond time scale. Also, because the velocities are determined by differentiation of the time-of-arrival curve, good relative positions of the gauges to its neighbors is sufficient for velocity and to check on the absolute position through $R = \int U\, dt$.

The essential idea in the Doppler system is to place a hollow coaxial cable on a radial line toward the device. An rf signal of 1580 megacycles is input and forms a standing wave. As the shock advances and crushes the outer conductor upon the inner conductor, the standing wave shortens; the reflected wave is heterodyned with the input, and the Doppler frequency of the mixed signal is displayed on an oscilloscope. The Doppler frequency is directly proportional to the shock velocity. The Doppler technique is greatly complicated by a "pinch jet," described in Section VII of Part B of this paper: the input signal is reflected from a shock in pure air induced ahead of the crushed cable. But even without special provision for jetting, the Doppler can provide an accurate value of shock velocity near the walls of the device chamber.

The blast switches and Doppler system offer an ideal combination for mutual check and support because the switches yield the integrated time-of-arrival for gross phenomenology and the Doppler system provides great

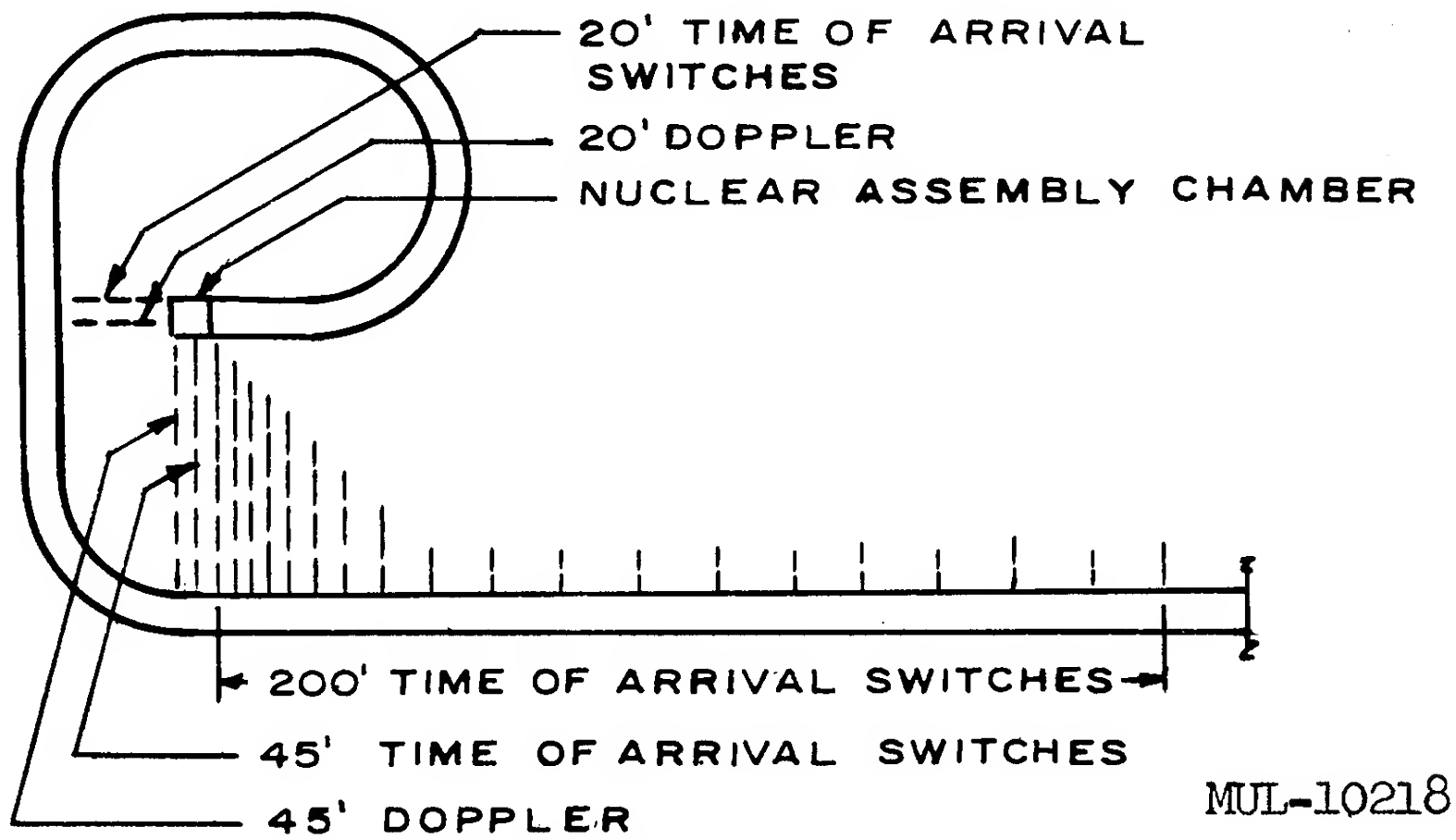

Fig. 3.1. Rainier equipment layout.

detail in the differentiated counterpart as shock velocity versus time.

II. Theory

As is well known, given the Rankine-Hugoniot adiabat, the measurement of the shock velocity permits the direct calculation of peak pressure, density, material velocity, and other hydrodynamic variables of interest at the peak of the main pressure pulse. It is important for the case of soil and rock to recall that these relations require only gross conservation of mass, momentum, and energy across a narrow domain and are not sensitive to the existence of a truly sharp shock front. By means of a derivation the author calls the "matrix formulation," it is then possible to derive the space gradients and time rate of decay on the interior of the wave from the measured peak values at the front and from their measured decay with distance and time. Finally by means of the analytic solution – being the repeated use of conservation of mass, momentum, and energy on the interior of the wave – the complete waveforms for all the hydrodynamic variables on the interior can be calculated as a function of space and time, and the hydrodynamic energy can be evaluated by integrating the energy waveforms.

The waste heat concept plays a controlling role in the description of explosions in solids and liquids; this concept is discussed in Section I of Part B. (Also in Part B are discussed: in Section II, the general characteristics of wave propagation; and in Section III, some implications regarding underground explosions.) The waste heat concept greatly simplifies the description for the behavior of the material on the interior of the wave during its expansion behind the shock, and the validity of the concept rests in good part on considerations of "grain size" of the mixture. Characteristically, strong shocks produce high temperatures in a gas phase but usually produce low temperature in the solid phase; simple considerations of the solutions to the heat conduction equation will show, as an example, that for particles approximately 0.1 millimeter in diameter, the heat flows from the gas phase into the solid phase in times like 0.1 millisecond. Such considerations justify the assumption of temperature equilibrium for the time scale of a nuclear explosion in soil, but it is to be expected that this assumption is not justified for the shorter time scale of explosions induced in soil from small charges.

The equation of state for Nevada soil along the Rankine-Hugoniot adiabat

has been experimentally determined by LRL, furnished to Armour Research Foundation, and will not be described here. Oddly enough, despite the complexity of the thermodynamics for rock, especially soils with high water and air content, elaborate thermodynamic detail is not required in the equation of state. The dynamic compressibility is largely controlled by the air content and controlled at somewhat higher pressures by the compressibility of the water fraction. A quite adequate equation of state can be constructed from the knowledge of the rock density in situ, the void fractions (essentially from the comparison of actual density to crystal density), the water content, and the gross mineralogical composition. We require, in addition, a specification of the waste heat up to the boiling point of water and up to effective vaporization of the soil. The latter quantities are rather easily estimated from the boiling temperature of water, the water content and its heat of vaporization. Surprisingly enough, Nevada soil is close to saturation in water and, except on the deep interior of the cavity, temperatures exceeding the local boiling point of water are quite unlikely. The ARF studies of these phenomena led to postulating the concept "decrepitation"; when the waste heat is sufficiently high to vaporize irreversibly the water fraction and waters of crystalization, the final state of the rock could only appear as exploded material, similar to the process of making puffed cereals and like the familiar phenomena of decrepitation in certain minerals. Because the rock samples obtained to determine the equation of state for Rainier had evidently dried out before testing, the actual void ratio for Rainier was calculated using the observed crushing and cavity radii. We assume (1) the gross hydrodynamic displacements are negligible beyond the crushing radius as far as they affect the cavity radius, and (2) the solid fraction of material on the interior was compacted in a spherical shell of inner radius essentially the cavity radius x, when the shock reached the crushing radius R. Conservation of mass then requires that the average density compression ratio (essentially the solid fraction only) is given by

$$\eta = \frac{1}{1 - \left(\frac{x}{R}\right)^3} = 1.08 \quad . \tag{1}$$

With x = 55 ft and R = 130 ft for Rainier, the result $\eta = 1.08$ indicates the small void ratio fraction of 0.08 in comparison with void fractions like 20 or 30% for dried-out samples.

III. Rainier Results

The Rainier explosion is characterized by good containment, with essentially spherical symmetry, in which the waste heat concept provides the controlling mechanism.

The idealized equation of state for Nevada soil and the observed shock velocity versus distance curve for Rainier are shown qualitatively in Figs. 3.4a and 3.4b of Part B, which also describes the interrelations of various regions on those two figures. The curves shown here represent the author's views at Armour Research Foundation for what should have happened and what did happen on Rainier, but the reader is cautioned that this interpretation, including the "decrepitation" concept, do not yet necessarily represent the views of the sponsor.

Doppler measurements fixed the shock velocity in soil as 70 meters/msec at the walls of the nuclear device chamber, an effective radius like 1.6 meters. The switches showed that the shock velocity fell quickly to a value of 3.2 meters/msec at 4.9 meters, and ran constant at this value out to 18.4 meters. This region corresponds to a peak pressure of 40,000 bars, and the flat portion of the curve represents the transition from an explosion in a gas (made by vaporization of rock for shock radii inside 4.9 meters) to the characteristics typical of an explosion in soil (beyond 18.4 meters). Ambient sound velocity in Nevada is about 8,000 ft/sec; shock velocity was measured as low as 7,400 ft/sec, and was still falling rapidly. As expected and as the gauges were so designed, the switches beyond the crushed zone limit at 130 feet did not close.

It is emphasized that the waste heat so strongly controls the phenomenology that a nuclear explosion in soil is best regarded as a calorimeter experiment: virtually all the heat was expected to be distributed within the cavity and the relatively thin shell of crushed material out to the crushing radius. One equation for yield – used for Rainier – is instructive on this point. The energy balance in Eq. (1) of Part B is readily put in the calorimetric form

$$W = \frac{4}{3}\pi R_2^3 \rho_0 Q_2 \left[1 + \left(\frac{Q_1}{Q_2} - 1 \right) \left(\frac{R_1}{R_2} \right)^3 + \frac{Pf}{\rho_0 Q_2} \right]. \qquad (2)$$

The term $\frac{4}{3}\pi R_2^3$ is the volume out to the point where any vaporization occurs in soil, which gives $R_2 = 18.4$ meters for Rainier; $\rho_0 Q_2$ is the energy density deposited by waste heat up to the boiling or decrepitation point. The term $(Q_1/Q_2 - 1)(R_1 R_2)^3$ is a correction factor to account for waste heat in excess of simply raising to the boiling point; on Rainier this term has the numerical value 0.07 in Eq. (2). The term $Pf/\rho_0 Q_2$ represents the available hydrodynamic energy when the shock reached 18.4 meters and had the value 0.23 for Rainier. The fraction $1/1+0.07+0.23 = 0.77$ means that 77% of the energy was dissipated within 18.4 meters or 60 feet from the device merely from raising the rock to the boiling point of water. The available hydrodynamic energy already represented only a relatively small fraction of total energy by then, and the total yield is not sensitive to an accurate specification of hydrodynamic waveforms.

With a crushing pressure of 700 bars (an upper estimate in UCRL-5124), Eq. (3) of Part B indicates that a maximum for the available energy left at the cessation of the crushing stage was

$$\frac{W'}{W} = 0.23 \left(\frac{700}{40,000}\right)^{1/2} = 0.03 \quad .$$

In short, only 3% of the energy was left, even at 130 feet, to go into the seismic wave; 97% of the energy had already been converted to heat.

The analytic solution provides a similar evaluation of the yield at any other radius and time by more elaborate counterparts of Eq. (2) above. The constancy of $W = W(t)$ so determined is an internal check on the validity of the theory, provided the data and the shot geometry are sufficient to insure reasonable spherical symmetry. The probable error of the Rainier hydrodynamic yield, about 1.7 ± 0.15 kt, is largely due to the uncertainty from the necessity to "construct" the equation of state for Nevada soil.

The principal damage to the Rainier tunnel, beyond the crushed zone, was due to the "pinch jet" similar to that described in Section VII of Part B. The temperatures in such an induced jet are significantly high. With a shock velocity in soil of 7900 ft/sec, the model of Fig. 3.6b, Part B, would require air shock pressures of the order of 100 bars, i.e., "fireball" temperatures. Such temperatures easily account for the observed carbon monoxide in the Rainier tunnel. The carbon monoxide may have been produced by air shock action on the mine timbers.

IV. Hardtack II Results

The Hardtack II events were characterized by the channeling concept, to about the same degree that Rainier was characterized by the waste heat concept.

The channeling concept and its implications are described in Sections VII and VIII of Part B. The shot geometry for each of the Hardtack II events involved line-of-sight pipes of relatively large diameters, such as 1 or 2 feet. Also, the accelerated time schedule of Hardtack II, due to the impending moratorium on weapons tests on 1 November 1958, required the positioning of blast switches in the floor of tunnels for some shots, precisely where the asymmetries due to jetting were most pronounced. As such, the time-of-arrival data are of excellent value as diagnostic hydrodynamics, whereas it would be naive to expect a reliable yield determination with such experimental improvisations and shot geometry. Here again, the reader is cautioned that the results given here represent the interpretation of the author at ARF for what should have happened and what did happen on Hardtack II, but this presentation does not necessarily imply the technical concurrence of the sponsor.

Tamalpais was instrumented like Rainier in rock, but not along the axis of any conjectured jets. The results confirmed the existence of subsonic velocities in the surrounding rock, even close to the device chamber, presumably due to the large fraction of energy which jetted elsewhere.

The results for Logan are shown qualitatively in Fig. 3.2. The line-of-sight pipe shown was evacuated, had a maximum diameter of 24 inches, and passed through three intermittent zones of sandbagging in the tunnel. The blast switches were placed on the floor of the tunnel, in both the open tunnel and the sandbagged sections. The measurements generally showed an abrupt increase in shock velocity at each of the open spaces, and a much slower velocity within each sandbagged layer. To Armour Research Foundation, this result appears to be a vivid demonstration of jetting down the pipe, flooding of energy into the open tunnel spaces, partial closure by sandbags followed by a new jet through the sandbag zone. The jet velocity showed a marked decrease in the third open space, as if the third set of sandbags held, but one switch at 187.5 feet, in this open section of the tunnel, closed earlier than a switch in the sandbags at 183.5 feet, indicating that the shock energy was flowing backward through the sandbags at this interface. It is not clear from the data that even the last set of sandbags (beyond the line-of-sight pipe) actually

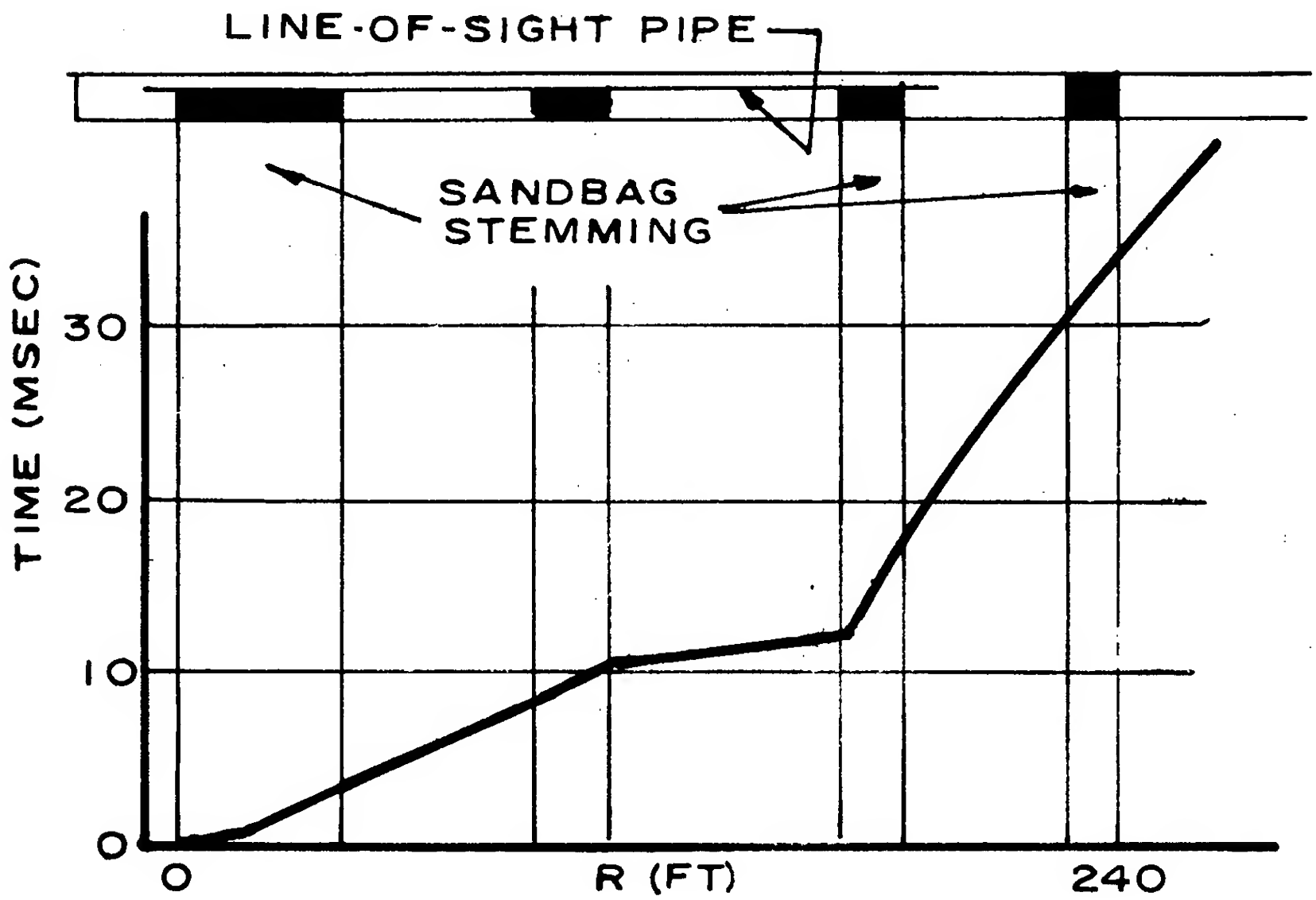

MUL-10219

Fig. 3.2. Logan – time of arrival.

held the jet at the far end of the tunnel; the last switches indicate the shock was possibly accelerating beyond that point. The Logan results indicate an apparent energy release as low as 5 kt where the explosion was partially stemmed at each sandbag barricade, but an apparent yield like 30 kt where jetting opened the tunnel. In the opinion of ARF, the jetting effect in the Logan tunnel is simply the explanation for the damage which occurred in the main tunnel.

Evans event again confirmed the subsonic velocities in soil, due in part (again in the author's opinion) to jetting. The Evans shot involved large air-filled line-of-sight channels, the first being about 130 feet long which opened into a large room. Significantly, a blast switch in that room, placed well off the line-of-sight, closed at 0.7 msec, at a time when the shock had advanced only about 4 feet into the rock surrounding the device chamber. The ratio 130/4 is in excellent agreement with the ratio of 30;1 (air shock velocity to ground shock velocity) suggested in Part B for jets at high pressures.

For Blanca, the tunnel damage from Logan precluded the use of the original nuclear device location and switch layouts, but attempts were made to improvise a layout as on Logan. The close-in string of switches failed for one of many possible but unknown reasons. The last string indicates that the last set of sandbags successfully stemmed the explosion at that point. The overall results for Blanca are sufficient to confirm the expectation that about 10 times as much energy from the nuclear device was available for crushing as would have resulted from a stemmed charge, and a correspondingly larger fraction of energy went into the seismic wave.

V. Summary

In summary of these Armour Research Foundation studies, it appears entirely feasible to measure the hydrodynamic yield by time-of-arrival methods, provided the explosion is either stemmed to permit spherical symmetry, or, in the presence of open line-of-sight channels, if sufficient strings of switches are placed along different radii to verify the jetting and measure its extent. A principal advantage of the switch method is the simplicity and reliability with which many hundreds of pertinent points of information can be obtained at pressure levels far in excess of the capabilities of usual pressure-instrumentation.

Some consequences of the waste heat concept on wave propagation are listed briefly in Section II of Part B, and their implications for underground explosions in Section III. Some implications of the channeling concept (Section VII) are discussed in Section VIII, "Controlled Excavation."

Part B

New Concepts for Control and Use of Nuclear Explosions

This section describes some new and basic concepts for control and use of nuclear explosions in peaceful uses. These applications involve large scale public works for which the designation "civil engineering" is particularly appropriate.

Because some of the ideas presented here may seem so novel as to oppose first intuition about them, it probably helps to state at the outset that the field "Fluid Dynamics of Strong Shocks" is literally a new branch of physics. Historically, this field grew out of the military necessity to understand the blast and other hydrodynamic effects of nuclear weapons; it is only fair to add that the progress would not have been possible without the enormous experience invested in that field during the past fifteen years. The military applications clearly could not be paralleled by a similar growth in the nonclassified literature. But the basic concepts are not classified, they are readily derived from conservation of mass, momentum, and energy. The field is characterized by the nonlinearity in the hydrodynamic equations of motion and in the equation of state of materials, due to the high pressures and stresses characteristic of such explosions. The end result is an emphasis on different mathematical disciples and theoretical techniques, new but no more difficult than their counterparts in "acoustic" theory. Unfortunately, the linearity assumption pervades so many fields of science and engineering — aerodynamics, elasticity, vibration, electronics — that we develop a corresponding intuition about the behavior of natural processes as if linearity were a universal characteristic of nature. But in the realm of very large displacements and unbalance of forces the concepts of linearity are more of a liability than an asset. In some cases, the linearity assumption literally annihilates the most significant terms in the equations of motion and denies the essence of the problem we are trying to understand. A corresponding confusion would result if we were trying to understand a radio or television set which was built with nonlinear resistances so that electrical resistance was not a constant property of material, independent of voltage and current, but proportional to some high power of the current itself.

This section is restricted to a discussion of two principal concepts and their applications: waste heat and channeling. The waste heat concept provides a categorical method for the control and use of an explosion by control of the properties of the medium surrounding the device or energy source; the applications are possible because of nonlinearity of the equation of state for compression. The channeling concept provides a categorical method for control and use of an explosion by control of the geometry of the material surrounding the energy source; the applications are possible mostly because of the nonlinearity in the shock velocity and in the material velocity behind the shock.

I. Waste Heat

Irreversible heating in a material, caused by the entropy change across a shock which traverses it, is well known. The effect is proportional to the cube of the overpressure at low pressures and is, therefore, vanishingly small in the acoustic approximation. There is a tendency to overlook the corresponding fact then that the entropy change is necessarily a controlling feature of the hydrodynamics at the high pressures which exist close to any rapid energy release. Thus, the fireball from a nuclear device in air is not due to the device parts directly but due to the passage of the shock wave over the surrounding

air; if the air were adiabatic in compression (let alone its nonlinearity) there would be no fireball from a nuclear device. Also, the "hole" represented by the bubble of an underwater explosion and the cavity in an underground explosion would exist for other hydrodynamic reasons, but they would be different from their present size.

We define the waste heat Q(P) to be the net energy per unit mass (above initial energy content) which remains in the material (originally shocked to pressure P) after it has finally expanded adiabatically down to the ambient pressure P_0 that existed before the explosion. The "waste heat concept" itself has a special meaining with regard to explosions in solids, liquids, and their mixtures with gases; it is a convenient, useful, and accurate engineering assumption which justifies the subsequent bookkeeping of internal energy by dividing it into "waste heat" and "available energy." The waste heat concept implies important but deceptively simple differences from entropy change: there would be no waste heat if the material returned to zero pressure instead of ambient pressure. This bookkeeping approximation is justified by the fact that the bulk modulus for compressibility is quite insensitive to temperature and for a variety of other compensating effects both in the process of shock and in the subsequent expansion.

The relative magnitude of several energy quantities and the method of calculating waste heat is indicated in Fig. 3. 3. The figure is a conventional pressure-volume diagram; energy is portrayed as an area on such a diagram. The full curve is called the "Rankine-Hugoniot curve" which gives the relation between pressure P and specific volume V at various shock strengths. By conservation of energy alone, the total energy added to the material by the shock is given by $E_T - E_0 = P(V_0 - V)$. This is the area of the rectangle below the pressure P and between V_0 and V. The kinetic energy E_k of the material, with velocity u behind the shock, is given by conservation of mass and momentum alone as: $1/2\ u^2 = 1/2\ (P - P_0)(V_0 - V)$. This is the triangle in the upper right of the total energy rectangle: whatever the actual path during shock compression, the latter equation shows that the compression is effectively as if the material were shocked along the straight line joining P_0 with P. It immediately follows that the internal energy in the material is the quantity of $E_i - E_0 = 1/2\ (P + P_0)(V_0 - V)$ which is clearly the total trapezoid in the total energy rectangle lying below the straight line joining P and P_0. Although these energy expressions and the Rankine-Hugoniot relations may be derived in a different manner with more restrictive assumptions, the simple derivation shown here is sufficient to indicate that these relations are quite general and apply without regard to the equation of state of the material or the details of the shock process.

For solids and liquids the subsequent expansion of the material behind the shock can be described in a simple manner: the material will expand by essentially adiabatic processes back to its original pressure P_0 and volume V_0, and for most practical purposes, will expand along the Rankine-Hugoniot curve. Since the area under that curve is the $\int P\ dV$ energy subsequently given up during the expansion, that area is defined as the available internal energy. It follows that the lens-shaped area lying between the straight line and the curve is by definition the waste heat itself. The energy represented by this area appears as a final temperature rise in the material left long after the shock has passed. Heat conduction processes occur on time scales much longer than the rapid process of compression and expansion described here, so the deposition of waste heat is literally forever so far as the shock hydrodynamics is concerned.

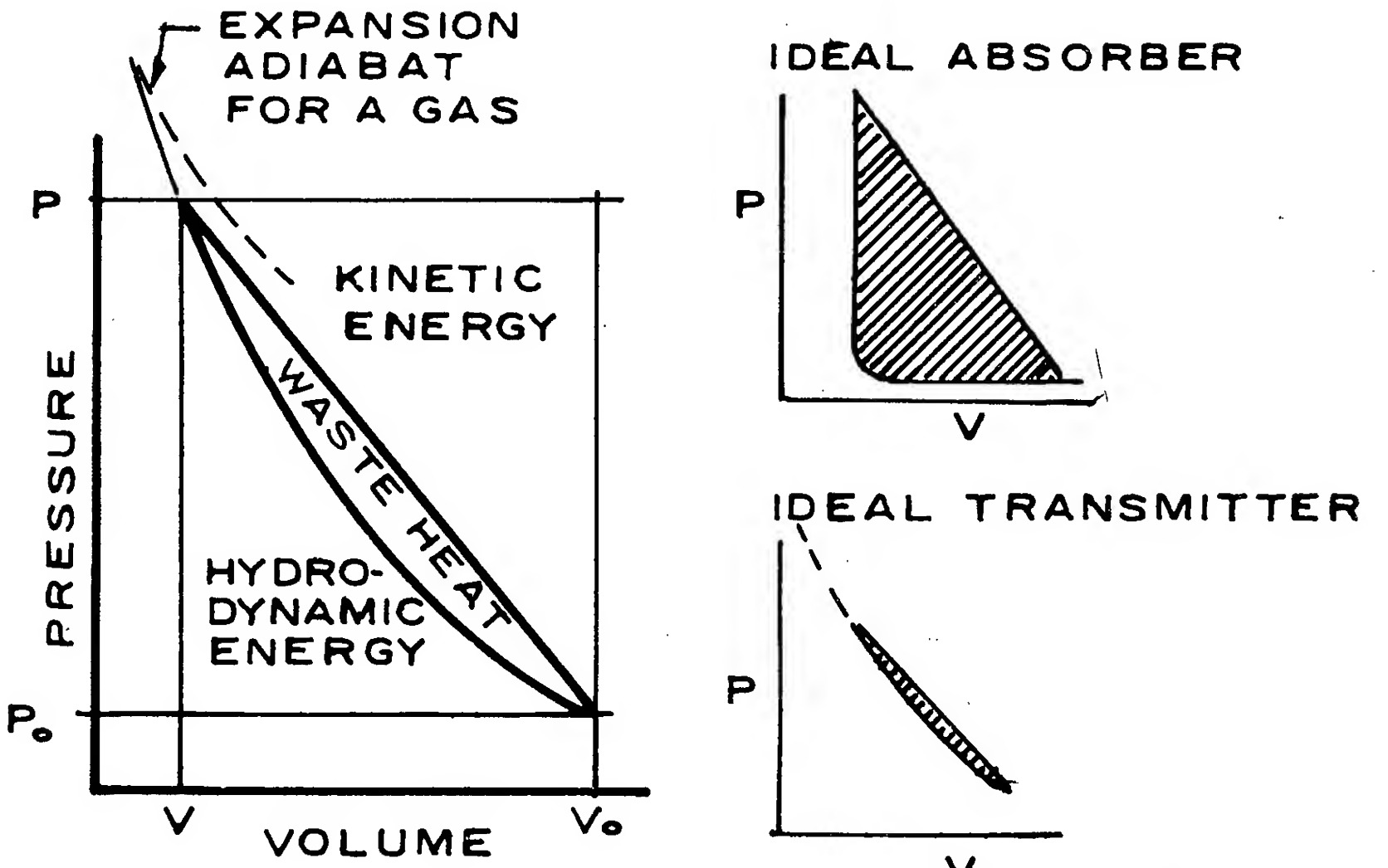

Fig. 3.3. Waste heat concept.

For all materials, there exists some shock pressure high enough that the waste heat is sufficient to vaporize the material irreversibly, even after it has expanded and cooled back to ambient pressure. We define that shock pressure to be the "vaporization" pressure, and the material inside the corresponding radius becomes part of the device cavity. The energy represented by the "waste heat area" in excess of the total heat to vaporization appears as superheat in a gas, is available by expansion, and is not counted as waste heat. Very close to the device, well in excess of vaporization pressure, all materials are initially good transmitters.

It is easy to find or to fabricate materials and mixtures which "crush down" at some relatively low pressure. In that case the Rankine-Hugoniot curve is much more sharply bowed, as shown in the diagram at the upper right of Fig. 3.3, and nearly all the internal energy appears as waste heat. As a result of the Rankine-Hugoniot relations, all materials compress to some limiting density ratio, like 10 to 1 or 4 to 1 even at infinite shock pressures. For this reason all materials display a vertical Rankine-Hugoniot curve at pressures high enough and all materials become ideal absorbers at such high pressures provided they are not greatly superheated.

At low pressures the curvature in the Rankine-Hugoniot curve is very slight; in the acoustic approximation the Rankine-Hugoniot curve is a straight line passing through (P_0, V_0). This is the domain of ordinary elastic theory. Strictly speaking, the straight line approximation is never really reached, but the waste heat area becomes very small and we speak of material as an ideal transmitter. All materials, at least below their crushing strength, are ideal transmitters at low pressures, as shown at the lower right of Fig. 3.3.

II. Wave Propagation

We discuss briefly the fraction of energy which is hydrodynamically available after the shock has run to some appreciable distance R from an instantaneous energy release in a liquid or a solid. The damage, and hence the difficulty of controlling an explosion, can often be specified in terms of the peak pressure P at the shock front.

At high shock pressures, the usual theory in the current literature is based on certain similarity assumptions, which are not really justified in their own right, but the similarity condition would require that the decay of pressure with distance be as $P \sim R^{-3}$, the quantity $PR^3 \sim W$, and $(d \ln P)/(d \ln R) = -3$. At low pressures the usual description is based on the acoustic approximation and gives $(P - P_0)\, R \sim W$ and $[d \ln (P - P_0)]/(d \ln R) = -1$. In both cases, the total energy W in the wave is taken to be constant and equal to the original energy released. These results, both at high and low pressures, are misleading oversimplifications and the reasons can be summarized briefly by means of the waste heat concept.

With the energy partitioned according to the waste heat concept, the energy balance at any time is:

Effective energy	=	Original energy	−	Dissipated energy	=	Available internal plus kinetic energy

$$W' = W - 4\pi \int_0^R \rho_0 Q R^2 dR = \frac{4}{3} \pi R^3 (P - P_0)\, f. \qquad (1)$$

The validity of this equation is wholly a matter of definition and conservation of energy. The effective energy is W', the energy left to propagate the shock and to do damage at the distance R. The extreme right-hand term contains the volume of the shock $(4/3)\pi R^3$ and the peak pressure P at the shock front, pressure having dimensions of energy per unit volume. The factor f is defined to relate the average energy density per unit volume on the interior of the wave (available internal energy plus kinetic energy) to the peak pressure at the shock front. Because the sum of compressional energy and kinetic energy decreases monotonically on the interior of the wave, the factor f will be less than unity, in terms of the peak energy density at the shock front itself; f will be a number like 1/2 for strong shocks in gases but be a much smaller number when the shock becomes weak. The waste heat concept makes it possible to calculate the dissipated energy by integrating over the past history of the shock front, since the functions P(R) and Q[P(R)] are known and the heat is "stored forever" in the material. Because the waste heat Q is always a positive quantity the integral is monotonically increasing. Equation (1) shows that the effective energy W' (or its counterpart on the extreme right) is not proportional to a constant W but decreases continually as the shock progresses and the waste heat accumulates in the material left behind.

Assuming that the original energy W is constant (it is not necessary to assume that the energy release was instantaneous), Eq. (1) may be differentiated with respect to time or distance R and after suitable manipulations the rigorous result is obtained that

$$\frac{d \ln (P - P_0)}{d \ln R} = -3 \left[\frac{1 + \dfrac{\rho_0 Q}{(P - P_0) f}}{1 + \dfrac{d \ln f}{d \ln (P - P_0)}} \right] . \qquad (2)$$

At high pressures, f = constant $\cong$ 1/2 or 1/3, $(d \ln f)/[d \ln (P - P_0)] \cong 0$ and at the same time the quantity $\rho_0 Q/(P - P_0)$ is itself close to 1/2. The result is that the logarithmic decay of pressure with distance is two or three times greater than the similarity assumption would indicate and means that the peak pressure decay is like the sixth or perhaps the ninth power with distance from the source. This rapid decay of pressure, says $P \sim R^{-6}$, with distance instead of $P \sim R^{-3}$ is due to dissipation of energy through the waste heat process; it results in dissipation of energy fractions like 99% of the original energy W before the shock wave reaches the crushing pressure or other pressures of practical interest.

It can be shown that at low pressures the factor f is proportional to the square of the overpressure, $f \sim (P - P_0)^2$, so that $(d \ln f)/[d \ln (P - P_0)] = 2$. It follows from Eq. (2) that $[d \ln (P - P_0)]/(d \ln R) = -\{1 + [\rho_0 Q/(P - P_0) f]\}$. But in the acoustic approximation $Q \sim (P - P_0)^3$ and because $(P - P_0) f \sim (P - P_0)^3$ it follows that the correction term $\rho_0 Q/(P - P_0) f$ (representing the waste heat) does not vanish but approaches a constant limiting value even in the acoustic approximation.

Despite the variations in the factor f with shock strength and the variation in the behavior of the waste heat with pressure, it is possible to specify the available energy W' by a simple relationship with pressure as:

$$W' = W'_1 \left(\frac{P}{P_1} \right)^{1/2} \cong \frac{W}{2} \left(\frac{P}{P_1} \right)^{1/2} . \qquad (3)$$

P_1 is the "vaporization pressure"; the term W_1' is the available energy at the vaporization pressure; the W' will usually be about 1/2 the original energy release W. The pressure P_1 will be of the order of tens of kilobars for most soils but may be of the order of megabars for dense homogeneous materials like concrete or steel if free of voids. In any case, Eq. (3) shows why the available energy W' will be only a small fraction of the original energy release W, and will decrease with distance.

Some consequence of the waste heat concept on wave propagation follow from such considerations as these.

1. Most of the energy from the explosion, fractions like 99%, is deposited as heat very close to the source, in the cavity and in a relatively thin shell of compressed material immediately surrounding the nuclear device cavity.

2. The energy available to produce damage or seismic waves bears no set direct relation with the original energy release; the residual energy fraction depends upon the initial configuration of the material and the room immediately surrounding the device, upon the vaporization pressure, and the dynamic crushing strength of the rock or soil. The apparent energy at long distances will be a small fraction of the original energy release, like 0.001.

3. The concept of energy partition, so much going into the bubble, so much going into blast, is essentially a misnomer; the available energy is a constantly decreasing fraction with distance and the accumulated waste energy rapidly approaches 100% of the original energy.

4. It is doubtful if the acoustic approximation ever applies, in the sense of a constant energy in the wave. For example, Cole's "Underwater Explosions" gives the universal experimental for TNT explosions in water in the form

$$(P - P_0) = \text{constant}\left(\frac{W^{1/3}}{R}\right)^{1.13} . \qquad (4)$$

From the exponent 1.13 and Eq. (2) we recognize that whatever the value of Q and f at low pressures, the limiting value is such that $\rho_0 Q/P - P_0)f = 0.13$.

5. If the attempt is made to measure the energy release from an explosion by measuring the kinetic and compressional energy in the shock at appreciable distances from the source, the results are bound to indicate very small energy releases perhaps in error by a factor like 100 from the original energy release. Such procedures have been used by a number of agencies, e.g., in attempting to evaluate the energy release from metal-water reactions suspected to occur in reactor explosions; the results indicated very small energy releases. The point is that a similar measurement from a TNT explosion would also lead to similarly small values of hydrodynamic energy, at large distances, entirely inconsistent with the known energy release of TNT, as used for scaling. Damage is usually predicted on the basis of $W^{1/3}$ scaling from TNT results, so that direct comparisons are valid, and this "apparent energy" grossly underestimates the damage.

III. Underground Explosions

A typical history from an explosion in soil displays striking features, indicated in Figs. 3.4a and 3.4b, which would not be suspected on the basis of either linearized or conventional shock theory. This description is the author's interpretation for what should have happened and what did happen in the Rainier underground shot at Nevada Test Site in September 1957; the reader is reminded that the interpretation is not yet universally accepted.

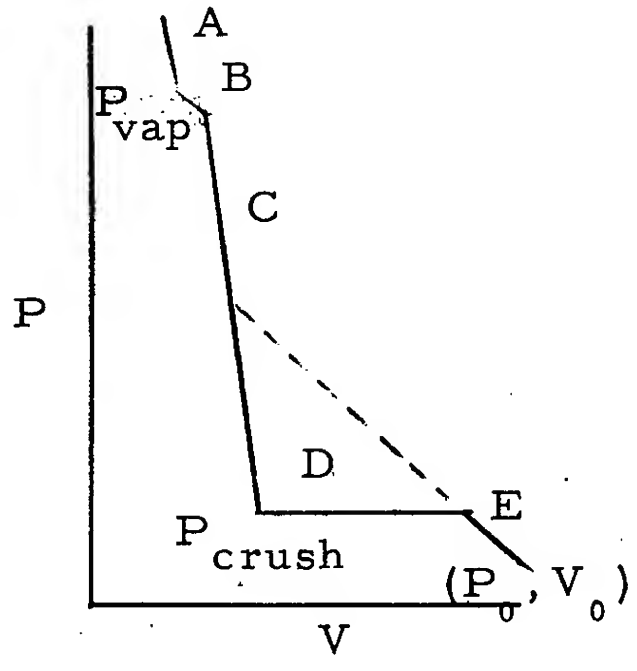

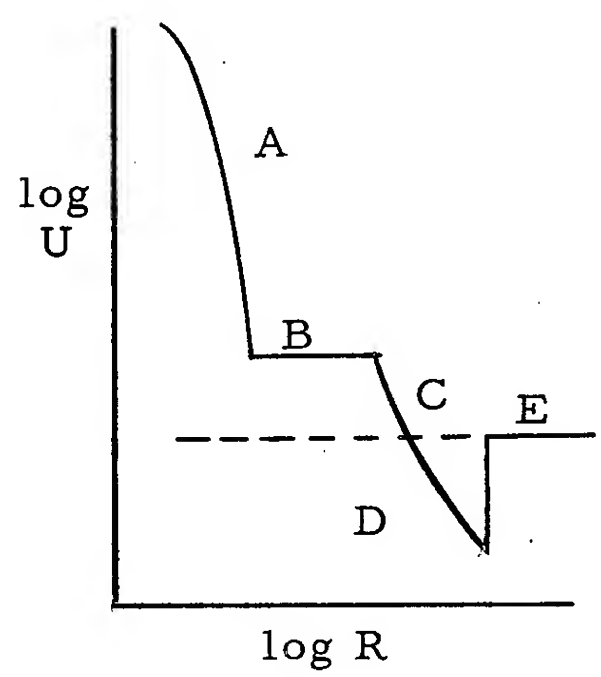

Fig. 3.4a. Pressure-velocity diagram for soil.

Fig. 3.4b. Shock velocity versus distance in soil.

The plot of shock velocity versus distance as in Fig. 3.4b is convenient to describe the various phases in the history of the shock growth. At high enough pressures, conservation of mass and momentum alone requires the shock velocity to behave as $U \sim P^{1/2}$ for any medium. The similarity condition $P \sim R^{-3}$ would require $d \ln U / d \ln P = -3/2$, which is a straight line of slope $-3/2$ on these logarithmic coordinates. At low pressures the shock velocity asymptotically approaches a constant, which is sound velocity; the general behavior according to conventional theory is shown as the dashed line in Fig. 3.4b. For the purpose of exposition now, we assume the Rankine-Hugoniot curve has the shape shown in the pressure-volume diagram of Fig. 3.4a. The corresponding regions of growth in Figs. 3.4a and 3.4b are shown by labeling portions of the curve A, B, C, D, and E. The region A is shocked well above the vaporization pressure of the material. The material behaves like a gas because the material behind it is irreversibly vaporized and superheated. But the shock velocity curve decays more rapidly with distance, than $U \sim R^{-3/2}$ (like $U \sim P^{1/2}$), because of the enormous energy expended on latent heat of vaporization of the material. The region B corresponds to the range of pressures between the pressure at which 100% of the material is irreversibly vaporized and some lower pressure at which all of the material can be heated to the boiling point by waste heat but too weak to vaporize any of it. B is a region of more or less constant temperatures. For other reasons also, the peak pressure is probably constant, and in any case, the shock velocity runs constant for some distance. In Rainier, this constant velocity region extended for all material which originally lay between 5 meters out to 17 or 18 meters from the device. The regions C and D shown are best understood by noting that the Rankine-Hugoniot equation for shock velocity requires:

$$U^2 = V_0^2 \frac{(P - P_0)}{V_0 - V} \qquad (5)$$

This equation means that the straight line joining P and P_0, as shown in Fig. 3.3, represents the square of the shock velocity, U^2. Ambient sound velocity has been indicated by the dashed line on Fig. 3.4a, as an extension of a straight line portion of the Rankine-Hugoniot curve at low pressures in the region E. The region C corresponds to those pressures below vaporization but at which the shock is still sufficiently strong to be supersonic with respect to ambient sound velocity. The region D is particularly interesting because it represents a region of pressures well above the crushing pressure but in which the shock velocity is below ambient sound velocity. In this region of pressures, precursor sound signals may precede the main shock pulse, but they are necessarily insignificant in strength compared with the main shock pressure. The region E represents the range of pressures below the crushing strength of the rock. By virtue of the simplification used to portray compressibility in the region E in Fig. 3.4b and in the corresponding region E in Fig. 3.4a, the crushing pressure is shown as a horizontal straight line.

We note that acoustic theory would require that the entire history of the explosion would be represented by straight lines, both for the compressibility in Fig. 3.4a (dashed line) and a constant value (sound velocity) represented by E in Fig. 3.4b.

Some comments on the history of an underground explosion are given below.

1. There is little meaning to a ≈constant seismic energy≈ in the acoustic region E, which is by definition beyond the crushed zone, a distance like 100 feet for one kiloton in a medium like Nevada soil. Surprisingly enough, Nevada rock is a relatively good transmitter of shock energy because of its high water content at depth. Energy fractions like 1% of the original energy may still be available in the seismic wave at this distance, but this would be significant only if the material beyond the crushed zone were completely homogeneous and linearly elastic.

2. The existence of faults, joints, fissures, and free-surfaces all constitute mechanisms whereby the compression (due to the shock transmitted beyond the crushed zone) is readily relieved (at the expense of the net energy transmitted further out in a seismic wave). As such, the "earthquakes" generated by these explosions are more or less coincidental to the shock process and their relationship to the energy release is ambiguous. Both the Rainier event (1957) and the Hardtack II events (1958) resulted in displacements of about two feet along joints or planes of structural weakness originally in the rock, much like the slippage along an earthquake fault. Very large amounts of energy may be represented as potential energy from a fault block lying above some plane of structural weakness, and the passage of the shock may literally trigger this energy. In any case, the subsequent movement of the block (which may relieve the shock stress by moving the block as a whole) generates a disturbance of its own along the induced fault entirely comparable to the mechanism in an ordinary earthquake, but of a much smaller magnitude of energy. It is suggested that the seismic signals alleged to be observed as a result of the Rainier event – if they had any significance at all – were probably due to these minor induced earthquakes. It is of considerable reassurance, therefore, in worrying about earthquakes from underground explosions, to note that earthquakes did occur but were very minor events. It is entirely probable that once a test site has been "fired in," by relieving the eons-old accumulation of stresses along planes of structural weakness, no further serious disturbances would result from subsequent shots, even like these very minor events.

3. Finally, it is noted that the typical disturbance produced by the shock wave itself is of short duration and of an entirely different nature from the train of waves associated with slippage along a fault block, which have a relatively long time duration. There is no strong reason to suppose that the initial compression wave in rock is different from any other shock; a sharp rise followed by a more or less rapid and asymptotic decay back to ambient pressure. In the low pressure approximations, the time decay of pressure just behind the front in such a wave can be derived explicitly in terms of the peak pressure, the time t from the source, and the properties of the material according to

$$\frac{\partial P}{\partial t} = \frac{\rho_0 c_0^2}{t} . \qquad (6)$$

Here ρ_0 is the density and c_0 is the sound velocity. Even gross considerations with this equation will show that the "positive duration" for pressure in the shock wave is likely to be of the order of milliseconds; this duration is probably too short for the average seismic instrument to resolve; what the instrument saw was the mountain settling slowly after its initial jolt.

VII. Channeling

By channeling we mean that the tendency for shock energy to propagate preferentially into rarified media instead of dense media is so pronounced that the energy can be directed almost at will by means of open channels.

The basic hydrodynamic reasons for channeling can be simply shown. Compare the rate of work $\dot{W}$ per unit area and time done by a shock front on the gas compared with that done on a solid medium, assuming the configuration shown in Fig. 3.5. The rate of work $\dot{W}$ in any medium is given by the product $\dot{W} = Pu$, a piston moving with the force P at the material velocity u. If the peak pressure at the shock front at a given time is the same in the two media – and the hydrodynamics will nearly always guarantee that it is – then the rate of work in either medium is described by the equation:

$$\dot{W} = Pu = P\,(P - P_0)(V_0 - V).$$

Under the condition that the shock pressure is equal across the interface, the ratio of the rate of work in each medium is readily obtained as

$$\frac{\dot{W}_{gas}}{\dot{W}_{solid}} = \sqrt{\frac{\rho_{0,\,solid}}{\rho_{0,\,gas}} \; \frac{\left(1 - \frac{V}{V_0}\right)_{gas}}{\left(\frac{\Delta V}{V_0}\right)_{solid}}} \qquad (8)$$

A factor of 10^3 to 10^4 or so occurs in the density ratio betwen the two media and is alone sufficient to introduce a factor of 30 to 100 for energy propagation in favor of the gaseous phase, even at high pressures where the compression in the solid is comparable to that in the gas. However, over a large range of pressures, V/V_0 in the gas is so substantially less than 1 so that the corresponding term in the numerator is practically 1. At the same time the density change $\Delta V/V_0$ in the solid is very small and this small fractional change in specific volume in the solid again introduces many factors of 10 to the relative rate of work in favor of the gaseous phase. At low enough pressures

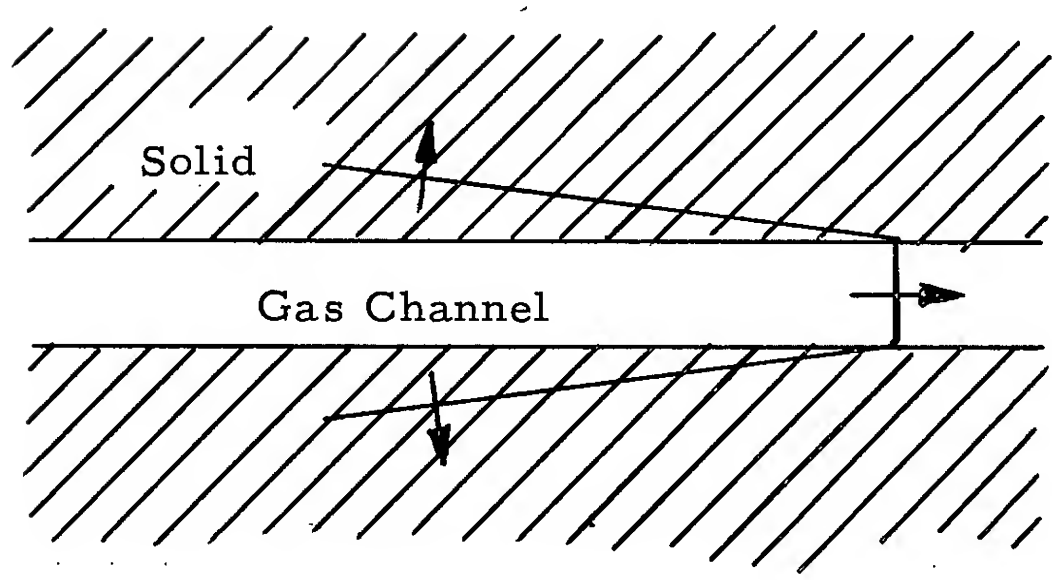

Fig. 3.5. Strong shock in a gas channel.

the relative rate of work in Eq. (8) approaches the ratio of the familiar "acoustic impedance"

$$\frac{\dot{W}_{gas}}{\dot{W}_{solid}} = \frac{(\rho_0 c_0)_{solid}}{(\rho_0 c_0)_{gas}} \quad , \tag{9}$$

which is a ratio like 10,000 in favor of propagation in the gas.

Such considerations show the enormous tendency for the shock energy to literally spill out into the gaseous phase – a factor of 1,000 at most pressure levels – with a corresponding depletion of the shock energy in the solid or liquid phases.

VIII. Controlled Excavations

Despite the well-known condition that the sound velocity in solid and liquid media may be five to ten times the sound velocity in air, a reverse situation occurs at nearly all pressures great enough to be of practical interest for excavations.

A strong tendency for the shock in the gaseous media to outrun the shock in the dense media is indicated by considering the equation for shock velocity, given as Eq. (5). Assuming we have equality in pressure across the interface as in Fig. 5, the ratio of the shock velocity in each media would be given by

$$\frac{U_{gas}}{U_{solid}} = \sqrt{\frac{\rho_0\text{, solid}}{\rho_0\text{, gas}} \frac{\left(\frac{\Delta V}{V_0}\right)_{solid}}{\left(1 - \frac{V}{V_0}\right)_{gas}}} \quad . \tag{10}$$

When the shock strength is high enough to achieve appreciable compression of the solid (which is widely significant if the solid contains any appreciable air

fraction) then the shock velocity in air outruns the shock velocity in soil by the square root of the density ratio. A factor of about 30 to 1 applies for many pressures of interest. At low enough pressures the shock velocity ratio must obviously approach the ratio of sound velocities in each medium, a ratio in favor of increased shock velocity in the solid medium. However, over the large range of pressures in which the compression in solid is small enough to be considered linear (although much too strong for the linear approximation to apply in air), the ratio of shock velocities behaves as

$$\frac{U_{air}}{U_{solid}} = \frac{C_{0,\ air}}{C_{0,\ solid}} \sqrt{\frac{6\frac{P}{P_0} + 1}{7}} \qquad (11)$$

From this equation it is clear that a shock in air will outrun the shock in solids at pressures above 30 atmospheres or roughly 500 psi. Close in, the ratio reaches the limit like 30 to 1 suggested by the square root of density ratios alone in Eq. (10). This result means that the angle of inclination of the ground shock in Fig. 5 is very flat; the shock in ground moves 1/30 the distance outward from the channel as the front moves forward in the channel. For practical purposes, the result is a nearly cylindrical jet.

As a result of such comparisons of shock velocity and with considerations of the detailed material velocity in each of the solid and gaseous phases, it is possible to derive some general criteria for the conditions under which such a channel may be stemmed or plugged. The details are more complex than can be shown here but the results are shown qualitatively in Figs. 3.6a and 3.6b. Figure 3.6a represents the before and after pictures for an open channel. Categorically, any open channel in a radial direction to the device will always open up. The criteria for stemming depend upon the physical properties of a plug shown in Fig. 3.6b. But a general rule-of-thumb appears that a plug with the same length as the diameter of the channel will usually be sufficient to stem the channel as shown. The hydrodynamic reasons are as follows.

When the shock first emerges from the far side of the plug, an enormous rarefaction in shock strength occurs, reducing the transmitted shock in the channel by a factor roughly equal to the density ratio between the gas and the solid phase. A corresponding rarefaction moves backwards through the plug. The pressures in the solid phase are not similarly reduced and the walls of the channel begin to move in toward the center, closing the channel. If the plug is too thin, the subsequent rarefaction back to the device chamber occurs with sufficient rapidity that the device energy breaks through. But if the plug is long enough the channel may already be closed before the breakthrough can occur. The net result is a continual closure of the channel. At the same time it will be clear from the figure that a pinch jet will almost always move down the channel, ahead of the ground shock because of the continual closure of the air channel behind it. The process is somewhat analogous to the boyhood trick of shooting watermelon seeds by squeezing them.

Surprisingly enough, despite the very much lower efficiency of a nuclear explosion with spherical symmetry in a homogeneous soil, the channeling concept provides the means to make nuclear explosions more efficient than TNT for many excavation purposes. The argument is as follows. Because of the close similarity of density between TNT and most rock-like materials, the initial shock transmitted outward from a tamped TNT charge is of the same

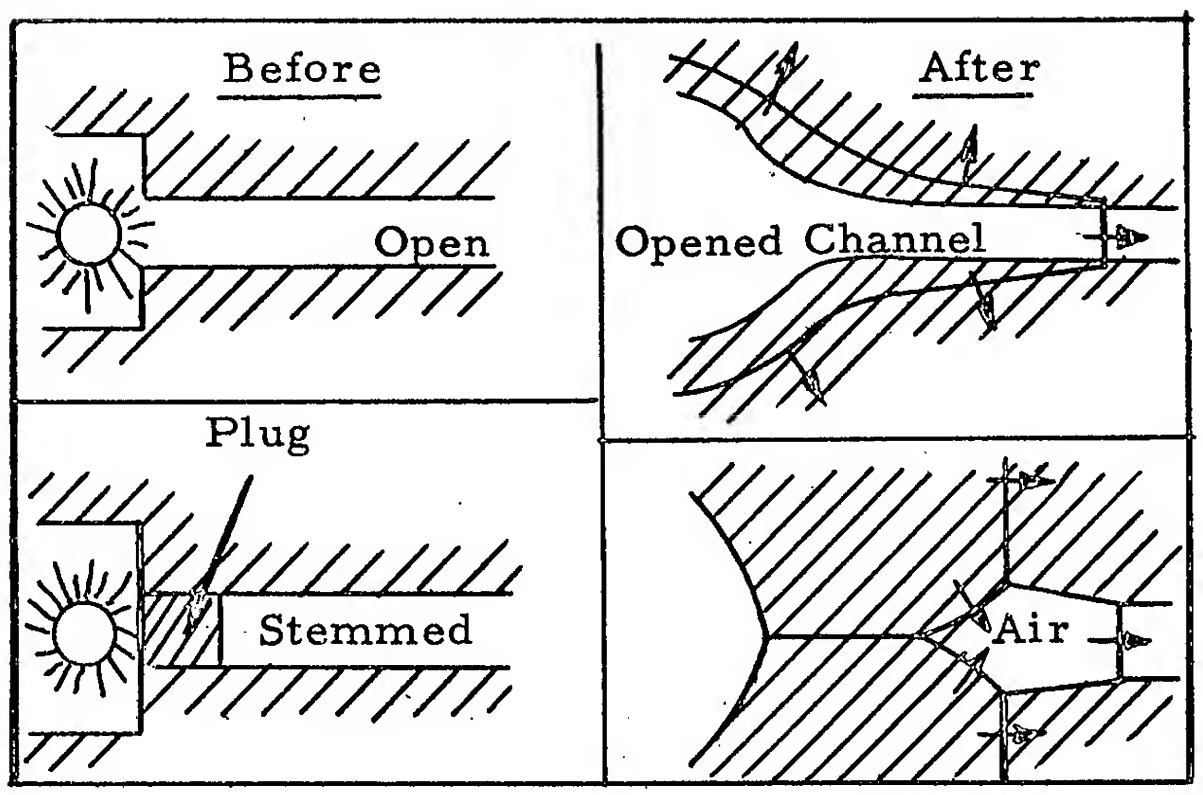

Fig. 3.6a. Open channel (upper figures).

Fig. 3.6b. Stemmed channel (lower figures).

order as the internal pressure initially in the high explosive, about 300,000 atmospheres. This results in the shattering by TNT with a large loss in energy due to crushing and waste heat within the rock, although, of course, not comparable to the waste heat of a tamped nuclear explosion. It is difficult to exploit channeling with TNT even with an open channel because the large mass effect of the TNT is itself almost equivalent to the stemming plug described above. No such mass effects exist for nuclear explosions; by the channeling process it appears possible to channel the energy into very large volumes of air, perhaps reducing the pressures down to levels like 500 psi quoted above, at least down to the crushing strength of the rock, or its yield strength in situ. Thus, because the pressure can be degraded quickly, the energy from a nuclear explosion can be made to lift the overburden with greater efficiency than is possible with TNT.

The area of a cylindrical shock front in soil ($2\pi r\ell$) relative to the area of the channel itself (πr^2), together with the ratio $\ell/r = 30$, is sufficient to indicate that the area of the ground shock is about 60 times the area of the shock at the front of the jet. This means that despite the larger rate of work per unit area in air a large fraction of the energy from an explosion can be directed through the jet to work the ground: the explosion behaves kinetically like a line charge.

The argument has often been advanced that an open radial channel from an explosion will close itself because of the greater sound velocity in dense media than in air. That this argument is invalid at pressures of interest is clear from Eq. (10) and (11). Furthermore, in a porous rock or soil, the sound velocities may actually be comparable. In any case, Fig. 3.4a shows that the shock velocity in a crushable dense medium can be quite low even where the pressure exceeds the crushing strength. Hence, the argument for automatic closure applies only at pressure levels which are too low for the channel to crush down. The argument for closure of an open radial channel is tantamount to the incredulous statement that a pipe leading from a suddenly pressurized boiler will implode because of the high sound velocity in steel.

4. SUBSURFACE EARTH MOTION

William R. Perret

Sandia Corporation

Subsurface earth motion is the time history of transient mechanical effects produced by large contained explosions and observed within the containing medium in the region extending from just outside the explosion cavity to an adjacent free surface or to the region of essentially pure elastic reactions. The studies performed in this region provide direct knowledge of reaction of the medium to explosive energy. Such knowledge is fundamental to understanding the mechanics of containment and its antithesis, cratering.

The instruments for observing such transient effects consist primarily of accelerometers, supplemented by several specially developed velocity gauges and stress or strain gauges. Chief dependence has been placed on accelerometers, not because acceleration is the most desirable parameter for analysis, but because gauges suitable for measuring velocity or displacement of the magnitudes and durations anticipated are only now emerging from proof test phases of development.

Programs designed to explore motion in the rock surrounding the Rainier, Tamalpais, and Evans shots of 1957 and 1958 were conducted by several agencies. The Rainier studies, undertaken by Stanford Research Institute (SRI), Sandia, and Engineer Research and Development Laboratories (ERDL), Fort Belvoir, included acceleration measurements on vertical and horizontal radii. Figure 4.1 shows the relative positions of the instrumentation for the Rainier explosion. SRI and Sandia instrumented borings adjacent to surface zero. ERDL and Sandia instrumentation was installed in the access tunnel. These projects met with only qualified success, primarily because the instrument ranges chosen were in some cases too low, and recording circuitry limited recorded peak signals.

Evans studies were designed to overcome some of the difficulties encountered by the Rainier projects. Two vertical instrumentation systems extending from about 200 ft from the zero point to the surface were installed by SRI and Sandia. Again dependence was placed primarily on accelerometers, but SRI included several newly developed velocity gauges in their array.

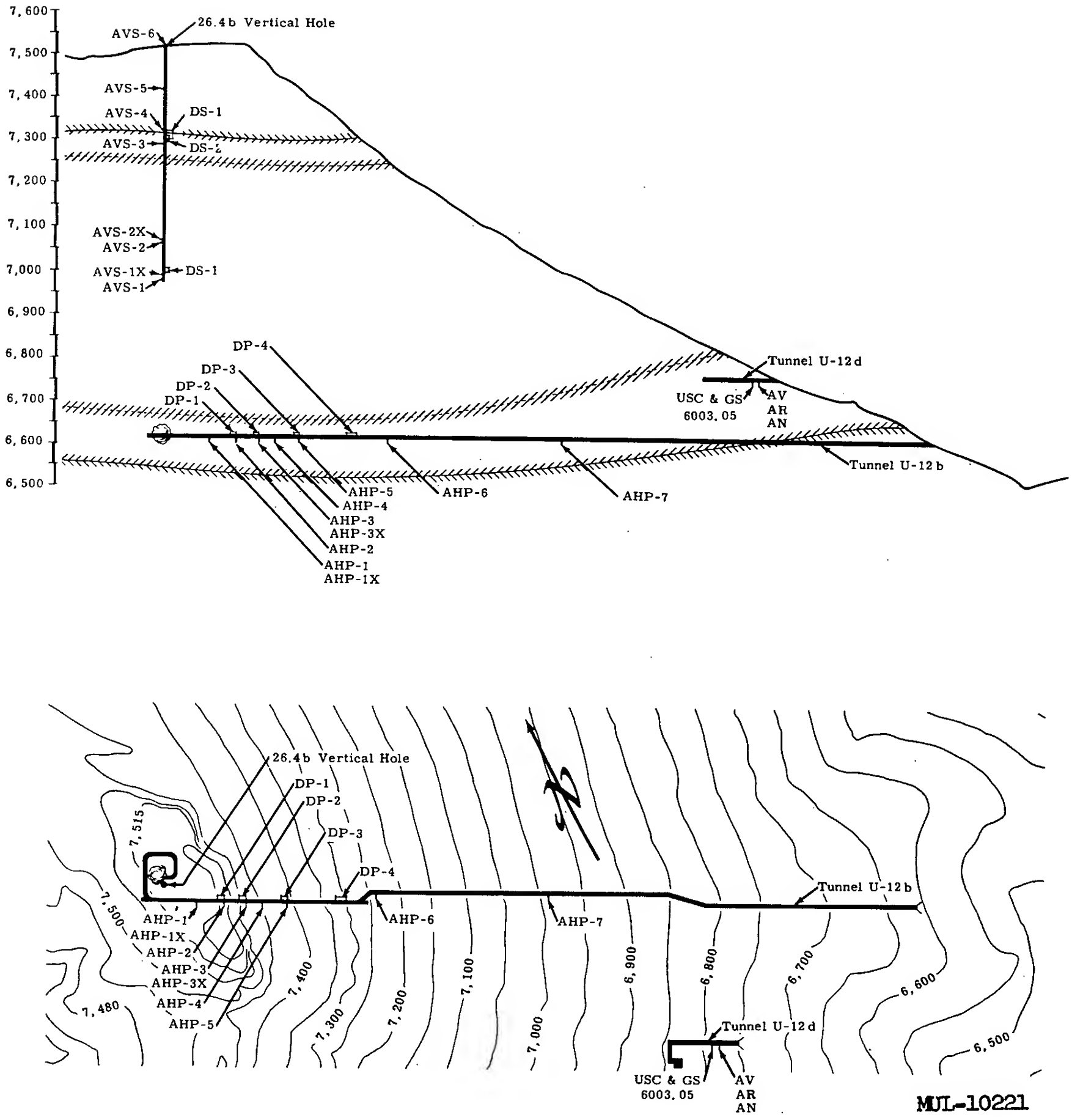

Fig. 4.1. Plan and elevation, Rainier tunnel.

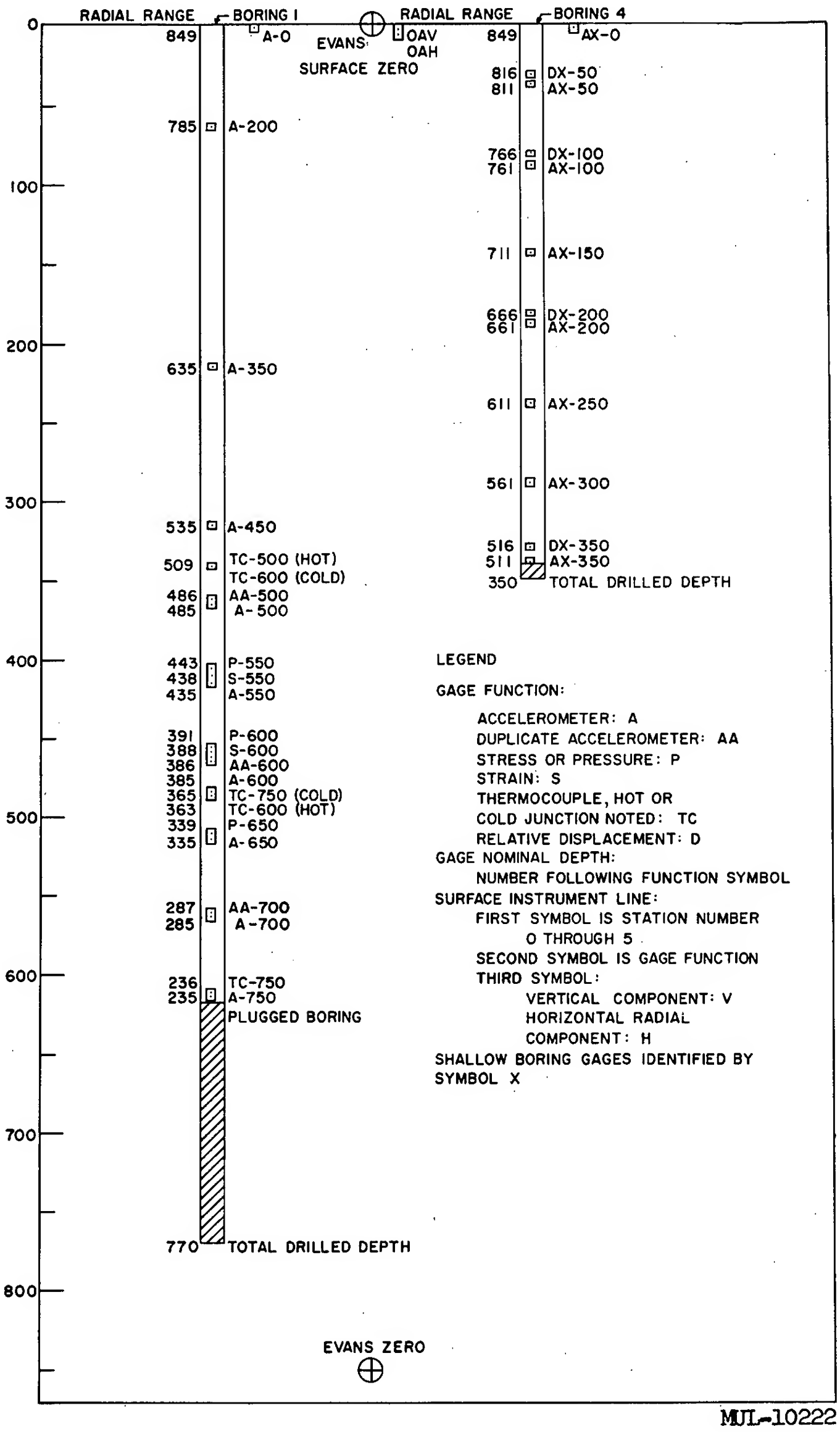

Fig. 4.2. Distribution of vertical instrumentation for Evans.

Figure 4.2 shows the distribution of vertical instrumentation. Horizontal radius instrumentation was installed adjacent to the access tunnel by ERDL and Ballistic Research Laboratory (BRL) for the Tamalpais and Evans event. Success of these programs was again seriously limited, this time principally by the fact that the energy derived from the Evans event was only about 1% of that anticipated and measuring and recording systems were operating in many instances close to the limit of resolution. Precision of the results is consequently low.

All acceleration data taken within the rock during Rainier and Evans events were radial. These data from both vertical and horizontal radii are shown plotted against range in Fig. 4.3. Two plots are shown, one of raw data, the second of scaled data. Dimensional analysis indicates that accelerations should follow a relationship of the form

$$AW^{1/3} \propto \left(RW^{-1/3}\right)^{n} ,$$

where $AW^{1/3}$ is scaled acceleration and $RW^{-1/3}$ is scaled range. The data suggest that the exponent should be -4 out to a range of about 700 ft, beyond which it changes toward -2. There is an obvious discrepancy in the scaled plot between the Rainier and Evans data, due in part to the fact that most Rainier peaks were low by a factor greater than 2, and the widths of Evans records were relatively large compared with deflections.

The inverse fourth power relationship between accelerations and range near an explosion appears valid for both plots although it is not evident that scaling laws are valid. Point-source theory implies that pressure varies inversely with the cube of radial range, but the radial derivative of pressure must be proportional to acceleration. Hence, inverse variation of acceleration with the fourth power of range indicates that, out to about 700 feet from an explosion, rock reacts as to a point source.

There is a slope inversion in each vertical radius data curve at ranges which encompass a region within 300 feet of the free surface. This region includes the welded-tuff caprock of the Rainier mesa. Peaks decrease with range up to a point about 250 feet below the surface. Above this point accelerations increase. Time relationships are such that surface reflection effects cannot cause the increase. In fact, one record, AVS-5 Fig. 4.4, shows a reflected peak following the major one; reflected signal arrivals indicated on other

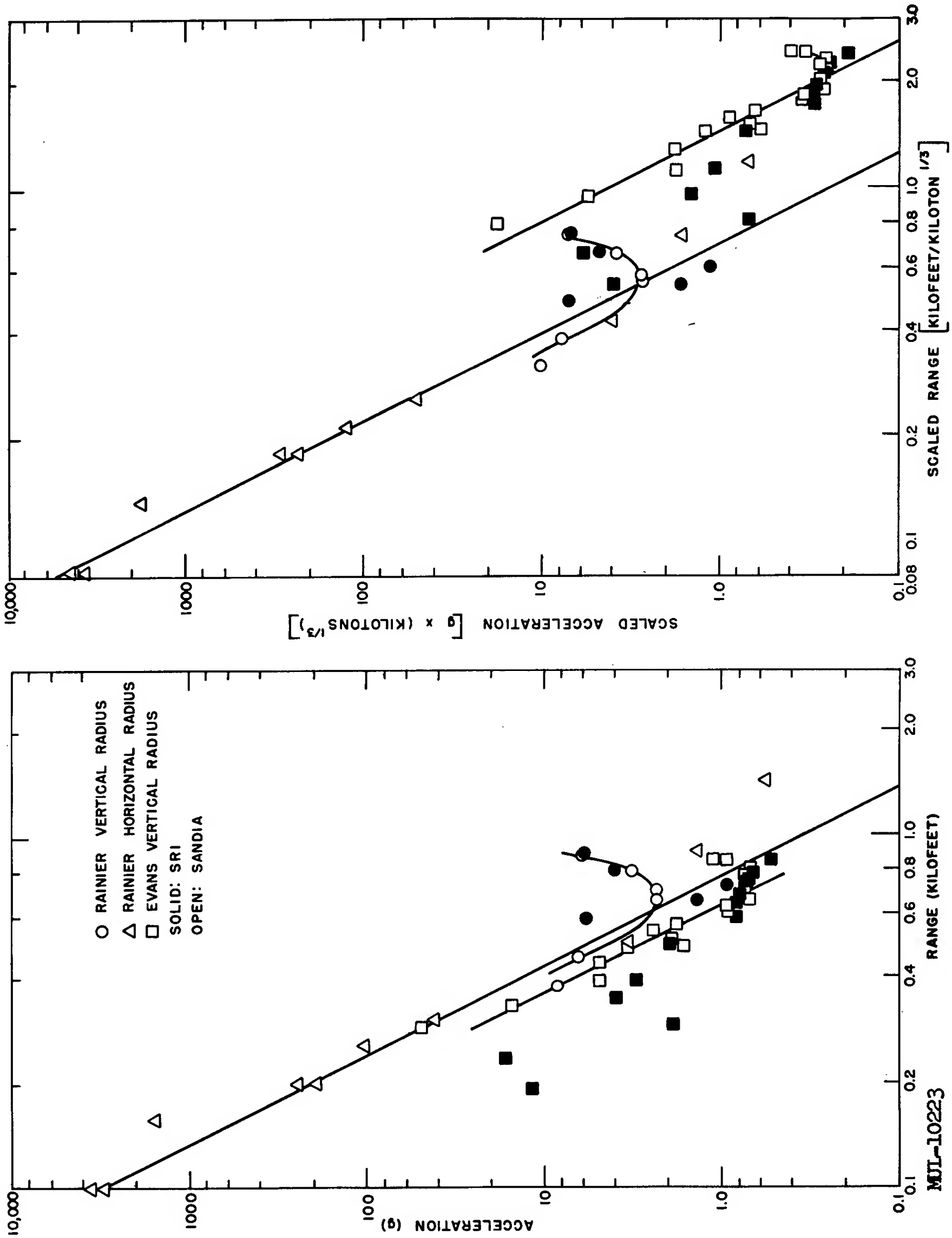
SCALED ACCELERATION [g x (KILOTONS^1/3)]
10,000
1000
100
10
1.0
0.1
0.08
0.1
0.2
0.4
0.6
0.8
1.0
2.0
3.0
SCALED RANGE [KILOFEET/KILOTON^1/3]
ACCELERATION (g)
RANGE (KILOFEET)
O RAINIER VERTICAL RADIUS
Δ RAINIER HORIZONTAL RADIUS
□ EVANS VERTICAL RADIUS
SOLID: SRI
OPEN: SANDIA
MUL-10223

Fig. 4.3.

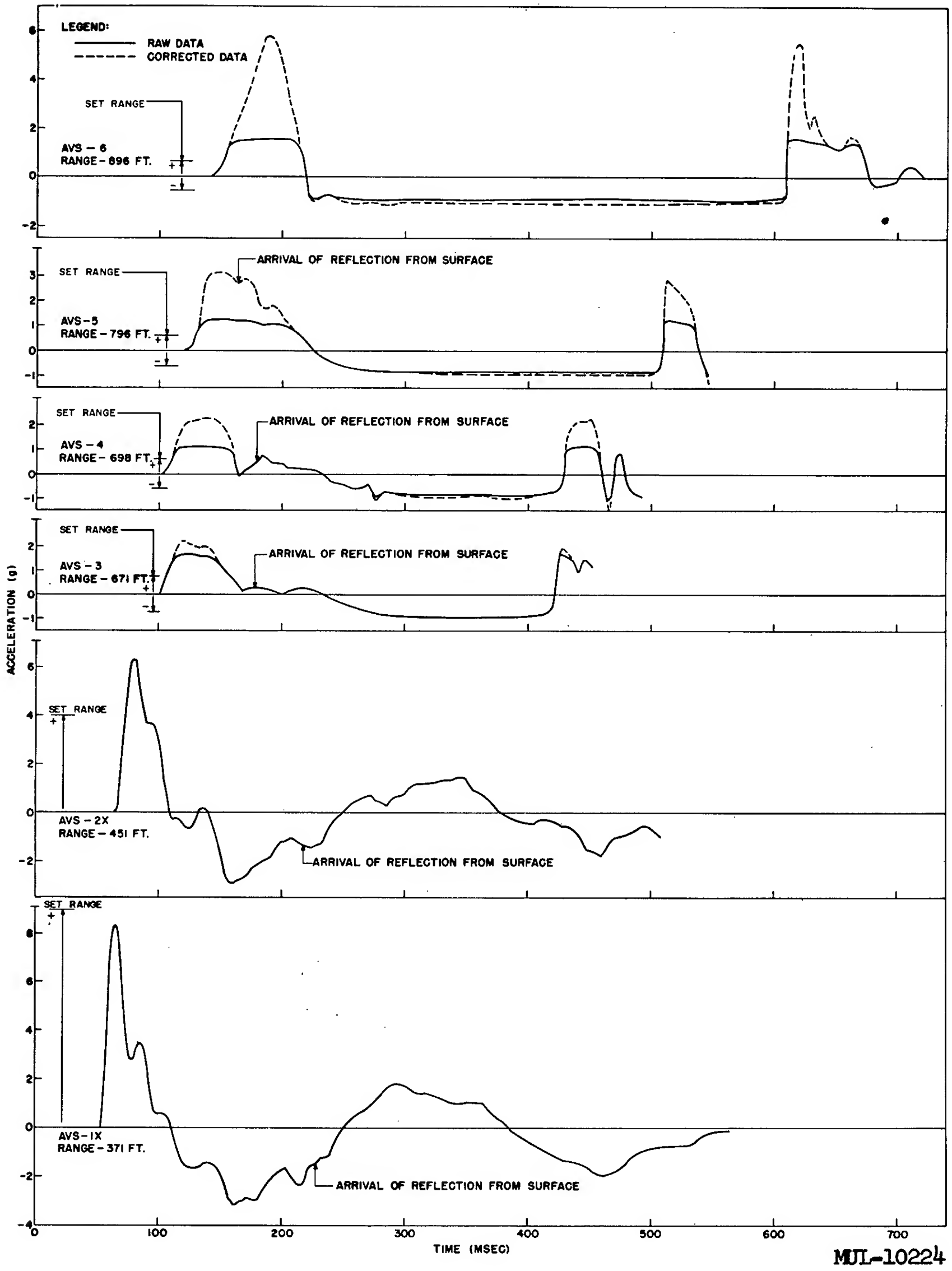

Fig. 4.4. Acceleration – time records, vertical radius.

records are derived times based on travel times to surface and return. Examination of propagation velocity data and rock densities shows that the velocity decreases through a factor of 3 more or less continuously from the base of the caprock toward the free surface. Densities vary by not more than 20%. Thus seismic impedance, the product of propagation velocity by density, decreases toward the surface from the base of the caprock and particle displacements and accelerations increase accordingly as a result of the amplitude relationship

$$X_2 = X_1 \frac{2\rho_1 C_1}{\rho_1 C_1 + \rho_2 C_2} ,$$

where ρ's are densities, C's propagation velocities, and X's amplitudes or displacements transmitted from medium 1 into medium 2. $\rho_1 C_1$ is greater than $\rho_2 C_2$.

This enhancement effect is more pronounced in the Rainier data than in the Evans results, but it appears in both sets of records at about the same depth. The Evans results involve small signals near the limit of resolution of the gauges, and energies too small to produce gross motion and partings of the caprock. Therefore, the enhancement in the Evans data does not follow as consistent a pattern as do the Rainier data. Only at the free surface were accelerations of markedly increased magnitude noted in Evans records.

Motion of the caprock, as described by the four uppermost acceleration records from Rainier in Fig. 4.4, indicate upward motion followed by a period of free fall. These records are a composite of Sandia and SRI data. Free fall ends for each gauge in a rebound pulse, implying that the floating rock came back to earth. Comparison of intervals between first arrivals and arrivals of rebound indicate, by differences, at least three partings between a depth of 250 feet and the surface.

Particle velocities have been derived from both Rainier and Evans vertical data. Those from Rainier were derived by integration of the acceleration-time records, but those from Evans were measured directly by the SRI gauges and were checked by integration of corresponding acceleration data. The plot of peak velocities versus scaled range, shown in Fig. 4.5, indicates that below the caprock discontinuity velocities vary with the inverse square of scaled range. Scaling relations for velocity and range should have the form

$$V \propto (RW^{-1/3})^n .$$

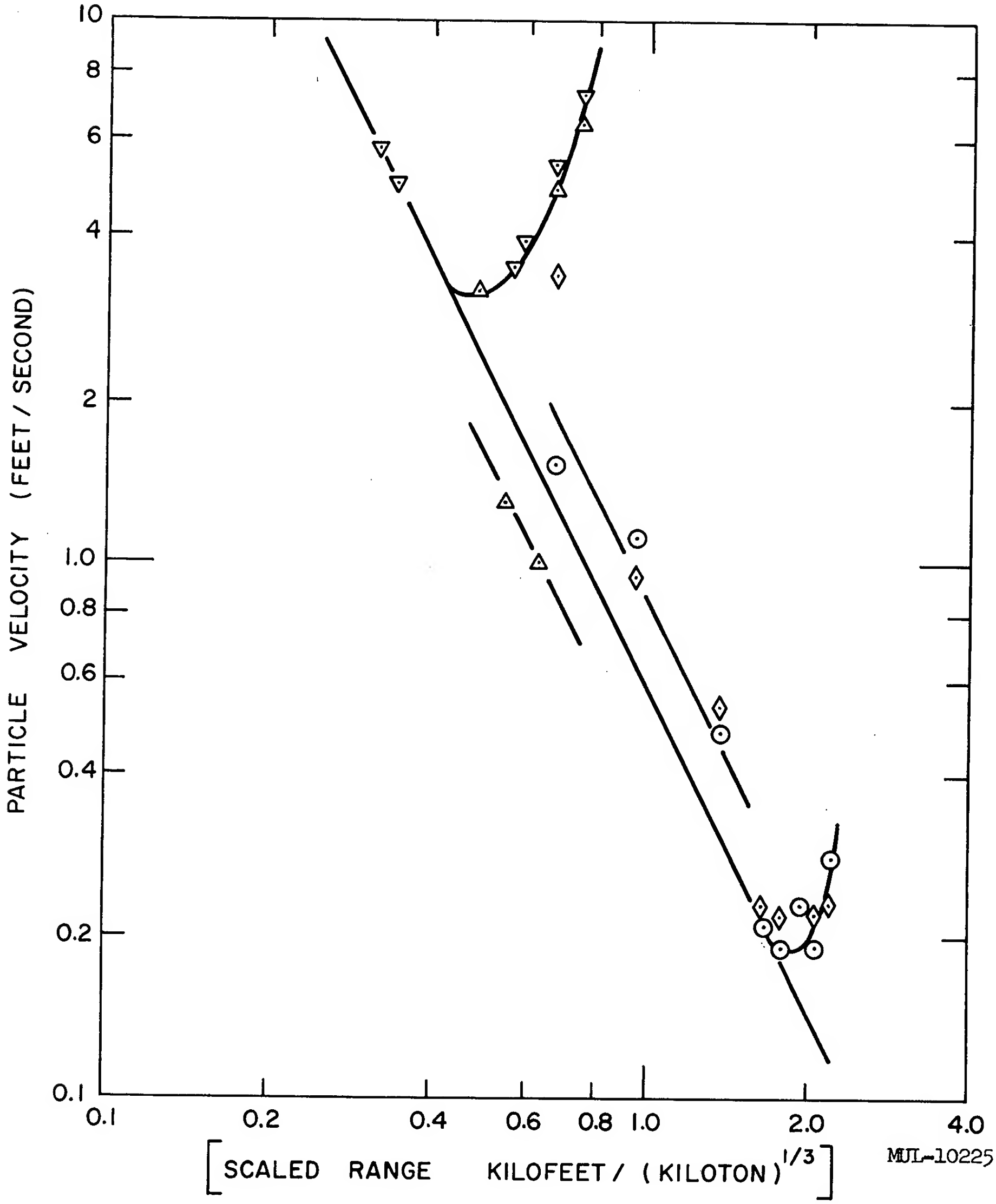
10
8
6
4
2
1.0
0.8
0.6
0.4
0.2
0.1
PARTICLE VELOCITY (FEET / SECOND)
0.1
0.2
0.4
0.6
0.8
1.0
2.0
4.0
[SCALED RANGE KILOFEET / (KILOTON)^1/3]
MUL-10225

Fig. 4.5.

The graph shows that the exponent, n, is -2. Slope of the velocity curves also undergo inversion within the caprock.

Finally, a few observations of stresses and strains are available from the BRL and ERDL Tamalpais instrumentation. The five observations of radial stress by BRL ranged from about 1100 psi at 100 feet downward to 18 psi at 1100 feet from the 57-ton shot. Tangential stresses were about 60% of radial stresses. The few data available indicate that both components of stress observed vary inversely with the cube of the radial range, again implying that within this region the rock reacts as to a point source.

ERDL strain data indicate that peak transient strains are compressions which vary inversely with the square of scaled radius. Compressive strains observed ranged downward from about 0.1% at 100 ft.

The data available concerning motion within the earth near a contained nuclear explosion imply that the rock reacts as to a point source in a homogeneous medium over the range of distances beyond the gross deformation of the cavity out to at least 700 ft. Scaling laws do not appear to apply to peak acceleration data, but circumstances which limit precision of the data may account for many of the discrepancies in scaling.

5. SURFACE EFFECTS

L. M. Swift

Stanford Research Institute

The surface effects of a deep underground explosion are not merely a continuation of the subsurface effects. Even in the case of the ideal but never attained "infinite, homogeneous, elastic, etc." solid, the stress wave arriving at surface ground zero is reflected as a negative of its former self. That is, a compressional wave is reflected as a tensile wave, and vice versa. What is not so obvious is that this reversal in both sign and direction of travel of the stress wave requires that the particle motion is not reversed. Thus the meeting of the remains of the incident wave with its reflections near the surface causes the stresses to cancel, but causes an amplification of the particle motions.

At points other than ground zero, where the incidence of the wave with the surface is other than perpendicular, these cancellations and amplifications are not direct, and changes occur in the directions of stresses and movements. The general effect is to translate more and more of the energy into a horizontal direction, that is, parallel with the free surface. When the medium is layered, as real conditions usually are, this tendency may be offset by the tendency of the energy to follow a refracted path in reaching the surface, so that, beyond a critical angle, the angle of arrival is constant, for high frequency waves at least. Further complications are added by the presence of faults and joints, and by reflections from moderately deep layers.

At great distances, most of the high frequency energy is lost, and the remaining signals are low frequency and consequently of long wavelength. These long waves simply cannot "see" the smaller discontinuities in the earth, and are affected primarily by the major features of the earth's structure. That region belongs to the seismologist, however, and I am sure he appreciates my oversimplification of his problems. With apologies, then, we will withdraw to the close-in surface effects, defined as those at distances no greater than a few times the depth of burial of the shot.*

On shot Rainier, records were obtained of the vertical acceleration at ground zero, and of vertical and horizontal accelerations at six other ranges

*This discussion applies to burial sufficient for containment.

out to about a half mile. At most of these points, records were obtained of the strain at the surface as well. A point of perhaps maximum interest on the surface is surface ground zero. It is usually the closest surface point to the shot, and hence the one where maximum effects are to be expected. Also, as mentioned previously, it is a region where the mechanisms of reflection are simple. Mr. Perret has described how the original violent, crushing shock wave was modified by dissipation and geometric spreading to a more complex wave of longer duration and lower peak magnitude. Beyond a few hundred feet, it differed little from a purely elastic wave. As this wave approached the surface, the motions were amplified by reflections from the surface, so that they were greater at the surface than at a depth of 250 feet, in spite of the greater distance from the shot. Figure 5.1 shows the motion of the surface, expressed in physical quantities. The vertical acceleration, shown here as a function of time, is seen to exhibit a sharp pulse, with a peak of about 6 g and a duration of 50 msec, followed by a flat region of -1 g magnitude and about 400 msec duration. (This -1 g is with reference to a normal zero established with the accelerometer being supported by the earth — -1 g actually represents a free fall condition.) Following this is another pulse similar to the first. These data can be converted into terms of velocity by integration of the acceleration with respect to time. The first acceleration pulse produced a velocity upward of about 6 fps. During the -1 g period, this velocity gradually dropped to zero and on to about the same velocity in a downward direction. At the time of the second bump, most of the velocity was lost, and the surface stopped moving, except for a moderate and more or less random vibration.

Integrating once more, to obtain displacement, we see a parabolic trajectory which begins to look familiar; it shows that what happened was simply that the surface was tossed into the air about nine inches, and landed again about where it started. The dotted curve of displacement is one obtained from motion picture photography of the surface, taken with telephoto lens from a point about 4000 feet away. The agreement is good.

These records alone do not demonstrate it clearly, but in combination with subsurface data they show that it was not only the very surface which was in free fall, but a layer some hundred feet or more thick. In fact there appear to have been several horizontal parting planes at depths down to 250 feet or more. This effect is familiar and similar to that of "spalling," frequently observed

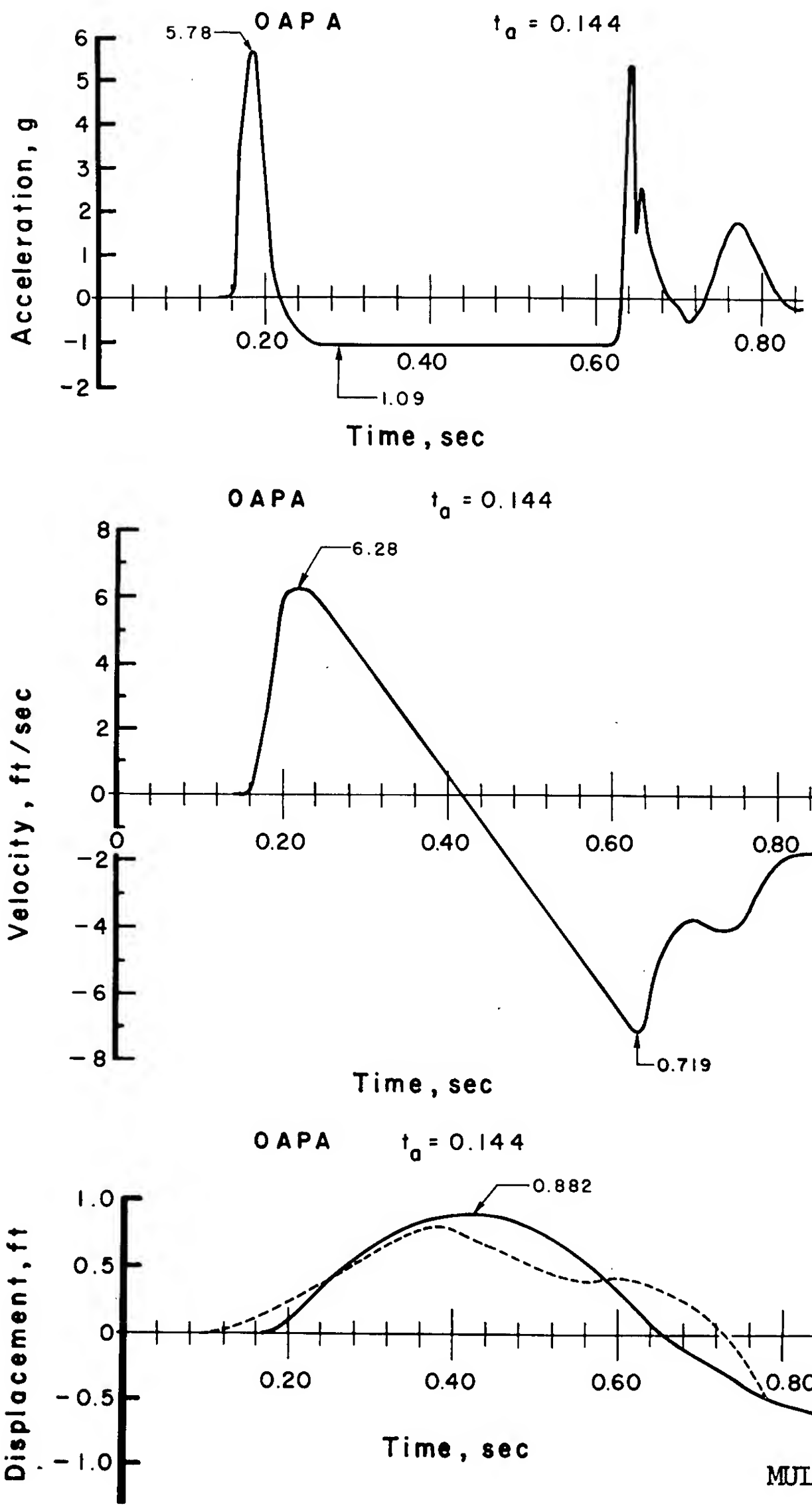
OAPA
t_a = 0.144
5.78
6
5
4
3
2
1
0
-1
-2
Acceleration, g
0.20
0.40
0.60
0.80
1.09
Time, sec
OAPA
t_a = 0.144
6.28
8
6
4
2
0
-2
-4
-6
-8
Velocity, ft/sec
0
0.20
0.40
0.60
0.80
0.719
Time, sec
OAPA
t_a = 0.144
0.882
1.0
0.5
0
-0.5
-1.0
Displacement, ft
0.20
0.40
0.60
0.80
Time, sec
MUL-10298

Fig. 5.1.

in small explosions, but here it is complicated by the fact that the formation is held together more by the force of gravity than by any tensile strength of the material.

Most of us have had the experience of unexpectedly stepping off a curb in the dark. It's startling, frequently painful, but seldom fatal. That is about the sensation that would have been experienced by an observer standing at ground zero when Rainier was fired, except that he would have felt two bumps, each of only about 5 or 6 g. But that was Rainier. I assure you that my hypothetical observer would have been much more embarrassed had he attempted to sit on some of those other underground shots.

One of those shots was Blanca. This was a larger shot at about the same depth as Rainier, so one would expect more surface effects. Unfortunately, this shot was under the slope; for this and other reasons close-in measurements were not feasible, but information is available on the movement of a couple of points on top of the mesa but near ground zero. Figure 5.2 gives the vertical displacement as a function of time, of a station (1205.18) displaced horizontally about 750 feet from ground zero. The dots are the actual data points as read, and the solid curve is the smoothed interpretation applied by the analysts, showing a peak upward displacement of some 33.4 inches, occurring about 436 msec after the first motion was observed. I have drawn the dotted curve, which is the calculated curve for an object in free fall, starting with an upward velocity of about 160 inches per second. I think this agreement is about as good as that in Fig. 5.1, so I suggest that the phenomena are similar. In any case, a velocity of 160-180 ips was attained in about 20 msec, calling for an acceleration of at least 25-g peak.

Figure 5.3 represents similar data from a station (1205.17) about 900 feet from ground zero and somewhat farther from the mesa edge. Its peak upward displacement is about 20 inches, and the apparent curve does not fit a free-fall parabola well, so at this range the formation must have held together.

On this curve, like the others, the photographic data stop when the shock reached the camera. In this case, the surface has returned practically to zero, and still has a downward velocity of near 40 ips. For this one station on this shot we have pre-shot and post-shot survey data which show that it finally stopped about 19 inches below its original position. This is partly in accord with data from permanent displacement surveys on Rainier, where the permanent displacements were found to be downward and inward toward ground

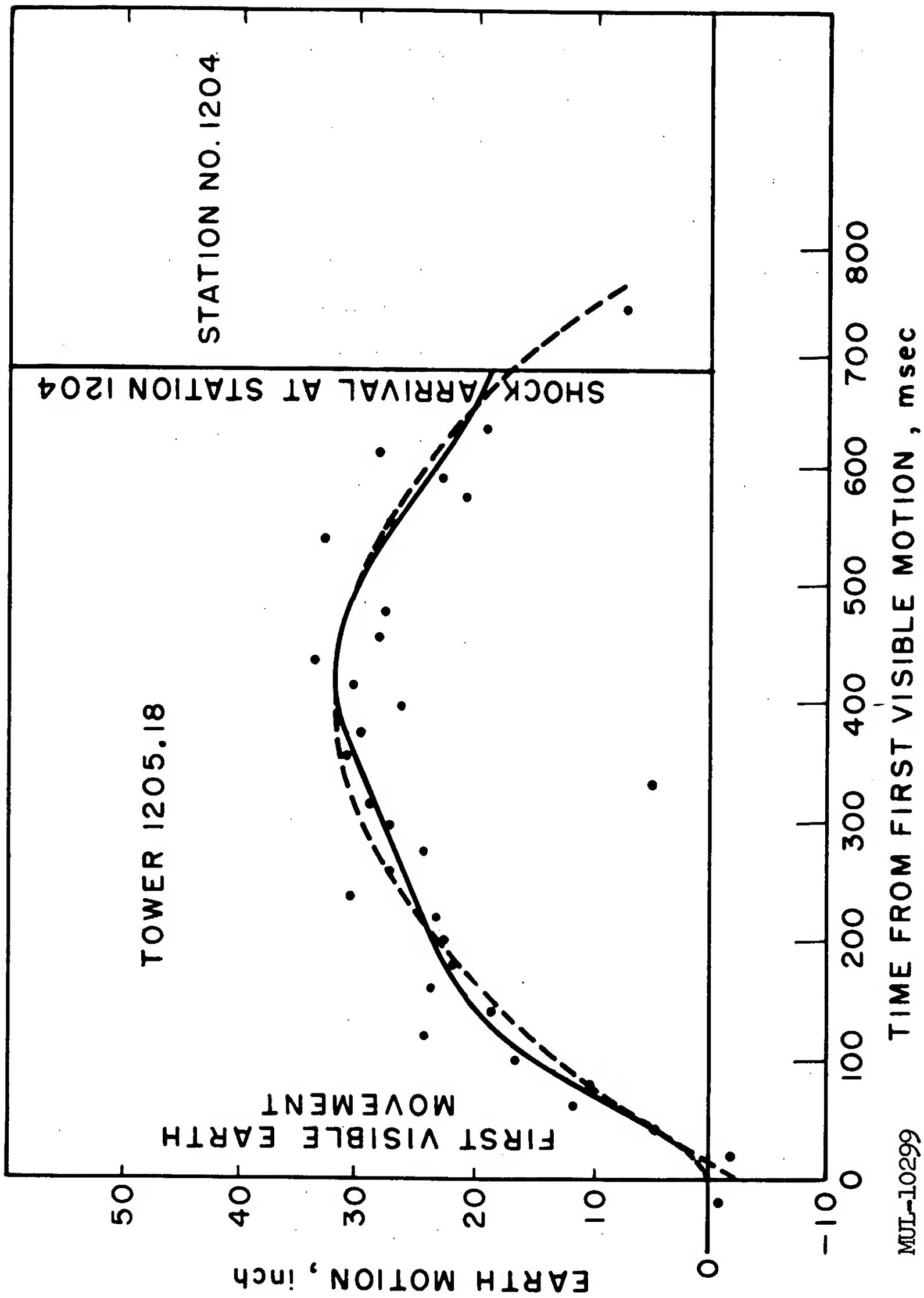
STATION NO. 1204
SHOCK ARRIVAL AT STATION 1204
TOWER 1205.18
FIRST VISIBLE EARTH MOVEMENT
EARTH MOTION, inch
50
40
30
20
10
0
-10
0
100
200
300
400
500
600
700
800
TIME FROM FIRST VISIBLE MOTION, msec
MUL-10299

Fig. 5.2

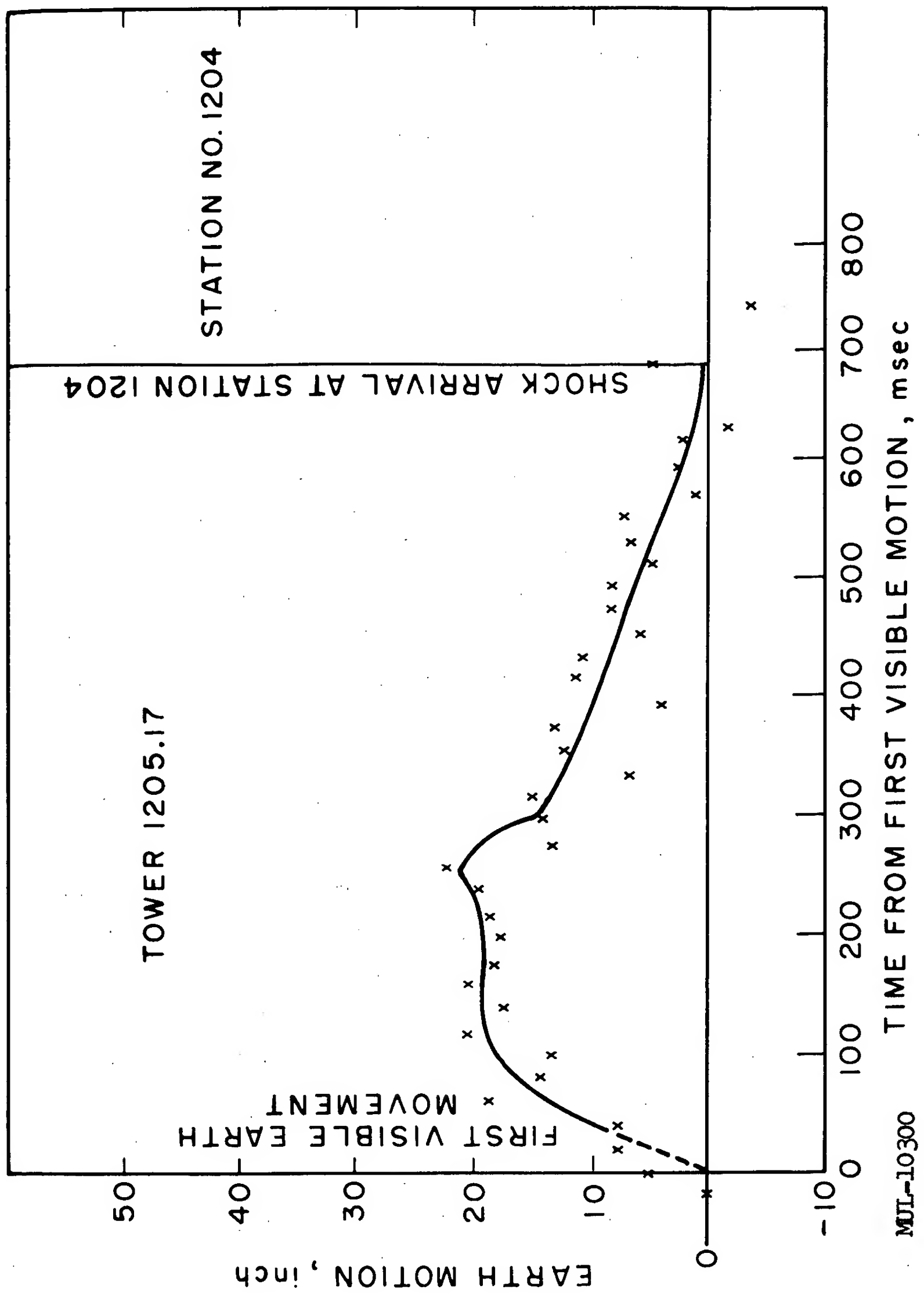
TOWER 1205.17
STATION NO. 1204
SHOCK ARRIVAL AT STATION 1204
FIRST VISIBLE EARTH MOVEMENT
EARTH MOTION, inch
50
40
30
20
10
0
-10
0
100
200
300
400
500
600
700
800
TIME FROM FIRST VISIBLE MOTION, msec
MIL-10300

Fig. 5.3.

zero. On Rainier, though, the displacements were small, none over 2 inches downward. The permanent displacement of the station 1205.18 on Blanca was large but not meaningful. It was near the edge of the cliff, and fell off.

Returning to Rainier, we have data on the ground motion as a function of time at a number of ranges. As might be expected, these fall off rapidly with distance. Figure 5.4 shows a profile, with the vertical scale greatly exaggerated, of the vertical displacements at different times. Superimposed is a curve which represents the calculated shape of the hump produced in an elastic medium by a pressure center at the depth of shot Rainier. The difference, though marked, is not surprising in view of the inelastic and layered condition of the medium and the fact that we are comparing a dynamic result with a static calculation.

In forming the hump shown here, an appreciable tensile strain was produced in the near-surface formations. Rocks of the general types found at the Nevada Test Site simply have no tensile strength in the gross form. An individual small rock may have appreciable strength, but in the rock in place there are faults and joints at frequent intervals, so that when a tensile strain is applied, cracks form every few feet. On Rainier, these cracks were small — they probably did not open more than two or three inches at their widest, and they all re-closed almost immediately.

Figure 5.5 shows the strain at the surface at ground zero, as measured by a gauge with a total span of 50 feet. The maximum observed was about four parts per thousand, or 0.4%. In the total span of 50 ft, this represents an elongation of about 2-1/2 inches. Post-shot observations showed that several cracks were covered by this span, so that at their widest these cracks could not have been open more than a couple of inches.

On the other hand, some of the cracks formed in the surface by shot Blanca must have been quite large, even when we do not include those quite near the edge of the cliff. A peak-recording strain gauge with a 50-foot span, located at station 1205.17, showed a peak strain of about nine parts per thousand, about twice the maximum recorded on Rainier, even though this station was about 900 feet from ground zero. Figure 5.6 is a photograph of the post-shot surface conditions near that station. Note that there is considerable vertical displacement across these faults. There is reason to believe that at-least some of the cracks opened quite wide, but most of them re-closed almost immediately.

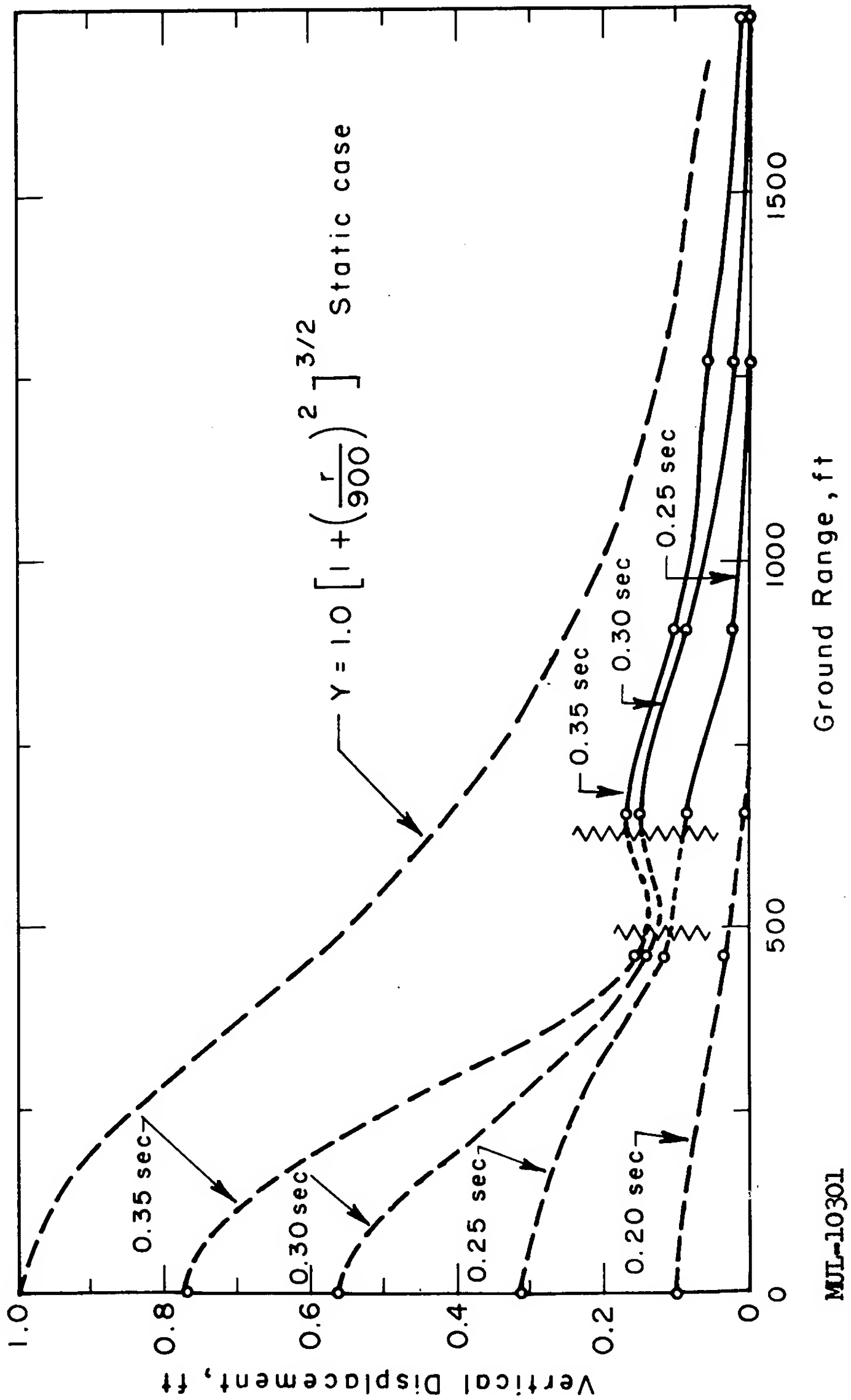
Vertical Displacement, ft
1.0
0.8
0.6
0.4
0.2
0
0.35 sec
0.30 sec
0.25 sec
0.20 sec
Y = 1.0 [1 + (r/900)^2]^3/2 Static case
0.35 sec
0.30 sec
0.25 sec
1500
1000
500
0
Ground Range, ft
MUL-10301

Fig. 5.4.

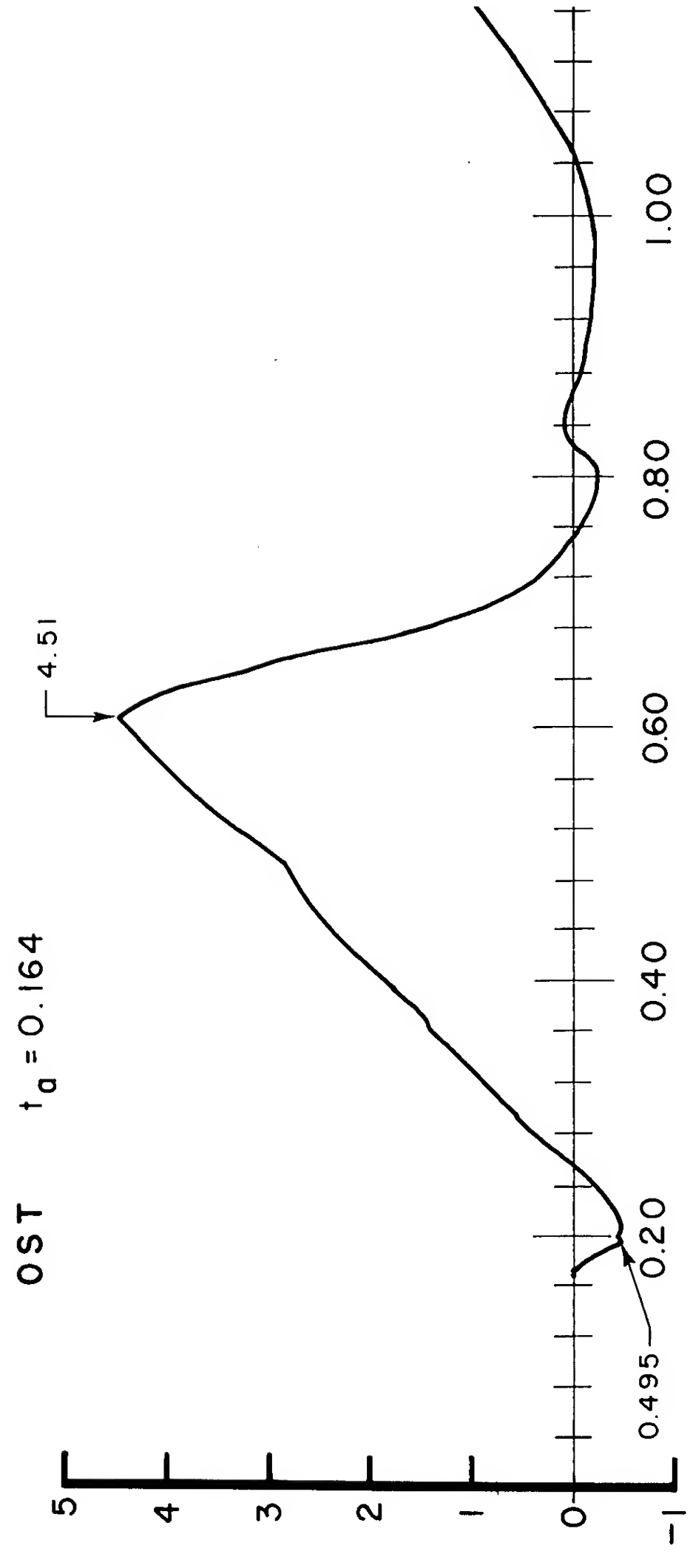
1.00
0.80
0.60
0.40
0.20
0.495
4.51
t_a = 0.164
OST
5
4
3
2
1
0
-1
Time, sec
Strain, ppk
MU-10302

Fig. 5.5.

SN-20960

Fig. 5.6.

In discussing the surface phenomena, I have avoided much discussion of movements on the slope of the mesa, since it would seem that many such movements can be utterly disproportionate to the excitation that caused them. The material of this slope is quite naturally lying at the maximum slope which is stable. Occasional slides occur naturally, from weathering, etc. It seems inappropriate, then, to pay much attention to the quantitative displacements of portions of the cliff which are displaced by the shock but which fall or roll great distances down the slope. On shot Rainier, an effort was made to measure the transient motion of a series of outcrops along the slope, but the gauges were either destroyed or disturbed by the rock slides, and the data obtained were not very helpful.

In summary, then, we may describe the close-in surface effects of a deep underground explosion as follows:

a. The first arrival is a relatively sharp pulse of upward acceleration which imparts an upward velocity to the surface formations.

b. Under the influence of this velocity, the surface continues upward, being decelerated only by the force of gravity or a little more, so that there is an appearance of a slow upward "heave."

c. During this upward movement, cracks tend to form in the surface, but there is little tendency toward lateral or vertical displacements across the cracks, unless a major discontinuity of the formation intersects the surface.

d. After reaching its peak, the "hump" falls back to its original position, landing with a second shock. At this time, most of the cracks close, except for those which are somehow wedged apart by loose rocks. In some cases, there are distortions producing vertical or lateral displacements across the cracks.

e. If venting occurs, it is usually in the late stages of c or d, unless the burial is really to be classed as shallow. In case of full containment, d is followed by more or less irregular vibrations, largely caused by reflections or refractions from irregularities in the formation.

f. The final position of points on the surface near ground zero has been found lower than their original position. This is not necessarily a general case – I have observed permanent humps from small contained shots, but this may not be possible with large shots.

g. The effects fall off rapidly with distance from ground zero. The peak accelerations tend to be proportional to the inverse fourth power close-in,

shifting rapidly to the inverse cube of the range; the peak displacement does not fall off so rapidly, since the frequency changes as well. At quite great distances, the rate of decline decreases, since indirect propagation effects become prominent.

6. SEISMIC MEASUREMENTS

Carl Romney

Headquarters, U. S. Air Force

I. INTRODUCTION

This report presents preliminary technical conclusions based on the analysis of seismograms recorded at more than 40 stations at the time of the Rainier explosion (September 1957) and seismograms recorded at more than 90 stations at the time of the Hardtack underground nuclear explosions (October 1958). Recordings are available for five underground nuclear explosions ranging in yield from about 50 tons to 20 kilotons. The basic information on the shot times, locations (including depth of burial) and yields of explosions has been made available to seismologists by the Atomic Energy Commission.[1]

II. FIELD PROGRAM

When it was recognized that the underground nuclear explosions planned for Operation Hardtack could provide important basic scientific information of value to seismologists, the Air Force undertook a program for the measurement of seismic effects from these shots. With the assistance of a contractor (The Geotechnical Corporation), the Air Force was able to install 17 temporary seismic stations.

The results to be reported here depend to a large extent on the measurements from these temporary stations supplemented, where possible, by data from the U. S. Coast and Geodetic Survey stations and from many stations operated by universities. Because of the vast amount of information available, the present report will be limited to a summary of the chief conclusions of interest to seismologists.

A. Location of Temporary Stations

The stations were disposed at distances extending from 60 kilometers from the shot points to a distance of slightly more than 4000 km. Many of the temporary stations were equipped with vehicles enabling them to move to various locations as required. The temporary stations were situated generally along a line extending eastward from the Nevada Proving Ground to Arkansas and thence

[1] AEC release on Hardtack, March 10, 1959, No. B-39. Also refer to Table I on page 81.

northeastward to Maine (Fig. 6.1). Each operating site and alternate sites had been preselected by a team of geologists who located suitable outcrops of hard rock remote from obvious sources of man-made noise. It was planned that five temporary stations would remain at fixed locations to provide control data on all shots, and it was hoped that the remaining ten mobile stations could be moved between shots in order to increase the amount of recorded data. These mobile teams were in fact able to move between shots Logan and Blanca. In all, recordings were made by the Air Force teams at 28 different distances from the shot point. Successful recordings were thus made at intervals of approximately 100 km out to 2300 km, and at intervals of about 250 km thereafter to a distance of 4000.

B. Equipment

The temporary stations were all equipped with Benioff short-period vertical seismographs; twelve of them were additionally equipped with two horizontal components which were oriented along the transverse to the path from the shot point to the station. Each station was provided with a good timing device and means for recording time signals from WWV on a continuous basis. Each station also was provided with equipment for calibrating the seismographs and for determining the polarity of each instrument under operating conditions. In addition, special efforts were made to check both the polarity and the calibration by independent methods at one time or another during the course of the observations.

III. TECHNICAL RESULTS

A. Longitudinal Waves

1. Amplitude-Yield Relation for P Waves

The Hardtack underground explosions produced almost identical waveforms at any given station. It was therefore possible to measure the amplitude of each shot at several corresponding points within the wave train. The separate measurements were then divided by the corresponding amplitudes recorded from Logan so that all results are normalized to Logan amplitude equals 1.0. The results of these observations are shown in Fig. 6.2. It may be seen that the points described in approximate first power relation between amplitude and yield. For reasons which are not understood, the amplitudes from shot Evans were less than one-tenth of those from Tamalpais, although the two shots released approximately the same amount of energy (55 and 70

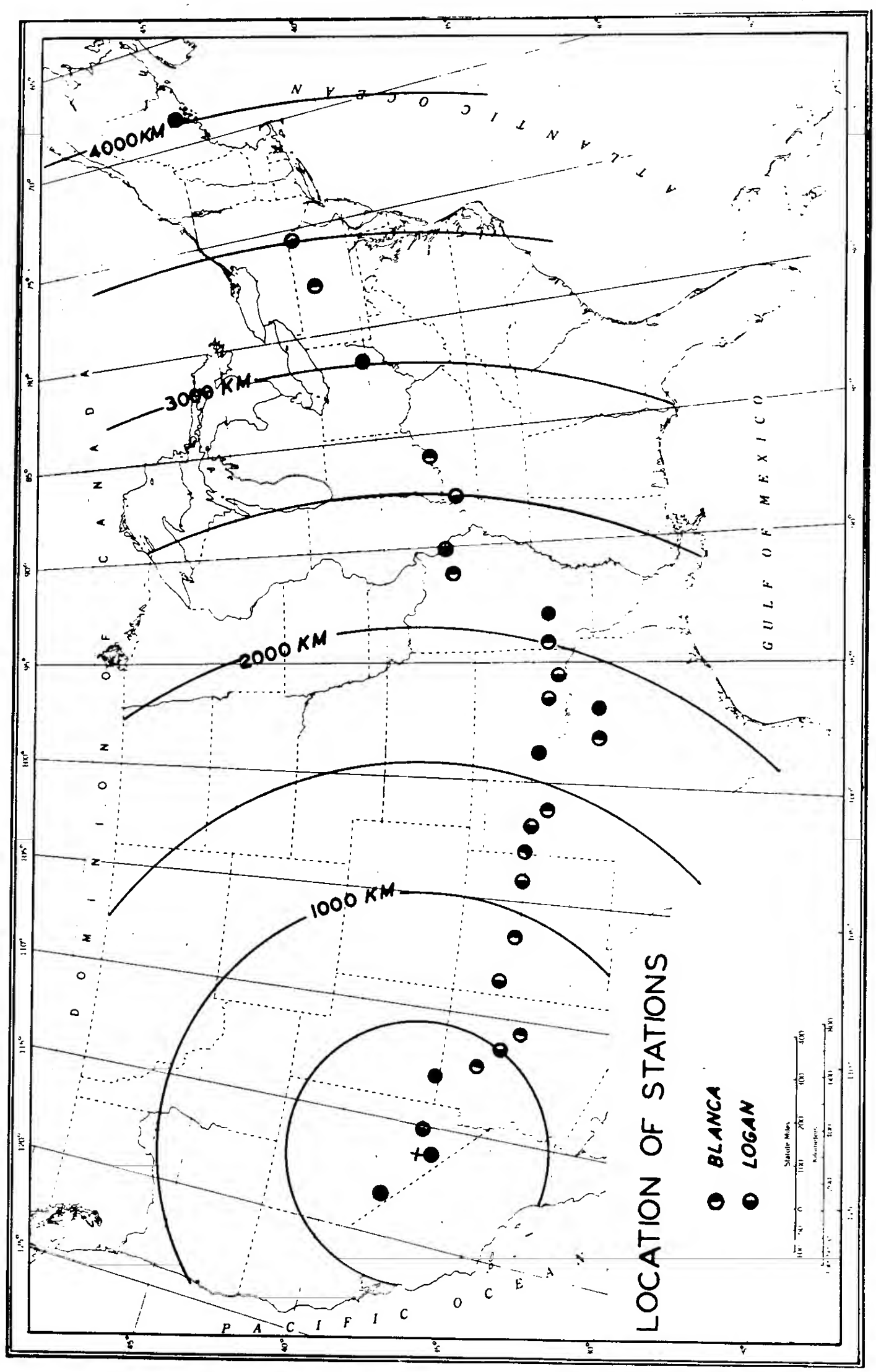

Fig. 6.1.

MUL-10226

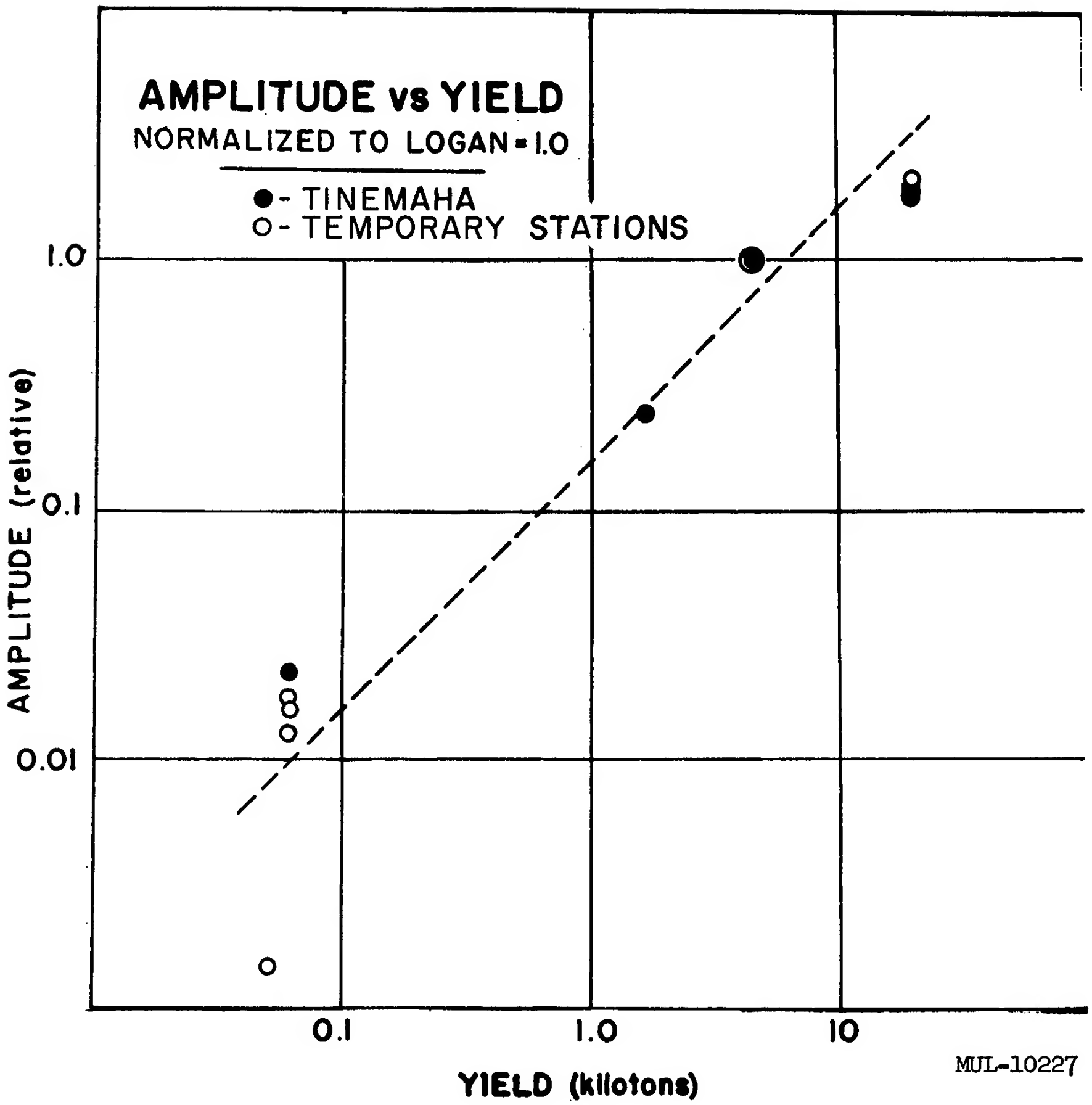
AMPLITUDE vs YIELD
NORMALIZED TO LOGAN = 1.0
● - TINEMAHA
○ - TEMPORARY STATIONS
AMPLITUDE (relative)
1.0
0.1
0.01
0.1
1.0
10
YIELD (kilotons)
MUL-10227

Fig. 6.2.

tons, respectively). For a comparison, the amplitudes recorded on the Wood-Anderson torsion seismograph at Tinemaha are plotted on the same graph. These measurements are of the maximum amplitudes in the shear waves rather than in the P wave group. It may be seen that the Tinemaha shear wave amplitudes have about the same dependence on yield as the amplitudes of P waves.

2. Amplitude of P Waves as a Function of Distance

The maximum amplitude in the first three cycles of P waves is shown as a function of distance in Fig. 6.3. The data indicated by the solid circles are from Blanca (20 kt). Logan data, indicated by open circles, were used to help define this curve by multiplying each observed Logan amplitude by 2.36, which was the average amplitude ratio of Blanca to Logan observed at fixed stations. Curves for other yields may be constructed by using the first-power scaling law mentioned above.

At distances between about 200 and 1000 km the amplitudes of Pn are inversely proportional to the cube of the distance, confirming measurements made from earthquakes and previously reported in the literature of seismology.

From about 1200 to 2000 km a strong P-wave arrival was observed in the "shadow zone" discussed by Gutenberg and Richter in several papers on earthquake magnitudes. These large amplitudes are associated with longer period waves and late arrivals. The abrupt change in the amplitude-distance relationship, the travel-time anomalies, and the change in period imply that a new kind of wave begins to arrive at about 1200 km. Pn waves may well precede the new wave, but are too small to be detectable at these distances.

Beyond 2000 km, the amplitudes fall off slowly and regularly, except that there is a low amplitude region at 3300 and 3500 km. Logan was not detected at 3500 km and Blanca was not detected at 3300 km. In each case, measurements of microseismic noise showed that the P-wave amplitudes must be less than 10 millimicrons. Figure 6.4 shows a selection of the vertical component seismograms obtained at distances from 200 through 2650 km; the figure includes recordings of both shots. The seismograms are arranged in order of distance and aligned in time so that the arrivals should all lie along a straight line parallel to the distance axis if the speed of the P waves is 8.1 km/sec. The marks on the seismograms are at 10-sec intervals; upward motion on the seismograms is compressional motion of the earth. It may be seen that the direction of first motion is observed as compressional at some stations and rarefactional at others. There seems to be no systematic dependence upon

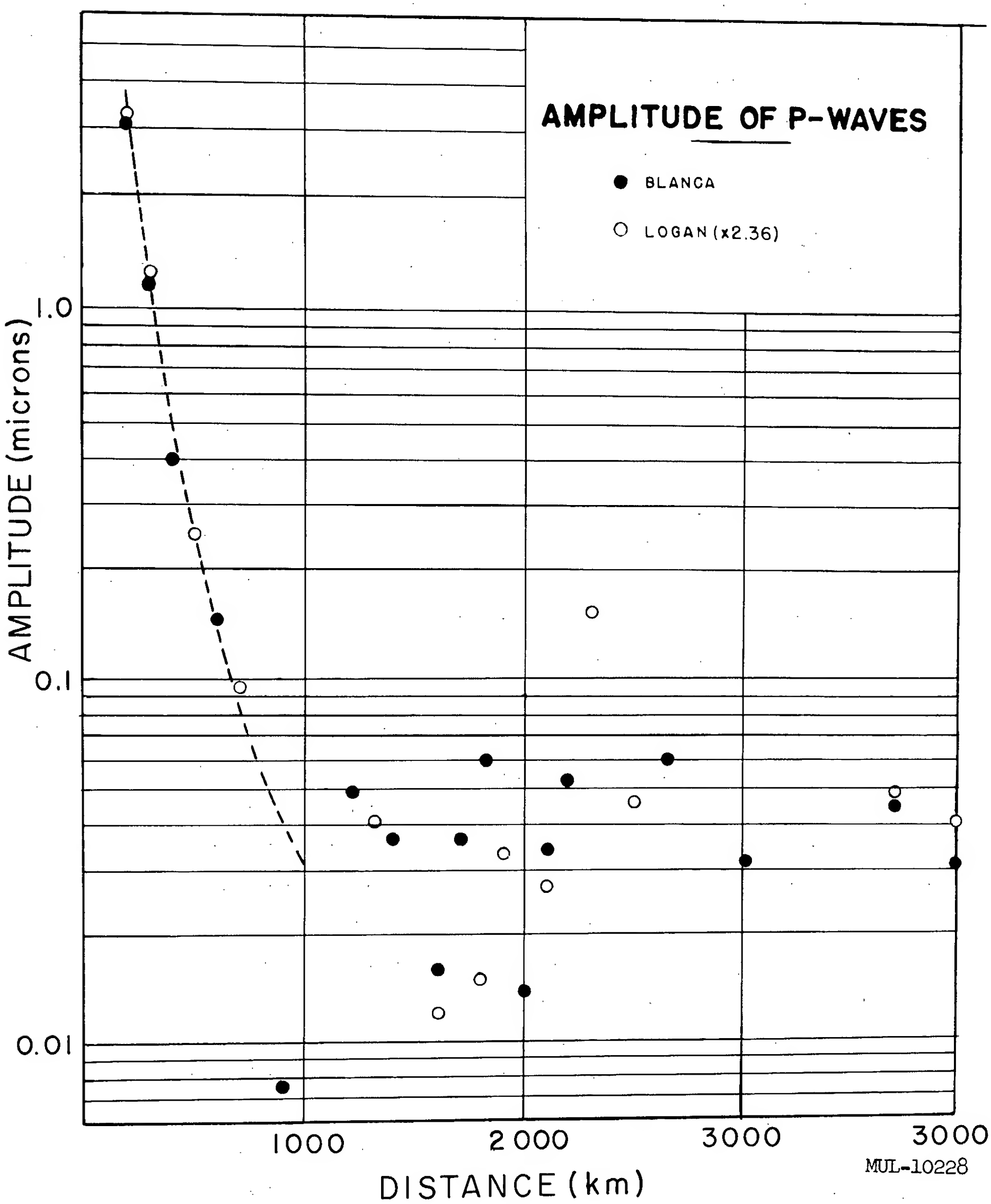
AMPLITUDE OF P-WAVES
BLANCA
LOGAN (x2.36)
AMPLITUDE (microns)
1.0
0.1
0.01
1000
2000
3000
3000
DISTANCE (km)
MUL-10228

Fig. 6.3.

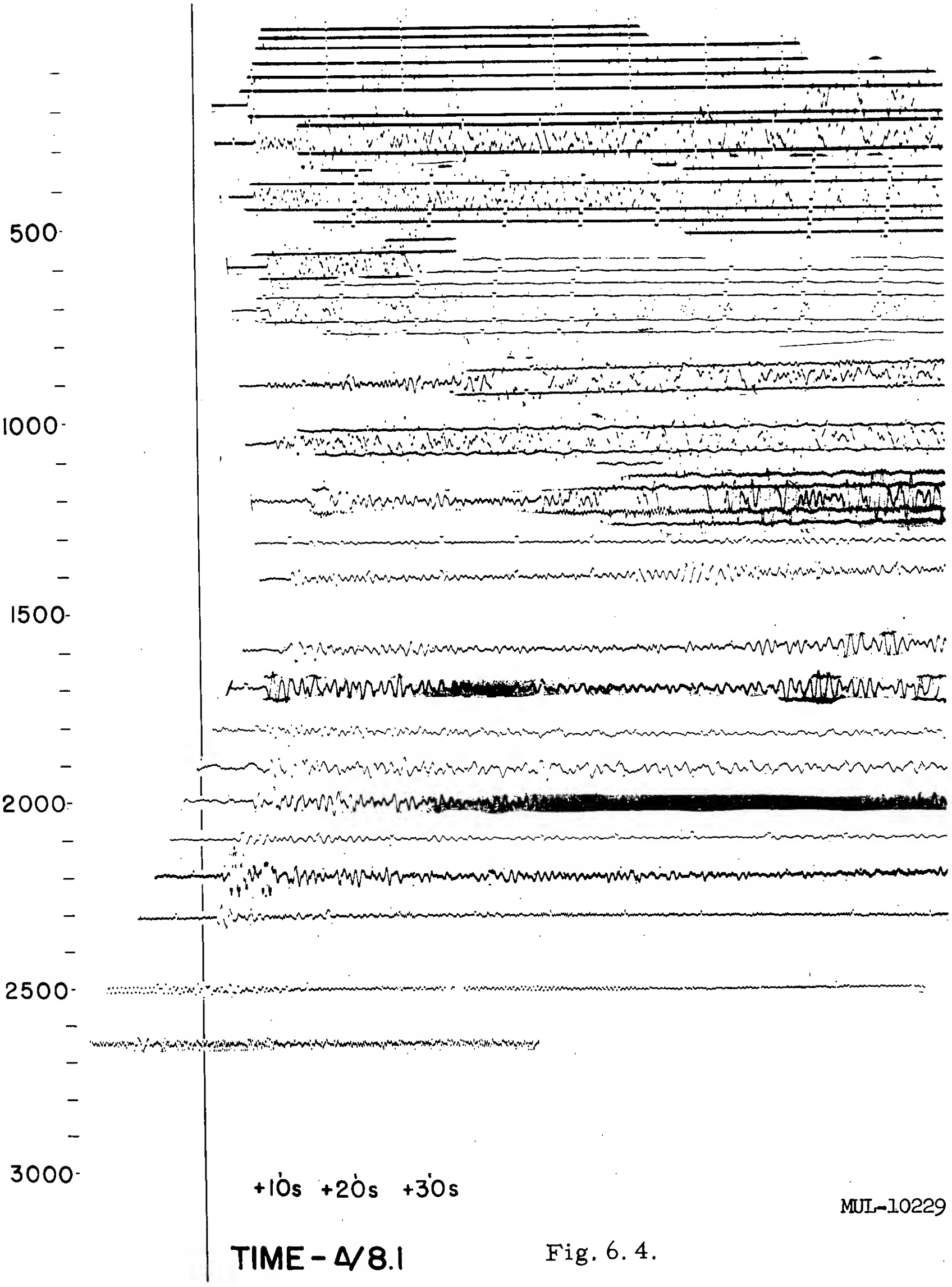

MUL-10229

Fig. 6.4.

the distance. At some stations (e.g., the station at 2300 km) there is apparently clear rarefactional first motion in spite of a signal-to-noise ratio of at least 10.

3. Travel-Times of P-Waves

Figure 6.5 shows the observed times of P as departures from a velocity of 8.1 km/sec. Last year at the annual meeting of the Seismological Society, I reported that the travel times of P from the Rainier explosion fit the equation:

$$t = 6.9 + \Delta/7.9$$

between 180 and 1023 km from the source. The new data may be seen to agree with that interpretation. Beyond 1200 km, most of the data show higher velocity arrivals, which initially are late with respect to the formula mentioned. Between 1500 and 2500 km, the travel times and the pulse shapes show multiple arrivals which may be interpreted to show one or more cusps in the travel-time curve. I am unable to explain the arrivals in detail at the present time. It seems probable that new data will be required to understand the propagation paths. A more detailed study, with more data, should provide great insight into the velocity structure just below the earth's crust. Beyond 2500 kilometers, the times approximately fit the Jeffreys-Bullen and the Gutenberg 1953 travel time curves.

B. Shear Waves

Shear waves, arriving at a speed of about 3.5 km/sec, were observed to a distance of about 2000 km. These waves have not been analyzed in detail at the present time. As a general observation, however, it can be stated that the radial- and transverse-horizontal components of motion are approximately equal in magnitude, and that these, in turn, are approximately equal in size to the vertical component of motion. At some distances there is the appearance of several discrete arrivals which might help to confirm that these waves are high-mode Love waves propagated in accordance with a method suggested by Oliver. Amplitudes are shown in Fig. 6.6. The fact that these amplitudes vary as the inverse cube of the distance is not consistent with the interpretation that these are surface waves, however.

C. Surface Waves

Rayleigh waves were detected by long-period seismographs at Berkeley, California; Laramie, Wyoming; Fort Sill, Oklahoma; and Palisades, New York. In addition, there are clear indications of Love waves at Berkeley and

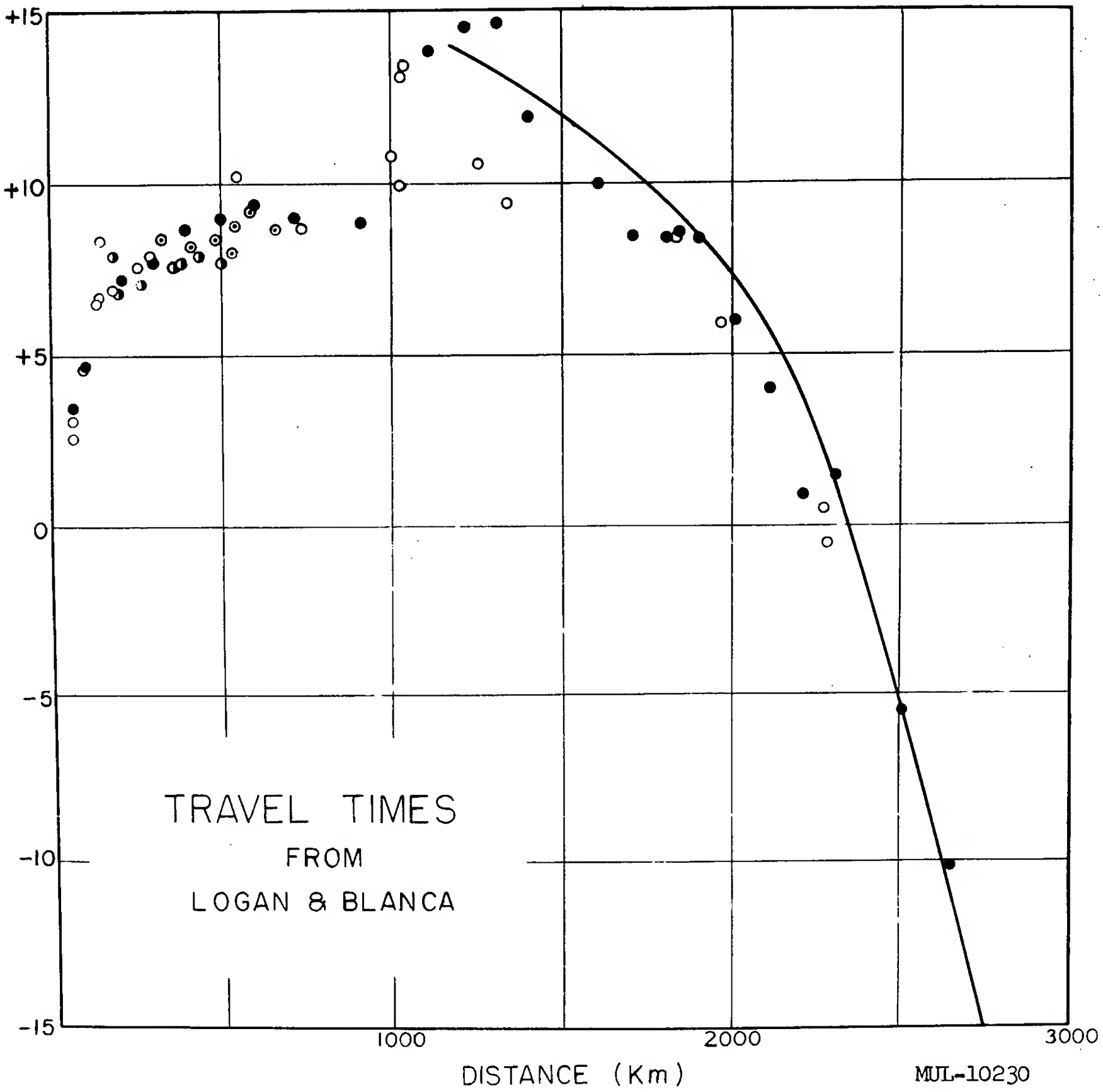
+15
+10
+5
0
-5
-10
-15
T-Δ/8.1 (Sec)
TRAVEL TIMES
FROM
LOGAN & BLANCA
1000
2000
3000
DISTANCE (Km)
MUL-10230

Fig. 6.5.

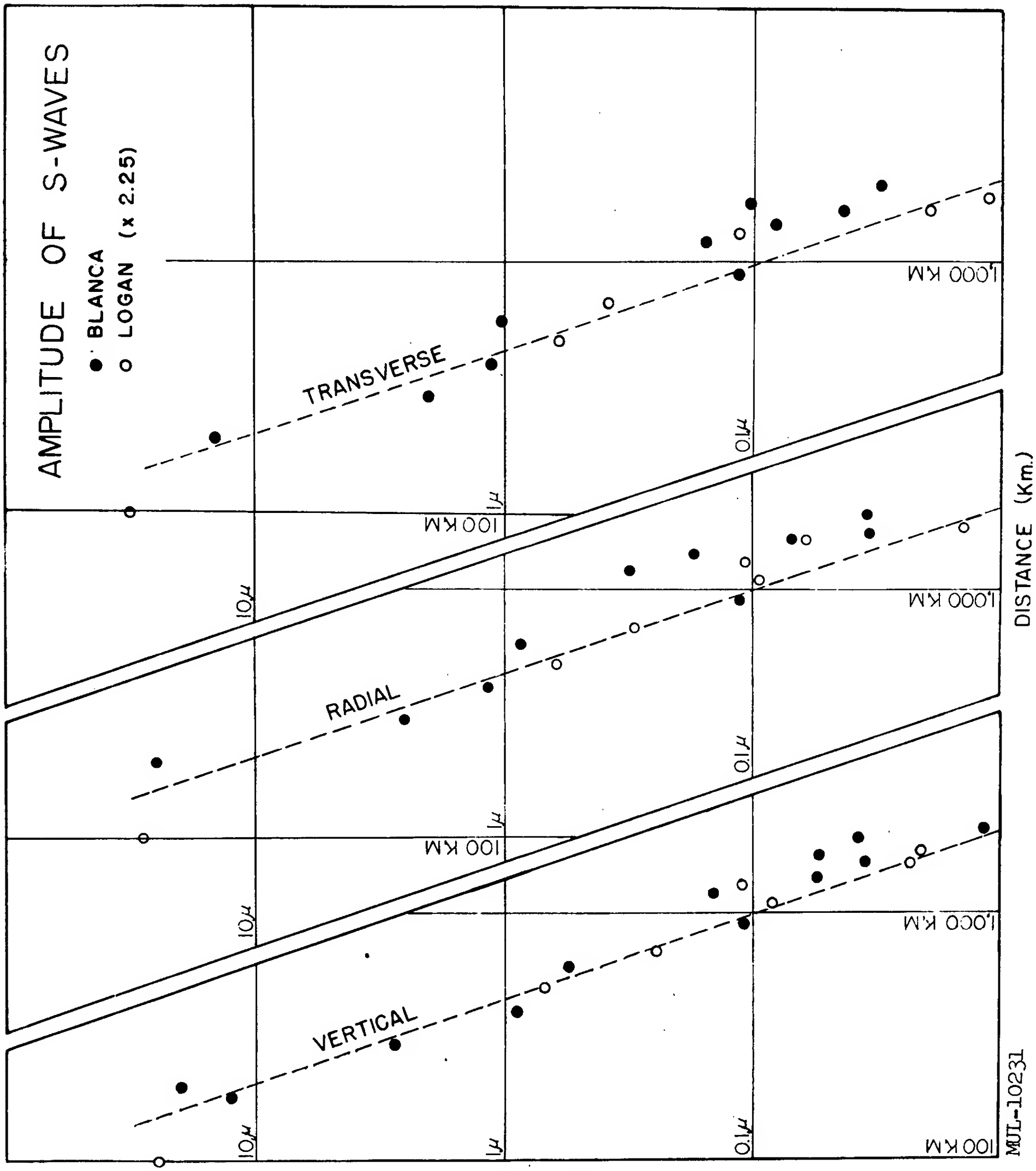
AMPLITUDE OF S-WAVES
● BLANCA
○ LOGAN (x 2.25)
TRANSVERSE
RADIAL
VERTICAL
10μ
1μ
0.1μ
100 KM
1,000 KM
AMPLITUDE (Microns)
DISTANCE (Km.)
MUL-10231

Fig. 6.6.

Palisades. These latter waves were completely unexpected from blasts, and their presence on the seismogram is believed to be due to mode conversion near the source, by processes which are not understood at the present time.

D. Magnitudes

Magnitudes were first determined for all shots recorded by Wood-Anderson torsion seismographs. It should be emphaiszed here that these magnitudes merely serve to compare the size of the seismic waves from blasts with those from earthquakes; it is not believed that the energies released can be compared by this means. The complete results are shown in Table I.

Table I. Magnitude Summary.

Station	Blanca	Logan	Rainier
Palo Alto	5.2	4.8	4.4
Berkeley	4.9	4.5	4.1
Mineral	4.8	4.4	4.3
Mt. Hamilton	5.4	5.0	4.7
USF	4.9	4.5	4.2
Tinemaha	5.1	4.8	4.2
Pasadena	4.8	4.4	4.0
Barrett	3.9	3.7	
Riverside	4.7	4.4	
Woody	4.2	3.9	

The magnitude of Blanca was found to be 4.8 ± 0.4* based on measurements from ten stations. The magnitude of Logan was found to be 4.4 ± 0.4* based on measurements from the same ten stations. Only seven stations recorded measurable amplitude for Rainier; these gave a magnitude of 4.25 ± 0.2*. The magnitudes for the smaller shots were observable only at one station and reliance should not be placed on these single estimates. It is perhaps important to note that if the magnitudes of Blanca and Logan are computed from the same seven stations that recorded Rainier, the result will be 0.2 of a unit higher than that found from the ten stations. The implication is strong that had the amplitudes been measurable at the other three stations (Barrett, Riverside, and Woody) the magnitude would have been estimated at 4.05 rather than 4.25.

Magnitudes were next computed for Blanca and Logan from nine and six stations, respectively, at greater distances. The results are: for Blanca, $M = 4.8 \pm 0.4$*; and for Logan, $M = 4.4 \pm 0.5$*. Thus, magnitudes estimated by the two methods are in agreement. Based on earthquake studies it might be expected that the magnitudes based on P-wave data from distant stations should exceed those based on shear wave data from nearby stations by about one-half magnitude unit.

A magnitude-yield relationship can be derived from the data so far presented. The basic definition of magnitude is

$$M = \log A_d - \log B_d \quad , \tag{1}$$

where A_d is the amplitude at distance d and B_d is the amplitude of a zero magnitude shock at the same distance. The observed relation between amplitude and yield (Y) is given by

$$A = K_d Y \quad , \tag{2}$$

where K_d is the amplitude observed at a distance d from an explosion of yield Y kilotons. From (1) and (2), it may be seen that

$$M = C + \log Y \quad , \tag{3}$$

where C is a constant [equal to log (K/B)] which can be evaluated if the magnitude is known for a given yield. Estimates for C can be made, based on the known yields and magnitudes of Rainier, Logan and Blanca. The relationship is then found to be

$$M = 3.64 + \log Y \quad .$$

This relationship may not apply for shots in other localities or in other media.

IV. SUMMARY

Seismic waves from recent underground nuclear explosions in Nevada were observed at a number of temporary stations along a line extending eastward to Maine. Studies of seismograms from these stations and from a large number of permanent stations have given the following tentative results:

(a) Between 150 and 1100 kilometers the times of P approximately fit a line of slope of 1/7.9 sec/km.

---

*Standard deviation of a single observation.

(b) At 1200 km a strong wave of higher apparent surface speed arrives about four seconds late with respect to the straight-line curve.

(c) Between 1200 and 2500 km the times and waveforms show multiple arrivals which may be associated with cusps in the travel-time curve.

(d) Short-period shear waves of speed near 3.5 km/sec were observed to about 2000 km.

(e) Between 200 and 1100 km the amplitude of P varies inversely as the cube of the distance.

(f) Between 200 and 2000 km the amplitude of S varies inversely as the cube of the distance. The vertical, radial, and transverse components are of approximately equal size.

(g) At large distances, the amplitudes of body waves are proportional to the first power of the explosive yield (Y).

(h) The explosions produced seismic waves equivalent in size to those from natural earthquakes of magnitude:

$$M = 3.6 + \log Y_{kt} \ .$$

7. TEMPERATURE AND RADIATION DISTRIBUTIONS IN THE RAINIER SHOT ZONE

J. L. Olsen, W. P. Bennett, and D. E. Nielsen

Lawrence Radiation Laboratory, Nevada

In an attempt to understand better the phenomenology of underground nuclear explosives and their applications to the Plowshare Program, extensive radiation and temperature measurements were made in the Rainier shot zone. Measurements are also being made at the present time in the shot zones of Blanca, Logan, Neptune and Tamalpais.

Prior to the Rainier event, some background temperature measurements were made in deep vertical holes at the Rainier site by the USGS.[1] Broadview Research Corporation made pre-Rainier temperature studies and did early planning for the post-shot temperature measurements for Rainier. The post-shot temperature and radiation measurements on this event and similar measurements on all subsequent underground nuclear detonations were conducted by LRL.

In order to make the measurements, it was necessary to drill holes through the zone of effect using standard underground drilling techniques with modifications for remote operations and radiation control. The cores taken from these holes were used for radiochemical analyses and physical properties studies.

The radiation distribution in the shot zones was determined by logging the drill holes for gamma radiation using a standard Jordon RAMS unit having a range of 1 mr/hr to 1000 r/hr. This unit utilizes as the detector a thick wall ionization chamber. For areas of low gamma intensity, a standard "Drill Hole" gamma probe was employed. This unit uses a Geiger tube mounted in a thick wall probe and has a range of 0.01 mr/hr to 20 mr/hr. Both units were calibrated with a Co^{60} source before and after each logging. The radiation values recorded are accurate to $\pm$ 15%.

Temperature distributions were measured using platinum resistance thermometers (100 ohms at 20°C) and thermistors (2000 to 18000 ohms at 20°C). These units were also calibrated before and after each logging. Calibration in

---

[1] T. C. Goodale et al., "Temperatures from Underground Detonation, Shot Rainier," Operation Plumbbob Report WT-1527, July 1958.

this case was done in a Fisher temperature bath using National Bureau of Standards mercury thermometers accurate to ± 0.05°C. The overall calibrations were reproducible to ± 0.5°C. The position accuracy for the probes in the holes was ± 6 inches.

Figure 7.1 is an elevation and Fig. 7.2 a plan view of the Rainier shot zone showing the locations of the drill holes and an exploratory drift driven through the zone.

The first hole drilled into the zone of effect was a vertical hole (No. R-6) drilled from the surface ground zero to a depth of 912 feet. This hole was completed approximately two months after the shot. No radiation above background (0.05 mr/hr) was detected in this hole to a depth of 848 feet. Measurements could not be made below 848 feet because of drilling tools lost in the hole. Gas and soil samples were obtained from the cavity (Fig. 7.1) 386 feet above the shot point. Radiochemical analysis of these samples showed a very small amount of Kr^{85} and traces of Nd and Y. Temperatures recorded in this hole by USGS (Fig. 7.3) were lower than the background temperatures measured by them in an adjacent pre-shot vertical hole (Fig. 7.4). This difference can be explained by the 68,000 gallons of drilling water (10 to 15°C) which were lost to the medium while drilling.

The B, C, and D holes (Fig. 7.1) were completed from 3 to 5 months after the detonation. Figures 7.5 through 7.10 show the results of the radiation and temperature measurements made in these holes both 5 and 18 months after the shot. In December 1958, the investigation of the Rainier zone, which had previously been suspended because of other activities at the test site, was resumed. Holes G, H, and I were drilled and an exploratory drift was driven as shown in Fig. 7.1. The results of the radiation and temperature measurements made in these holes are shown in Figs. 7.11 through 7.15. No radiation above background (0.05 mr/hr) was observed in the G hole. Figure 7.16 shows the radiation levels measured along the wall of the exploratory drift.

All of the radioactivity was found within a radius of 68 ± 9 feet from ground zero (Fig. 7.17) except for the small quantities of Kr, Nd and Y mentioned earlier.

Figure 7.18 is an isothermal plot of the temperatures observed in the B, C, and D holes approximately 5 months after detonation. Figure 7.19 is an isothermal plot of the temperatures observed in the B, C, D, G and H holes approximately 18 months after the shot. Temperatures above background were

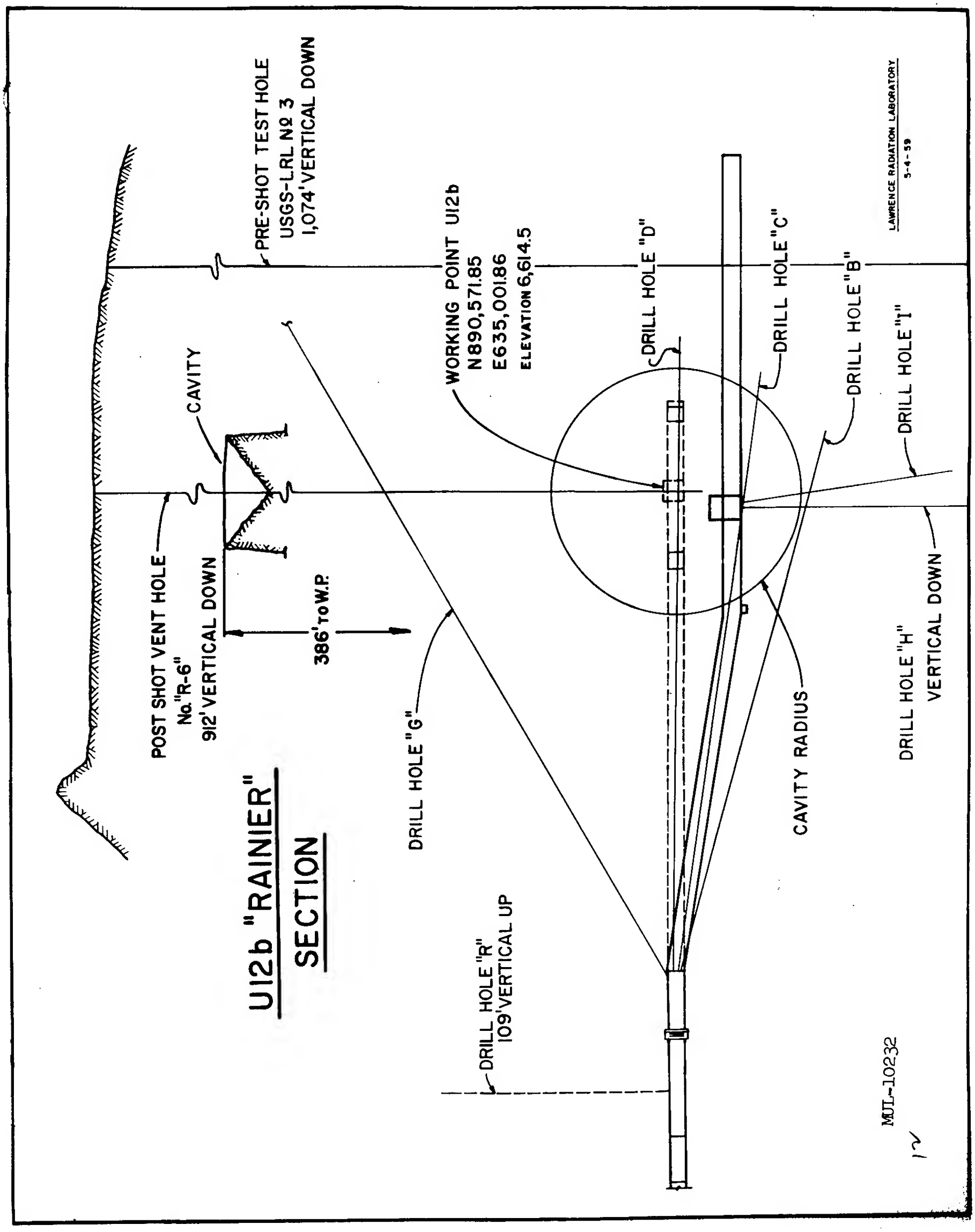
U12b "RAINIER"
SECTION
PRE-SHOT TEST HOLE
USGS-LRL Nº 3
1,074' VERTICAL DOWN
WORKING POINT U12b
N890,571.85
E635,001.86
ELEVATION 6,614.5
DRILL HOLE "D"
DRILL HOLE "C"
DRILL HOLE "B"
DRILL HOLE "I"
DRILL HOLE "H"
VERTICAL DOWN
CAVITY
POST SHOT VENT HOLE
No. "R-6"
912' VERTICAL DOWN
386' to W.P.
DRILL HOLE "G"
CAVITY RADIUS
DRILL HOLE "R"
109' VERTICAL UP
LAWRENCE RADIATION LABORATORY
5-4-59
MUL-10232

Fig. 7.1.

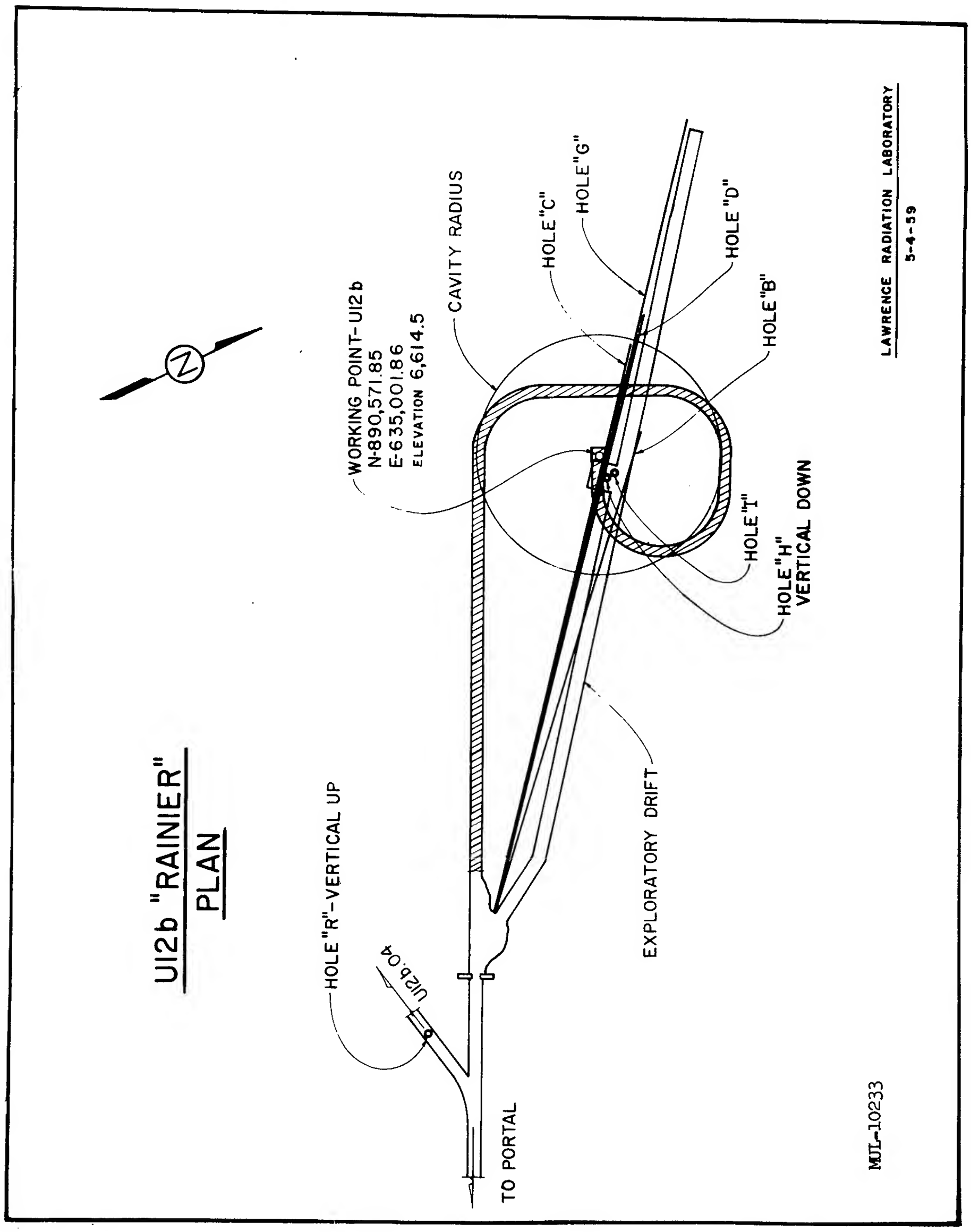
U12b "RAINIER"
PLAN
N
WORKING POINT-U12b
N-890,571.85
E-635,001.86
ELEVATION 6,614.5
CAVITY RADIUS
HOLE "C"
HOLE "G"
HOLE "D"
HOLE "B"
HOLE "I"
HOLE "H"
VERTICAL DOWN
HOLE "R"-VERTICAL UP
U12b.04
TO PORTAL
EXPLORATORY DRIFT
LAWRENCE RADIATION LABORATORY
5-4-59
MUL-10233

Fig. 7.2.

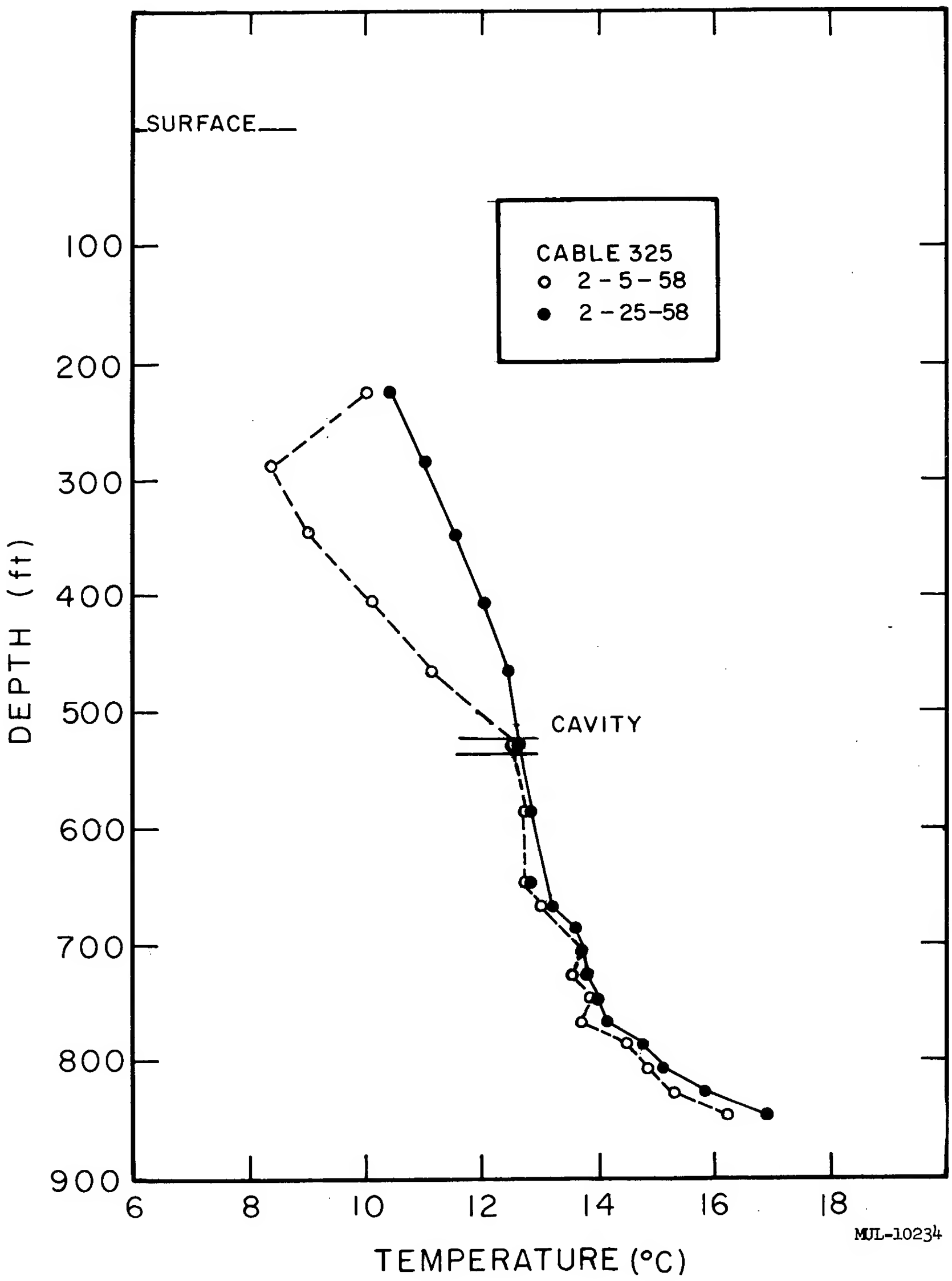

Fig. 7.3. Temperature vs depth in ground-zero vertical hole, as measured by USGS.

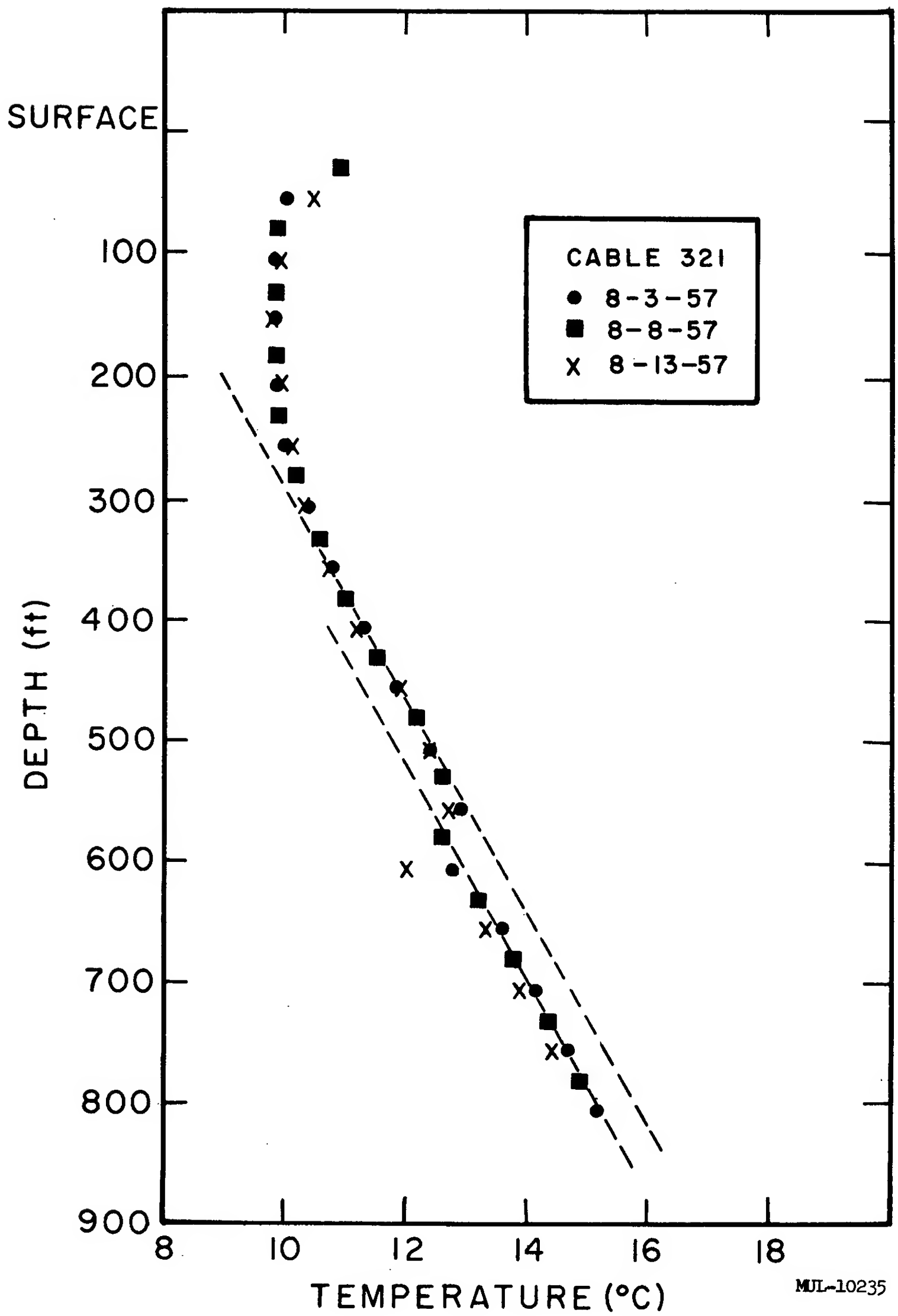

Fig. 7.4. Temperature vs depth in UCRL hole No. 3, as measured by USGS.

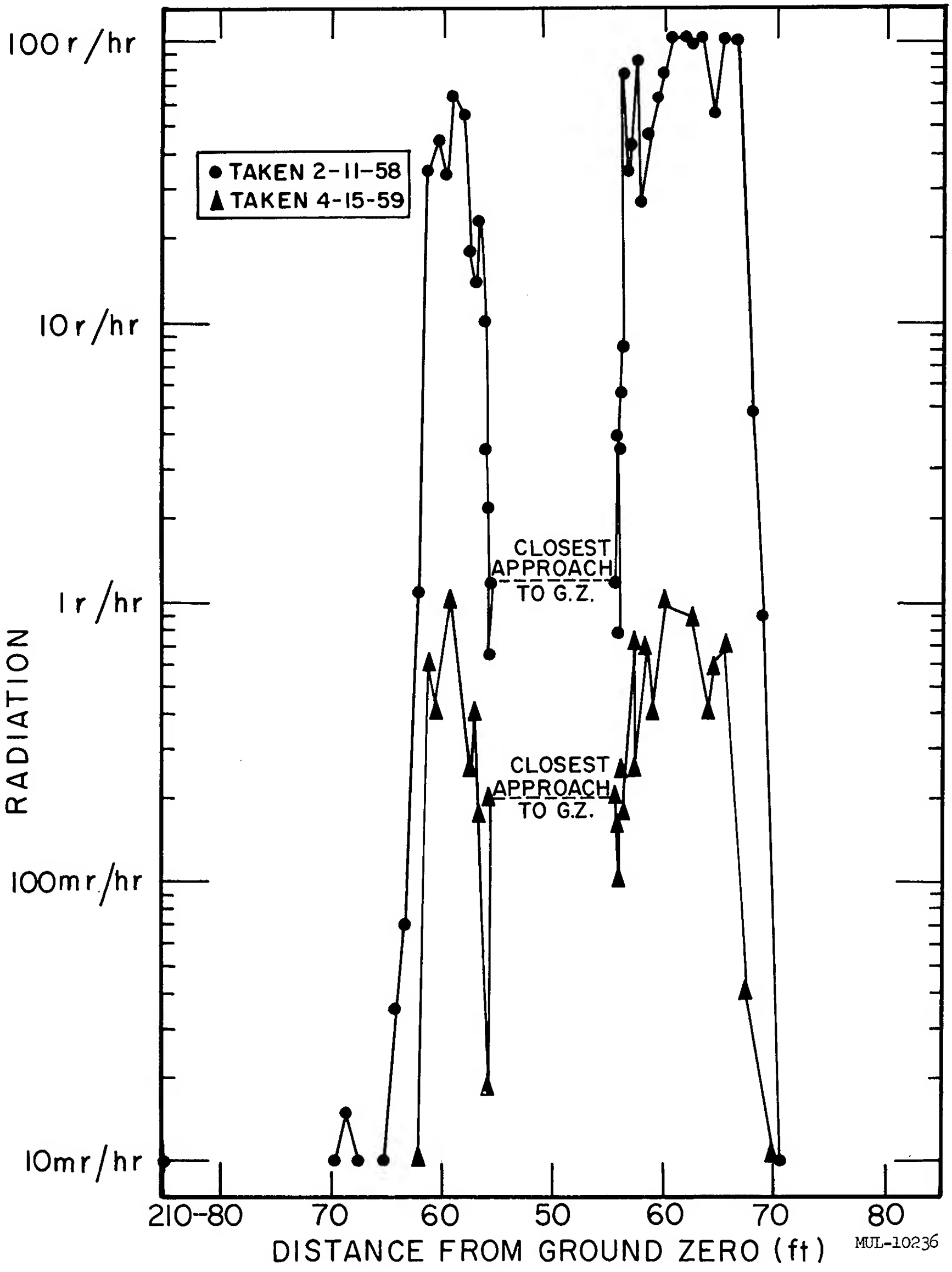

Fig. 7.5. Radiation measurements vs distance from ground zero, drill hole Rainier B.

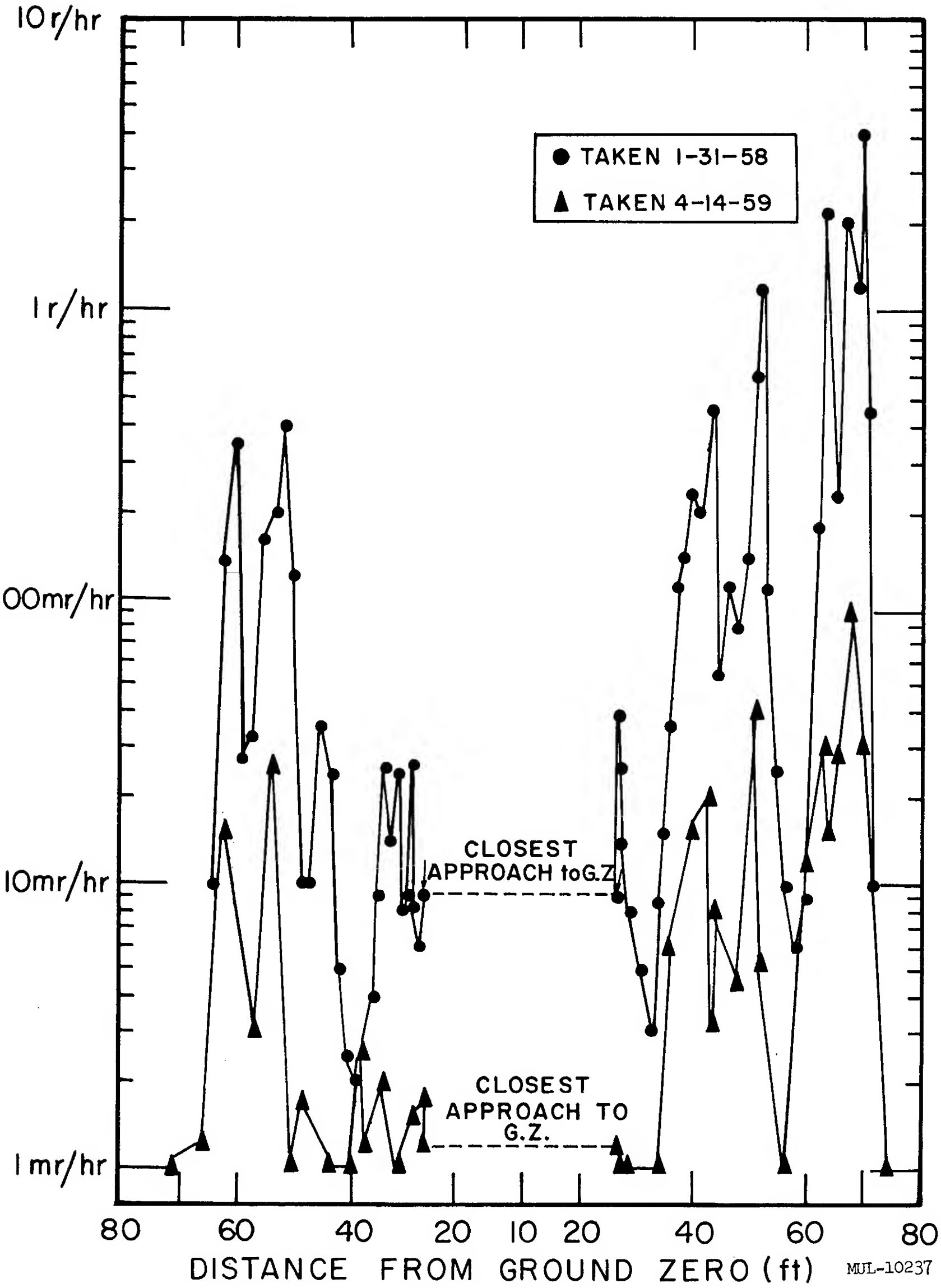

Fig. 7.6. Radiation measurements vs distance from ground zero, drill hole Rainier C.

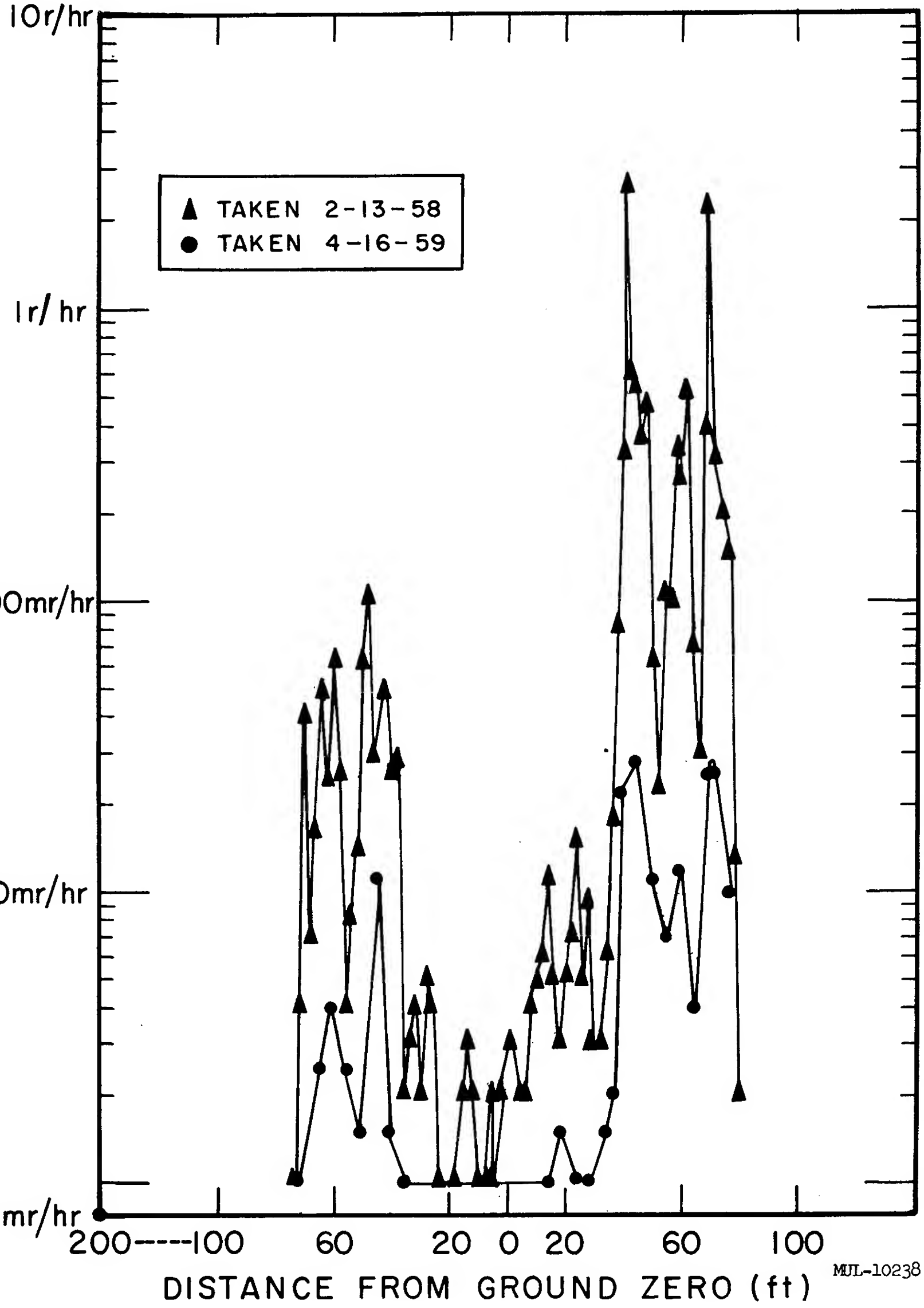

Fig. 7.7. Radiation measurements vs distance from ground zero, drill hole Rainier D.

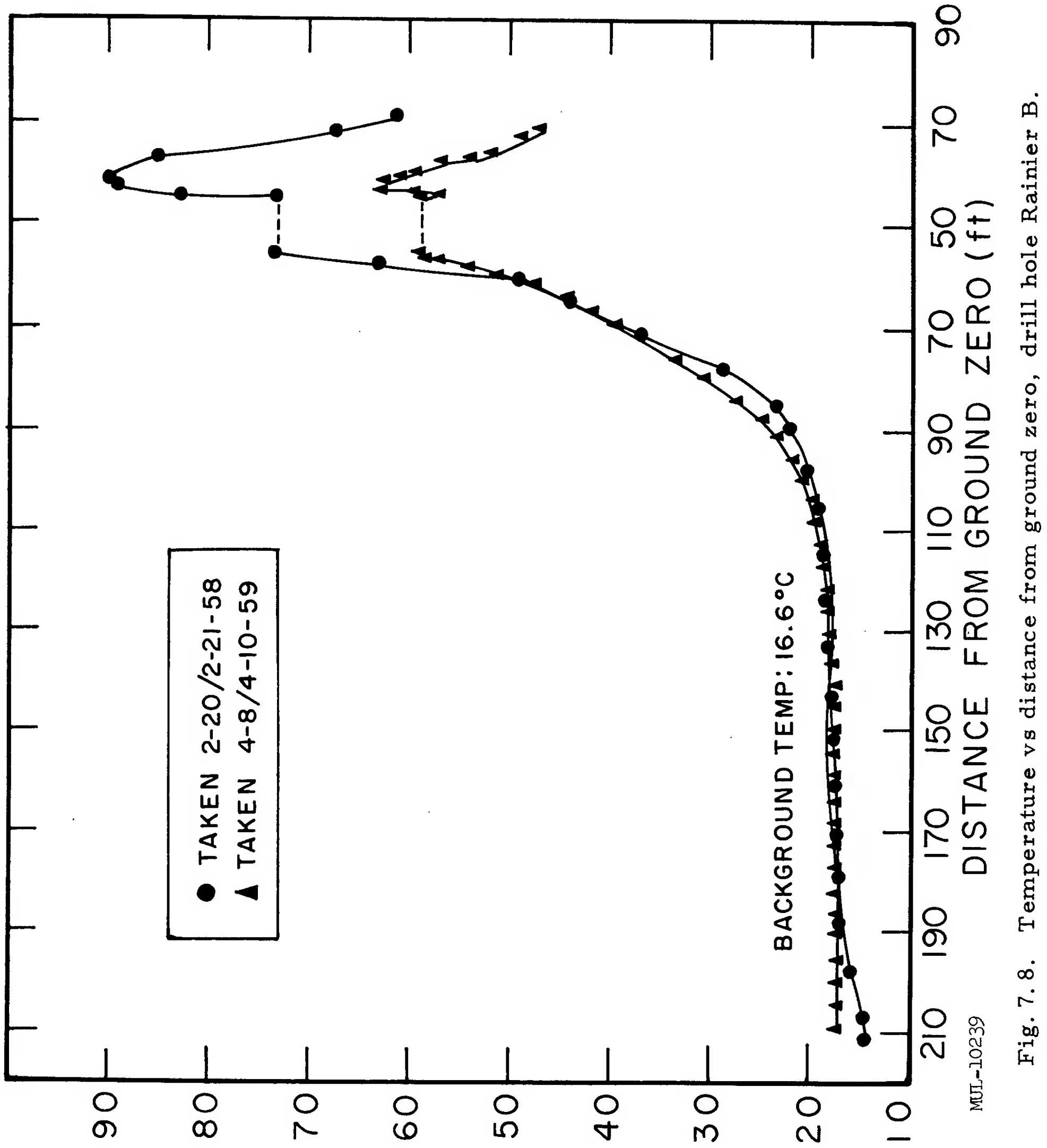

Fig. 7.8. Temperature vs distance from ground zero, drill hole Rainier B.

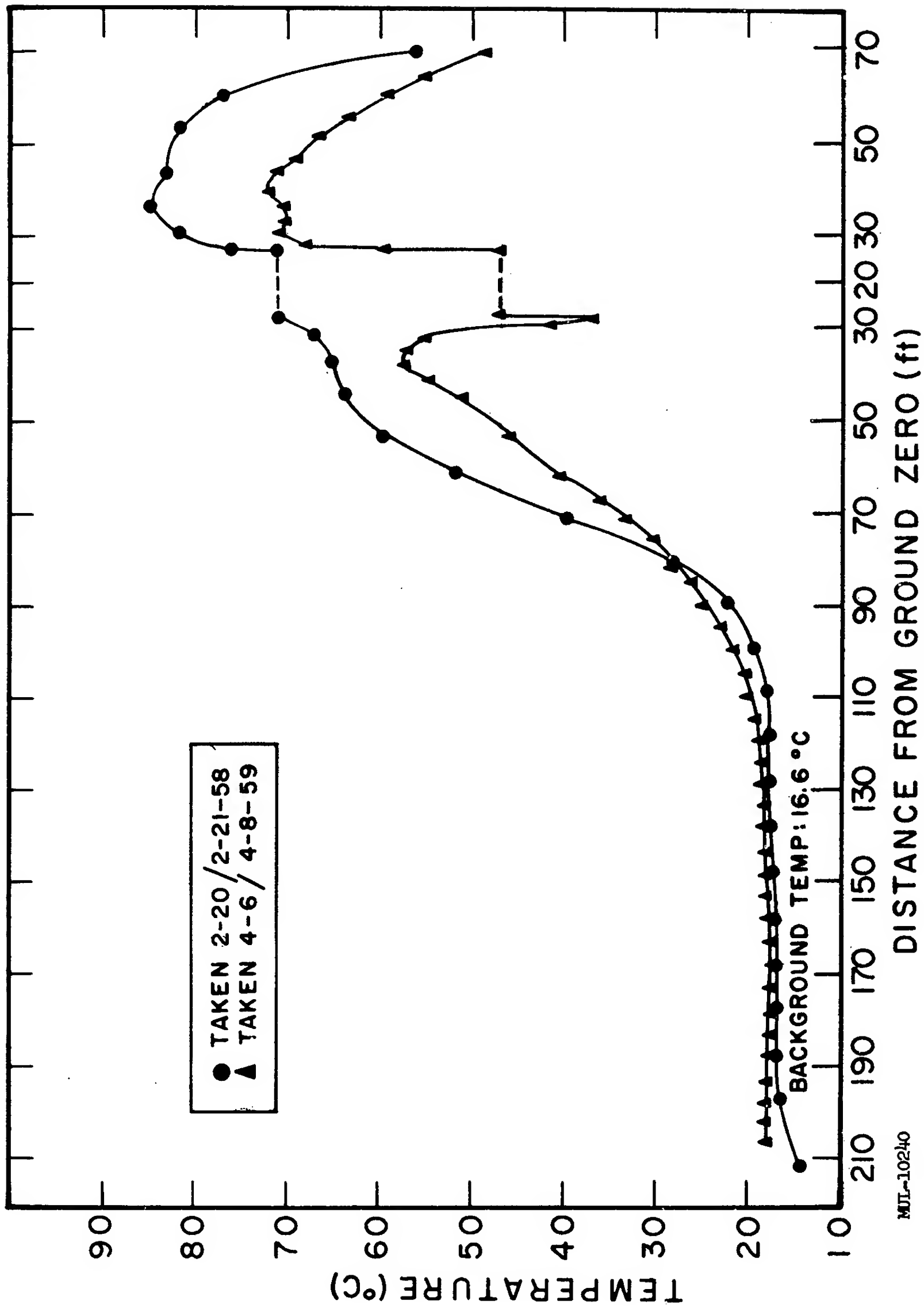

Fig. 7.9. Temperature vs distance from ground zero, drill hole Rainier C.

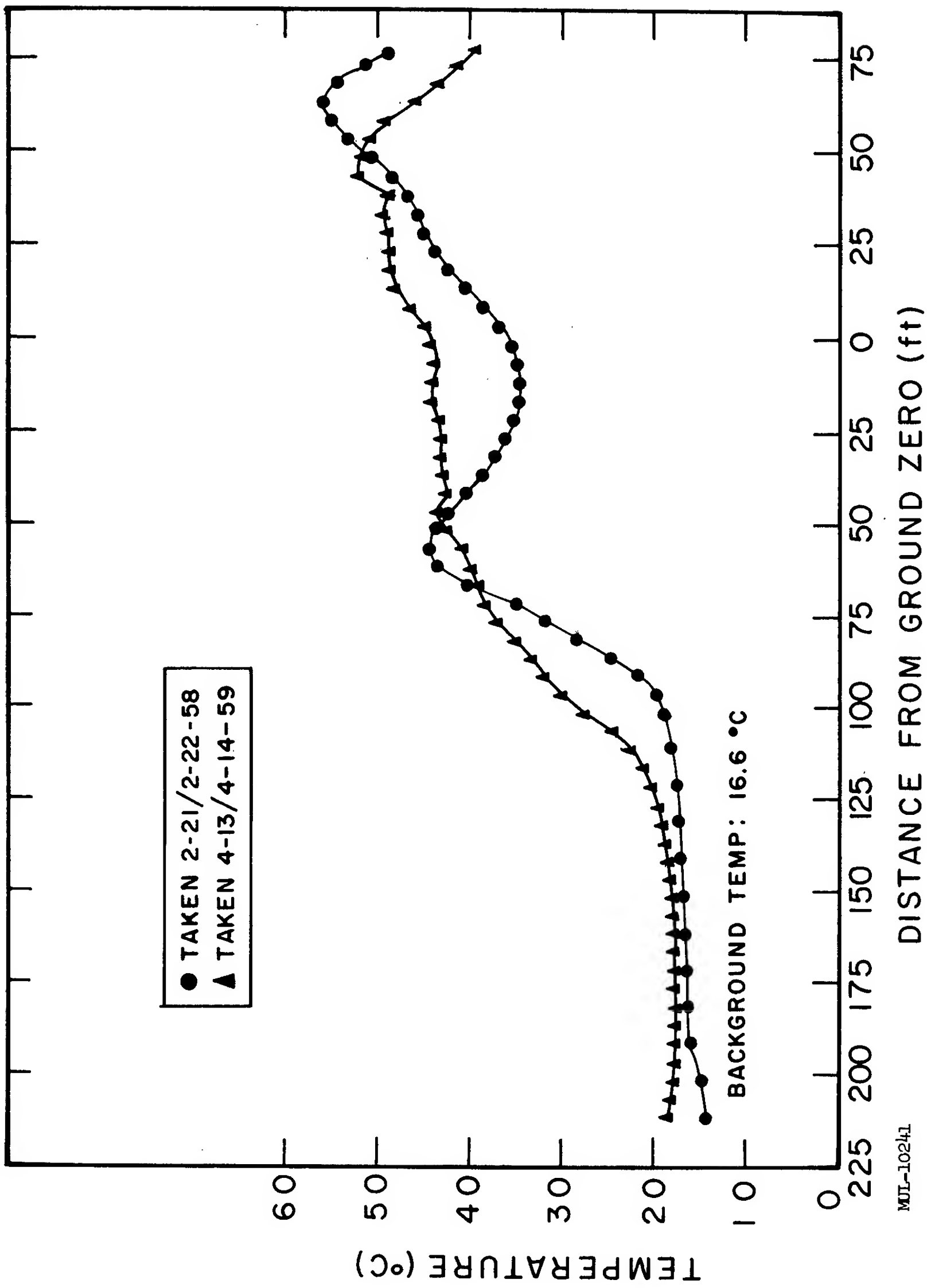

Fig. 7.10. Temperature vs distance from ground zero, drill hole Rainier D.

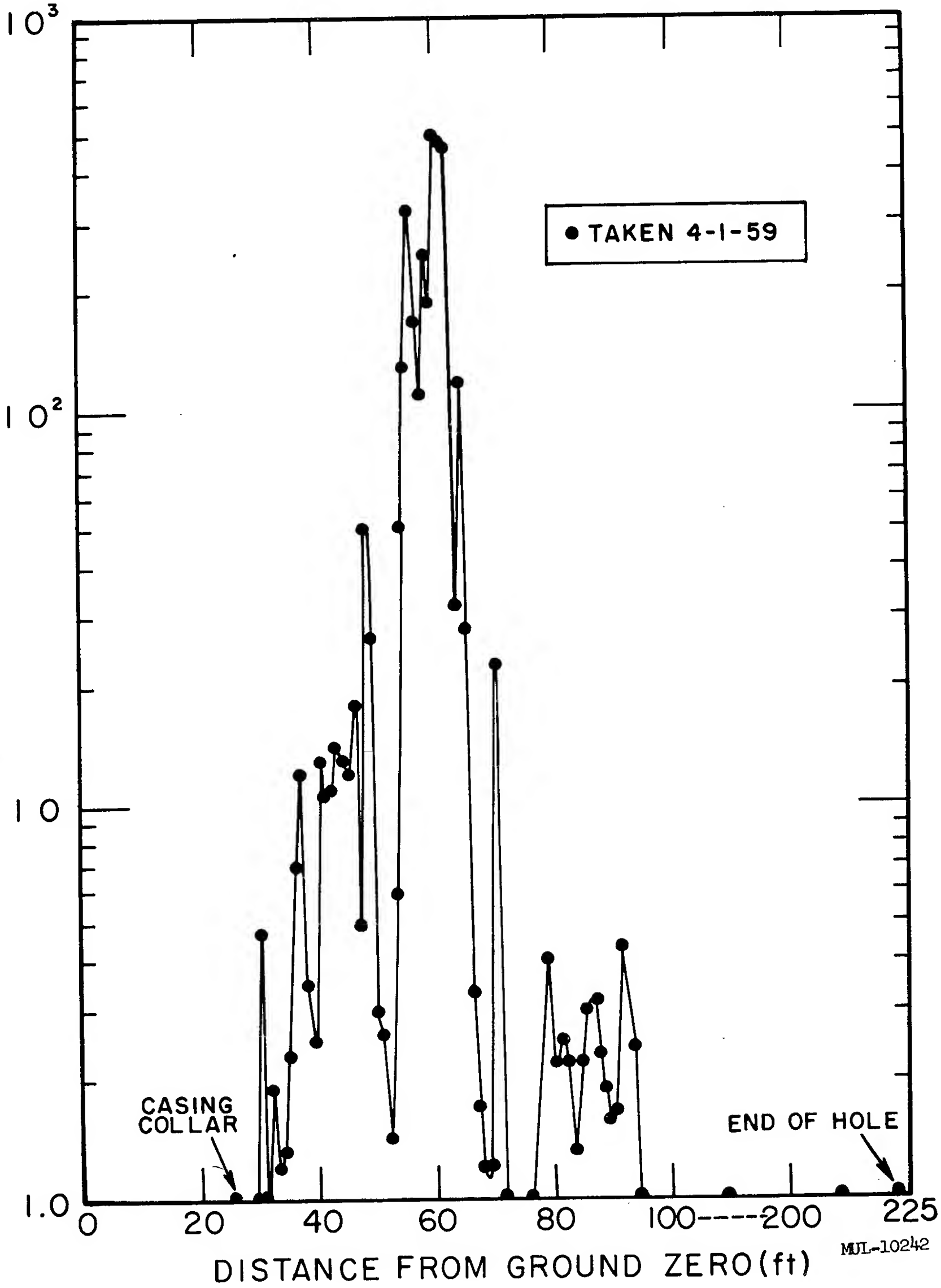

Fig. 7.11. Radiation vs distance from ground zero, drill hole Rainier H.

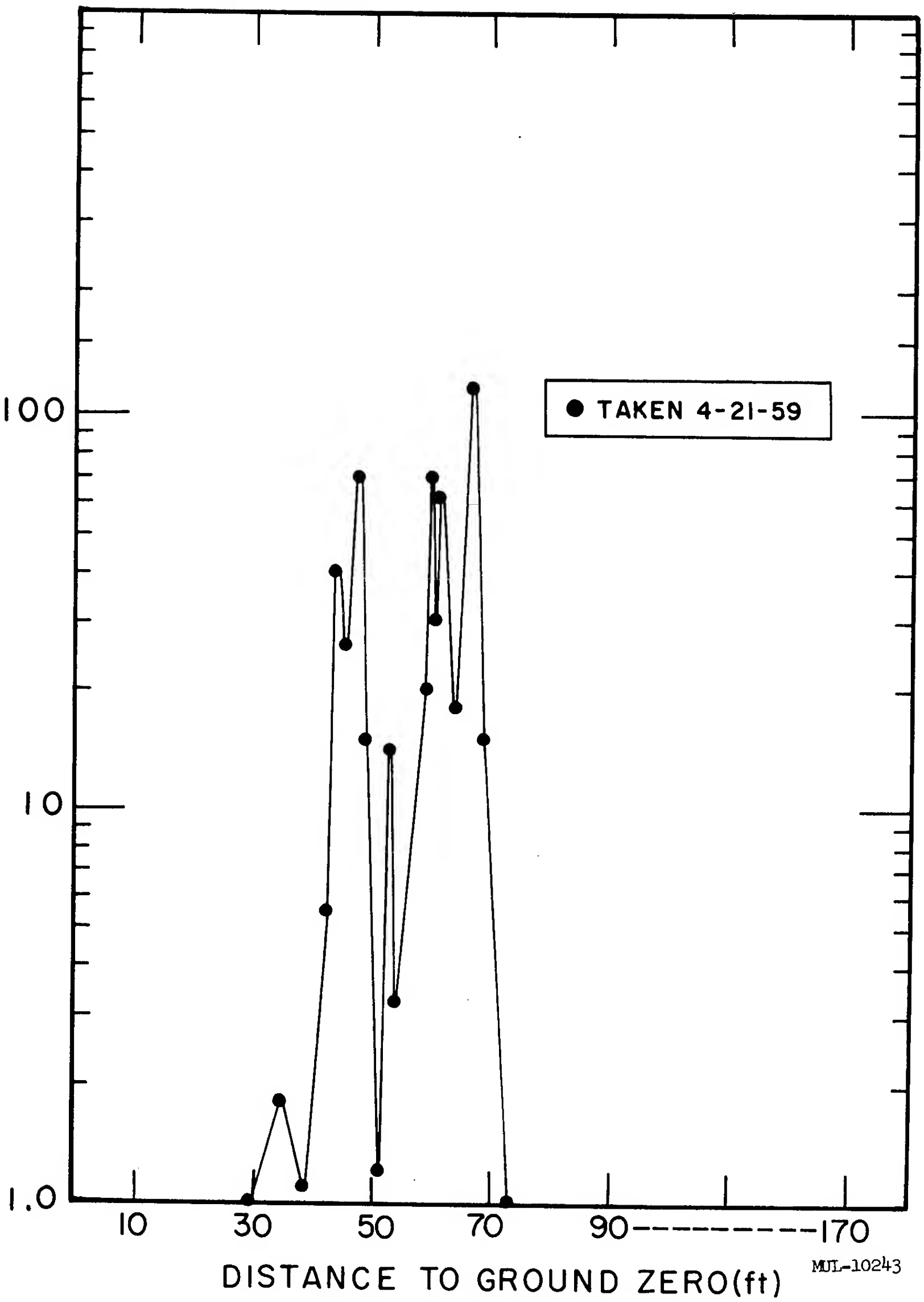

Fig. 7.12. Radiation vs distance to ground zero, drill hole Rainier I.

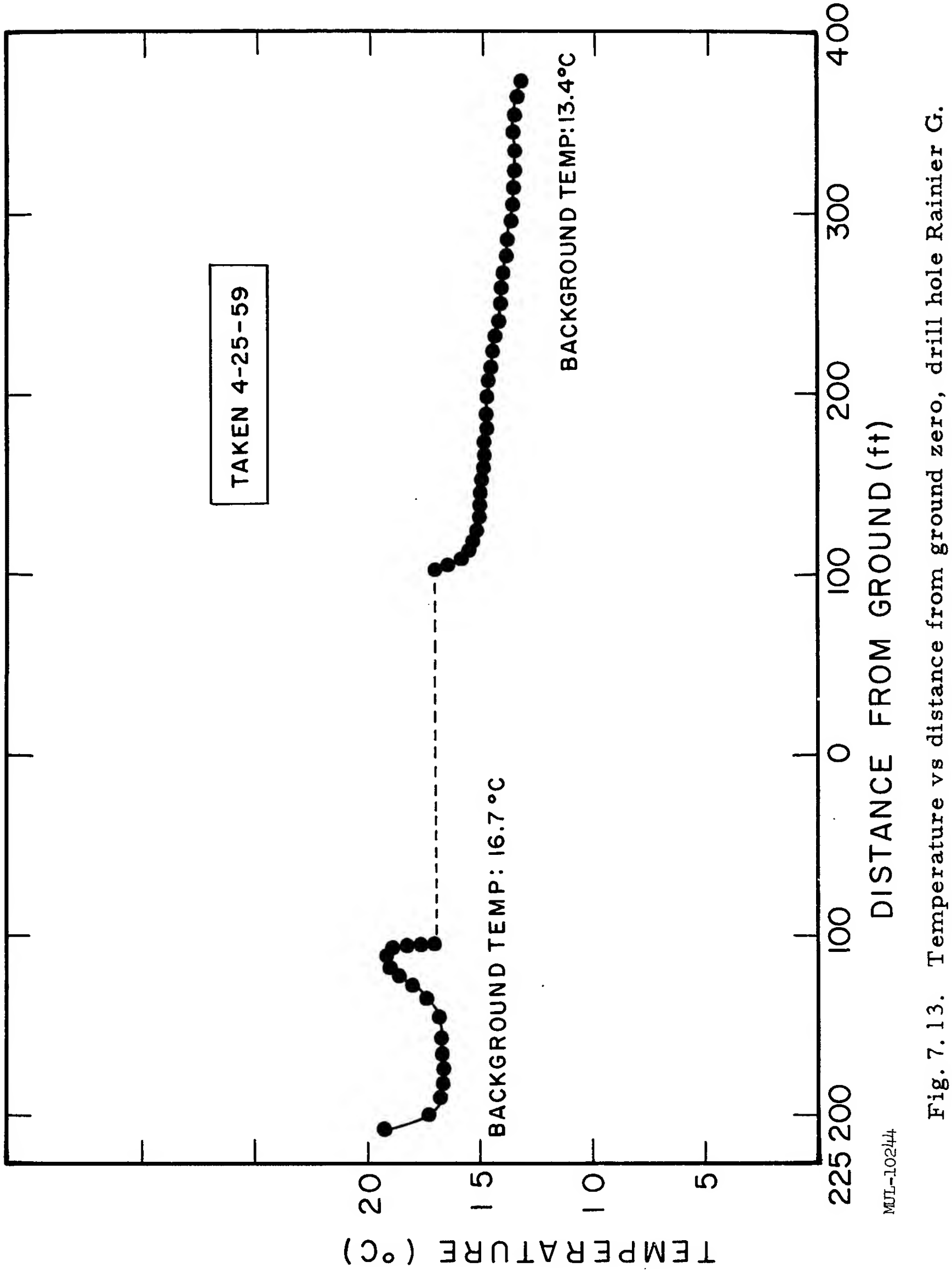

Fig. 7.13. Temperature vs distance from ground zero, drill hole Rainier G.

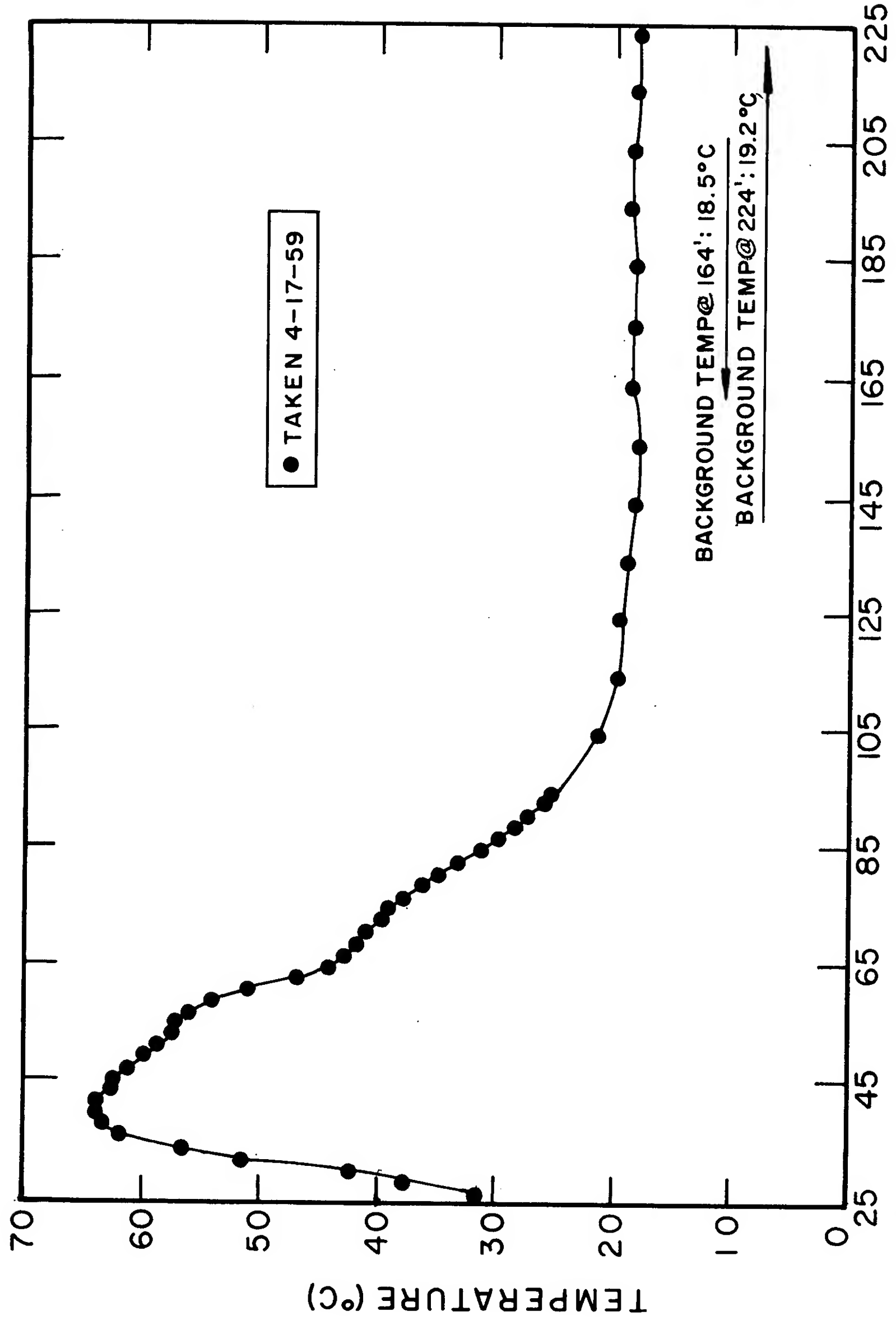

Fig. 7.14. Temperature vs distance from ground zero, drill hole Rainier H.

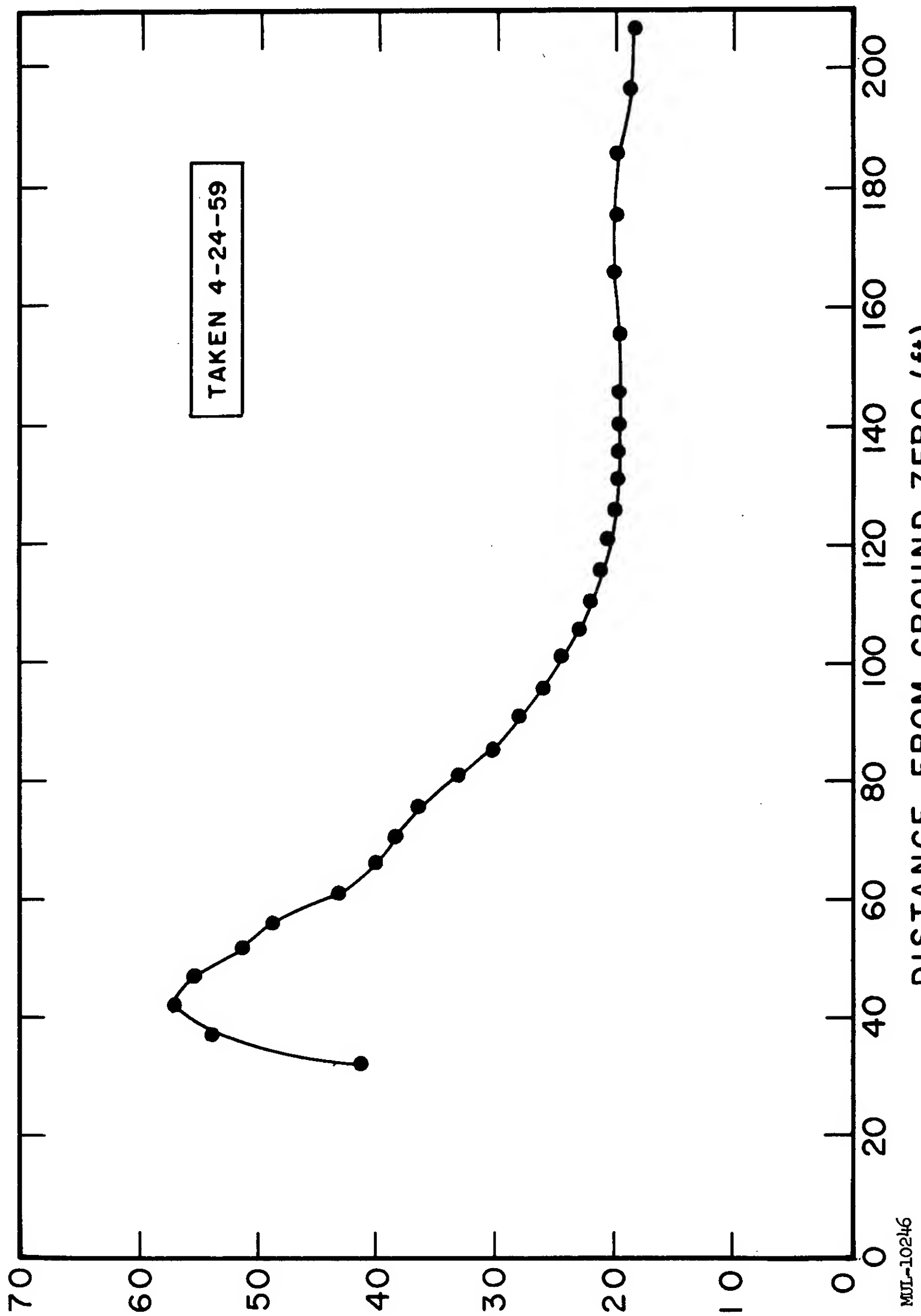

Fig. 7.15. Temperature vs distance from ground zero, drill hole Rainier I.

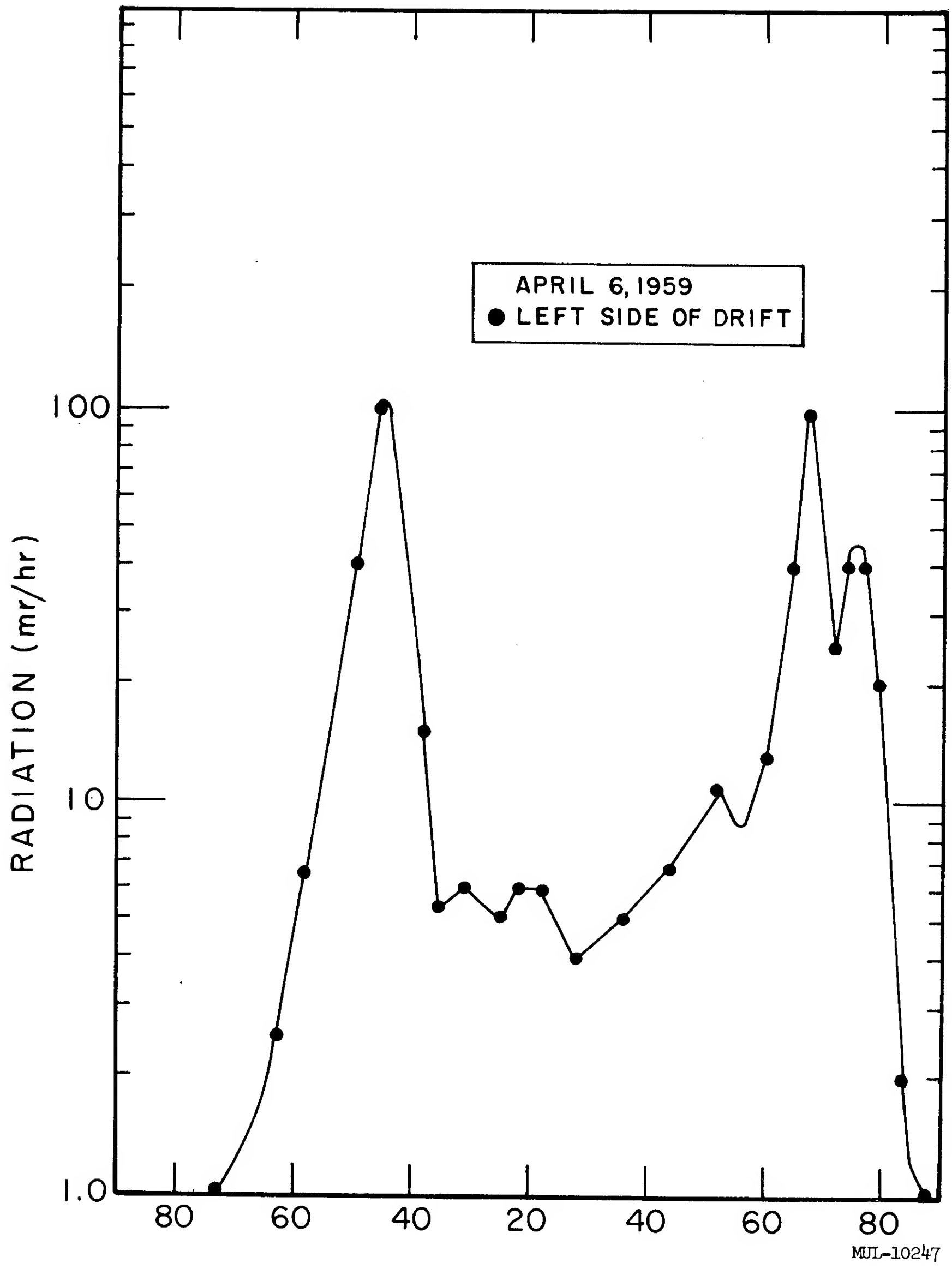

Fig. 7.16. Gamma-ray intensity vs distance from ground zero, Rainier exploratory drift.

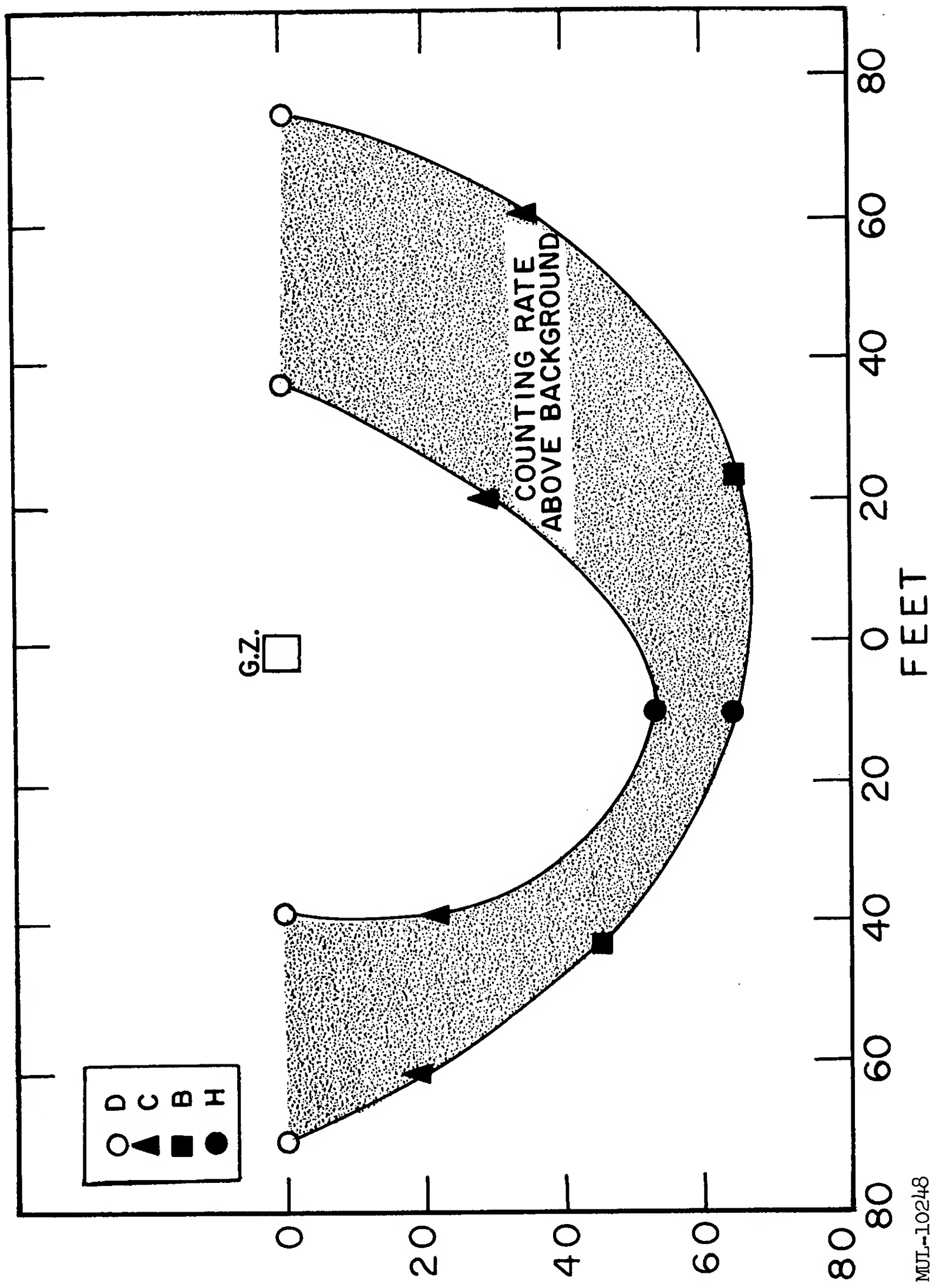

Fig. 7.17. Radioactivity distribution, Rainier. 2-21-58 and 4-16-59.

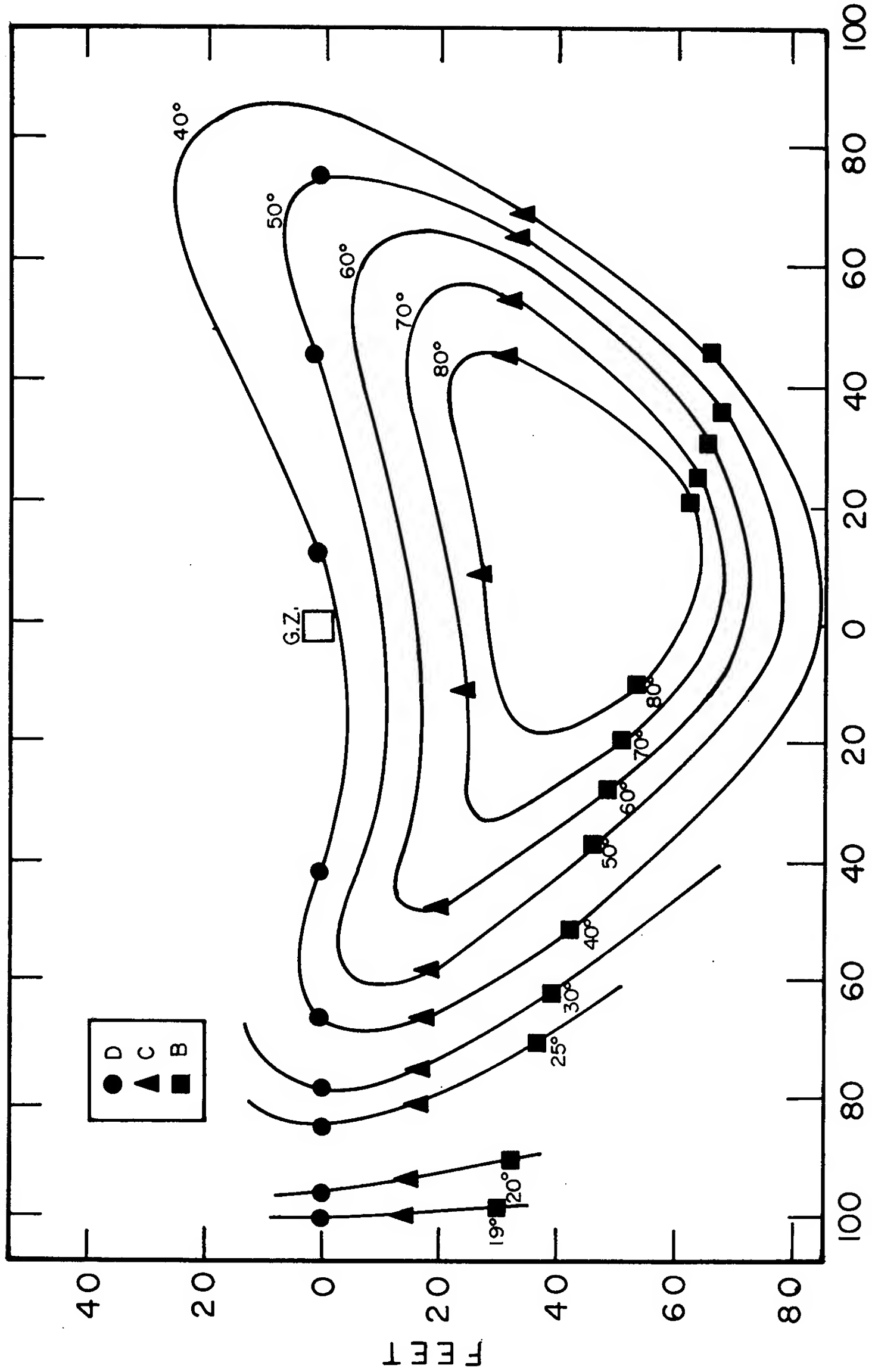

Fig. 7.18. Temperature distribution (°C) in Rainier holes B, C, and D on 2-21-58.

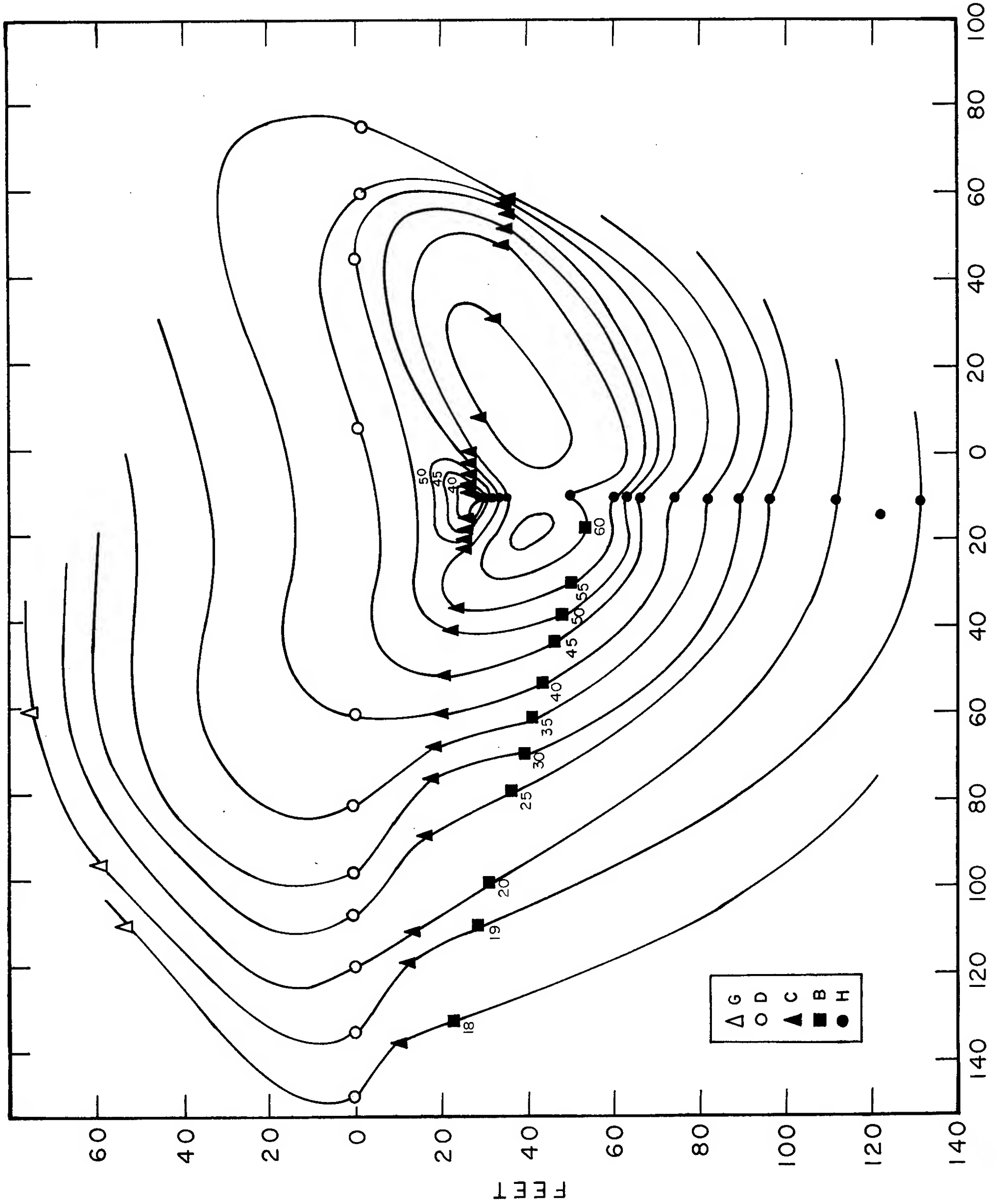

Fig. 7.19. Temperature distribution (°C) in Rainier holes B, C, D, G, and H on 4-8-59.

observed to a radius of approximately 180 feet from ground zero. However, since the temperature profiles approach background asymptotically, temperature differences of the order of the accuracy of the measuring equipment corresponded to large changes in the volume. Therefore, it was necessary to select a well-defined point for thermal energy calculations. The knee of the temperature curve, that is, the point at which the temperature begins to rise sharply above background, was selected.

On Rainier, the knees of the curves from the B, C, and D holes as measured approximately 5 months after the shot all correspond to a temperature of 20°C and a distance of 96 $\pm$ 1 ft from ground zero. A rough integration of the temperature distribution given in Fig. 7.18 shows that the heat added to the medium within a radius of 96 feet is equal to 8.4×10^{11} calories or approximately 1/2 the total energy of the device (1.7×10^{12} calories). An integration over the same volume using the temperature distribution shown in Fig. 7.19 as measured 18 months after detonation shows that the heat remaining is 7.2×10^{11} calories, a decrease of 14% in 13.5 months. In this same period, the zone heated above 20°C increased in volume by 57%.

Acknowledgments

The members of the staff of LRL who have contributed actively to this program are A. L. Anderson, W. P. Bennett, B. Cook, D. E. Nielsen, J. L. Olsen, J. D. Peterson, P. L. Stephenson.

8. THE DISPOSITION OF RADIOACTIVITY

R. H. Goeckermann

Lawrence Radiation Laboratory, Livermore

The material of this paper is based on radiochemical analyses by the forty members of the Radiochemistry group at LRL, Livermore, of samples obtained from underground explosions of 0.07 to 19 koloton yield range in tuff at the NTS during 1957-1958. The sampling included rock cores and assorted samples of the vented material from totally- or partially-contained explosions. The radionuclides studied included tracer activities, fission products, and induced activities of observable half-life – weeks to years.

It is necessary to review briefly the early history of an underground nuclear explosion in tuff. In explosions of a few kilotons, the maximum bubble radius is reached in 5-10 milliseconds. This time scales roughly like $W^{1/3}$. The vapor phase in tuff is at high temperature (1200-1500°C) and pressure (~40 atmospheres) and consists largely of water vapor. The viscous fused tuff acts to seal the cavity. Collapse begins at times ranging from immediately to tens of seconds later depending on the nature of the medium and degree of containment. If the cavity persists, flow and dripping of the fused material will occur. With collapse comes a sudden release of pressure and the escape of the vapor phase from the immediate vicinity of the cavity.

The tracer species that have been studied in several explosions are plutonium, uranium, the actinide earths, protactinium, arsenic, cesium, hafnium, and tantalum. Almost all of the plutonium has been found in the glass resulting from solidification of the fused tuff. The concentration indicates 200-500 tons of fused rock mixed with debris per kiloton yield results from explosions in the 1 to 20 kiloton range. Spongy-looking material containing a factor of 20 lower concentration of Pu has been found in fissures in the rock at distances of four cavity radii. The disposition of uranium is such as to indicate its behavior is considerably more volatile than plutonium as a reference species. Glassy shell samples have been found which have only one-third the expected uranium content and samples away from the cavity such as the fissure material are enriched in uranium by a factor of approximately 2. When collapse occurs immediately, as much as half of the uranium possibly escapes. The actinide earths behave more like plutonium, as do protactinium, hafnium, and tantalum. Arsenic

behaves like a very volatile species in these circumstances. The majority of the fused rock retains less than 1% of the arsenic, although isolated droplets have been found which have a normal concentration. When venting to the ground surface occurred, the vented debris was enriched in arsenic by an order of magnitude. Studies with cesium tracer have shown that approximately half of the cesium is retained in the glass while vented material is enriched by a factor of 2 in cesium.

The detonation of a nuclear explosive produces fission products in proportion to the fission yield of the explosive. Twenty kilotons of fission energy produces approximately 1 kg of fission products, including 20 g of strontium-90, which is comparable to the waste resulting from one day's operation of a 1000-Mw reactor. The distribution of fission product activity follows the familiar fission yield curve. The behavior of the observable species can be understood only after examination of the decay chains leading to them (these chains are listed in Table I).

Table I. Fission Product Decay Chains.

Mass 85:	$As \xrightarrow[s]{0.43} Se \xrightarrow[s]{40} Br \xrightarrow[m]{3.0} Kr$
89:	$Kr \xrightarrow[m]{3.2} Rb \xrightarrow[m]{15} Sr$
90:	$Kr \xrightarrow[s]{33} Rb \xrightarrow[m]{2.7} Sr$
91:	$Kr \xrightarrow[s]{9.8} Rb \xrightarrow[m]{2 \text{ and } 14} Sr \xrightarrow[h]{9.7} Y$
95:	$Rb \xrightarrow[25\%]{sh} Sr \xrightarrow{sh} Y \xrightarrow[m]{10} Zr$
99:	$Zr \xrightarrow[s]{30} Nb \xrightarrow[m]{2.5} Mo$
137:	$I \xrightarrow[s]{22} Xe \xrightarrow[m]{3.8} Cs$
140:	$Xe \xrightarrow[s]{16} Cs \xrightarrow[s]{66} Ba$
141:	$Xe \xrightarrow[s]{1.7} Cs \xrightarrow{sh} Ba \xrightarrow[m]{18} La \xrightarrow[h]{3.7} Ce$
144:	$Cs \xrightarrow[15\%]{sh} Ba \xrightarrow[60\%]{sh} La \xrightarrow{sh} Ce$

The history of the products of these chains is given below:

Krypton-85 : less than 1% appears to be trapped in the glass in a 2-kt explosion, the majority was diluted into ~10^9 cu ft of air in the chimney.

Strontium-89 : 3-10% in the major part of the glass, enriched in the rubble by several-fold and in the vented debris by nearly an order of magnitude.

Strontium-90 : 20-30% in the glass, vented debris enriched by 5-fold, local fallout less enriched.

Yttrium-91 : 30-50% in the glass, vented debris and rubble enriched several-fold.

Zirconium-95 : 70-100% in the glass, rubble enriched.

Molybdenum-99 : no data on glass, vented debris enriched by 30-60%.

Cesium-137 : 20-40% in the glass, vented material enriched by several-fold.

Barium-140 : 30-60% in glass decreasing as yield increases, vented debris enriched several-fold.

Cerium-141 : approximately 60% in the glass, escaping debris enriched few-fold.

Cerium-144 : ~100% in the glass, vented debris has same proportion as plutonium.

Neodymium-147 : precursors are rare earths, behavior like plutonium.

The species calcium-45, produced by neutron capture in the small percentage of calcium in tuff, has been measured in several samples. The activation has varied from (1 to 20) $\times 10^{-4}$ atoms Ca^{45} per fission, depending on the amount of neutron absorbing material around the nuclear explosive. In a given explosion, the ratio of Ca^{45} to plutonium varies by a factor of 2 in different glass samples. Isolated debris, such as the fissure sample, is low in Ca^{45}.

In conclusion, the disposition of the radioactivity is a function of the yield as it affects the time-temperature history, the degree of containment and associated collapse phenomena, and certainly the nature of the medium in which the explosion takes place. Subsequent measurements will be made in explosions which approximate more closely typical Plowshare applications.

9. THE LEACHING OF RAINIER DEBRIS

W. D. Bond and W. E. Clark

Oak Ridge National Laboratory

The possibility of serious ground water contamination is an important consideration in the peaceful application of contained nuclear explosions. A series of leaching tests were performed on Rainier debris to establish the extent of ground water contamination which would result from such debris. Leaching conditions were chosen so that the results would represent the maximum extractability of radioactivity.

Samples of the most radioactive Rainier debris available were crushed and sieved to divide the particles into five size classifications defined by diameters as follows:

(1) less than 53 microns (< 270 mesh)

(2) 53 to 74 microns (200-270 mesh)

(3) 74 to 149 microns (100-200 mesh)

(4) 149 to 297 microns (48-100 mesh)

(5) 297 to 1190 microns (14-48 mesh).

Specific activities were determined for the size ranges (1), (2), and (4), respectively, and one-gram samples of these size ranges were digested overnight with 100 ml of the various reagents of interest as indicated in Tables Ia-Ic. Solids were then centrifuged off, the activity of the supernatant liquid measured, and the percentage of each type of activity extracted was calculated.

The results are listed in Tables Ia-Ic. Though there is considerable scatter in the data it is obvious that extraction of any material represented by the measured activities would be completely impractical since the highest recoveries obtained are about 27%. The addition of MnO_2 to give the leach oxidizing power shows no clear trend so far as extraction efficiency is concerned. It is possible that any increase in extraction due to oxidation is offset by adsorption on the suspended particles of MnO_2.

The extraction of activity by ground water from the Nevada Test Site (Hagestad Hole) is of interest because it gives a measure of the amount of activity which can be expected to be leached from the residue after a test shot. The room temperature data are presented in Table II and Fig. 9.1. Since

Table Ia. Leaching Experiments on Rhyolite Debris from Rainier.

Conditions: 100 ml of solution, 1 g of debris, temperature boiling. < 53 μ diam fraction of the debris. No stirring.

Leaching agent	MnO_2	Leach time (hr)	Activity extracted (%)		
			Alpha[a]	Beta	Gamma
H_2SO_4					
0.5 M	Excess	15	9.12	0.85	0.28
0.5 M	Excess	16	4.84	0.98	0.29
0.5 M	None	16.5	20.2	2.02	0.90
3.0 M	Excess	16	4.64	0.81	0.43
3.0 M	None	16.5	26.8	2.00	1.26
HNO_3					
6 M	None	16	2.69	1.74	0.82
HCl					
6 M	Excess	16.5	6.87	2.99	1.29
6 M	Excess	16	6.26	2.65	1.30
6 M	None	16.5	16.4	1.29	0.69
NaOH					
1 M	None	16.5	20.1	1.22	3.20
Na_2CO_3, $NaHCO_3$					
0.5 M - 0.5 M	Excess	16.5	12.2	0.28	0.10
0.5 M - 0.5 M	Excess	16	6.34	0.12	0.03
0.5 M - 0.5 M	None	16.5	14.5	0.66	0.28
Distilled H_2O	None	21.5	0	0.31	0.28
Distilled H_2O	None	21.5	0	0.32	0.38
Ground H_2O[b]	None	16.5	3.21	0.55	0.41

[a]Includes all alpha activities except uranium.

[b]From the Hagestad Hole on the NTS. pH ≅ 10.2.

Table Ib. Leaching Experiments on Rhyolite Debris from Rainier.

Conditions: 149-297 μ diam fraction of the debris.
Solutions stirred.

Leaching agent	MnO_2	Leach time (hr)	Activity extracted (%)		
			Alpha[a]	Beta	Gamma
H_2SO_4					
0.5 M	Excess	16.5	2.47	0.38	0.25
0.5 $\overline{M}$	None	16.5	2.01	1.08	0.70
3.0 $\overline{M}$	Excess	16.5	2.48	0.56	0.45
HCl					
6 M	Excess	16.5	1.50	1.16	0.65
6 $\overline{M}$	None	16.5	1.32	0.89	0.71
Na_2CO_3, $NaHCO_3$					
0.5 M - 0.5 M	Excess	16.5	2.49	0.092	0.044
0.5 $\overline{M}$ - 0.5 $\overline{M}$	None	16.5	1.29	0.31	0.35
Ground H_2O[b]	None	16.5	1.44	0.52	0.44
Ground H_2O[b]	Excess	16.5	0.69	0.30	0.17
HNO_3					
6 M	None	16.5	2.32	1.18	0.73

[a]Includes all alpha activities except uranium.

[b]From the Hagestad Hole on the NTS. pH ≅ 10.2

Table Ic. Leaching Experiments on Rhyolite Debris from Rainier.

Conditions: 297-1190 μ diam fraction of the debris.
Solutions stirred.

Leaching agent	MnO_2	Leach time (hr)	Activity extracted (%)		
			Alpha[a]	Beta	Gamma
H_2SO_4					
0.5 M	Excess	16.5	1.64	0.19	0.01
0.5 $\overline{M}$	None	16.5	1.31	1.27	0.75
HCl					
6 M	Excess	16.5	1.05	0.56	0.035
6 $\overline{M}$	None	16.5	5.61	0.68	0.40
HNO_3					
6 M	None	16.5	1.87	0.55	0.029
Na_2CO_3, $NaHCO_3$					
0.5 M - 0.5 M	Excess	16.5	1.31	0	0.005

[a]Includes all alpha activities except uranium.

Table II. Leaching of Rainier Debris by Ground Water at Room Temperature.

1-g samples ground to < 53 μ diameter, stirred magnetically with 100 ml H_2O (Hagestad Hole).

5-ml specimens removed periodically for analysis.

Activity of solid specimen:

Gross alpha (except U)	= 150 counts/min/mg
Beta	= 1.82×10^3 counts/min/mg
Gamma (scintillation)	= 9.05×10^3 counts/min/mg

Specimen No.	Total leach time (hr)	Percent activity extracted		
		Alpha[a]	Beta	Gamma
1	2	0.20	0.11	0.065
1	4	0.20	0.14	0.050
1	6	0.20	0.20	0.11
1	8	0.39	0.26	0.12
2	16	0.20	0.29	0.15
1	24	0.39	0.40	0.28
2	24	0.20	0.34	0.18
1	32	0.39	0.53	0.39
2	40	0.59	0.48	0.34
2	48	0.52	0.54	0.41

[a]Includes all alpha activities except uranium.

these tests were run on the finest size classification, under stirred conditions and with a 100/1 weight ratio of water to specimen, it is believed that this should represent the most favorable condition for removal of activity from the rock. Since the maximum activity leached is less than 0.6% it appears that there will be relatively little contamination of the ground water. It should, however, be pointed out that at the end of the 48-hr contact period the rate of leaching appeared to be relatively constant at about 0.05%/hr; it is, therefore, possible that over longer residence times very sizeable activities could be built up. Long residence time, however, implies a slow rate of movement for the water through the ground water table with a correspondingly good chance of removal of activity by the inert medium traversed. It should be noted (Table Ia) that less activity is removed from the rhyolite by distilled water than by the ground water which had a pH of approximately 10.2.

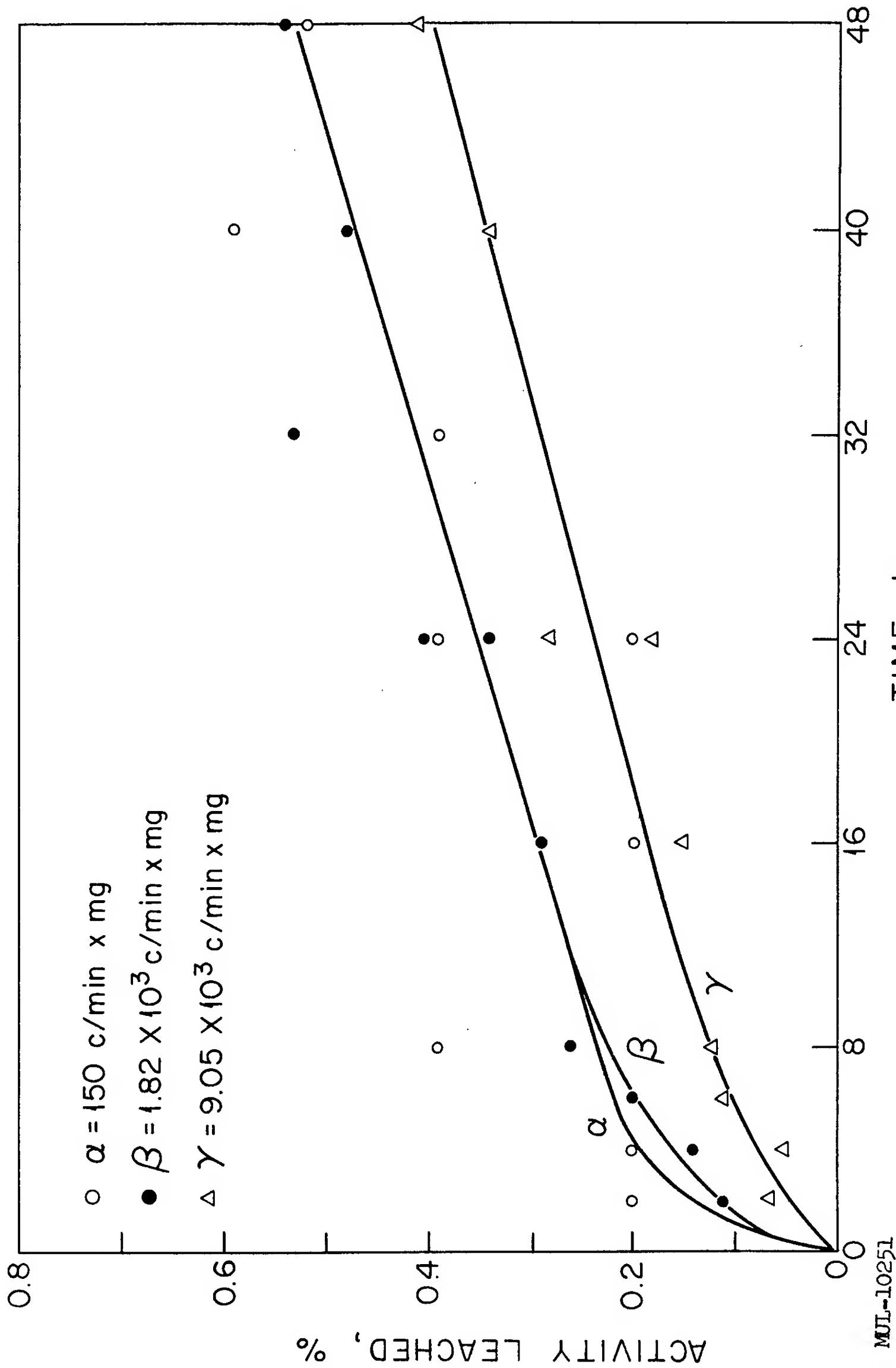

Fig. 9.1. The leaching of activity from Rainier debris by ground water.

C. The Theory of Underground Nuclear Explosions

1. CAVITY FORMATION

G. T. Pelsor

Lawrence Radiation Laboratory, Livermore

In Fig. 1.1 the solid curve approximates the Hugoniot for water saturated tuff which surrounded the Rainier nuclear detonation. A shock of 1.1 Mb pressure would increase the specific internal energy of this material by an amount equal to the area of the triangle below the straight line joining the initial and final states. As the pressure of this same material falls, the material expands nearly adiabatically. Using the Hugoniot as an approximation to the adiabat, the hatched area represents the net gain in internal energy when the pressure has fallen to, say, 100 bars. The 3200 cal/g was assumed to be sufficient to vaporize the rock under this pressure.

A one-dimensional hydrodynamic calculation was made on a rather crude machine code (as few as 4 zones were used occasionally) which did, however, provide for two different behaviors of the material after passage of the shock. That is, if the shock pressure exceeded 1.1 Mb, the expansion was that of an ideal gas of $\gamma = 1.4$; on the other hand, material subjected to weaker shocks than this was allowed to expand along the Hugoniot. Figure 1.2 shows two pictures taken from this calculation. In the one at the top, the shock pressure has just gotten down to 1.1 Mb. Material which was on the wall of the cavity initially at 1.2 m has now moved out to about 2 m and has a larger specific volume than it had initially. The material now at the front at 2.65 m will move, as shown in the later picture below, to a point where there is a jog in the specific-volume curve, indicating the difference in behavior of the two phases. Many milliseconds later, the material outside this jog forms the liquid wall of the cavity at a radius of about 55 ft.

But the situation in the liquified rock is complicated by the fact that one component, namely, water, is much more volatile than the rest. Most of this water will eventually be found as part of the cavity vapor. Its emergence is slowed by the viscosity and surface tension of the liquid rock. In fact, the water in a thin outer layer of the fused rock is trapped in the viscous glass. It may be that most of the water vapor from the molten rock gets into the cavity so late in the process that it takes little part in determining the cavity size.

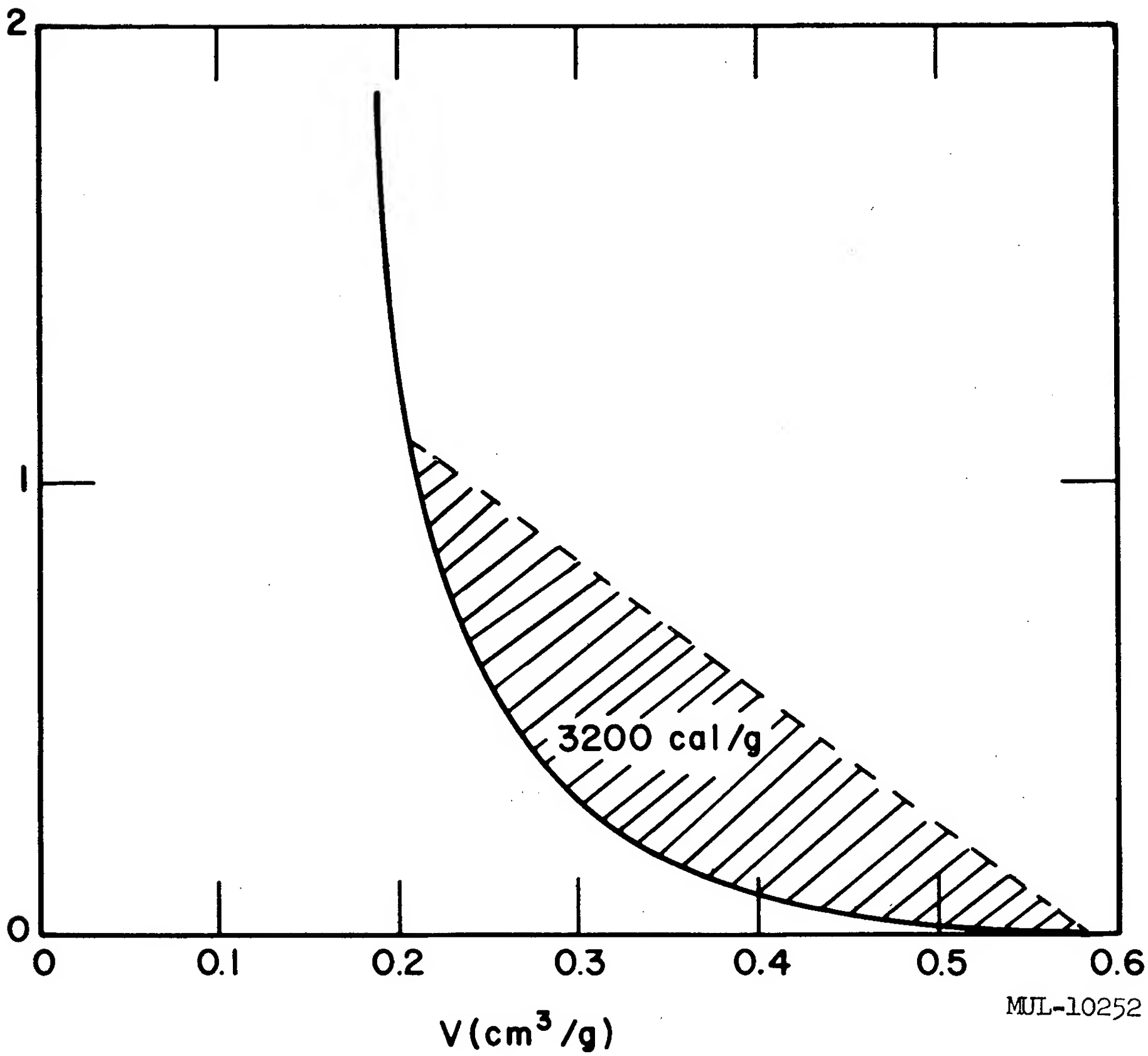

Fig. 1.1.

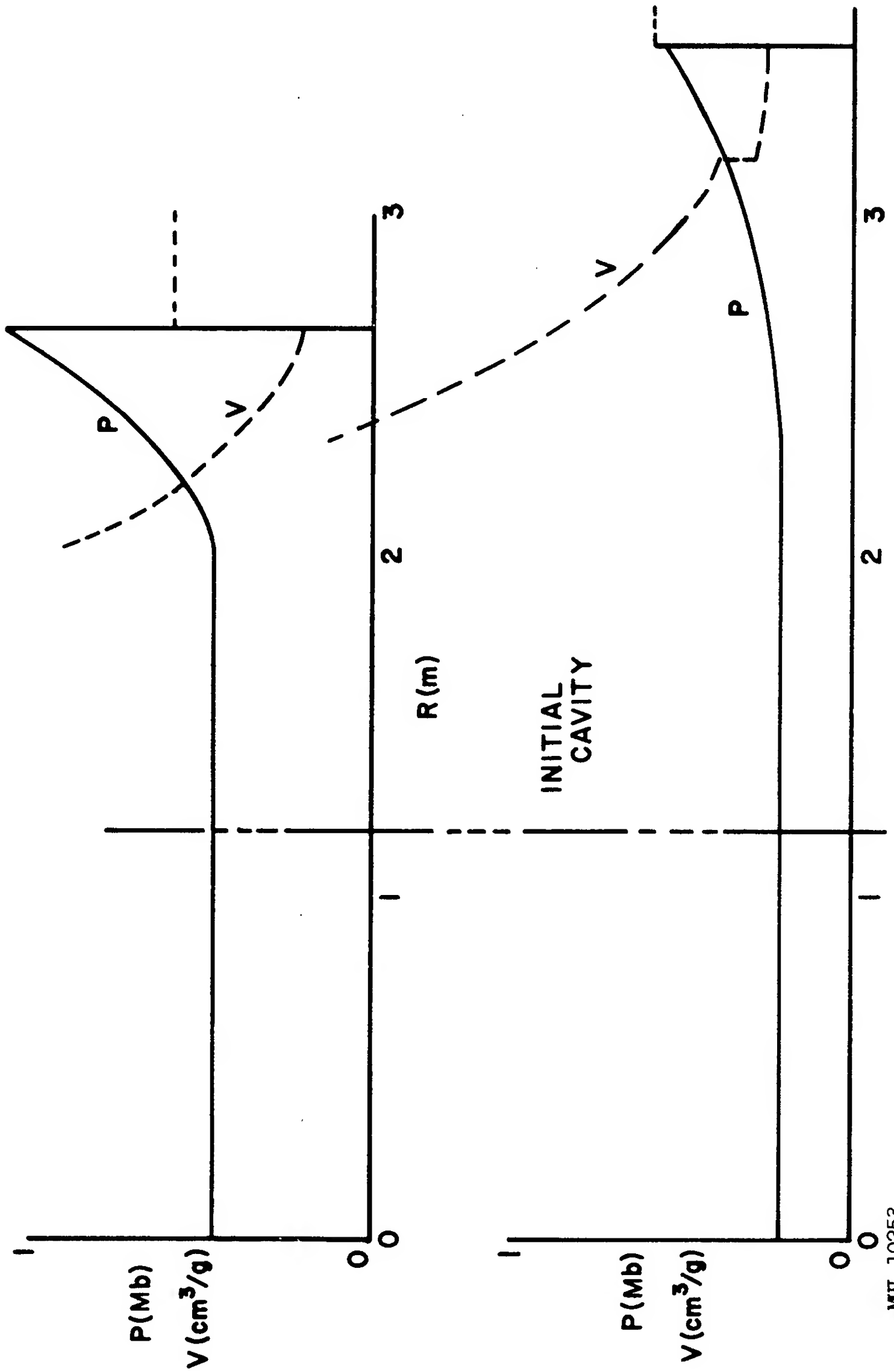

Fig. 1.2.

When this water does arrive, having started from a region of lower temperature than the cavity vapor and having cooled still further by expansion, it chills the rock vapor and leads to some condensation as has been discussed by Kennedy and Higgins. They deduce a water vapor pressure of 40 bars during the growth and freezing of the small beads which have been recovered in drilling through the Rainier site after the shot. The total pressure in the cavity including that exerted by the rock vapor was probably considerably higher, perhaps even higher than the overburden pressure, since the thick cushion of crushed rock between 55 ft and 130 ft would allow a higher equilibrium pressure in the cavity than the radial stress at the outer edge of the crushed zone. The fact that the roof took a minute or two to collapse is further indication of cavity pressure higher than overburden pressure.

Radioactive products found beyond the cavity wall lead one to suspect the formation of fissures (see Fig. 1.3). Although the location was such that fissure propagation could have been influenced by proximity of the tunnel or a weak faulted zone in the rock, there may have been other fissures which have been missed in the limited drilling and in the exploratory drift. One might imagine these fissures to be formed somewhat as follows: In the early stages of the explosion, the material just outside the liquid is deformed plastically with radial compression and lateral spreading as it moves to larger radii. Eventually as the pressure decreases this material is able to resist further distortion. This point may be reached while it is still moving outward so that, having low tensile strength, it tears along radial cracks. These cracks grow rather slowly at first because they are moving into a region where the pressure is higher than the cavity pressure. But if the cavity pressure is higher than the overburden pressure, as the pressure wave goes out and so becomes weaker, the pressure gradient is soon reversed. Then the cracks grow longer rapidly because of stress concentration at the end of the crack. This gives a large area of cold rock on which vapor can condense and leads to the sudden fall in pressure inferred by Kennedy and Higgins. The cracks would form preferentially in the roof of the cavity where overburden pressure is least and the unstable, water-saturated, crushed rock, no longer supported by cavity pressure, would fall into the cavity in a pile of rubble (Fig. 1.3). The displaced vapor would then be even more intimately mixed with cold rock and would further condense. The crushed rock beyond the cracks, and even the unaltered rock above, left without support, would proceed to collapse — perhaps in a succession of falls which in a

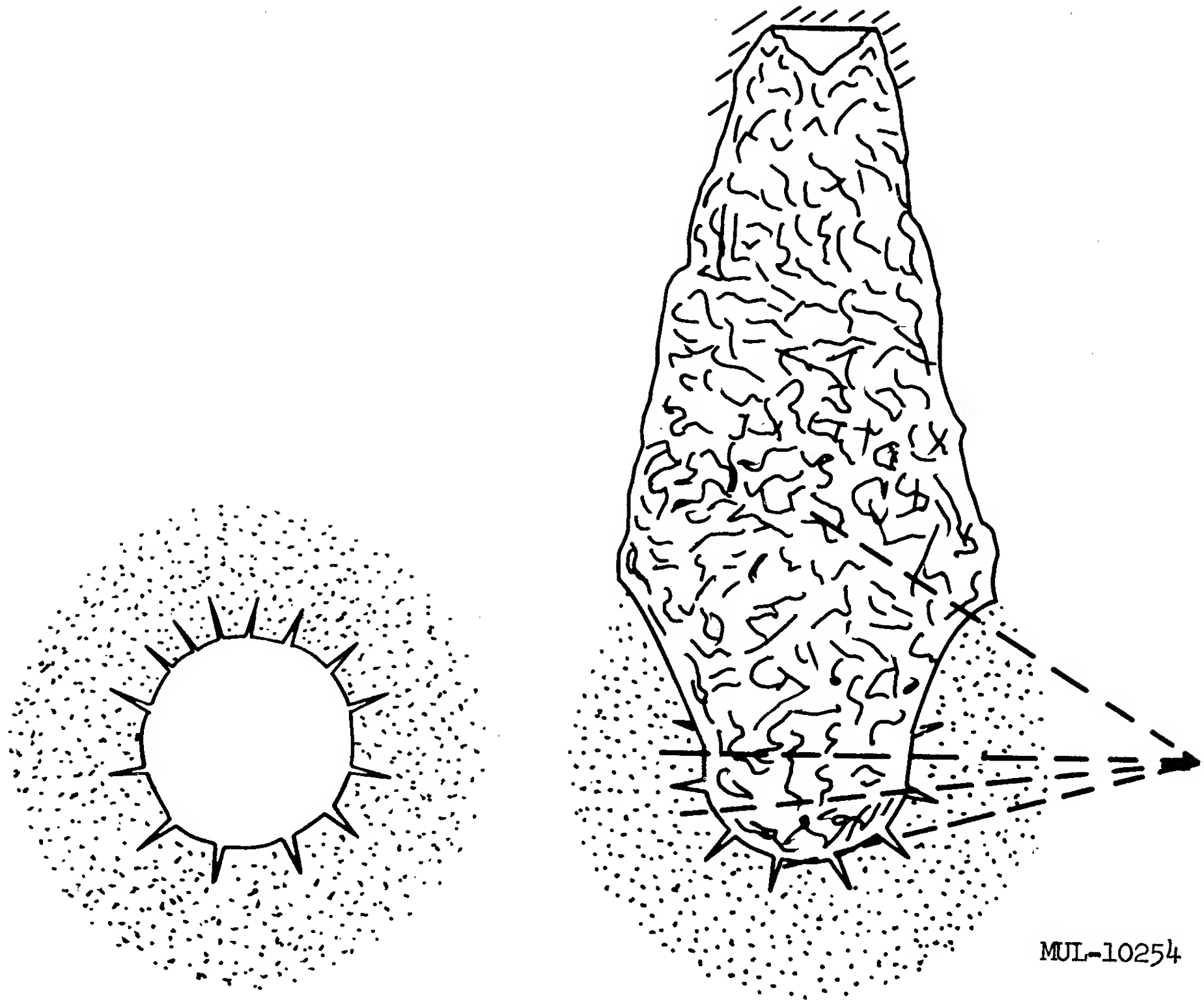

Fig. 1. 3.

couple of months had reached a height of 386 ft above the detonation point. The condensed water percolated back down to the hot region where it evaporated and started another cycle of diffusion upward, condensation in the cold chimney, and so forth. This gradually decreased the maximum temperature in the system to the boiling point of water, after which the chief mechanism of cooling is the conduction of heat through the surrounding rock.

The compressed rock, in place, is relatively impermeable while that which was broken in the cave-in is open and permeable. In a recent hole inclined upward through the Rainier chimney, circulation of drilling mud was lost at a point about 34 ft horizontally outward and 74 ft above the similar point on the horizontal hole through the detonation point. Thus the caving region flares out about 25° from the vertical.

If the process description we have given is correct, it depends at a number of points and in a rather sensitive way on the properties of the medium in which the detonation takes place. For example, the strength of the medium for dynamic, one-dimensional loading may be an important factor in the formation of fissures and thus in the final shape and state of the cavity. We hope eventually to have data on cavities formed in media other than tuff.

2. A COMPUTER CALCULATION OF RAINIER
(The First 100 Milliseconds)

John H. Nuckolls

Lawrence Radiation Laboratory, Livermore

The purpose of these calculations is to test and develop our capability for predicting the phenomena of underground nuclear explosions from the laws of physics and the properties of materials. We also seek to understand the experimental observations and measurements. Analytic methods are extremely difficult because of the nonlinearity of the partial differential equations, the complexity of the stress-strain relations, and the transitions between gaseous, liquid, plastic, fractured, and elastic states.

A special code, UNEC (Underground Nuclear Explosion Code), was developed for the IBM 709 Electronic Computer to make these calculations. They extend in time from a few microseconds to approximately 100 milliseconds after the Rainier explosion, and in space to a radius of several hundred feet from the site of detonation. Results are generally in good agreement with experiment.

METHOD, ASSUMPTIONS

Technically, UNEC is a spherically symmetric Lagrangian hydro-elasto-dynamic code. The basic difference equations are derived from the partial differential equations for conservation of momentum and energy:

$$\frac{\partial}{\partial r}(\tau_{rr}-q) + \frac{2}{r}(\tau_{rr}-\tau_{\theta\theta}) = \rho\ddot{r} \qquad \text{Conservation of momentum}$$

$$e = \frac{1}{2}\left(\tau_{rr}\frac{\partial S}{\partial r} + \tau_{\theta\theta}\frac{2S}{r}\right) - \int q\,\frac{dV}{V_0} \qquad \text{elasto-dynamic}$$

$$= -\int (P+q)\,\frac{dV}{V_0} \qquad \text{hydrodynamic}$$

} Conservation of energy

where r = radius

S = radial displacement

V = volume

ρ = density

e = internal energy per initial volume

P = pressure

$\tau_{rr}, \tau_{\theta\theta}$ = radial and tangential components, in spherical coordinates, of the stress tensor

q = viscosity.

The system of integration automatically conserves mass.

Outside the elastodynamic region (where the elastic limits of the tuff have been exceeded), a generalized Richtmyer-von Neumann artificial viscosity is used.[1] It spreads the shock front over several zones, and increases entropy as required by the second law of thermodynamics. In the elastodynamic region, the viscosity is proportional to the rate of strain and produces Kelvin-Voigt type damping of small amplitude stress waves.[2]

The tuff is represented by the generalized Hooke's law when elastic, by a bulk modulus type equation when fractured, by the initial shock Hugoniot in the plastic and liquid states, and as a Thomas-Fermi-Dirac gas when vaporized:

$$\tau_{rr} = (\lambda + 2\mu)\frac{\partial S}{\partial r} + 2\lambda\frac{S}{r}$$

elastic (generalized Hooke's law)

$$\tau_{\theta\theta} = \tau_{\phi\phi} = \lambda\frac{\partial S}{\partial r} + 2(\lambda + \mu)\frac{S}{r}$$

$$P = -k\frac{\Delta V}{V} \qquad \text{fractured}$$

$$P = F(V)_{\text{Hugoniot}} \qquad \text{crushed, plastic}$$

$$P = P(V, e)_{TFD}, \qquad \text{gas}$$

---

[1] J. von Neumann and R. D. Richtmyer, "A Method for the Numerical Calculation of Hydrodynamic Shocks", J. Appl. Phys. 21, 232, (1950).

[2] L. Knopoff and G. J. F. MacDonald, "Attenuation of Small Amplitude Stress Waves in Solids", Revs. Modern Phys. 30, 1178 (1958).

where λ, u = Lamé constants

k = bulk modulus.

In "vertical" calculations, a uniform radial gravitational field is superimposed on the system.

MODEL

Initially, the energy of the nuclear explosion is distributed uniformly as the internal energy of a gas contained in a sphere of the same volume as the original room (rectangular, $6 \times 6 \times 7$ feet). It is assumed that the initial density of this gas is approximately equal to the mass of material vaporized during the first few microseconds divided by the volume of the room.

It is assumed that the tuff has negligible large-scale tensile strength. As long as the tension does not exceed the compressive stress due to the overburden, and the shear strength is not exceeded, the tuff is treated as a linear elastic solid. The elastic constants were determined by static laboratory tests to be:[3]

bulk modulus, $k = 0.036$ megabars (Mb) ($1\text{Mb} = 1.01 \times 10^{12}$ dynes/cm^2)

shear modulus, $\mu = 0.055$ Mb

sound speed, $c = 0.241$ cm/μ-sec.

After the tension in a spherical shell exceeds the lithostatic stress the shear modulus there is set to zero, (i.e., the diagonal components of the stress tensor are set equal to a pressure which is related to the volume by a bulk modulus type equation of state).

When the shear stress exceeds the dynamic confined shear strength, it is assumed that the tuff flows plastically. This plastic material resembles mud and is relatively impermeable to water. Laboratory tests indicate the static unconfined shear strength of tuff is 175-350 bars.[4] The dynamic strength is not known. The assumption that it is twice the maximum static strength (i.e., 0.7 kilobars) leads to a crushing radius of 130 ft and is consistent with experimental ratios of dynamic to static strengths of concrete.[5] The plastic tuff is assumed to obey an equation of state identical with the initial shock Hugoniot.[6] At pressures less than 10 kilobars,

---

[3] G. W. Johnson and C. E. Violet, "Phenomenology of Contained Nuclear Explosions," UCRL-5124, Rev. I.

[4] G. W. Johnson and C. E. Violet, op. cit.

[5] D. Watstein, J. Am. Concrete Inst., April 1953, pp. 729-44.

[6] Measured experimentally at LRL with high explosives. Method is described by J. M. Walsh and R. H. Christian, Phys.Rev. 97, 1544 (1955).

the slope of the Hugoniot is faired into static measurements of the bulk modulus. Although use of the Hugoniot equation produces the correct conditions at the shock front, it results in the deposition of somewhat too much waste heat during the subsequent expansion.

When the shock is strong enough to vaporize the tuff upon rarefaction, an irreversible transition is made to a gaseous equation of state calculated by the Thomas-Fermi-Dirac theory[7] and normalized to the Hugoniot at the transition point. It is estimated that the total heat of fusion is 715 cal/g and the total heat of vaporization is 3200 cal/g.[8] These energies will be deposited by shocks with peak pressures of 0.4 and 1.0 Mb, respectively.

Summarizing, the calculations with this model will predict a vaporized region determined by a 1.0-Mb peak shock pressure, a melted region corresponding to 0.4 Mb, a plastic region where the shear strength is exceeded, a fractured region where the tension exceeds the overburden, and beyond this an elastic region.

RESULTS

Shock

The calculated shock arrival times are shown in Fig. 2.1. At approximately 60 feet the shock velocity becomes subsonic. Thereafter, the curve is the arrival time of the dilatational elastic wave. The results of Dickens and Porzel's measurements[9] are represented by circles. Disagreement at small radii is probably mainly due to the initial nonspherical geometry. At larger radii, the shock quickly approaches sound speed and the arrival time becomes relatively insensitive to yield.

Figure 2.2 shows the peak shock pressure as a function of distance. To 10 meters, it decreases as $r^{-2.35}$. Tuff is vaporized to a radius of 7 feet (peak pressure 1.0 Mb) and melted by the shock to 10 feet (0.4 Mb). Enough energy is deposited within a radius of 14 ft to melt all the tuff to this distance, or 660 metric tons. Radiochemical analysis indicates that 600 ± 250 tons were melted.[10] At 130 ft the peak pressure is 0.7 kilobars, twice the static shear strength.

---

[7] See R. D. Cowan and J. Ashkin, Phys. Rev. 105, 144 (1957).

[8] G. T. Pelsor, private communication.

[9] R. G. Dickens and F. B. Porzel, "Close-In Time of Arrival Measurements for Yield of Underground Shot," ARF-D-133 (PR-13).

[10] R. H. Goeckermann, private communication.

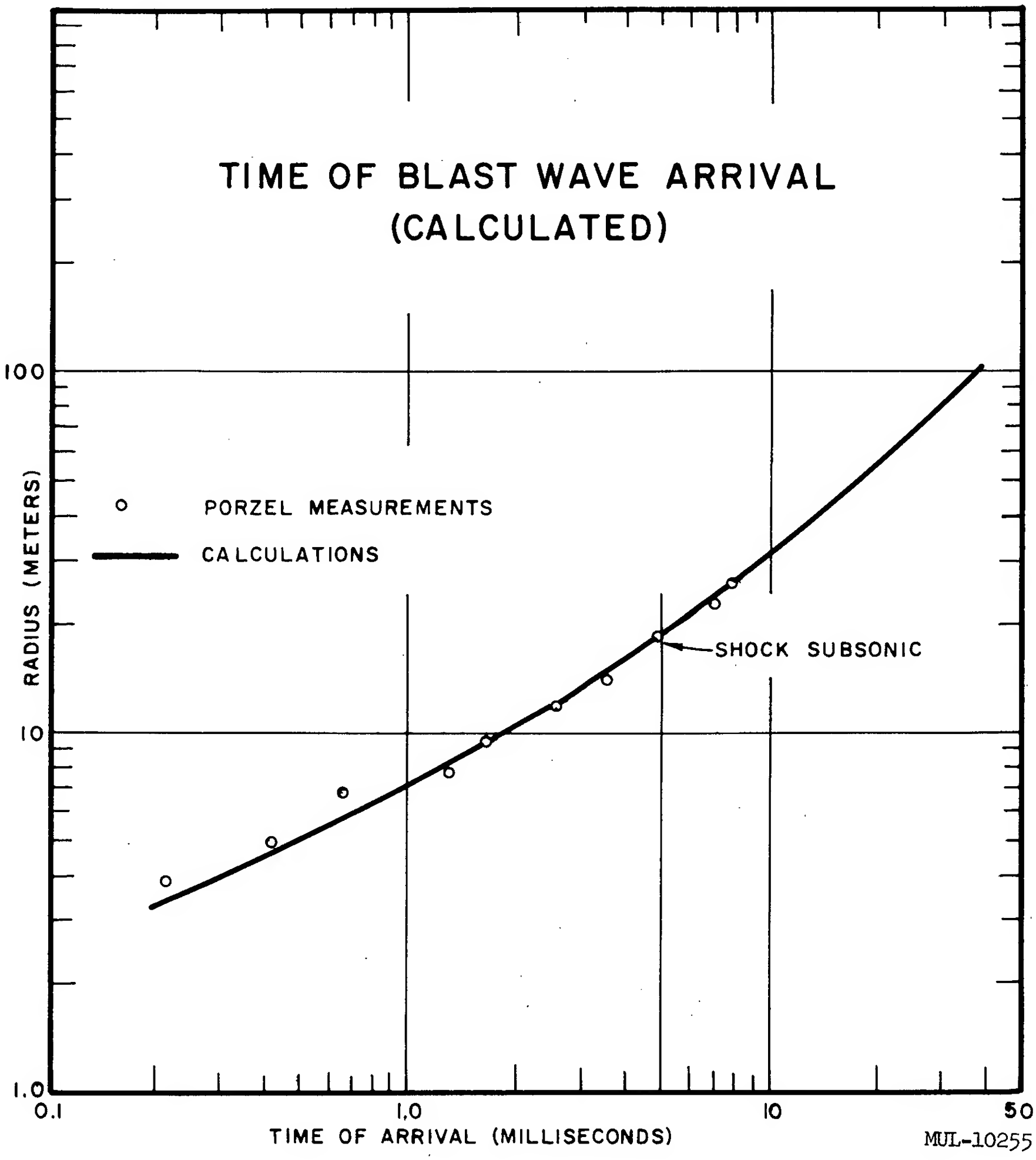
TIME OF BLAST WAVE ARRIVAL
(CALCULATED)
100
10
1.0
RADIUS (METERS)
PORZEL MEASUREMENTS
CALCULATIONS
SHOCK SUBSONIC
0.1
1.0
10
50
TIME OF ARRIVAL (MILLISECONDS)
MUL-10255

Fig. 2. 1.

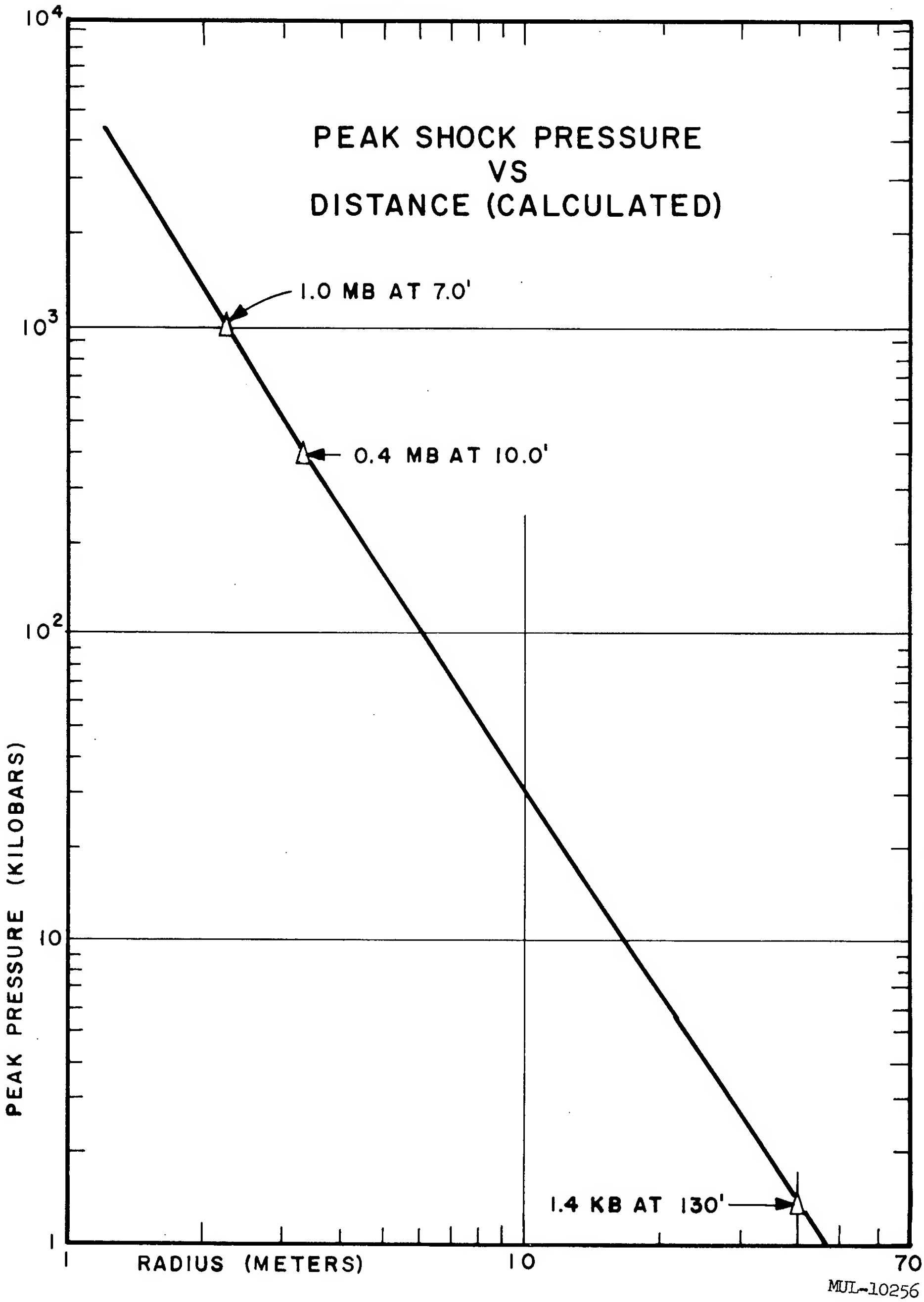
PEAK SHOCK PRESSURE
VS
DISTANCE (CALCULATED)
1.0 MB AT 7.0'
0.4 MB AT 10.0'
1.4 KB AT 130'
PEAK PRESSURE (KILOBARS)
10^4
10^3
10^2
10
1
1
10
70
RADIUS (METERS)
MUL-10256

Fig. 2.2.

Figure 2.3 (pressure vs time at 60 feet) is a typical supersonic shock. A subsonic pressure pulse is fundamentally different as shown in Fig. 2.4 (pressure vs time at 130 ft). The elastic precursor travels at dilatational sonic speed, $[(\lambda + 2\mu)/\rho]^{1/2}$, and the main pressure pulse moves approximately 40% as fast between 130 and 200 ft.

As it propagates, the shock becomes broader. Figure 2.5 shows the times for the pressure to decay to 1/2 and 1/10 peak values as a function of distance. For example, at 60 ft (peak pressure 9 kilobars) the pressure is greater than 4.5 kilobars for ~1.5 msec, and greater than 0.9 kilobar for ~12 msec. To about 20 meters, the lines in Fig. 2.5 are approximately parallel to $r^{-1.65}$.

CAVITY

Figure 2.6 shows the growth of the central cavity. The maximum radius is about 63 ft, compared to 62 ft determined by post-shot investigation.[11] The average cavity pressure as a function of time is plotted in Fig. 2.7. It decreases from 4.5 megabars to 1 kilobar in less than 10 msec, and to about 100 bars in 35 msec.

ENERGY

At 90 msec, less than 10% of the energy is kinetic. The total energy is distributed as follows:

State	Radii	% of total energy
Gas	0-62'	8.2
Liquid	62'-62'3"	19.1
Crushed	62'3"-130'	47.0
Fractured	130'-280'	21.2
Elastic	>280'	

At this time, the temperature distribution is as in Fig. 2.8.

---

[11] G. H. Higgins, private communication.

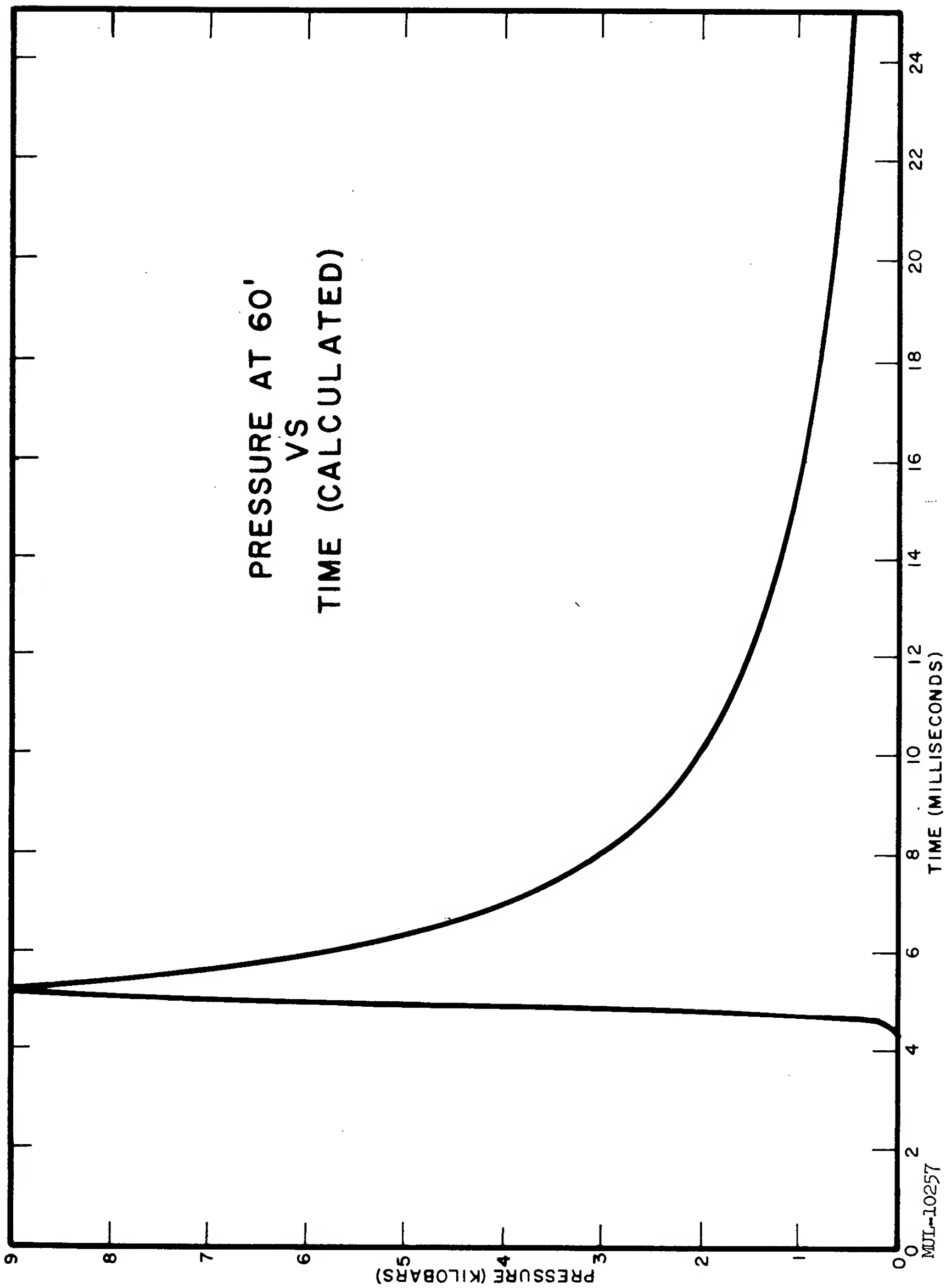
PRESSURE AT 60' VS TIME (CALCULATED)
PRESSURE (KILOBARS)
TIME (MILLISECONDS)
0
1
2
3
4
5
6
7
8
9
0
2
4
6
8
10
12
14
16
18
20
22
24
MUL-10257

Fig. 2.3.

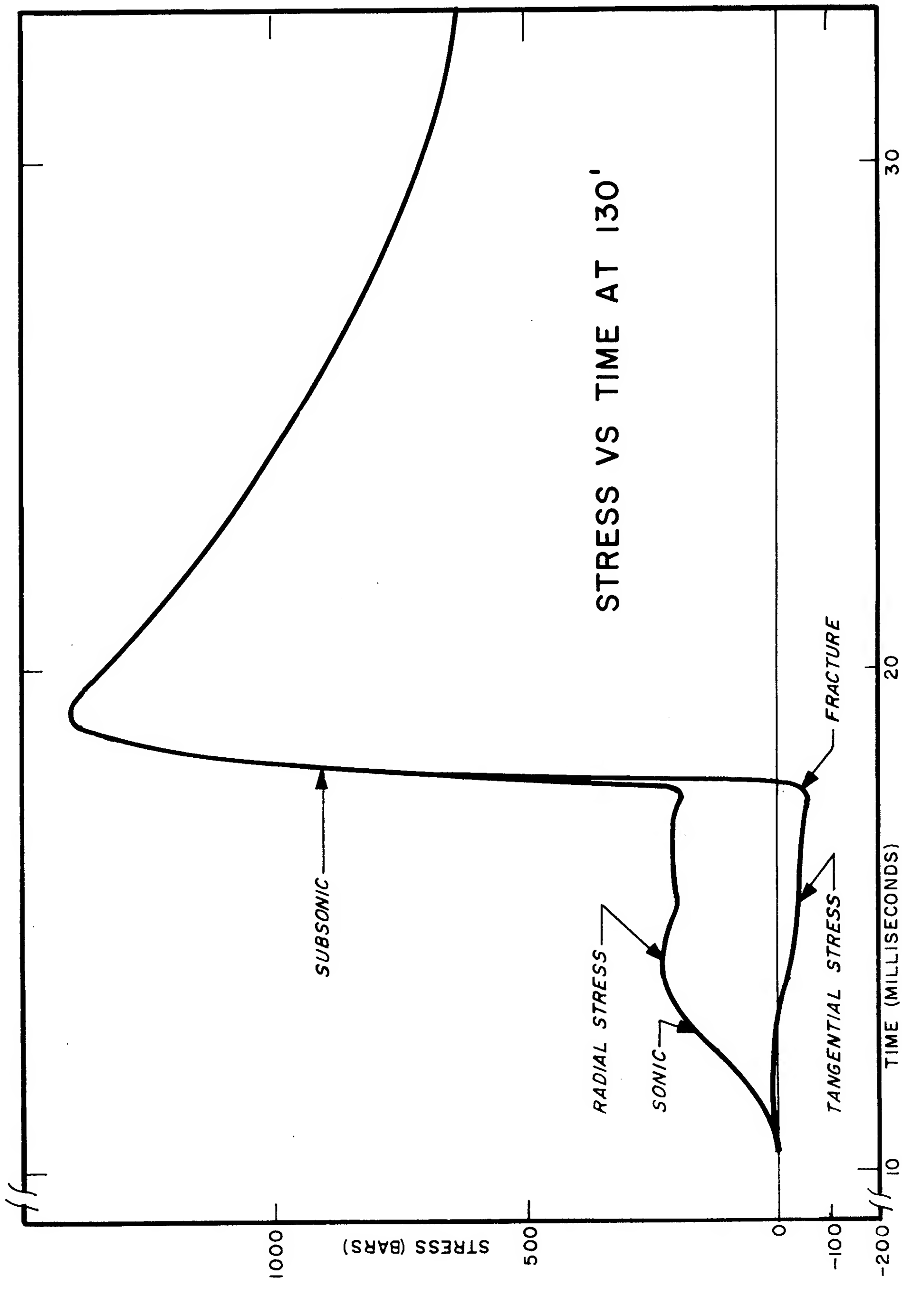
STRESS VS TIME AT 130'
SUBSONIC
FRACTURE
RADIAL STRESS
SONIC
TANGENTIAL STRESS
STRESS (BARS)
1000
500
0
-100
-200
10
20
30
TIME (MILLISECONDS)
MUL-10258

Fig. 2.4.

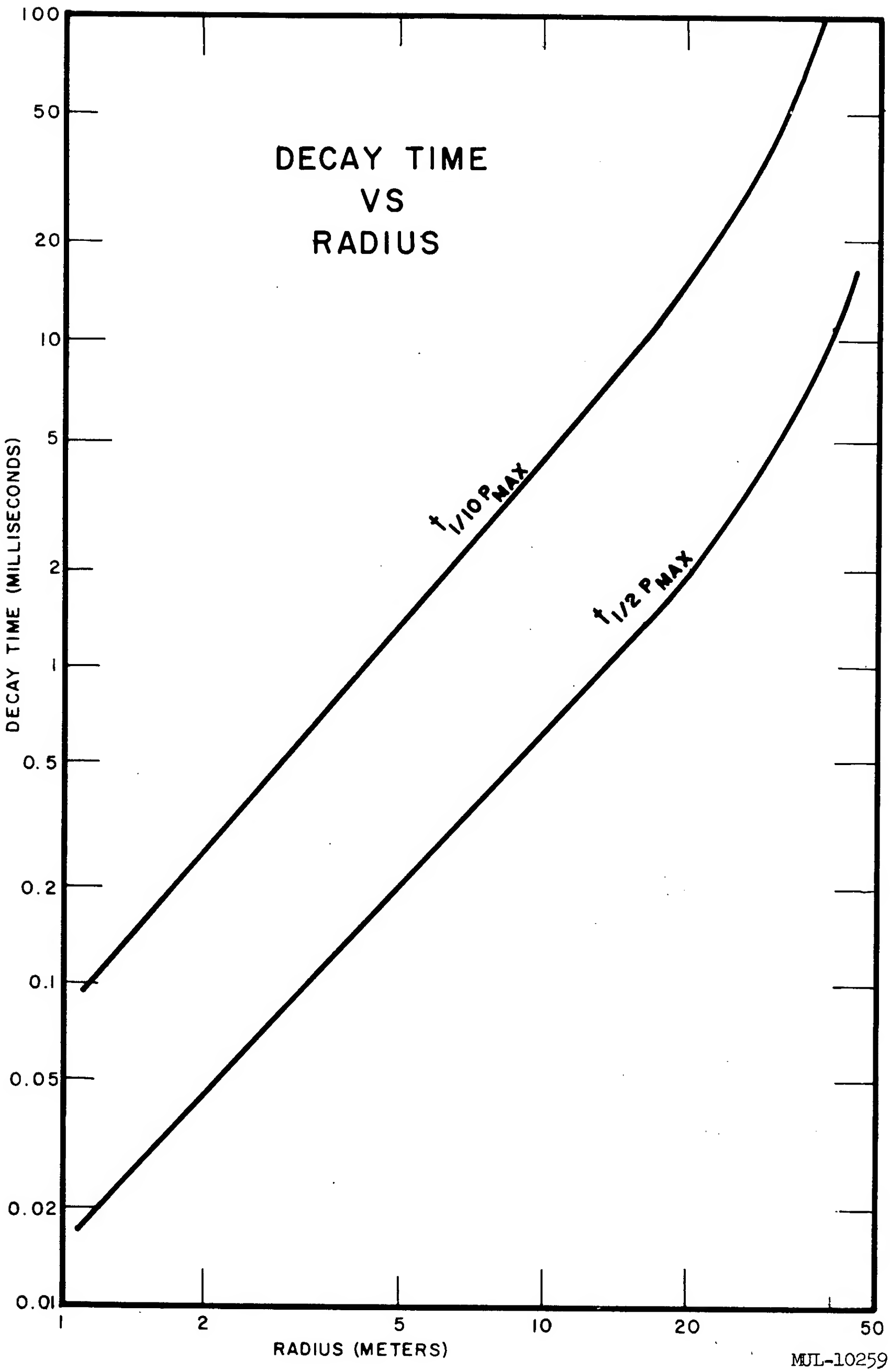
DECAY TIME
VS
RADIUS
DECAY TIME (MILLISECONDS)
100
50
20
10
5
2
1
0.5
0.2
0.1
0.05
0.02
0.01
$t_{1/10 P_{MAX}}$
$t_{1/2 P_{MAX}}$
1
2
5
10
20
50
RADIUS (METERS)
MUL-10259

Fig. 2.5.

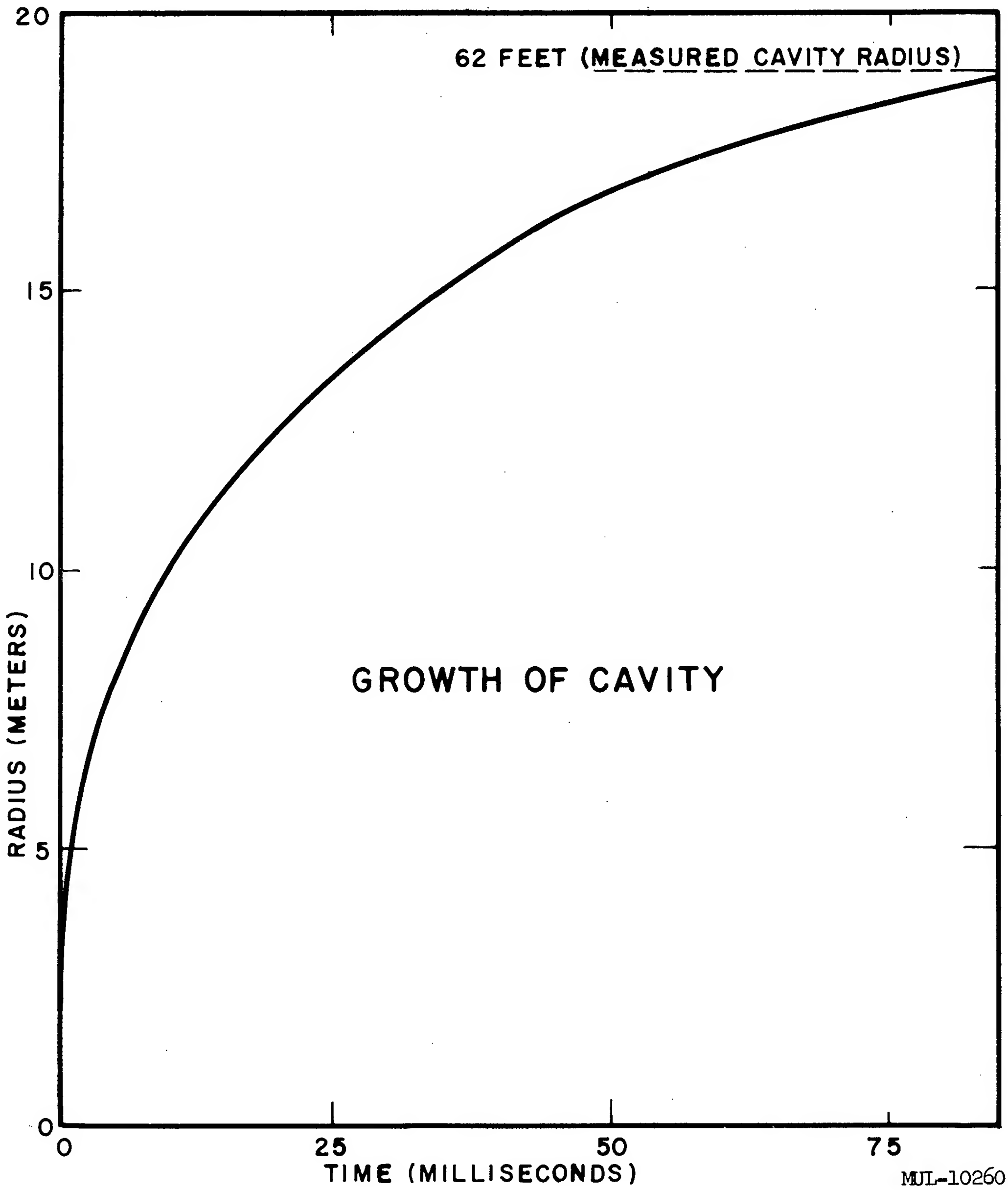
62 FEET (MEASURED CAVITY RADIUS)
GROWTH OF CAVITY
RADIUS (METERS)
TIME (MILLISECONDS)
0
5
10
15
20
0
25
50
75
MUL-10260

Fig. 2.6.

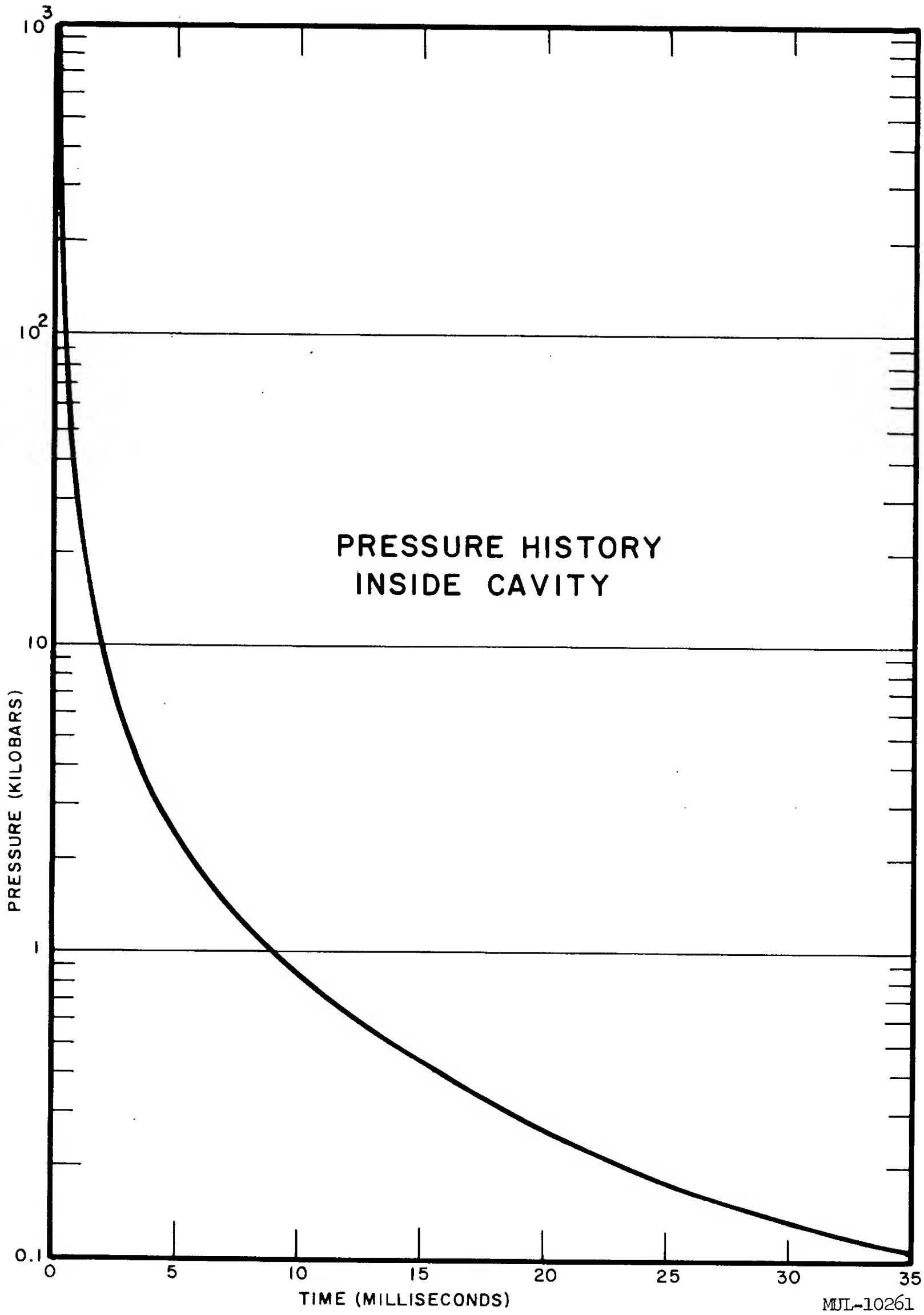
PRESSURE HISTORY
INSIDE CAVITY
PRESSURE (KILOBARS)
10^3
10^2
10
1
0.1
0
5
10
15
20
25
30
35
TIME (MILLISECONDS)
MJL-10261

Fig. 2. 7.

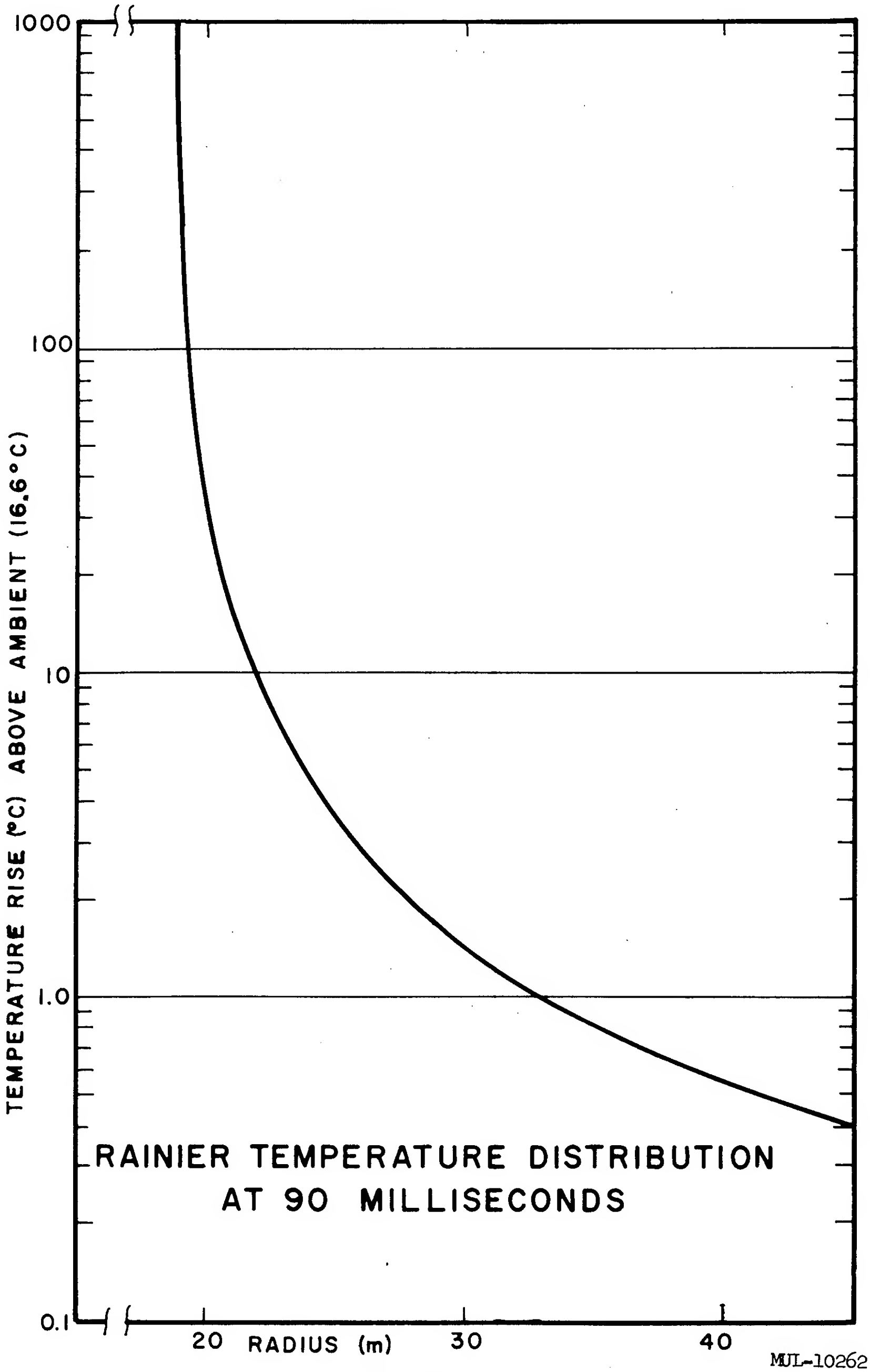
1000
100
10
1.0
0.1
TEMPERATURE RISE (°C) ABOVE AMBIENT (16.6°C)
RAINIER TEMPERATURE DISTRIBUTION
AT 90 MILLISECONDS
20
RADIUS (m)
30
40
MUL-10262

Fig. 2.8.

CONCLUSIONS

Much of the phenomena that occur during the first 100 msec after a contained underground nuclear explosion in tuff can be predicted with considerable accuracy. Calculations are now being made of other proposed Plowshare experiments.

NOTE ADDED DECEMBER 1959

The elasto-hydrodynamic model used for these calculations is being generalized to a reversibly cracked elasto-plasto-hydrodynamic system: Radial and tangential cracks are opened and closed reversibly. At initial time the diagonal components of the elastic stress are compressive by amount ρgh (ρ = density, g = acceleration of gravity, h = depth of burial). When one of these compenents (radial or tangential) becomes tensile (due to the deformation resulting from the explosion), it is set to zero during the current time cycle and the other component is calculated from its strain. When the stress becomes compressive again, the material is treated as a linear elastic solid with no cracks.

Under high confining pressures the rock flows plastically and supports large shearing stresses. The magnitude of the shear is calculated from a function of the pressure (where pressure is the average of the stress components), and the sign is determined by the sign of the radial velocity. The pressure is computed from the initial shock Hugoniot. Upon liquifaction a transition is made to the hydrodynamic phase (no shear). The main effect of the plasto-dynamic theory is to damp the system, i.e., slow the expansion of the cavity and increase the rise time of the disturbances generated by the explosion. Experiments are being planned to determine the constants needed for the theory.

The various states and transitions are indicated in the following diagram:

UNEC Material Behavior

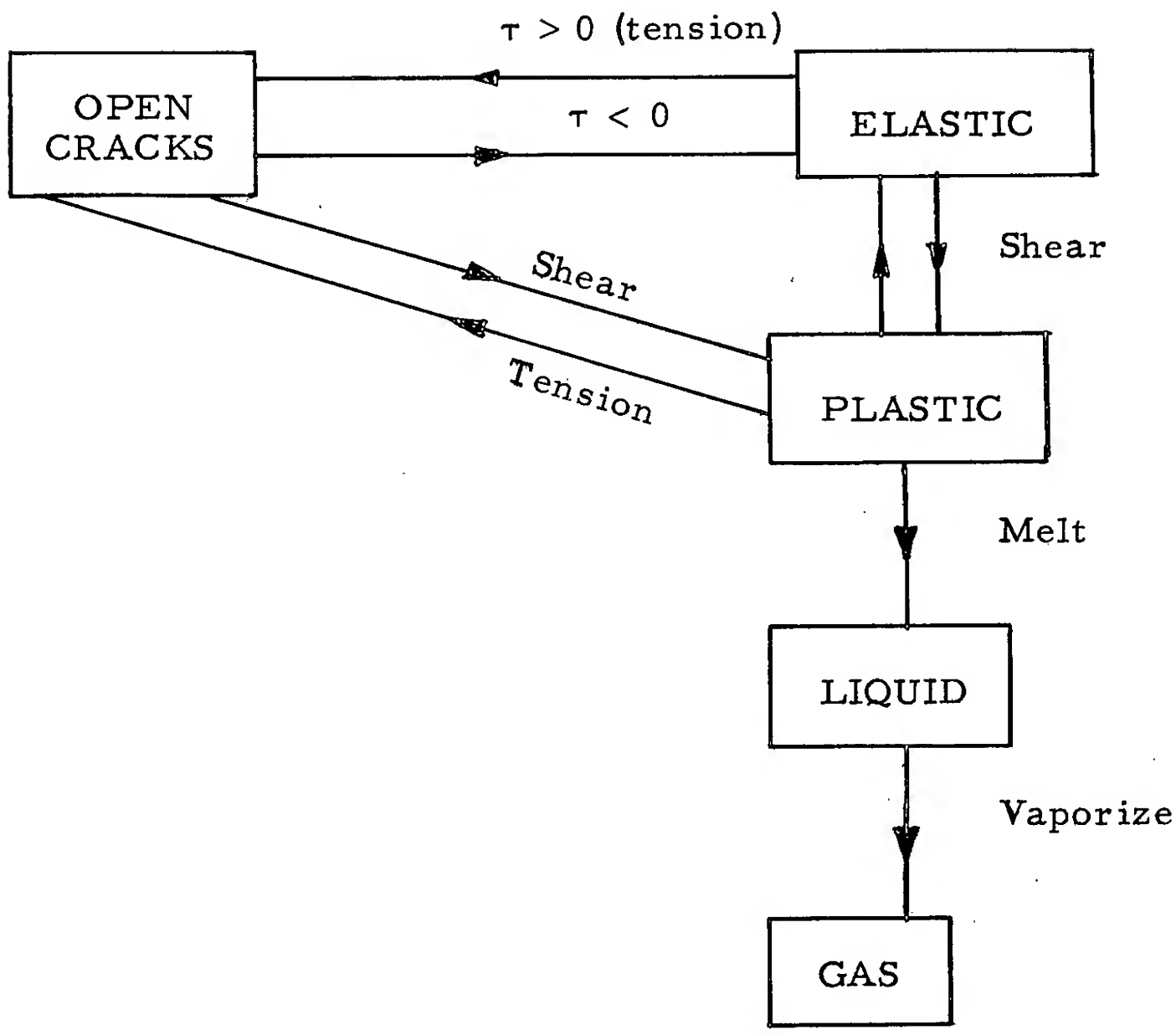

3. SPALLING AND LARGE BLASTS

John S. Rinehart

Professor of Mining Engineering, Colorado School of Mines

INTRODUCTION

Large contained nuclear blasts impart tremendous forces to their immediate surroundings and these forces, becoming distributed in accordance with well known laws of physics, produce damage in areas both near and remote from the blast. Many qualities of damage manifest themselves and of these one of the most esoteric is spalling, i. e., separation of rock, frequently close to a free surface, as a consequence of preferential partitioning of the momentum of the stress wave. The elemental principles of the dynamics and mechanics of spalling in soils and rocks are discussed here. These principles are then used to appreciate more fully the significance of the observations of ground movement at the Rainier blast.

PROPAGATION OF TRANSIENT DISTURBANCES

When a buried nuclear device explodes, the action of the blast is not instantaneously transmitted to regions remote from the blast. Changing stress situations will be communicated through most materials at velocities of several thousand feet per second, the exact value depending upon the material, the type of stress distribution, the state of stress within the medium, and the various boundaries involved. In large earth masses, velocities of two general types are encountered:

The dilatational velocity, c_l, the velocity of propagation of longitudinal waves in a medium of infinite extent, is given by

$$c_l = \left[\frac{3K(1-\nu)}{\rho(1+\nu)}\right]^{1/2} ,$$

where K is the bulk modulus; ρ is the density of the material; and ν is its Poisson's ratio. Variations of K, ρ, and ν with stress affect the value of c_l.

Shearing displacements advance through a material with a velocity given by c_t

$$c_t = (G/\rho)^{1/2} ,$$

where G is the rigidity modulus.

If the stress level is exceedingly high, the material will behave as a fluid, having no rigidity, and transverse or shear waves cannot exist within it. Under these conditions, stress changes will be propagated with a velocity, c_f, given by

$$c_f = (K/\rho)^{1/2}$$

The state of stress will affect both K and ρ. Indeed, at the exceedingly high pressures produced by nuclear blasts, changes in values of K and ρ can amount to 30 or 40%.

A stress disturbance passes through a body in the form of a transient wave of particle motions. A point or infinitesimally small particle within the body will be subjected to forces which impart transitory motions to it. The instantaneous velocity, v, of such a particle is directly related to the instantaneous stress σ at that point by the equation

$$\sigma = \rho c v \quad ,$$

where c is the velocity of propagation, viz., c_l, c_t, or c_f, of the disturbance. Particle velocity in a longitudinal wave is parallel to the direction of propagation of the wave, moving along with an advancing compressional wave and opposite to an advancing tension wave. Particle motion within a transverse wave is normal to the direction of propagation of the wave. In a typical granite, a particle velocity of 3 fps corresponds roughly to a stress of 1000 psi.

A typical disturbance, such as might have been generated by an underground nuclear blast, is shown in Fig. 3.1. The particular parameters used in plotting the curve are selected for convenience. Note that there is a 1:1 correspondence between stress and particle velocity and that whether time or distance is used as the abscissa will depend upon whether the phenomenon is viewed at all points in space simultaneously or at a single point through which the disturbance is passing. The instantaneous velocity of propagation of any point on the wave depends upon the level of stress at that point, being given by the expression

$$c = [(d\sigma/d\epsilon)/\rho]^{1/2},$$

where $(d\sigma/d\epsilon)$ is the slope of the stress-strain curve at that stress level. Unless the stress-strain curve is linear, which is seldom the case, the different points on the disturbance will range in velocities. Thus the shape of the

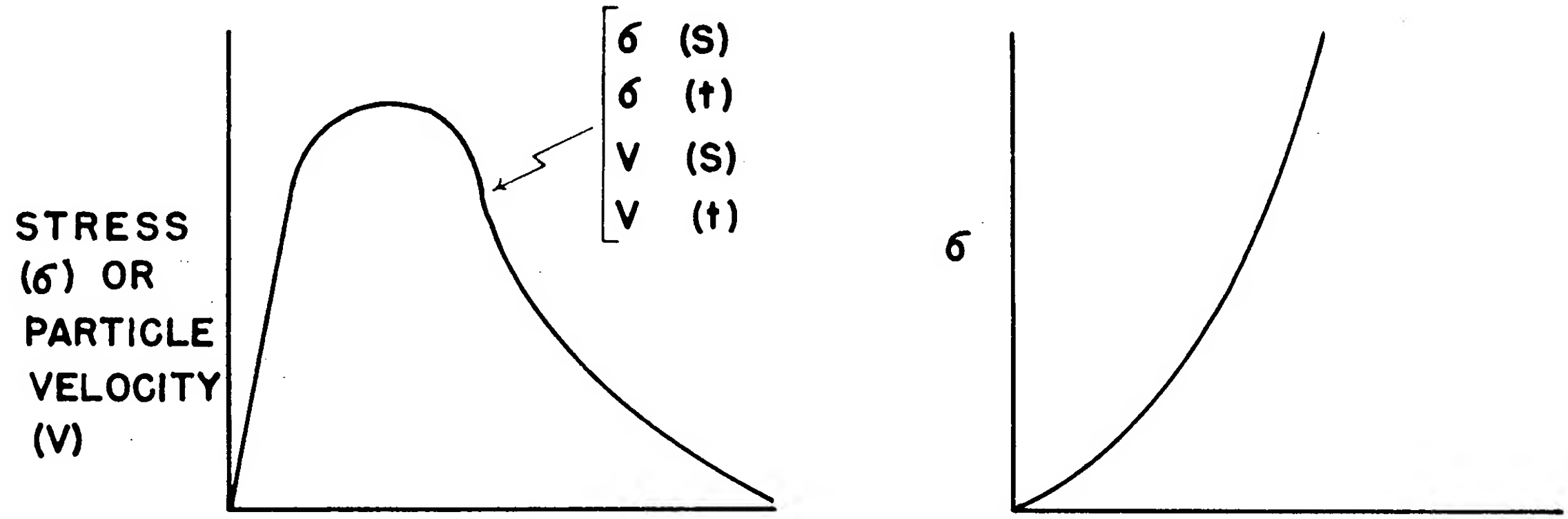

$$\sigma = \rho C V \qquad C = \sqrt{\frac{d\sigma}{d\epsilon}/\rho} \qquad \sigma = \sqrt{\rho \frac{d\sigma}{d\epsilon}} \cdot V$$

C IS VELOCITY OF POINT ON WAVE

MUL-10263

Fig. 3.1.

disturbance will be continually changing as it moves along. In the particular case shown in Fig. 3.1, the wave would tend to steepen its front since the higher stresses would be traveling at greater velocities than the lower stresses.

Rocks exhibit a wide variety of stress-strain curves. Typical curves for limestone and sandstone are shown in Fig. 3.2. Note that the limestone curve is concave downward which means high stresses will travel at relatively low velocities while the sandstone is concave upward, implying that the high stresses will travel at high velocities. In limestone, the waves will tend to elongate and flatten out, with just the reverse being true in sandstone.

DYNAMICS OF SPALLING

Viewed simply a material is said to spall when one segment of its parts and moves off from another segment. This will occur if the velocity of the one segment is greater than the velocity of the other, as illustrated in Fig. 3.3. Stress waves, on reaching a free surface and reflecting, are prone to give rise to this type of partition of velocity or momentum. Consider the semi-infinite body of Fig. 3.4, in which a stress wave of the shape shown is advancing toward a free surface. Assume, further, that the stress-strain curve is linear. When a disturbance strikes the free surface, it will be reflected as a tension wave without change in form. The incident compression wave and its reflected tension counterpart will interfere with each other as indicated. The resultant distribution of stress within the body at a slightly later instant is shown in the right hand drawing, the tension, AB, increasing as the reflected wave moves to the left. At some point, the material will no longer be able to support this tension; it will fracture; and a spall will fly off, trapping much of the momentum of the wave. The stress required to rupture the material is called its critical normal fracture stress, σ_c. In metals, this fracture stress is exceedingly high, corresponding to differential particle velocities of 100 to 200 ft/sec. In rocks, the stress is quite low, being in the neighborhood of 500 psi (1 to 2 fps particle velocity for granite). The critical normal fracture stress is an extremely important mechanical property of the material and is the factor that governs parting of the material. Note that two factors are important in describing spalling: the shape of the stress wave, and the critical normal fracture stress. Determination of the thickness of the spall is a simple geometrical problem, provided σ_c and the shape of the

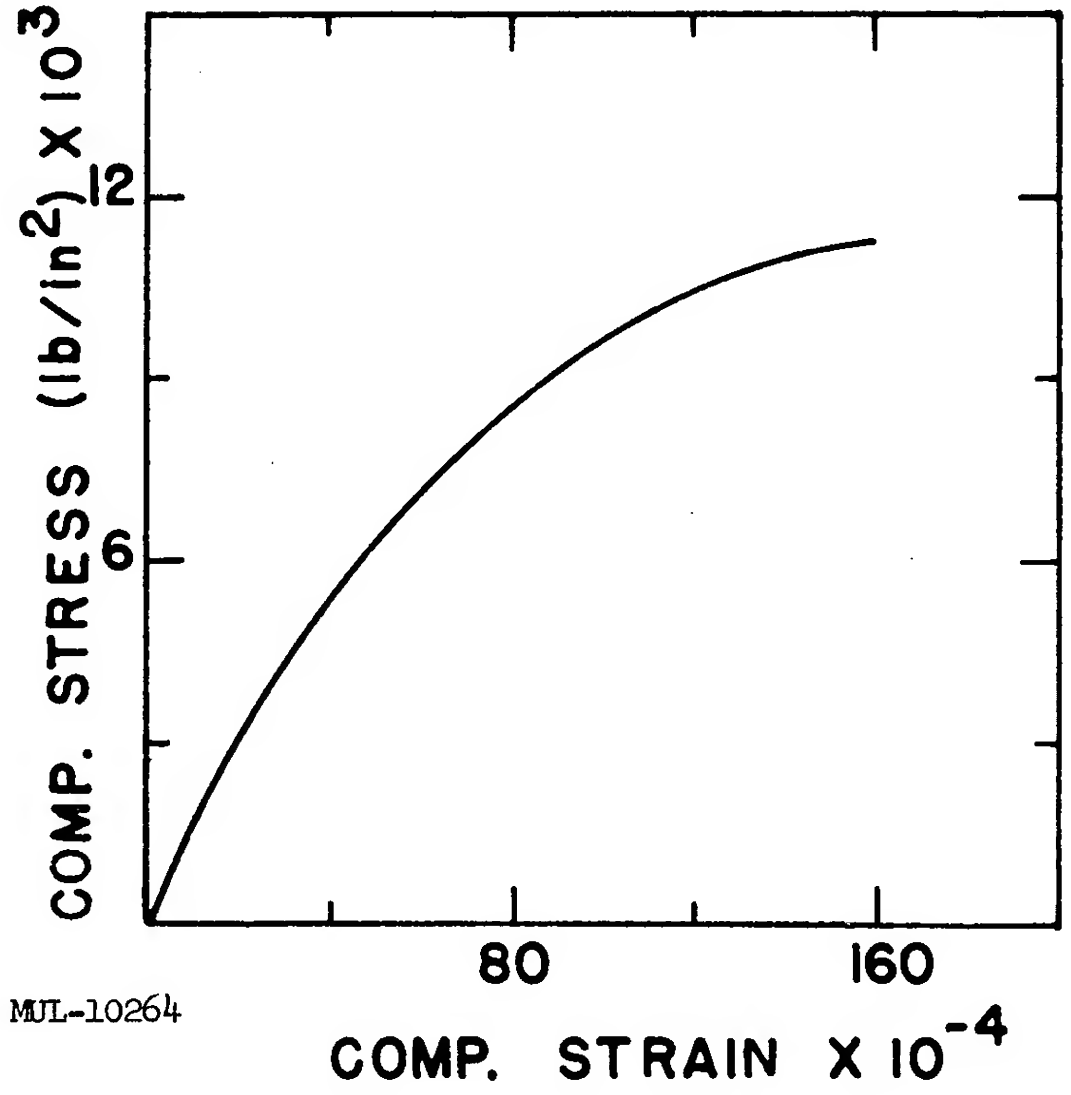

DOLOMITIC LIMESTONE
(GREEN RIVER)

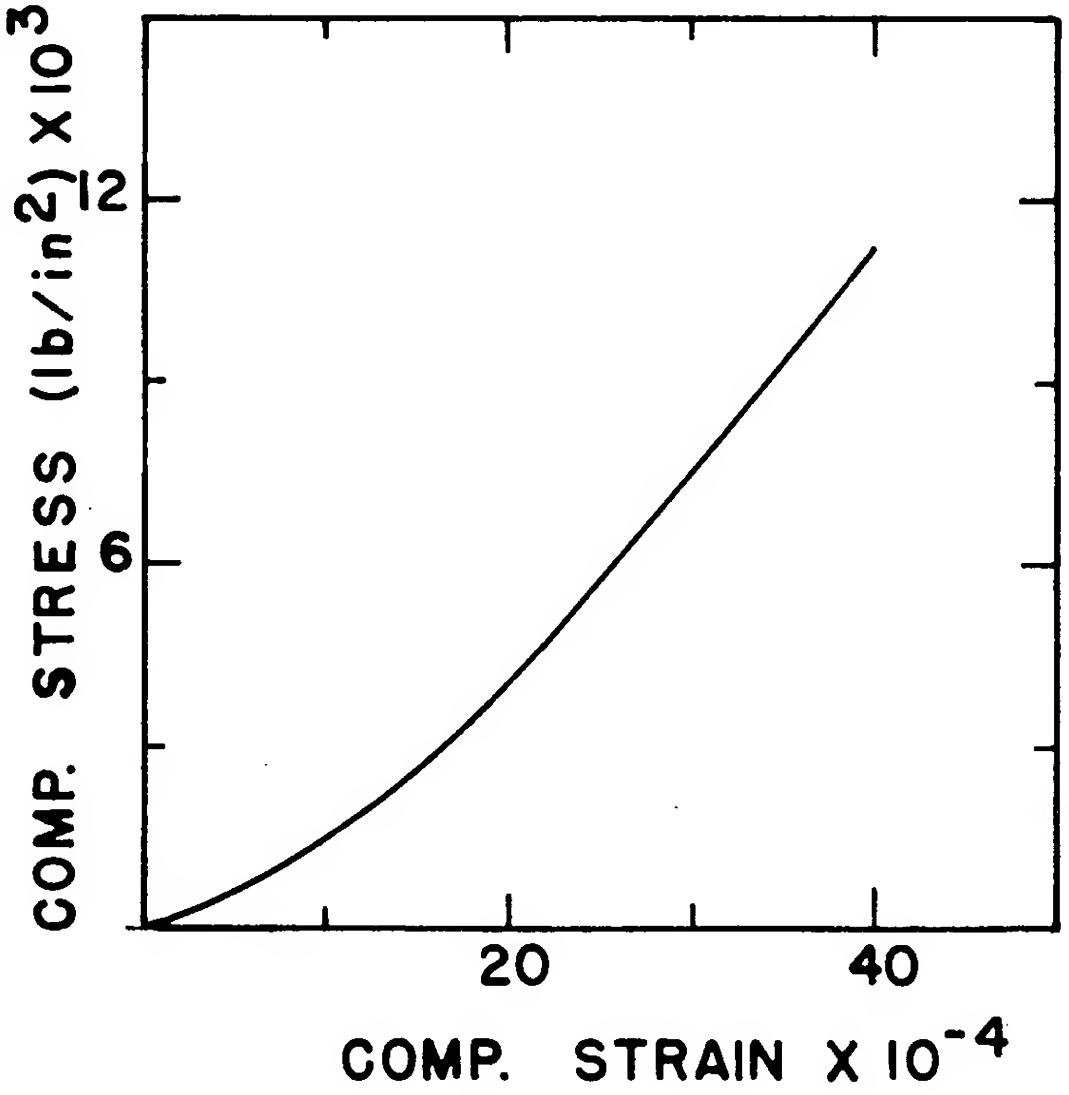

SANDSTONE
(NAVAJO)

Fig. 3.2.

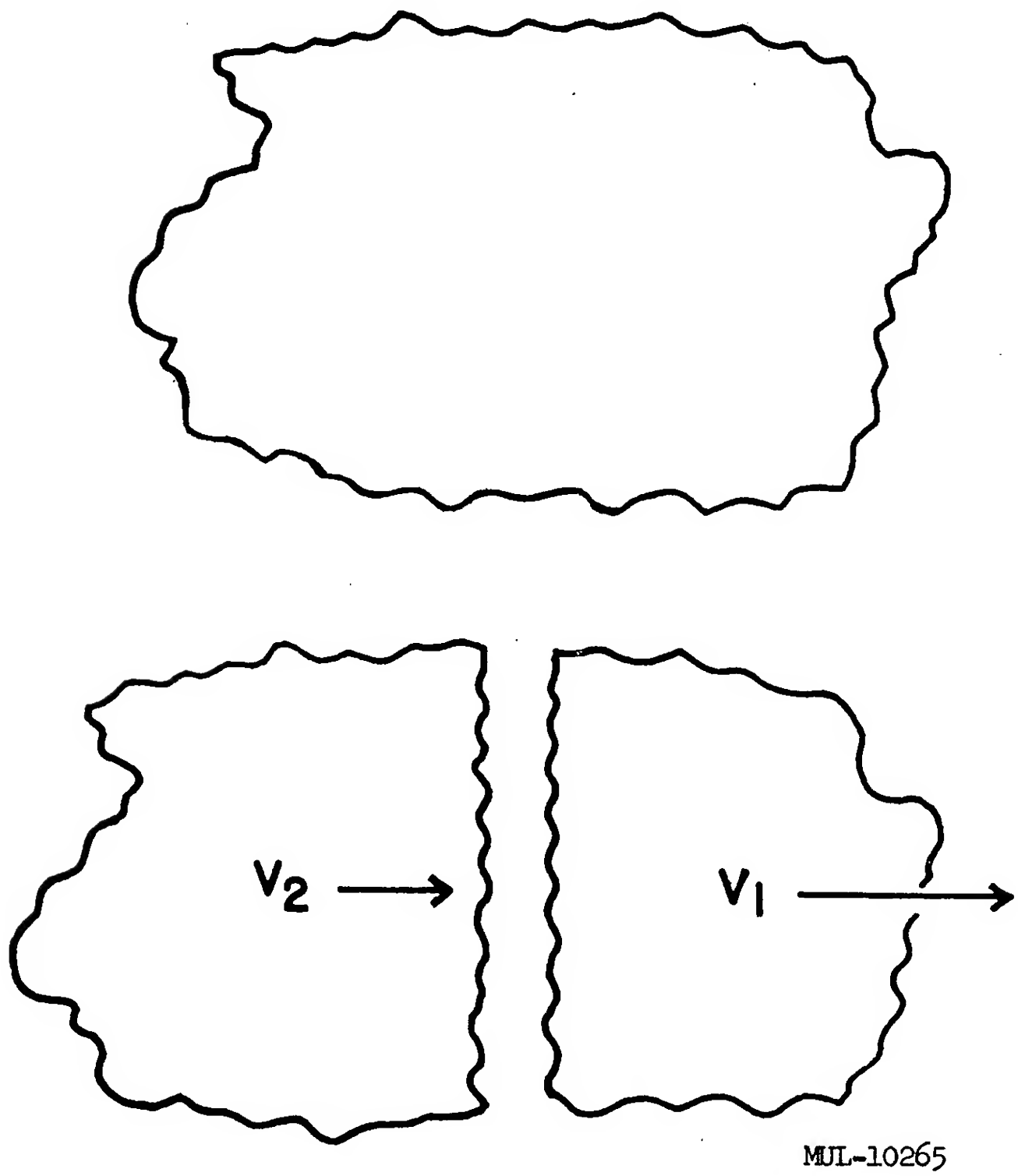

MUL-10265

$$V_1 > V_2$$

Fig. 3. 3.

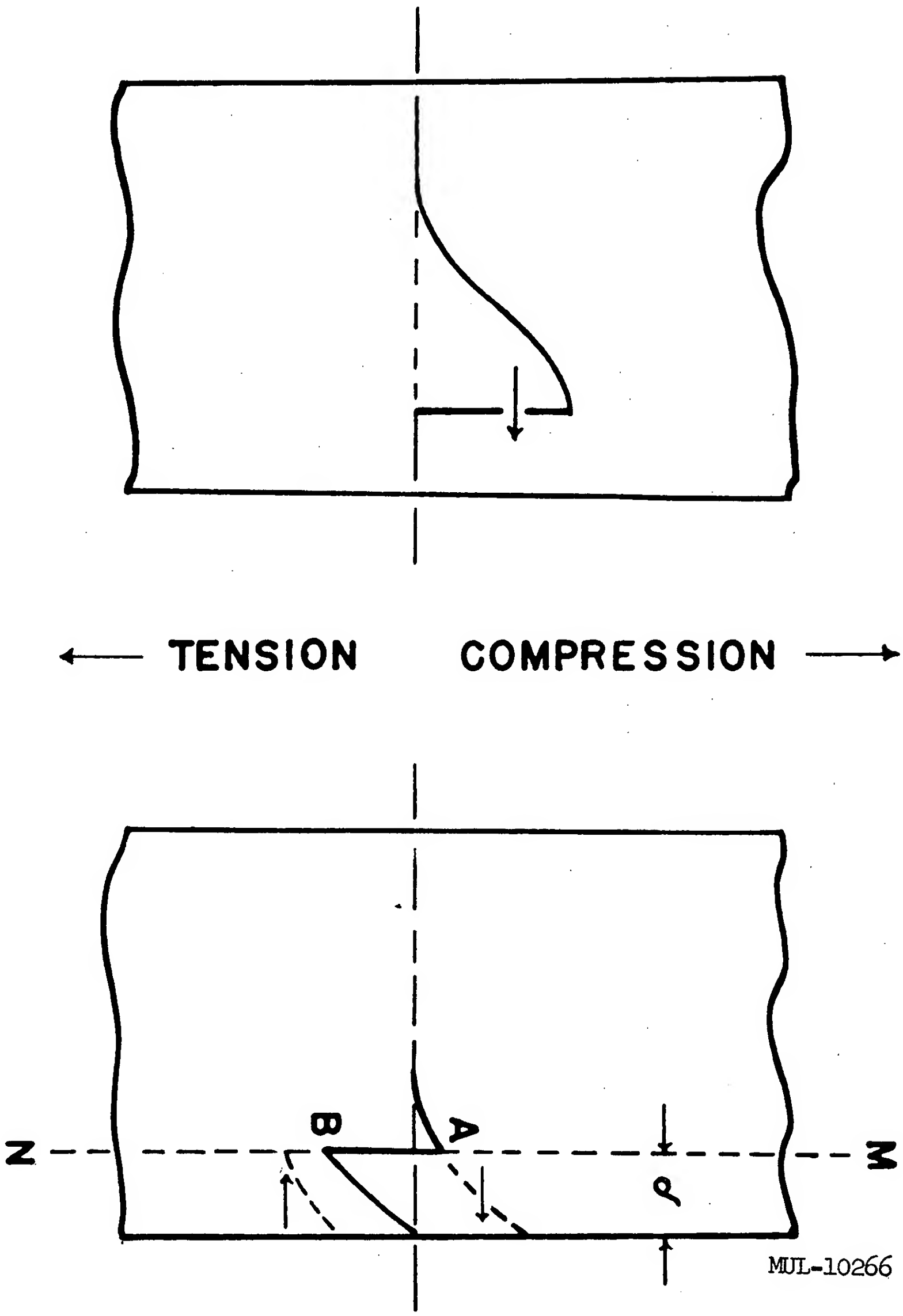

Fig. 3.4.

wave are known. Thickness of spall will be equal to 1/2 the distance within the wave that corresponds to a decrease in stress equal to σ_c.

Multiple spalling occurs when the stress level within the wave is more than double the critical normal fracture stress of the material. In such cases, several juxtaposed and parallel spalls are generated as illustrated in Fig. 3. 5. These arise in the following way: Assume that the first spall is generated in the manner just described. The remainder of the wave will suddenly find itself impinging on a freshly created, free boundary surface. The result will be the formation of another spall. This process will repeat itself until the stress level of the wave has been reduced to a value less than σ_c. In the case illustrated the thickness of the two spalls are vastly different. The first spall is quite thick because the leading portion of the wave is relatively flat. The subsequent abrupt decrease in stress thins down the second spall.

As pointed out earlier, underground blasts can give rise to disturbances of a wide variety of shapes which continually change as they propagate. Four idealized shapes are illustrated in Fig. 3. 6. In view of the strong dependence that the thickness of the spall has upon shape of disturbance, it is apparent that each particular shape of disturbance generates its own characteristic spalls. Given the shape of the wave and the fracture stress of the material, it is, of course, possible to describe precisely the character of these spalls. The simplest shape to consider is the sawtooth curve in the upper left hand corner of Fig. 3. 6. This shape does not differ appreciably from that of the disturbance produced in the consolidated tuff 900 feet from the Rainier shot (see Fig. 3. 7).

INFLUENCE OF MATERIAL PROPERTIES ON SPALLS

The tensile strength, compressive strengths, competencies, and anisotropics in mechanical properties range widely in rocks and soils. The foregoing section described spalling for the very particular situation where the rock is perfectly elastic and anisotropic. It was also tacitly implied that the material could support a compressive stress greater in magnitude than the tensile stress it could support. In real situations such an ideal circumstance will not be obtained. Compare now the three differing situations shown in Figs. 3. 8, 3. 9, and 3. 10.

The first of these, Fig. 3. 8, illustrates the spalling which will occur when a sawtooth wave, of length λ and maximum stress σ_0, strikes the free

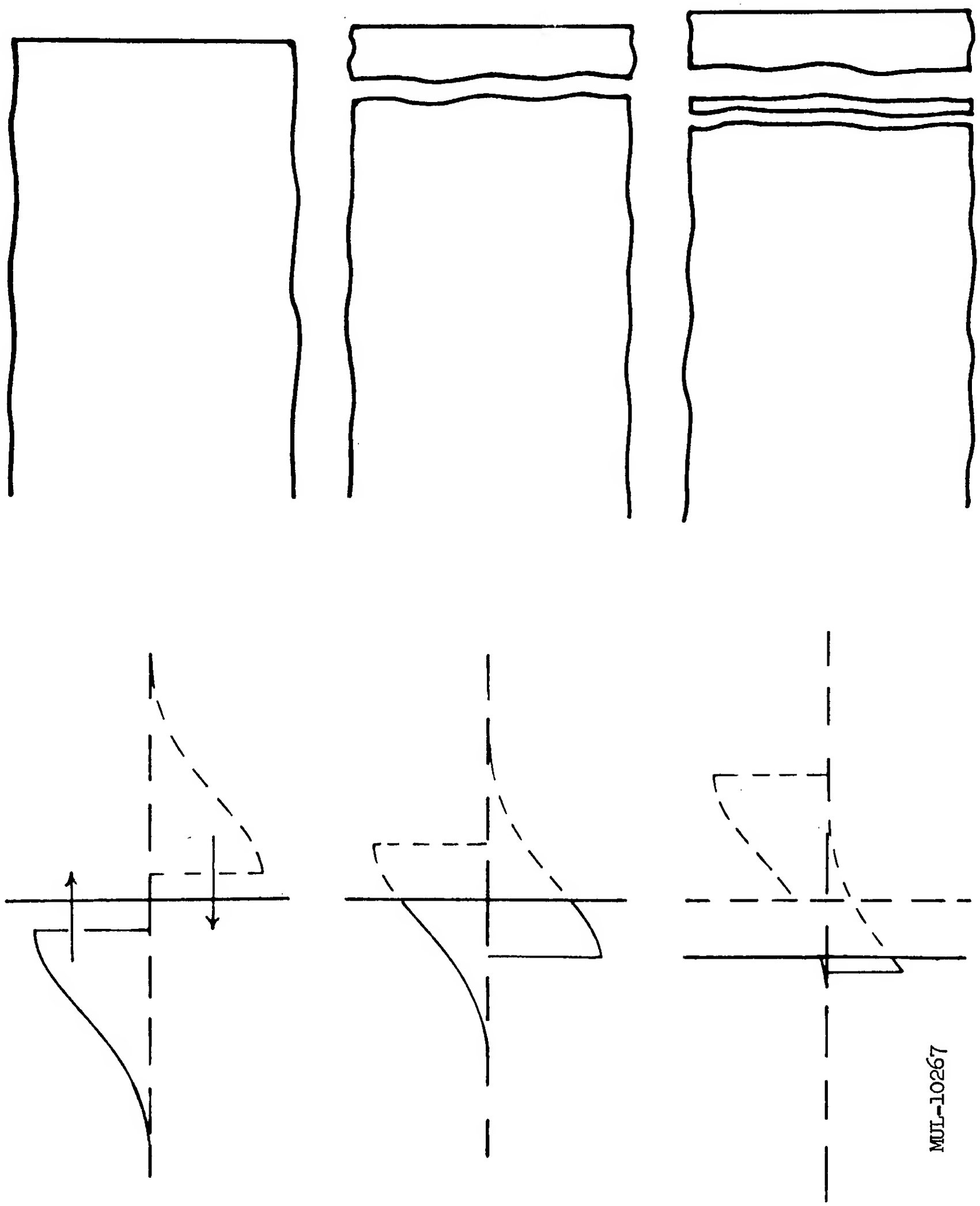

MUL-10267

Fig. 3.5.

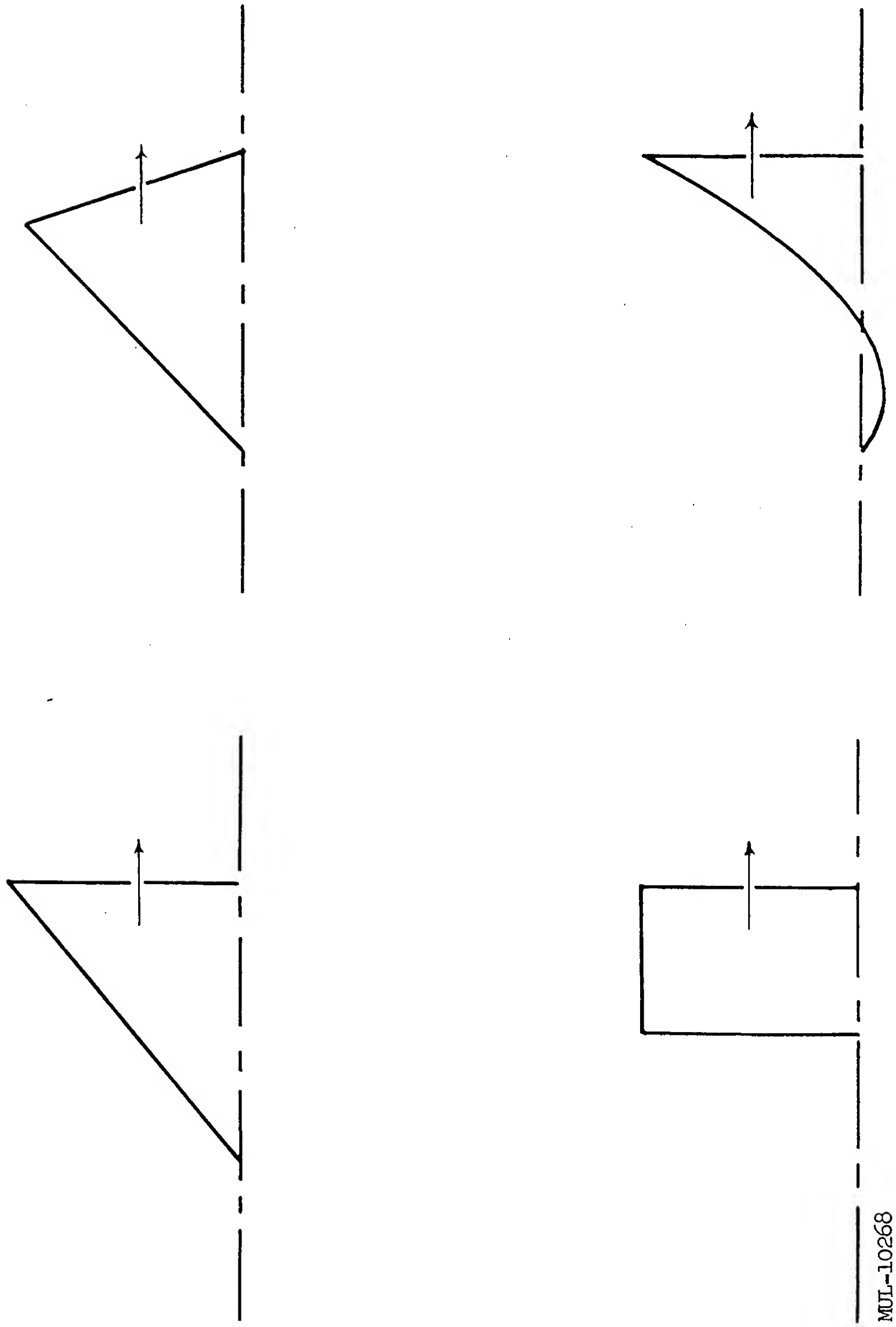

MUL-10268

Fig. 3.6.

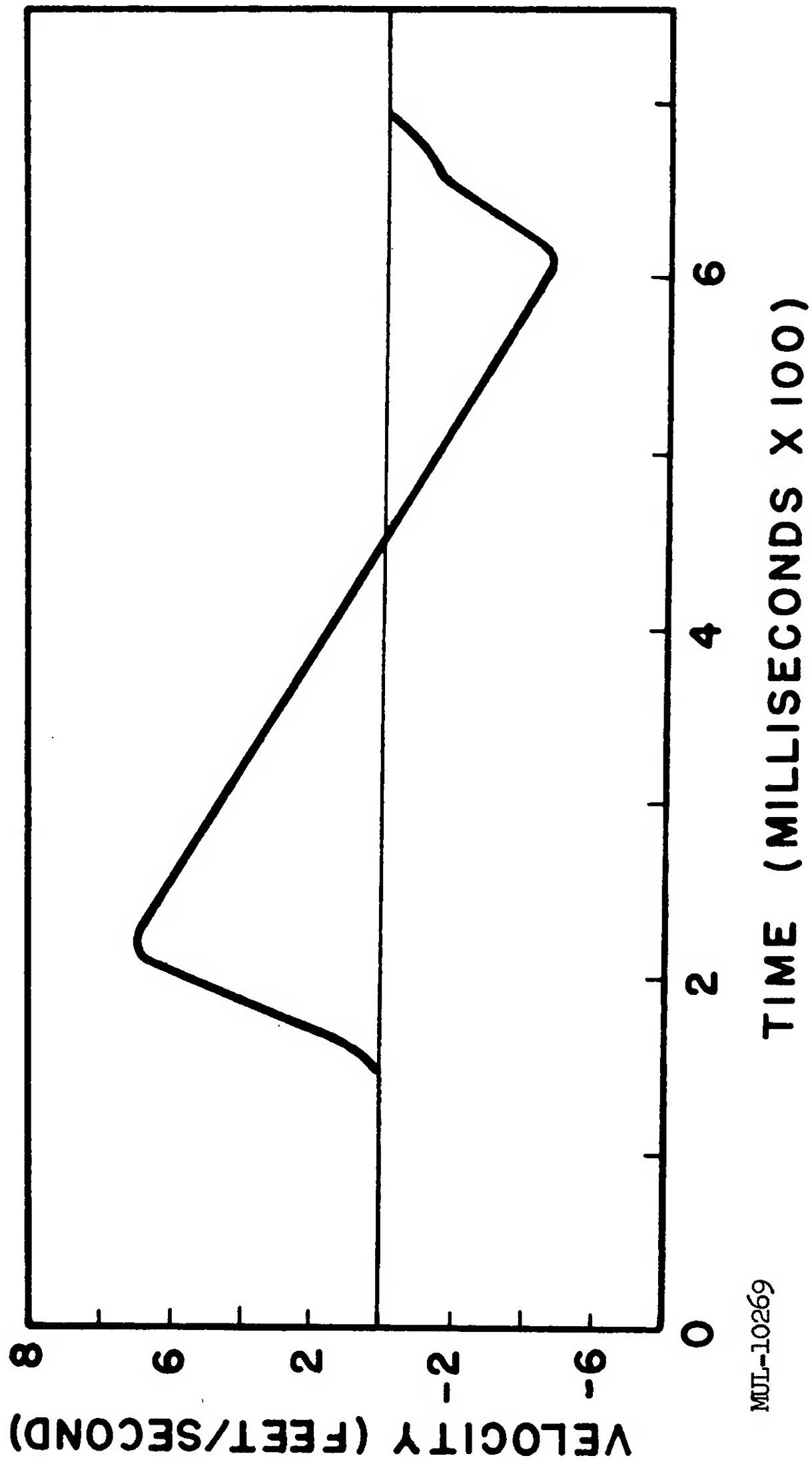
VELOCITY (FEET/SECOND)
8
6
2
-2
-6
0
2
4
6
TIME (MILLISECONDS X 100)
MUL-10269

Fig. 3.7.

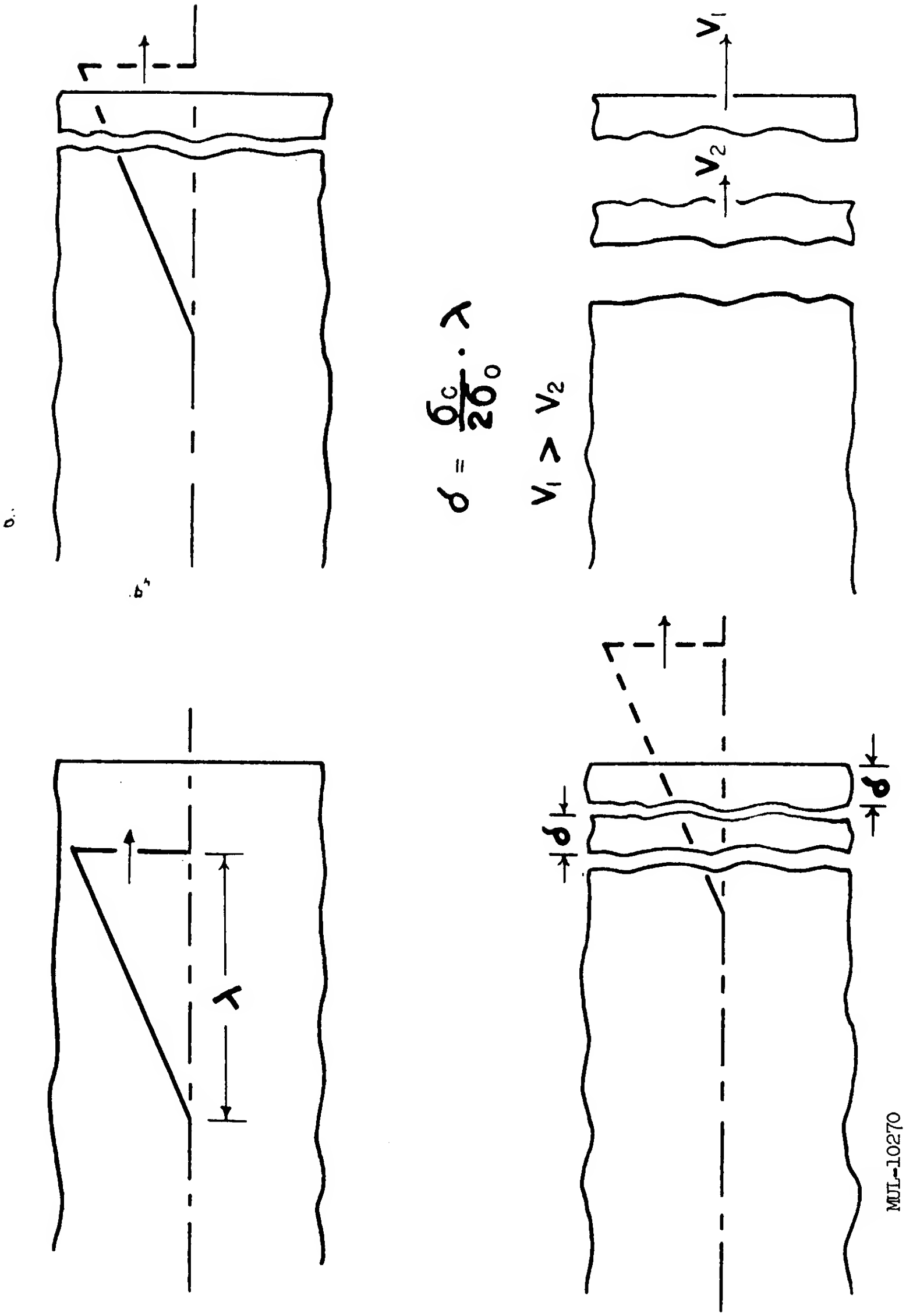
λ
a.
b.
$\gamma = \frac{\sigma_c^c}{2\sigma_o} \cdot \lambda$
$V_1 > V_2$
V_1
V_2
d
d
MUL-10270

Fig. 3.8.

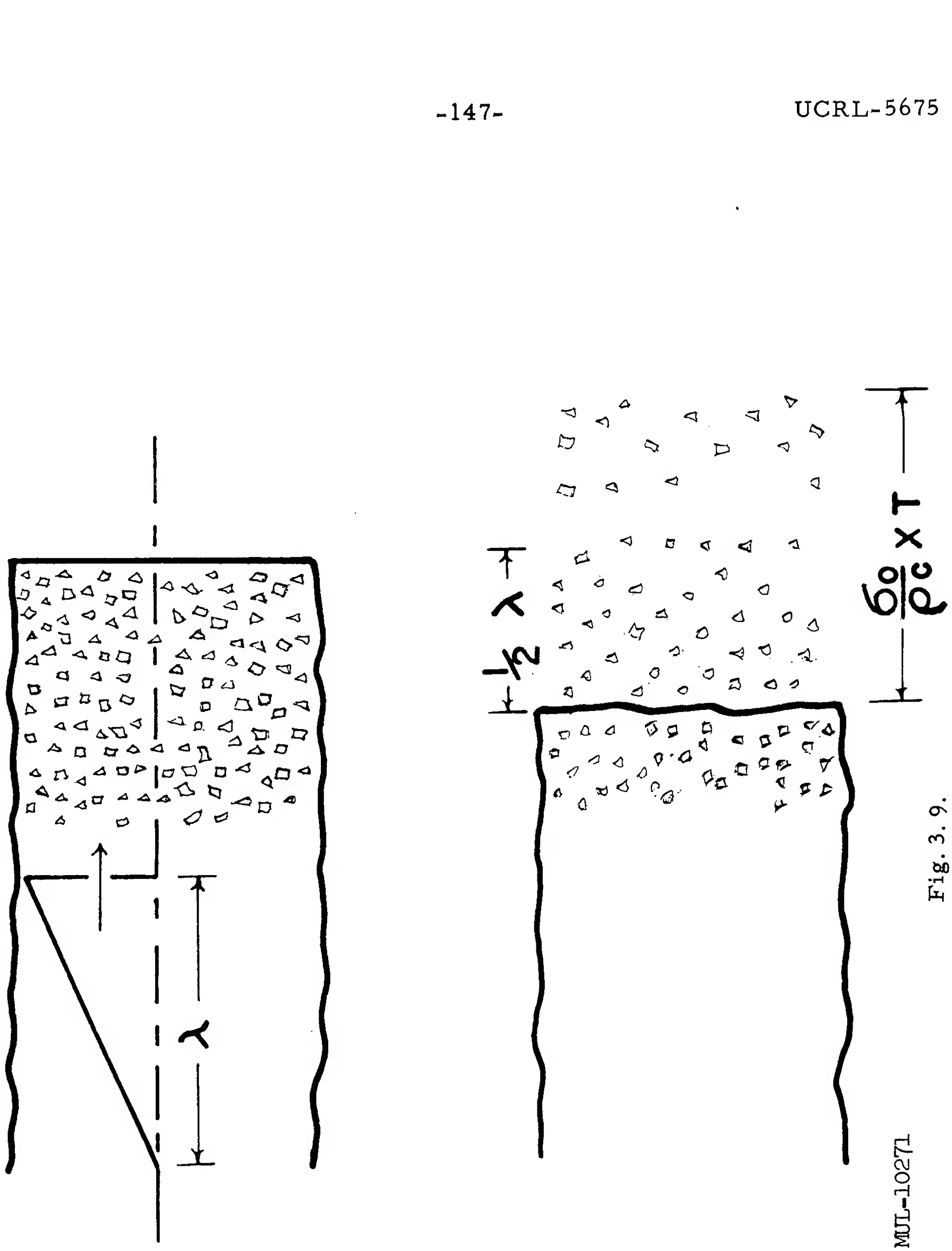

Fig. 3.9.

MUL-10271

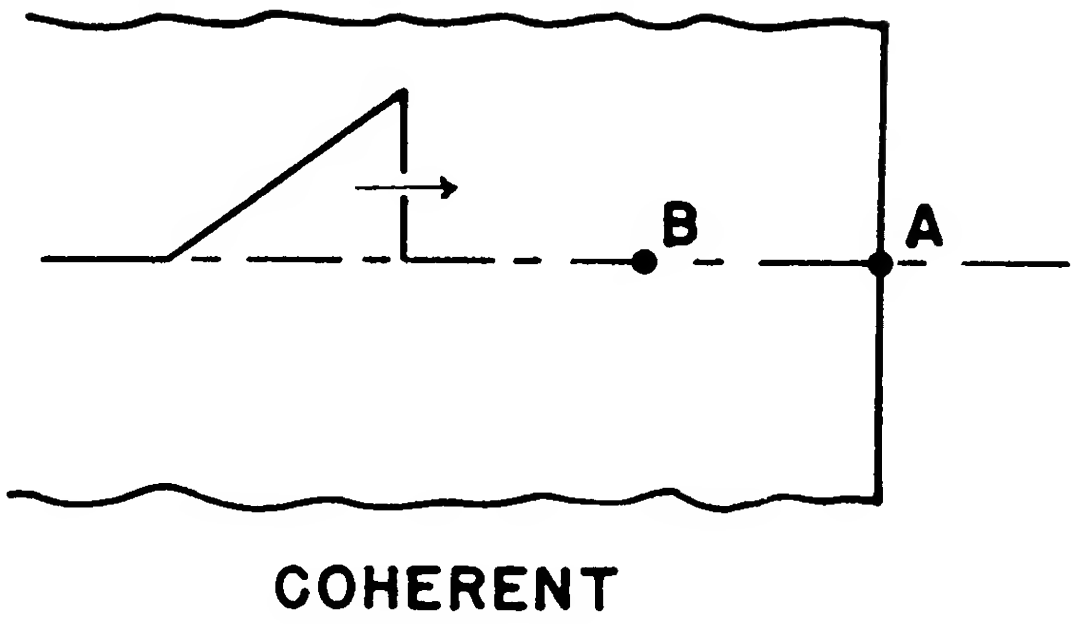

COHERENT

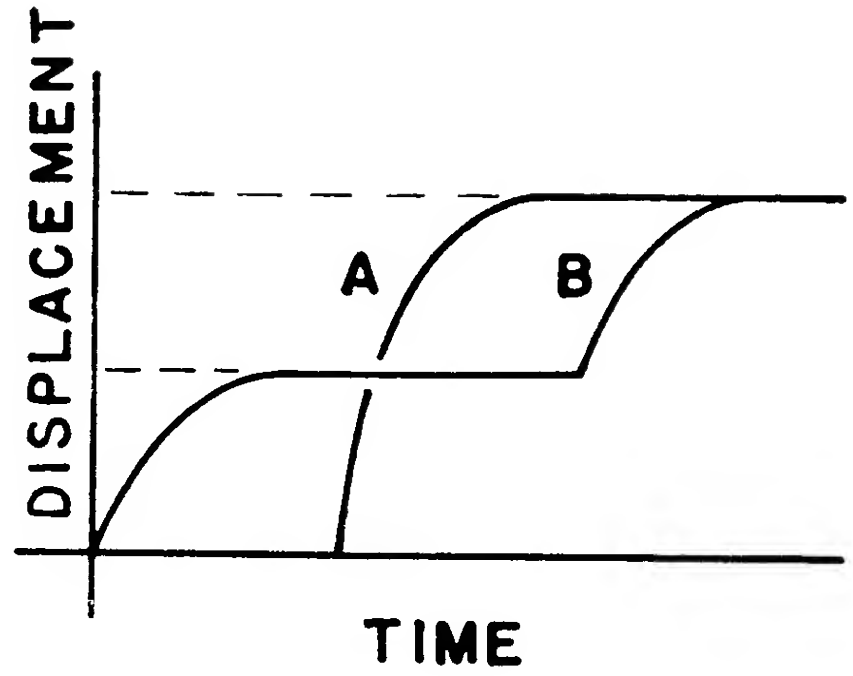

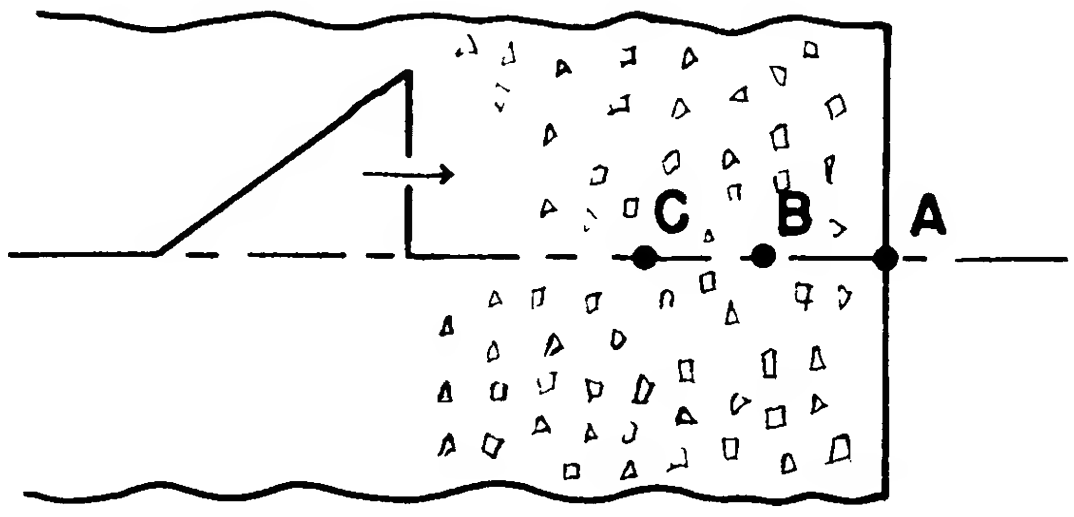

MUL-10272

NON - COHERENT

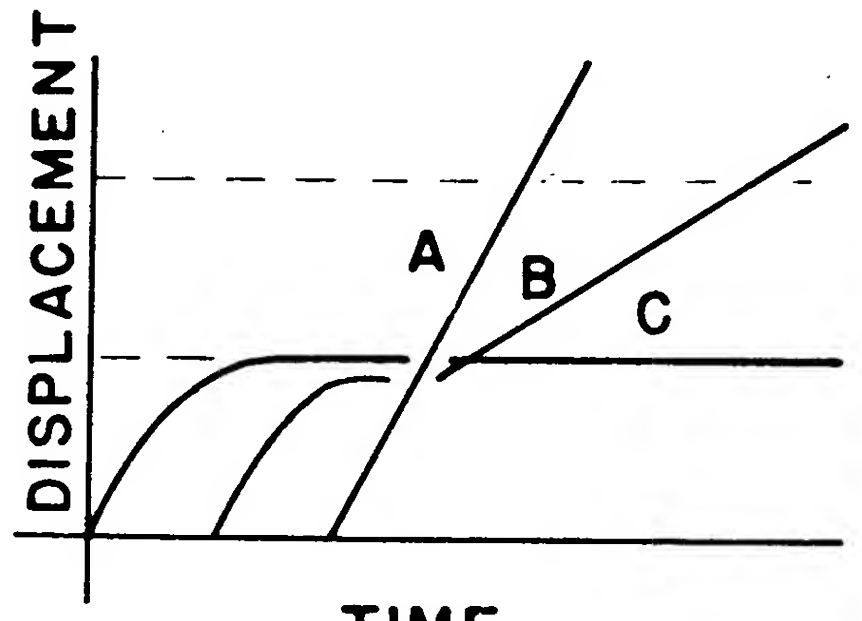

Fig. 3.10.

surface of an elastic material having a critical normal fracture stress σ_c, which is between 1/2 and 1/3 of σ_0 . Two spalls are thrown off. Both are of equal thickness, given by

$$\sigma = \left(\sigma_c/2\sigma_0\right)\lambda$$

but of different velocities, the piece to the right having the highest velocity. Specifically, the two velocities, v_1 and v_2, are

$$v_1 = 2v_0 - \left(\sigma_c/\rho_c\right); \qquad v_2 = 2v_0 - \left[3\left(\sigma_c/\rho_c\right)\right].$$

As the detached spalls move to the right they will become separated by an amount which is easily calculable using the above equations.

Figure 3.9 illustrates what will happen under similar circumstances when the material is incompetent, incapable of supporting any tension whatsoever. It is assumed, however, that a compressional wave will be transmitted without change in form. As soon as the wave reaches the free surface, the material will begin to flake off. The velocities of these first flakes will be equal to $2v_0$ where v_0 is given by

$$v_0 = \sigma_0/\rho_c \ .$$

Each bit of flaking absorbs a small portion of the momentum of the incident wave. The remaining portion of the incident wave will continue to advance against the freshly created free surface, flaking continuing so long as any portion of the wave remains. The velocity, v_p, of any small particle will be given by

$$v_p = \sigma/\rho_c \ ,$$

where σ is the value of the stress at the front of the incident wave at the time the particle leaves the surface. The initial thickness of the flaked off material will be $(1/2)\lambda$. The flakes themselves will appear as a cloud of debris, the rear portion of which is stationary and the front moving forward with a velocity $2v_0$. Thus the extent of the cloud of debris is continually increasing, its forward portion becoming less dense.

The situation for incompetent rock or soil is examined in a little more detail in Fig. 3.10. Here are compared the displacements of points within a

competent, elastic solid which does not spall and an incompetent mass which flakes off. Note that in the competent solid, the two points, A and B, eventually undergo the same displacement but do not do so simultaneously. The reason their total displacements are the same is simply that the material does not fly apart, and such must therefore be the case. The incompetent material behaves differently. Point A initially acquires a velocity which is maintained so that A moves farther and farther away from C. B moves along at a somewhat lower velocity. If the free surface of such a mass were horizontal, the restraining force of gravity would affect the material so that it would be brought to rest. These two drawings illustrate graphically the primary reason why damage is so much greater in unconsolidated soils and unconsolidated material than in solid rock.

The action of the wave on a series of juxtaposed slabs is illustrated in Fig. 3.11. The joints between the slabs are assumed to be perfect transmitters of compression but possessing no strength in tension. Each slab is of thickness L. On striking the free surface, the incident wave will be reflected, with the reflected portion proceeding backward (into the left) into the rightmost slab. When the wave reaches the first joint, the rightmost slab will fly off, trapping in it the momentum in the wave back to a distance 2L. The velocity of this slab, v_{s1}, will be

$$v_{s1} = v_0 + v_1 \ .$$

The second slab will then be carried off in a similar fashion with a velocity given by

$$v_{s2} = v_1 + v_2$$

and finally, the third slab with a velocity

$$v_{s3} = v_2 + v_3 \ .$$

THE RAINIER SHOT

It was observed in the Rainier shot that one or more large slabs of consolidated tuff, or rhyolite, situated about 900 feet above the blast, as illustrated in Fig. 3.12, rose to a height of 9 in. and then fell. From these data and accelerometers placed in a vertical hole situated directly above the blast, it was possible to make a reasonable guess of the shape of the stress wave

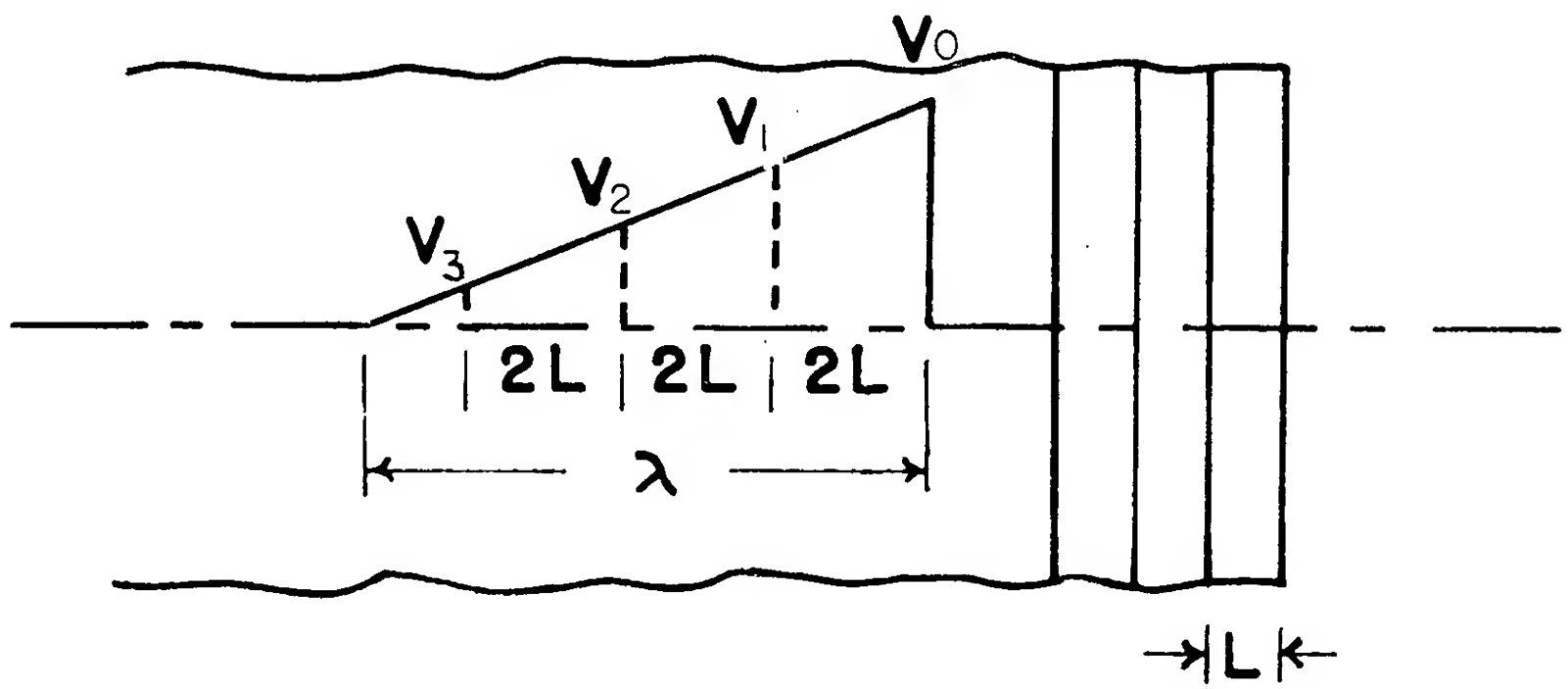

$$V_1 > V_2 > V_3$$

$$V_{S1} = \frac{V_0 + V_1}{2} \cdot 2$$

$$V_{S2} = \frac{V_1 + V_2}{2} \cdot 2$$

$$V_{S3} = \frac{V_2 + V_3}{2} \cdot 2$$

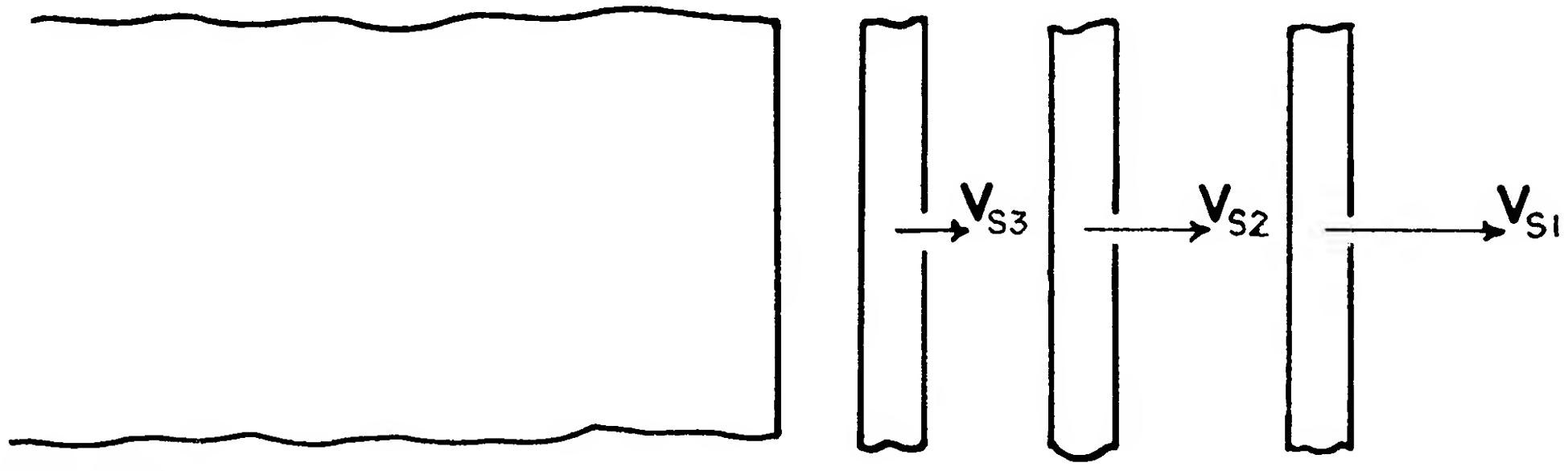

MUL-10273

Fig. 3.11.

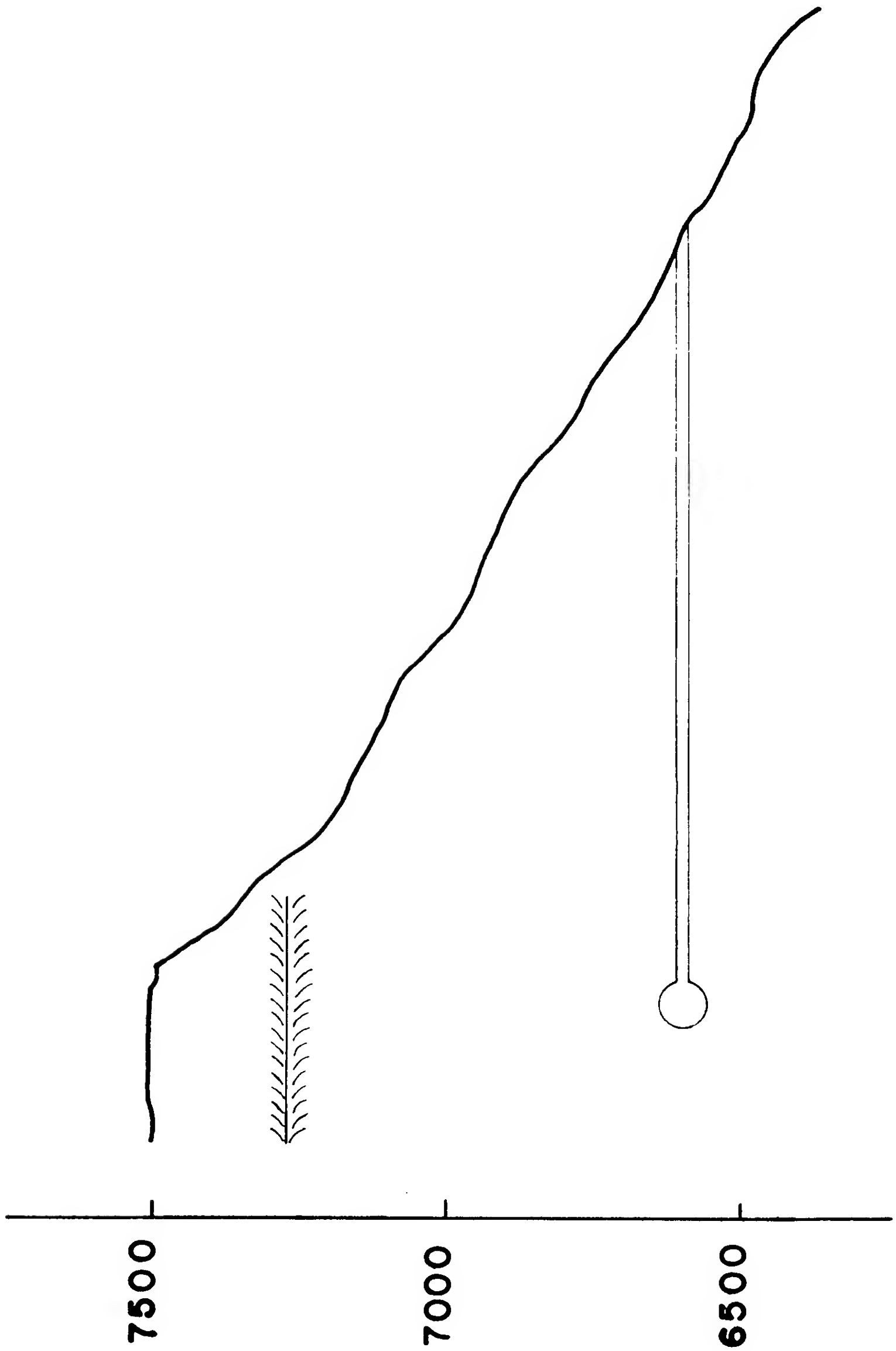

Fig. 3.12.

which reached this top layer of rock. The most probable curve is shown in Fig. 3.7. The leading portion of this curve approximates the sawtooth waves whose actions have been discussed above. In Fig. 3.13, the wave is redrawn as a stress versus distance plot and shown approaching the free surface of the rhyolite. The specific gravity of the rhyolite was taken as 2.7. The maximum stress in the wave is 1500 psi, corresponding to a maximum velocity of 7 fps, taking an average velocity for propagation of a wave of 6000 fps, close to the measured value. Such a wave would produce three spalls of equal thicknesses in a material having a tensile strength of 500 psi, a value reasonably close to that which might be expected for rock of this type. The three spalls would move away with initial velocities, 5.8, 3.5, and 1.5 fps. Gravity would slow these slabs down so that the total excursion of the top slab would be 7 to 9 in. Taking a somewhat lower tensile strength, say 250 psi, several more, but thinner, slabs would be generated. The thickness of the consolidated tuff layer was 230 ft. It seems likely that the entire slab probably moved as a unit with additional spalling taking place in the material below. All of the observations made are entirely consistent with what can be predicted from an appreciation of the elements of spalling. The two most important parameters needed are the shape of the wave and the fracture strength of the rock. In most situations, the rock will be stratified so that it will come off in layers of thicknesses preselected by nature.

In considering the possibility of damage, it should be noted that the effect of gravity restricts substantially the movement of rock, primarily because the velocities involved are so low. Spalling produced on the walls and roofs of tunnels and other underground openings will not have the mollifying effects of gravity.

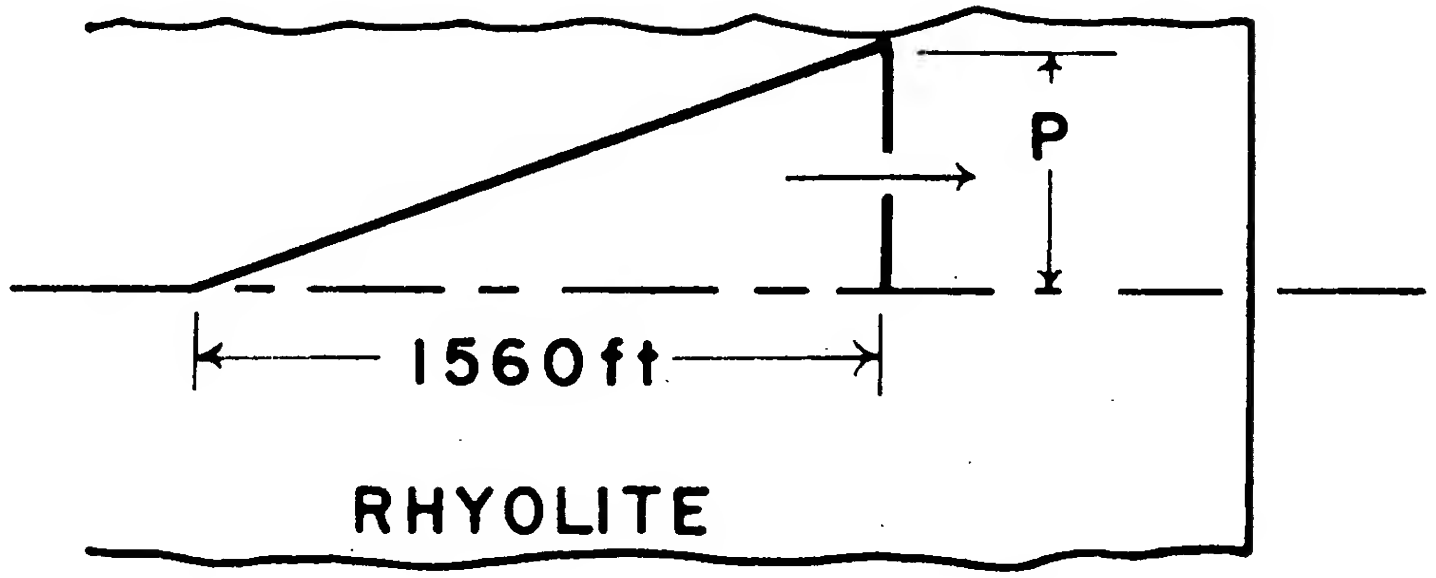

$P = 1530\ lb/in^2$

$L = 255\ ft$

$V_1 = 5.8\ ft/sec$

$V_2 = 3.5\ ft/sec$

$V_3 = 1.5\ ft/sec$

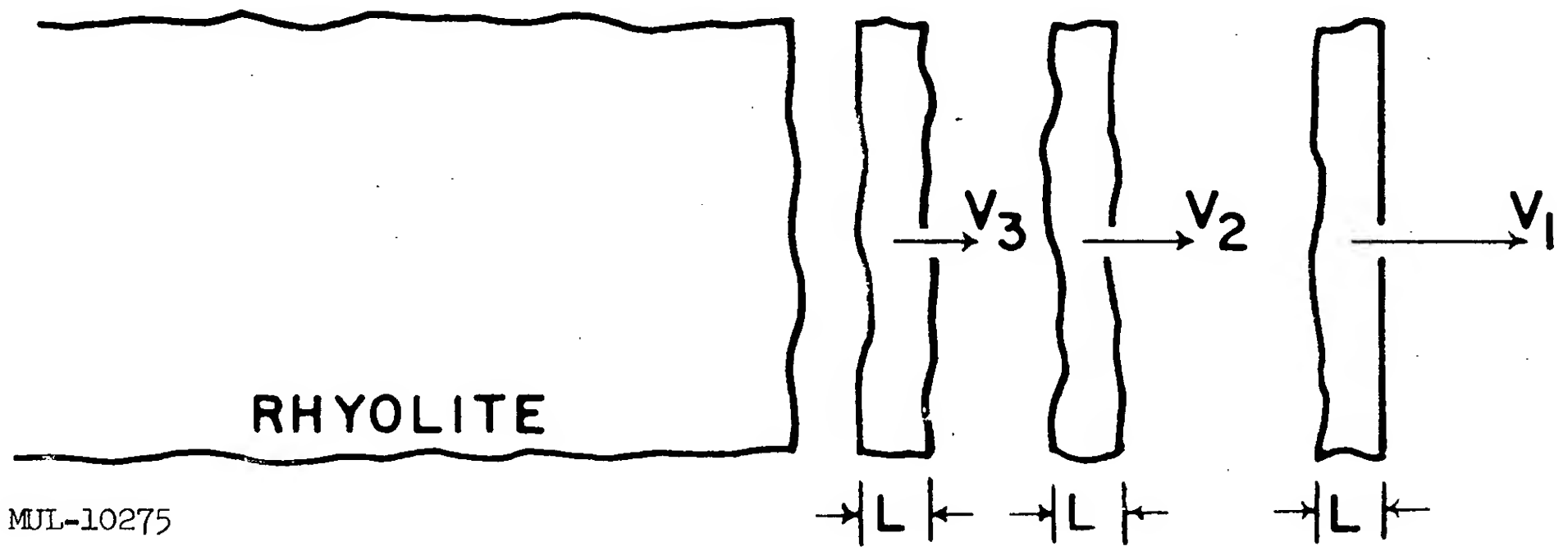

MUL-10275

Fig. 3.13.

BIBLIOGRAPHY

1. G. R. Pickett, "Seismic Wave Propagation and Pressure Measurements Near Explosions," Quarterly, Colorado School of Mines, Vol. 50, No. 4, Oct. 1955.
2. W. R. Perret and R. G. Preston, "Preliminary Summary Report of Strong-Motion Measurements from a Confined Underground Nuclear Detonation," ITR-1499, June 1958.
3. R. G. Wuerker, "Annotated Tables of Strength and Elastic Properties of Rocks," Petroleum Branch, AIME, Dec. 1956.
4. G. W. Johnson and C. E. Violet, "Phenomenology of Contained Nuclear Explosions," UCRL-5124 Rev. I, Dec. 1958.
5. W. R. Perret, "Subsurface Motion from a Confined Underground Detonation - Part I," ITR-1529, Nov. 1958.
6. B. E. Blair, "Physical Properties of Mine Rock, Part III," Bureau of Mines, R. I. 5130, June 1955.

4. A SEISMIC SCALING LAW FOR UNDERGROUND EXPLOSIONS

A. L. Latter and E. A. Martinelli, RAND Corporation

Edward Teller, Lawrence Radiation Laboratory

Seismic measurements have been made on five underground nuclear explosions ranging in energy release from about 70 tons to 19 kilotons TNT-equivalent. All these explosions took place in the same general area of the Nevada Atomic Test Site. The table lists the names, dates, depths of burial and sizes of the five shots.

Name	Date	Depth of burial (feet)	Energy release (kt of TNT-equivalent)
Blanca	10/30/58	835	19 ± 1.5
Logan	10/15/58	830	5 ± 0.4
Rainier	9/19/57	790	1.7 ± 0.1
Neptune	10/14/58	99	0.09 ± 0.02
Tamalpais	10/8/58	330	0.07 ± 0.01

Relative amplitude of horizontal earth motion as a function of the explosion energy is shown in Fig. 4.1. These data were obtained at the Tinemaha Station of the Cal-Tech Seismological Network using a Wood-Anderson torsion seismograph. The distance between the test site and the point of observation is approximately 180 kilometers. The relative amplitudes shown in the figure refer to the amplitude maxima, which were shear waves, but within the accuracy of the measurements, the same relative values appear to hold for the P-wave motion as well. (Frequency is not a function of yield, but constant.) The observed periods were similar for all the shots and roughly equal to one second. Although the precise values of the energy release are uncertain, a best power-fit indicates that the amplitude is roughly proportional to the first power of the energy. This dependence is somewhat unexpected since, for an elastic wave of a given period, the amplitude scales as the square root of the energy.

An explanation of the observed dependence is proposed on the basis of the following simple model. Close to the point of the explosion there is a shocked region in which energy is propagated and dissipated by nonlinear processes.

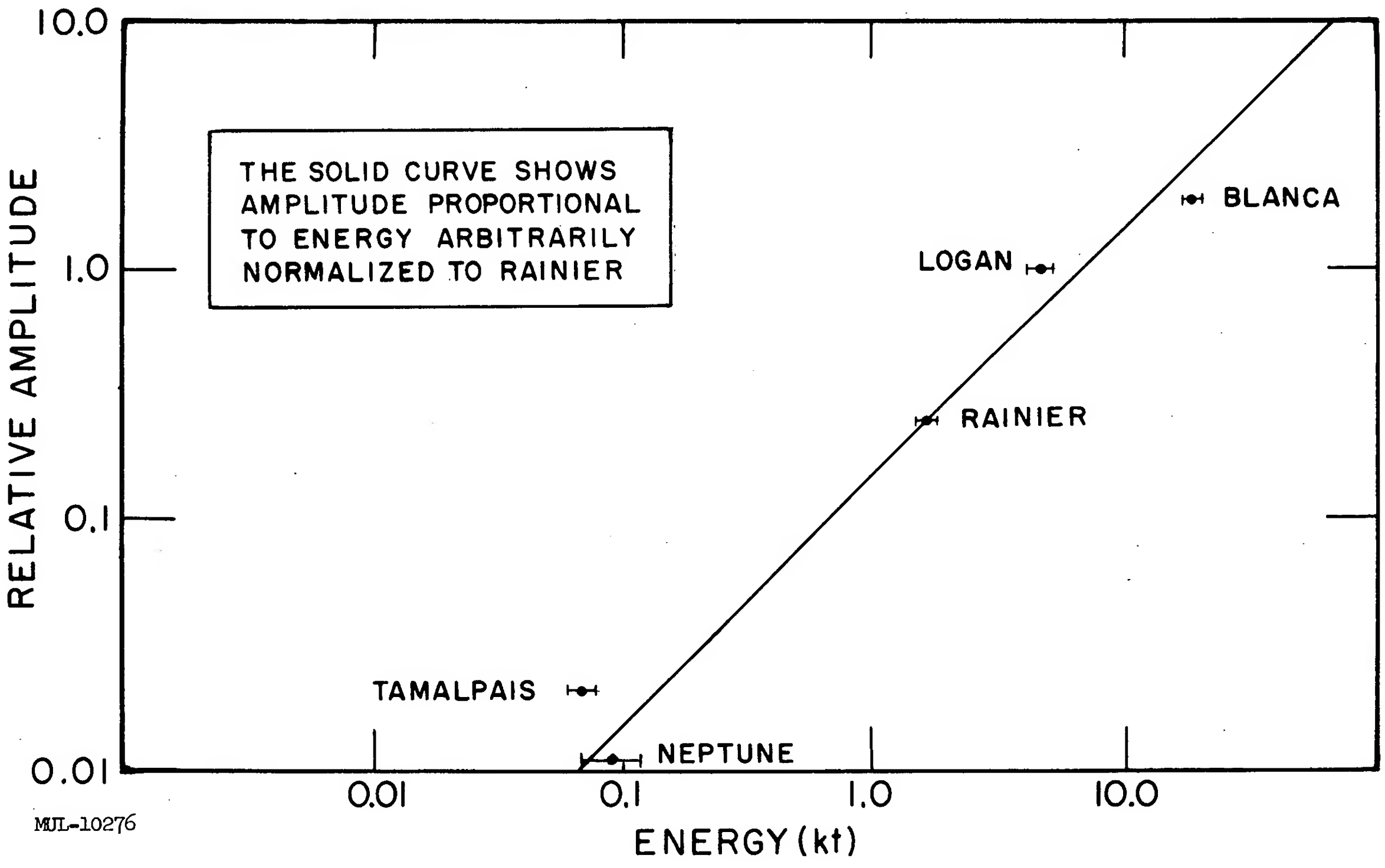

Fig. 4. 1. Relative amplitude of horizontal earth motion as a function of the explosion energy.

This region is assumed to be similar for all explosions so that its radius a scales like the cube root of the energy, consistent with the assumption that the nonlinear processes stop at a definite shock pressure p_0. In the region $r > a$ the medium is assumed to be elastic and linear so that a harmonic analysis of the pressure wave is permissible in the sense that the modes do not mix. It is further assumed that energy is being dissipated in this region in a way which depends on the frequency but not on the amplitude. The effect of this dissipation is to damp the high-frequency components of the pulse, allowing only the low-frequency components to be transmitted to large distances.

In the elastic region $r > a$ the seismic propagation is complicated by the free surface, inhomogeneities, and dissipation. If we were interested in the detailed wave shape of the distant signal, we would have to deal with these complications. However, we are interested only in the way in which the magnitude of the earth displacement depends on the radius a and hence on the energy of the explosion. For this purpose the free surface and inhomogeneities can be neglected, and the dissipation can be treated in a simplified manner. We assume only that the medium is homogeneous within a fixed radius $r = R$ which is at least a few times greater than any of the values of a considered. At this radius the displacement is determined as a function of time for each value of a. This function is then regarded as the boundary condition for the seismic propagation in the region $r > R$. It is necessary of course that R be much less than the distance between the explosion point and any surface of discontinuity (in particular the free surface) in order that interference between the outgoing wave and reflected and refracted waves at $r = R$ be negligible. Since R is chosen independent of a, all the a-dependence of the seismic signal is contained in the boundary condition at R.

With this model a simple argument can be given to determine the dependence of the amplitude of the distant seismic signal on the energy of the explosion. It follows from the assumption that the pressure p_0 at the elastic-inelastic interface a is independent of the yield, that the amplitude of the displacement produced at a is proportional to a. Since R is taken reasonably large compared to a, only the radiated wave need be considered and from a to R the amplitude will decrease by the factor a/R. The amplitude of the displacement at R is therefore proportional to a^2/R.

If the pressure at a remains high for a long time compared to the period a/c in which the sound velocity c traverses the distance a, then the displacement

at a will reach its maximum value in a time approximately equal to a/c and will thereafter be rapidly damped to the static value. It follows that at the point R a disturbance will arrive whose amplitude is proportional to a^2/R and whose duration is proportional to a/c. In the model we are now considering this disturbance will have essentially only outwardly directed components. The Fourier amplitude of a wave of sufficiently long wavelength will then be proportional to the product of amplitude and duration at the point R. Thus we obtain an amplitude which is proportional to a^3 and therefore proportional to the energy of the explosion.

Another limiting case of interest is one in which the pressure is not sustained but disappears in a time proportional to a/c. In this case the outward motion is followed by a similar inward displacement in a time which is proportional to a/c. The result at R is the superposition of a positive and negative pulse, each of an amplitude proportional to a^2/R and of a duration proportional to a/c, and separated by a time interval again proportional to a/c. The Fourier component of a long wave will then be proportional as before to the product of a^2/R and a/c, but will furthermore be proportional to the time interval between the positive and negative pulses. This introduces a further factor a/c and the resulting Fourier amplitude is therefore proportional to a^4 or the $\frac{4}{3}$-power of the energy of the explosion.

These simple arguments will now be verified by a more rigorous calculation. Since the explosion is spherically symmetrical in the region $r < R$, the equation of elasticity in this region reduces to the one-dimensional wave equation in terms of a displacement potential ψ, which is related to the displacement by

$$\zeta = \frac{\partial}{\partial r}\left(\frac{\psi}{r}\right) \quad . \tag{1}$$

The one-dimensional wave equation is satisfied if $\psi = \psi(\tau)$, where $\tau = t - \frac{r-a}{c}$, the retarded time. The form of τ has been chosen to represent an outgoing spherical wave.

We shall analyze the problem by relating the Fourier analysis of the source pressure p at point a to the displacement ζ at the greater distance R which is in turn related to the displacements at great distances. The pressure p(t) at $r = a$ is connected to the displacement and its derivative at $r = a$ through Hooke's law:

$$p(t) = -(\lambda + 2\mu)\left.\frac{\partial \zeta}{\partial r}\right|_{r=a} - 2\lambda \left.\frac{\zeta}{r}\right| \quad , \tag{2}$$

where λ and μ are the Lamé constants. In terms of the displacement potential,

$$p(t) = -\frac{\lambda+2\mu}{ac^2}\,\psi''(t) - \frac{4\mu}{a^2c}\,\psi'(t) - \frac{4\mu}{a^3}\,\psi(t) \quad . \tag{3}$$

Denoting the Fourier transform of $p(t)$ by $\hat{p}$ and the Fourier transform of ζ by $\hat{\zeta}$, it follows from Eqs.(1) and (3) that $\hat{\zeta}$ at $r = R$ is

$$\hat{\zeta}(\omega) = \frac{\hat{p}a}{4\mu}\left(\frac{1}{R^2} + \frac{i\omega}{Rc}\right)\frac{c^2}{\omega_0^2 + \omega_0\,\omega i - \frac{\lambda+2\mu}{4\mu}\omega^2} \quad . \tag{4}$$

To treat the dissipation we assume that the earth acts as a filter characterized by a response function $S(\omega)$. This means that if the displacement at $r = R$ is given by

$$\zeta(\tau) = \int_{-\infty}^{\infty} \hat{\zeta}(\omega)\, e^{i\omega\tau}\, d\omega \quad ,$$

then the distant signal will contain Fourier components given by

$$\hat{\zeta}_{dist}(\omega) = \hat{\zeta}(\omega)\, S(\omega) \quad . \tag{5}$$

τ is time measured after the arrival of the wave front, i.e., retarded time.

The function $S(\omega)$ depends on the nature of the physical mechanism which causes the energy loss. It will not be necessary for us to consider this mechanism in detail nor will we need to know the precise form of $S(\omega)$. We shall assume only that $S(\omega)$ has the property of admitting low frequencies and suppressing high frequencies. The cut-off frequency ω_c of $S(\omega)$ will further be assumed to be much less than the natural elastic frequency ω_0 of the inner region ($r < a$).

In this case ω can be neglected compared to ω_0 and

$$\hat{\zeta}_{dist}(\omega) \propto a^3\hat{p} \text{ for } |\omega| < \omega_c$$

$$\sim 0 \text{ for } |\omega| > \omega_c \quad . \tag{6}$$

The constant of proportionality in this equation is independent of $\underline{a}$. If we assume that p(t) is a jump function, equal to zero for $t<0$ and equal to $p_0 e^{-\alpha t}$ for $t>0$, then

$$\hat{p} \sim \frac{p_0}{\alpha + i\omega} , \qquad (7)$$

where p_0 is a constant independent of $\underline{a}$.

There are several cases to be considered depending upon the value of α. If α is independent of $\underline{a}$, $\hat{p}$ will be independent of $\underline{a}$ and the amplitude of the distant signal will be proportional to a^3 and therefore proportional to the first power of the explosion energy. If α depends on a but is much smaller than ω_c, i.e., the pressure falls off very slowly compared to the period of the transmitted waves, $\hat{p}$ is again essentially independent of $\underline{a}$, and again the distant signal goes like the energy to the first power. If, however, $\alpha \gg \omega_c$ and α is also proportional to $\omega_o = c/a$, then it follows that the amplitude of the distant signal is proportional to a^4 or energy to the $\frac{4}{3}$-power. To fix the dependence more precisely requires an analysis of the nonlinear region which we shall not undertake here.

The data shown in Fig.41 are not adequate to distinguish between the first power and the $\frac{4}{3}$-power for the amplitude yield relationship. In fact the data are intrinsically uncertain due to lack of knowledge of the precise energy release of the shots, particularly for Blanca and Tamalpais. Furthermore, as can be seen from the table, the depth of burial for the five shots varies over a considerable range and this may introduce effects not described by the model.

We have seen how the displacement depends on the energy of the explosion. It is also of interest to see how the acceleration depends on the energy of the explosion. This can be done readily from the preceding arguments. The Fourier analysis of the acceleration is ω^2 times the Fourier analysis of the displacement. For the distant seismic signal the Fourier analysis of the displacement cuts off in the neighborhood of ω_c, and the factor ω^2 does not introduce any further $\underline{a}$-dependence. At large distances therefore the acceleration and the displacement depend in exactly the same way on the energy of the explosion. Close-in, however, where the high frequency waves have not been dissipated, the Fourier analysis of the displacement cuts off in the neighborhood of ω_o instead of ω_c, and the factor ω^2 does introduce some additional

a-dependence. In this case, since $\omega_o = c/a$, the Fourier analysis of the acceleration is proportional to $(1/a^2)$ times the Fourier analysis of the displacement. From Eq. (4) it can be seen that the Fourier analysis of the displacement at close-in distances (but still in the radiation zone) is proportional to a^2. It follows that the acceleration at close-in distances is independent of a, and therefore independent of the energy of the explosion. Experiments should be made to check this amusing consequence of the model.

We are grateful to Dr. Frank Press for providing us with the seismic data contained in Fig. 4.1.

/ro

LIST OF PREVIOUS PLOWSHARE AND/OR RELATED REPORTS

Report No.	Title
UCRL-4659	Deep Underground Test Shots.
UCRL-5026	Non-Military Uses of Nuclear Explosions
UCRL-5124 Rev. I	Phenomenology of Contained Nuclear Explosions.
UCRL-5253	Industrial Uses of Nuclear Explosives.
UCRL-5257 Rev.	Peaceful Uses of Fusion.
UCRL-5281	Temperatures and Pressures Associated with the Cavity Produced by the Rainier Event.
UCRL-5457	Large Scale Excavation with Nuclear Explosives.
UCRL-5458	Mineral Resource Development by the Use of Nuclear Explosives.
UCRL-5538	Evaluation of the Ground Water Contamination Hazard from Underground Nuclear Explosions.
UCRL-5542 Rev.	Properties of the Environment of Underground Nuclear Detonations at Nevada Test Site. Rainier Event.
UCRL-5623	Radioactivity Associated with Underground Nuclear Explosions.
UCRL-5626	Underground Nuclear Detonations.
UCRL-5709	Hydroclimatology and Surface Hydrology of San Clemente Island.
UCRL-5757	Geologic Studies of Underground Nuclear Explosions Rainier and Neptune.
UCRL-5766	The Neptune Event. A Nuclear Explosive Cratering Experiment.
UCRL-5882	Chemical Reactions Induced by Underground Nuclear Explosions.
UCRL-5932	The Soviet Program for Industrial Applications of Explosions.
UCRL-5949	An Application of Nuclear Explosives to Block Caving Mining.
UCRL-6013	Probing the Earth with Nuclear Explosions.

LIST OF PREVIOUS PLOWSHARE AND/OR RELATED REPORTS

Report No.	Title
	Plowshare Series: Report No. 2. Proceedings of the Second Plowshare Symposium (Held at San Francisco, May 13-15, 1959):
UCRL-5675	Part I : Phenomenology of Underground Nuclear Explosions.
UCRL-5676	Part II : Excavation.
UCRL-5677	Part III: Recovery of Power and Isotopes from Contained Underground Nuclear Explosions.
UCRL-5678	Part IV: Industrial Uses of Nuclear Explosives in the Fields of Water Resources, Mining, Chemical Production, and Petroleum Recovery.
UCRL-5679	Part V : Scientific Applications of Nuclear Explosives in the Fields of Nuclear Physics, Seismology, Meteorology and Space.

Printed in USA. Price $3.00 Available from the
Office of Technical Services
U. S. Department of Commerce
Washington 25, D. C.